The laminar profile of spatial attention in macaque V1 and V4

Michael Boyd

A thesis submitted for the degree of Doctor of Philosophy

Institute of Neuroscience, Newcastle University

22nd September 2016

Abstract

Spatial attention allows processing to be prioritised for one or more locations in the visual field, even in the presence of other distracting or irrelevant stimuli. Previous work has shown that attention modulates the activity of the brain at the level of spiking activity, local field potentials and coherence between and within neuronal groups. However currently little is known about how these attentional modulations differ between groups of neurons in different cortical layers and areas.

We trained two adult male rhesus macaques to perform a covert visuospatial attention task whilst we recorded simultaneously from V1 and V4. Recordings were taken with multichannel laminar electrodes allowing recording from supragranular, granular and infragranular cells within the same cortical microcolumns. We used current source density analysis to align our recording contacts to the cortical laminar profile (layers). The receptive fields of the V1 and V4 cells we recorded from were overlapping which meant they could be driven by the same stimulus in the task. To measure the attentional modulation of information flow between different groups of neurons we calculated field coherence, Granger causality and spike-rate correlations.

Attention increased firing rates for all of the cell types, layers and areas in our study. We also show that variability as measured by gain variance and noise correlations is reduced by attention. Although we find differences between the two monkeys regarding LFP power changes and regarding coherence measures within and between the areas investigated, we find that attention consistently increased the Granger causality in the gamma frequency band between V1 and V4. We demonstrate that the flow of information in the alpha/beta and gamma bands follows expected interareal feedback and feedforward patterns between V1 and V4. We also provide evidence that feedforward gamma oscillations are generated, contrary to expectations, in the infragranular layers of V1.

Supported by the Wellcome Trust

Table of Contents

Table of Figures

Table of Abbreviations

ANOVA	Analysis of variance
AUROC	Area under receiver operating characteristic
BOLD	Blood-oxygen-level dependent
CRT	Cathode ray tube
CSD	Current source density
DP	Dorsal prelunate gyrus
DVA	Degrees of visual angle
ECoG	Electrocorticography
FDR	False discovery rate
FEF	Frontal eye fields
FF	Fano factor
FFC	Field-field coherence
FFT	Fast Fourier transform
fMRI	Functional magnetic resonance imaging
FST	Fundus of the superior temporal area
GC	Granger causality
IT	Inferior temporal area
JND	Just noticeable difference
K-cells	Koniocellular cells
LFP	Local field potential
LGN	Lateral geniculate nucleus
LIP	Lateral intraparietal
M-cells	Magnocellular cells
MI	Modulation index
MST	Medial superior temporal area
MT	Middle temporal area
MUAE	Envelope multiunit activity
P-cells	Parvocellular cells
PFC	Prefrontal cortex
PO	Parieto-occipital sulcus
PPC	Posterior parietal cortex
RF	Receptive field
ROC	Receiver operating characteristic
SC	Superior colliculus
SFC	Spike-field coherence
SNR	Signal to noise ratio
SU	Single unit
VEP	Visually evoked potential
VPA	Ventral prearcuate region
VPS	Ventral bank of the principle sulcus

Chapter 1: Introduction and Aims

This chapter contains a literature review relevant to this thesis. Based on this, the aims of the study are set out (Section 1.4) and the techniques and methods which we used to investigate these are detailed (Chapter 2). The results obtained from recordings in V1, V4 and the interactions between V1 and V4 are described in Chapters 3, 4 and 5 respectively. These results are discussed and put into context in Chapter 6.

1.1 Vision

1.1.1 The main visual pathway

The main visual pathway for conscious perception in mammals is the thalamocortical pathway. It sends visual information from the eye to the cortex, starting in the retina. From the retina (from retinal ganglion cells) axons are sent through the optic tract to the lateral geniculate nucleus (LGN) of the thalamus, where information is processed and then relayed to the visual cortex. This pathway and the areas involved in visual processing will be discussed here, with particular emphasis on the structure of visual cortical areas V1 and V4, as these areas are the focus of my experiments. Another pathway of importance for vision is the retinotectal pathway, which sends information to the pretectum and the superior colliculus (Johnson and Harris, 2000). Given that this pathway is not investigated in the current thesis, it will be described in much less detail.

At the first stage of vision, light enters the eye and reaches the retina, activating light sensitive photoreceptors located in the outer nuclear layer (Kandel *et al.*, 2000). The two types of photoreceptors are rods and cones, each with different photopigments and separate roles in the visual system. Cones are light sensitive primarily at medium to high intensities (mesopic and photopic illumination conditions) , whereby the three subtypes show light absorption selectivity centred on short (~426nm), medium (~530nm) and long (~555nm) wavelengths (Merbs and Nathans, 1992). The cones are arranged in a mosaic in the retina and their outputs combine to form the basis of

colour vision (Roorda and Williams, 1999). Luminance perception under mesopic and photopic light conditions also arises from the cones, with input from the medium and long wavelength cones summed together to give luminance sensitivity (Lee *et al.*, 1989). Rods, conversely, function at lower light levels (scotopic, <20-40cd/m^2) and so allow vision in dark environments (Masland, 2001). The spatial acuity of rods and cones also differs, with cones responsible for capturing fine detail in vision, due to the higher density of cones and the smaller number of cones converging onto individual interneurons in the retina. Spatial acuity is highest at the centre of the visual field in many mammals, which maps onto an area of the retina named the fovea in primates (note that not all mammals have a fovea [Woollard (1927)]). The increased spatial acuity is a consequence of the increased cone density in the fovea, compared to the rest of the retina. Rods are not present in the fovea (Curcio *et al.*, 1990).

In the inner nuclear layer of the retina, three classes of interneurons (horizontal, bipolar and amacrine cells) integrate the information from the photoreceptors (Kaneko, 1970). Horizontal and amacrine cells process information laterally and bipolar cells transmit information vertically from the photoreceptors to the retinal ganglion cells. Retinal ganglion cells in the ganglion cell layer are the last stage of processing in the retina before the signal is transmitted through the optic nerve to the next recipient stages.

The optical nerve projects from the retina to the lateral geniculate nucleus (LGN) of the thalamus. The LGN contains three projection type cell classes, categorised by their input from the retina and their location within the thalamus (Kaplan and Shapley, 1986). The two main groups of LGN cells are parvocellular (or P-cells) and magnocellular cells (or M-cells). M-cells have a shorter latency than P-cells, and are selective for lower spatial and higher temporal frequencies, while P-cells are unique in that they have colour (red-green) opponency (Kaplan and Shapley, 1982). The final group of cells within the LGN, koniocellular cells (or K-cells), appears to be more heterogeneous than the other two and their primary function (Hendry and Clay Reid, 2000; Stewart and Reid, 2000) is still somewhat unknown. The three cell classes are organised into separate layers within the LGN. In primates the M-cells reside in layers 1 and 2, the P-cells in layers 3-6 and the K-cells are present between these (in the intercalated layers).

The visual cortex comprises of many different areas (for details see Section 1.1.4), which reside in the occipital lobe, and in primates to some extent in the temporal and parietal lobe. As its name suggests, it is involved in the processing of different aspects of visual information. The first visual cortical processing stage is the primary visual cortex, also referred to as V1 or striate cortex. The separation of the magnocellular and parvocellular pathways is conserved in projections from the LGN into V1, with the M-cells projecting to layer 4cα and P-cells to layers 4a and 4cβ (Casagrande and Xu, 2004).

1.1.2 Alternative visual pathways

Although the majority of inputs to the visual system are processed along the pathway described above, there are additional pathways through which it may route. For example, the LGN does not project solely to the striate cortex, but also has direct projections to the extrastriate cortex, projecting to V2, V4 and MT (Bullier and Kennedy, 1983; Sincich *et al.*, 2004; Ninomiya *et al.*, 2011).

The retinotectal pathway diverges from the main visual pathway at the level of retinal ganglion cells, some of which project to the superior colliculus (SC), located in the tectum of the midbrain, rather than to the LGN (Schiller and Malpeli, 1977). One of the primary roles of the SC in mammalian vision is its coordination of saccadic eye movements (Krauzlis, 2003) along with stability of fixation (Goffart *et al.*, 2012). Stimulating the macaque SC elicits saccades towards the RF of the stimulated cells (Robinson, 1972). The SC receives input from several cortical regions, including the frontal eye fields (FEF), the lateral intraparietal cortex (LIP) and visual cortex (Fries, 1984), making it a viable target for top down attention. Conversely, the SC projects to several cortical areas, raising the possibility that it acts as a centre for top-down attention control (Zénon and Krauzlis, 2014).

1.1.3 Receptive fields

Receptive fields (RFs) describe the spatial extent of external space for which a cell is responsive. Retinal ganglion cells and bipolar cells in the retina have “on-off” receptive fields, which are composed of a centre and surround (Kandel *et al.*, 2000).

The centre and surround always oppose each other so that one is excitatory (“on”) and one is inhibitory (“off”).This means that “on-off” RFs respond optimally to contrast, such that either the centre or surround are stimulated individually by their respective preference, and ideally opponently.

Many visual areas are organized in a retinotopic manner. This describes the finding that neighbouring cells in the area of interest have neighbouring receptive fields in the external world. The retinotopy in the primate LGN and V1 arise due to the organisation of their inputs (i.e. neighbouring retinal ganglion cells project to neighbouring LGN cells, etc.). Retinal ganglion cells project to only one LGN side individually, but each retina sends projections to both hemispheres (Tassinari *et al.*, 1997), with input from the contralateral and ipsilateral visual fields arriving in separate layers. Moreover, the upper and lower portions of the visual field are represented by the inferior and superior regions of the LGN respectively (Chen *et al.*, 1999).

In the primary visual cortex of primates, there is a retinotopic map for the contralateral (but not the ipsilateral) visual field. There is a lateral-medial gradient for foveal-peripheral portions of the visual field and separation of the upper and lower portions of the visual field superior and inferior to the calcarine fissure (Kandel *et al.*, 2000). This continuous retinotopy is not (or at least less) present in higher areas of the visual stream, where adjacent neurons and subregions may have less overlap in RF locations.

1.1.4 Multiple visual pathways in the cortex

An influential way of thinking about information processing in the visual system is along a subdivide of visual areas into a dorsal and a ventral stream (Mishkin *et al.*, 1983). The dorsal (or “where”) pathway is associated with spatial visual processing, with activity progressing from the visual cortex to the parietal cortex. The ventral (or “what”) pathway is responsible for recognising the features of an object and the object itself. In this pathway, activity is processed from the visual cortex to the temporal lobe. In the macaque visual cortex, the dorsal stream comprises of V1, V2, V3, the middle temporal (MT) area and the medial superior temporal (MST) area before projecting to the parietal cortex (Boussaoud *et al.*, 1990). The ventral stream includes V1, V2, V3, V4 and finally areas of the temporal lobe (areas TEO, TE and

the inferior temporal cortex (IT)) (Gross *et al.*, 1969). Both pathways receive input from the magno- and parvocellular pathways, however there is a strong bias for the dorsal areas to receive magnocellular input and a mild bias for the ventral areas to receive parvocellular input (Merigan and Maunsell, 1993).

1.1.5 Structural organization and local connectivity of the striate cortex (V1)

One of the regions of interest for our study is the striate cortex (V1). At a coarse level, primate V1 can be subdivided into supragranular, granular and infragranular layers. Supragranular layers can be further subdivided into layers 1, 2, 3A and 3B (Lund and Wu, 1997). The name striate ('striped') cortex is derived from a clearly visible granular layer, which is discernible to the bare eye in Nissl stained anatomical sections. This makes it distinct to other (visual) cortical areas, where the granular layer is substantially thinner (or sometimes absent). The granular layer of V1 is ~500μm thick (Lund and Yoshioka, 1991), and it can be further separated into layers 4A, 4B, 4Cα and 4Cβ, each with its own structure and input-output specificity. The deepest layers in V1 are the infragranular layers, which can be subdivided into layers 5A, 5B and 6 (Lund *et al.*, 1988).

Additionally, V1 is functionally organised into individual cortical microcolumns that span all of the cortical layers. Since cells within microcolumns have similar input, they also have similar receptive field locations (Mountcastle, 1957). As outlined previously (Section 1.1.1), the main input to V1 arises from the magno- and parvocellular layers in the LGN. These terminate in V1 layer 4Cα and 4Cβ, respectively. The separation of magno- and parvocellular activity is maintained in granular layers, with layer 4Cα projecting predominantly to layer 4B and 4Cβ projecting mainly to layer 4A (Boyd *et al.*, 2000).

The next step of processing (or information channelling) in the V1 microcircuit is from the granular to supragranular layers (Livingstone and Hubel, 1982). This is where the separation of the M and P pathways begins to break down, with spiny neurons in both layers 4Cα and 4Cβ projecting to layer 3B (Callaway and Wiser, 1996). Horizontal connectivity between different microcolumns is typically observed in the superficial layers (Rockland and Lund, 1983), where pyramidal cells in layer 3 project

to other microcolumns (McGuire *et al.*, 1991). However there are also horizontal connections between microcolumns in the other cortical layers, albeit in smaller quantities (Blasdel *et al.*, 1985).

Neurons in layers 2-4B show prominent projections to layer 5 (mainly 5B) in the infragranular layers. The majority of the layer 5 cells then project back to layers 2 to 4B (Callaway and Wiser, 1996). As well as projecting reciprocally back to the supragranular layers, layer 5 projects to layer 6 (Blasdel *et al.*, 1985). From layer 6, activity is then routed back to the more superficial layers, forming modulatory connections. An additional fraction of cells in the top and bottom portions of layer 6 project back to layer 4C, while neurons in the middle section project mainly to layer 5B (Wiser and Callaway, 1996).

Although these connections describe the main flow of visual activity through V1, there are also a large number of other cell types making modulatory connections between the different layers. For a review on the remainder of these connections see Lund (1988) and Callaway (1998).

The above connectivity pattern and the associated predicted flow of information has given rise to the notion of the canonical microcircuit (Douglas and Martin, 2004), which argues that the flow of information (and the associated processing steps) is repeated in all neocortical areas. The model of the canonical microcircuit argues that granular layers are responsible for integrating feedforward recipient input (from e.g. the thalamus or upstream cortical areas). The integrated information is passed on to cells in the supragranular layers. These also receive input from the supragranular layers of other cortical microcolumns (and from layer 5 [infragranular] neurons of the same microcolumn, see below). The integrated activity is then passed sent to layer 5 neurons, which provide feedback to the supragranular cells, as well as sending output to layer 6 and to subcortical structures. Layer 6 cells project back to the input layers, and to the thalamic input. Their role is often seen as modulatory, regulating the input into the microcolumn. Based on this description, the connections from 4 to layers 2/3, as well as the connections from layer 2/3 to layer 5, could be seen as feedforward connections, while those from layer 5 to layer 2/3, and those from layer 6 to layer 4 could be seen as feedback connections. This, distinction will be important when considering the predictions regarding the flow and directionality of oscillatory activity interactions within cortical microcolumns (see Section 1.2).

1.1.6 Input into the striate cortex

Input into the striate cortex can be subdivided into feedforward and feedback. Since V1 is the earliest visual cortical region, its feedforward input arrives from subcortical areas (the LGN, and partly the pulvinar). As already discussed in Section 1.1.1, the LGN projects from its magnocellular and parvocellular layers into layers 4Cα and 4Cβ respectively. Additionally, there are other smaller projections from the LGN to V1, terminating outside of layer 4. For example, the parvocellular layers project to layer 4A and both the parvocellular and magnocellular layers project to layer 6 (Blasdel and Lund, 1983). Projections to layer 5 of V1 from the LGN have also been demonstrated in the rat (Constantinople and Bruno, 2013), cat (Ferster and Levy, 1978) and in layer 5A of the macaque (Blasdel and Lund, 1983), however these occur less frequently than the projections to the granular layers, even though they may be as (if not more) important as granular terminals in the rodent (Constantinople and Bruno, 2013).

In addition to its feedforward inputs, V1 also receives feedback input from higher areas in the visual stream. Extrastriate area V2 projects back to V1, mainly from infragranular layers but supragranular sources also exist (Rockland and Pandya, 1979; Kennedy and Bullier, 1985; Markov *et al.*, 2014). Feedback projections arise predominantly in the infragranular layers, throughout the brain, whereby the relative proportion of infragranular over supragranular feedback projections increases with increasing distance from V1 (Markov *et al.*, 2014). The projections from V2 most frequently terminate in regions of V1 which have similar receptive fields to the origin of the projection (Gattas *et al.*, 1997). V1 does receive some direct feedback from V4, however only from regions representing the foveal portion of the visual field (Ungerleider *et al.*, 2008). Felleman and Van Essen (1991) summarised the connections reported between cortical areas and ranked them in order of their position in the cortical hierarchy. This hierarchy categorises V1 as the lowest in the visual stream.

V1 also receives feedback from areas outside of the traditional visual stream. Borra and Rockland (2011) showed that association areas in the parietal cortex project directly to the portions of V1 representing the peripheral visual field. The combination of the sensorimotor role of the parietal cortex and peripheral V1 locations could mean that these connections are linked to motor planning, for example the planning of

saccades into the peripheral visual field. Interestingly, though these projections were considered to be feedback terminations they predominantly targeted layers 1, 2, 3, and 6 (with boutons even found in layer 4), but spared layer 5 (Borra and Rockland, 2011).

1.1.7 The projections of the striate cortex

The main output from V1 is to V2, from where visual activity is then sent further down the visual stream. Rockland (1992) found that the majority of V1 projections to V2 are from layers 3A and 4B, with a smaller number of connections coming from layers 2, 3B, 4A and 5. The superficial projection neurons are more likely to be responsive to chromatic stimuli, whereas the granular projection neurons are more likely to be selective for motion and disparity (El-Shamayleh *et al.*, 2013), suggesting a functional divide for these pathways.

In addition to the projection to V2, there are several other feedforward projections which bypass V2. Cells in layers 2/3 of V1 representing the foveal part of the visual field project directly to V4 (Nakamura *et al.*, 1993). The authors suggest that the importance of this projection could be in improving the speed of information flow by sending coarse representations ahead of the fine grain representations traveling via V2. They also highlight its importance in allowing vision to function even if V2 is damaged.

In addition to receiving the majority of its input from the LGN, V1 pyramidal cells in layer 6 project back to the LGN, completing a thalamocortical loop (Lund *et al.*, 1975). The separation of parvo and magnocellular LGN inputs is also maintained here, with cells in the upper portion of layer 6 projecting mainly to the parvocellular LGN layers and the lower portion of layer 6 projecting mainly to the magnocellular layers. Since attention has been shown to increase spiking activity in thalamic reticular neurons and these in turn inhibit thalamic relay cells, this means that the thalamocortical loop could be responsible for attentional modulation of spiking activity occurring as early as the LGN (McAlonan *et al.*, 2006; Briggs *et al.*, 2013).

The striate cortex also has projections back to the inferior and lateral subdivisions of the pulvinar (Ogren and Hendrickson, 1976). This is part of a pulvinocortical loop, an important circuit for visual processing, since deactivation of the pulvinar diminishes

visual responses in supragranular V1 neurons (Purushothaman *et al.*, 2012). In addition to the role of attention in the pulvinar discussed later in Section 1.3.3 (Zhou *et al.*, 2016) this puts forward the possibility that the pulvinocortical loop plays a role in attentional modulation of V1 activity.

1.1.8 The local connectivity of extrastriate area V4

Extrastriate visual cortex comprises areas beyond area V1, of which there are many (Felleman and Van Essen, 1991). This section will describe some anatomical features of the extrastriate area V4, which was the other area investigated in this study.

V4 is equally organised into cortical microcolumns, and along the depth axis into supragranular, granular and infragranular layers. However, there are fewer layer subdivisions than reported for area V1 (Hendry *et al.*, 1990). The supragranular layers comprise of layer 1, 2 and 3 and the input/granular layer is layer 4. The input layer does not have the same parvocellular and magnocellular separation which V1 does, nor is it subdivided any further. Measuring only 200µm in depth, it is also substantially thinner than the granular layers in V1 (Hof and Morrison, 1995). The deep/infragranular layers are layers 5A, 5B and 6.

Following feedforward input into layer 4, the information is then processed and passed on by spiny stellate cells which mainly project up to layers 2 and 3 within the same cortical microcolumn (Yoshioka *et al.*, 1992). Connectivity between microcolumns occurs primarily in layers 2/3, where pyramidal cells project horizontally up to 6mm (Lund *et al.*, 1993). From the supragranular V4 layers the main intracolumnar projections are down to layer 5 (Rockland and Pandya, 1979). Layer 5 connects reciprocally back to the superficial layers and to layer 6 (Yoshioka *et al.*, 1992), completing the canonical microcircuit (Douglas and Martin 1984).

1.1.9 V4 afferents

The predominant input into V4 is from extrastriate area V2, which in turn receives its input from V1 (Zeki, 1971). Cells in layer 3C of V2 project directly to layer 4 of V4 (Rockland and Pandya, 1979). V4 also receives input from V3, again from the

supragranular layers to the granular layers (Felleman *et al.*, 1997) and, as discussed previously (Section 1.1.7), directly from V1 (Nakamura *et al.*, 1993) .

Additionally, V4 receives a direct (sparse) projection from the koniocellular layers of the LGN to layers 4 and 5 of V4 (Benevento and Yoshida, 1981).

A repeating pattern of processing in the visual cortical system is the existence of pulvinocortical loops, already described in relation to V1 processing (Section 1.1.7). The pulvinocortical loop in V4 emerges from layers 5 and 6, sending axons to the pulvinar, whereby the pulvinar projects back to granular and supragranular layers of V4 (Shipp, 2003). As has been suggested for the V1 pulvinocortical loop, this connection may have an important role in attention (Zhou *et al.*, 2016).

The feedback from higher cortical areas to V4 typically originates in layers 5B and 6 and projects back to V4 layers other than layer 4 (Rockland and Pandya, 1979). Ungerleider *et al.* (2008) used this definition in combination with retrograde tracers injected into V4 to establish which areas project feedback connections into V4. The feedback connections they found were from the temporal areas TEO and TE, the lateral intraparietal cortex (LIP) and area 7a. Feedback from the frontal eye field (FEF), one of the main areas controlling attention (Moore and Fallah, 2004; Gregoriou *et al.*, 2009) terminated across different layers in V4, including the granular layer.

1.1.10 Efferent projections of V4

V4 cells in layers 3C and 5A project to IT (Rockland and Pandya, 1979). Given IT's primary role of object recognition (Lueschow *et al.*, 1994) and V4's role in colour vision (Heywood *et al.*, 1992), this projection might be providing IT with the colour information required for identifying objects.

Projections from V4 to the posterior parietal cortex (PPC) have been found in macaque, but these are present mainly between regions representing peripheral parts of the visual field (Baizer *et al.*, 1991). Projections were also found from V4 IT in that study, but mainly for the foveal visual field representation. This means that the separation of information flow into dorsal and ventral streams can be maintained,

since the projection origins are mostly non-overlapping. Both of these projections originate in the supragranular layers.

Ungerleider *et al.* (2008) injected an anterograde tracer into macaque V4 and categorised the projections as feedforward from the area if the origin was supragranular and the terminal was granular. The areas found to receive feedforward projections from V4 were the fundus of the superior temporal area (FST), the medial superior temporal area (MST), inferior temporal areas TEO, TE and TF, LIP, parieto-occipital sulcus (PO) and area 7a.

Unlike in V1, it is not always clear whether cortical projections to or from V4 are feedforward or feedback. Ungerleider *et al.* (2008) classify connections with V3A, V4t, the middle temporal area (MT), the dorsal prelunate gyrus (DP), ventral intraparietal area (VIP), the posterior intraparietal area (PIP), and the FEF as an intermediate type because the laminar projection patterns do not match up with the canonical feedforward (supragranular to granular) and feedback (infragranular to non-granular) circuits. Given the suggested role of the FEF as a top-down attentional centre (Gregoriou *et al.*, 2009; Bichot *et al.*, 2015), this area can still be considered higher than V4, at least with respect to spatial attention even though it does not project preferentially to specific layers of V4 (Anderson *et al.*, 2011).

This method of distinguishing feedforward and feedback projections based on the laminar origin/destination was also utilised by Markov *et al.* (2014). This study showed that supragranular feedback connections most frequently have an origin in layers 2/3A, while feedforward connections originate in layer 3B. The origins of infragranular connections are less segregated, with feedback neurons typically located in layer 6 and the bottom of layer 5, whereas the feedforward neurons are located throughout the infragranular layers.

1.2 Feedforward and feedback connections: origin, termination, and spectral signatures of interareal interactions.

As described above, feedforward connections arise predominantly in the superficial layers of an area and terminate predominantly in the granular layers of the target area (Ungerleider *et al.*, 2008; Markov *et al.*, 2014). Conversely, feedback (top-down) projections arise predominantly in infragranular layers and mostly terminate in layer 1 and layer 5 of the target areas (Rockland and Pandya, 1979; Markov *et al.*, 2014). These preferences increase with hierarchical distance between areas (Markov *et al.*, 2014). These laminar differences map onto patterns of local field potential (LFP) activity seen for inter-areal interactions. Specifically, it has been suggested that feedforward influences are predominantly mediated through gamma frequency synchronisation of neurons (measured using the LFP) and to some extent through theta frequency synchronisation (Bosman *et al.*, 2012; Van Kerkoerle *et al.*, 2014; Bastos *et al.*, 2015), while feedback influences are predominantly carried through alpha band synchronisation (Bosman *et al.*, 2012; Van Kerkoerle *et al.*, 2014; Bastos *et al.*, 2015) or beta band synchronisation (Bastos *et al.*, 2015). Based on these findings it has been suggested that bottom up-stimulus processing is facilitated in a feedforward manner through gamma-band coherence/influences (Bosman *et al.*, 2012; Van Kerkoerle *et al.*, 2014; Bastos *et al.*, 2015), while tasks (or more general: stimulus processing requirements) that necessitate feedback interareal interactions, would modulate beta-band influences from higher to lower areas (Bastos *et al.*, 2015). During normal vision, both rhythms (coherences) are present simultaneously. Despite this, the strength of interareal interactions in specific frequency bands (measured by Granger causal analysis) is modulated by presentation of visual stimuli, which boosts gamma frequency Granger casual interactions from lower to higher areas (Bosman *et al.*, 2012; Van Kerkoerle *et al.*, 2014; Bastos *et al.*, 2015), and by task demands which boost beta frequency Granger causal interactions from higher to lower areas (Bastos *et al.*, 2015). We currently have no (or only very limited (Van Kerkoerle *et al.*, 2014)) data on whether a similar preference/organisation exists within an area along the cortical microcolumns. In principle this should occur, as the canonical microcircuit argues for a feedforward processing loop from granular to

supragranular to infragranular layers, and a feedback loop from infragranular layers to supragranular layers. It would thus predict, that the gamma-frequency causal interactions are dominant along the directionality of the feedforward pathway, while alpha/beta frequency causal interactions dominate the directionality from infragranular to supragranular layers.

1.3 Attention

Attention describes the ability to focus on one or more stimuli in the presence of other irrelevant or distracting information. There are several defined forms of attention; it can be split into covert or overt attention (Posner *et al.*, 1982), exogenous or endogenous attention (Posner, 1980; Theeuwes, 1991) and also categorised based on sensory domain. In overt attention, attention is directed to a stimulus by shifting the centre of gaze to its location, thereby increasing salience and the ability to resolve fine detail due to the higher resolution of photoreceptors in the fovea. Conversely, covert attention operates in the absence of eye movements, allowing a stimulus to be attended to without moving the centre of gaze towards it. Endogenous attention refers to a voluntary orienting of attention to a stimulus, often referred to as top-down attention because it is a wilful process and because of the idea that higher cortical areas are acting as an attentional control to enhance processing abilities in sensory cortices. Exogenous (or bottom-up attention) is a stimulus driven process which allows unexpected events to be reacted to. The final categorisation of attention is based on sensory domains, for example visual attention is concerned with the visual domain and auditory attention involves attention in the auditory domain, but in everyday life they would often be linked. Visual attention can be further divided into spatial, feature and object based attention. Spatial attention involves directing attention to one or more portions of the visual field (Posner, 1980), feature based attention refers to attention to features such as shape or colour (Rossi and Paradiso, 1995), whereas object based attention refers to attending to an object as a whole, rather than to its basic features (Duncan, 1984).

1.3.1 Visual cortical contributions to attention

1.3.1.1 Attentional modulation of spiking activity

Over the past 30 years numerous studies have demonstrated that attention alters neuronal firing rates. A full literature review thereof would be excessive, and thus this review will remain somewhat incomplete. The first studies to observe attention effects in the brain were performed in the visual cortex. Moran and Desimone (1985) recorded single cells in the macaque visual cortex and showed that the firing rates of V4 cells were increased when the animal attended to the cell's RF rather than away from it. Initial studies did not find an effect of attention in striate cortex. However, a later study (Motter, 1993) showed an attention effect in V1 when multiple (3 or 4) competing stimuli were used, which means that the initial lack of an attentional modulation in V1 may have been due to low attentional demand and a lack of competition between the stimuli. Luck *et al.* (1997) placed two stimuli within the RFs of V2 and V4 neurons. When the stimuli were presented simultaneously the effect of attention was larger than when they were presented sequentially. Similar results have been obtained by Treue and Maunsell (1999). This suggests that attention most effectively affects firing rates when stimuli are competing for the same resources. These findings have led to the biased competition model of attention (Desimone and Duncan, 1995), arguing that stimuli compete for processing resources, and attention is able to bias that competition, such that the attended stimulus 'wins'. In this model attention prioritises resources to behaviourally relevant stimuli.

1.3.1.2 Additional models of attention

While an early study by Spitzer *et al.* (1988) has argued that attention sharpens orientation tuning curves, various follow up studies failed to replicate these changes. Instead many authors found that attention increases firing rates for preferred and for non-preferred stimuli, whereby responses to stimuli are increased in proportion to the responses elicited in the absence of attention (McAdams and Maunsell, 1999; Treue and Maunsell, 1999; Williford and Maunsell, 2006). This has led to the response gain model of attention, which argues that attention increases the gain of neuronal responses, resulting in a fixed amplification factor (Treue and Maunsell, 1999). While influential, it was not supported by all investigations. For example, Reynolds *et al.*

(2000), using stimuli of differing contrast, showed that attention had the greatest effect on V4 firing rates when low contrast stimuli were used, a finding incompatible with a simple increase in response gain. They concluded that attention is increasing the salience of stimuli and argued that attention alters the contrast gain of neurons, effectively shifting the contrast response function to increase neuronal sensitivity for low salience stimuli, while having little or no effect for high salience stimuli. Yet others have reported additive effects of attention (Thiele *et al.*, 2009), and even suppressive effects when attention was directed to non-preferred stimuli (Reynolds *et al.*, 1999; Martinez-Trujillo and Treue, 2004) The latter gave rise to the feature similarity gain model of attention. The multitude of effects appears puzzling, but many of these effects can be explained by the normalisation model of attention (Reynolds and Heeger, 2009; Ni *et al.*, 2012; Sanayei *et al.*, 2015), which assumes that attention acts by affecting excitatory and inhibitory circuits. The balance between excitatory and inhibitory drive in this model is determined by the size of the stimulus and the size of the attentional focus. By altering these sizes, attention can appear to either cause contrast or response gain (Reynolds and Heeger, 2009), or a mix thereof, and it can even reproduce results predicted by the feature similarity gain model.

1.3.1.3 Attention effects in V1 and V4

Given that the data reported herein were obtained in areas V1 and V4, I will mostly focus the next sections on describing attentional effects in V1 and in V4. As reported above, early studies either failed to find effects of attention in area V1 (Luck *et al.*, 1997) or only found it when competing stimuli were present (Motter, 1993). However, many studies have now also found attention induced firing rate changes in V1 when non competing stimuli were presented (Roelfsema *et al.*, 1998; McAdams and Maunsell, 1999; McAdams and Reid, 2005; Roberts *et al.*, 2007; Herrero *et al.*, 2008).

Many of these studies instructed animals to attend to a spatial location (McAdams and Maunsell, 1999; McAdams and Reid, 2005; Roberts *et al.*, 2007; Herrero *et al.*, 2008), thereby employing spatial attention. Others, however, have used paradigms of object based attention (Roelfsema *et al.*, 1998). Roelfsema *et al.* (1998) trained monkeys to attend to one of two curves and showed that attention to a preferred object increased V1 firing even when the curves overlapped, eliminating spatial

attention as a possible cause. McAdams and Maunsell (2000) also demonstrated that feature based attention is able to modulate neuronal activity in macaque area V4. This shows that the visual cortex is affected by different types of visual attention.

The above shows that attention can alter firing rates to attended/non-attended stimuli, but an important question to ask is whether it also alters the receptive field size and/or receptive field location, as these would affect the filter properties of the visual system and possibly the spatial resolution available. This question has been addressed in a variety of different ways, as outlined below.

Responses to stimuli in V1 increase when stimuli are shown along with additional flanking stimuli with similar orientation and location (Kapadia *et al.*, 1995). Exploiting this finding, Ito and Gilbert (1999) showed that attention can enhance this effect, however only when attention was focused into the receptive field of the cells and not when attention was focused away or distributed across the visual field. The authors suggest that this effect occurs due to feedback from higher visual areas gating the horizontal connections in supragranular layers. Despite the high profile placement of this study, the effects found were opposite for the two monkeys, whereby attention reduced the flanker effects in one animals (where recordings were performed near foveally), while it increased the flanker effects in the other monkey (where recordings were performed more peripherally). A potential explanation for this inconsistency was provided by Roberts *et al.* (2007). They showed that attention does not have the same effects across the visual field in V1, by systematically recording from cells with foveal and peripheral receptive fields in the same monkeys. Doing so, they found that attention decreased spatial integration for cells with foveal receptive fields but increased spatial integration for cells with peripheral receptive fields. These contrasting effects could arise due to the differences in projections to/from foveal and peripheral representations (Ungerleider *et al.*, 2008; Borra and Rockland, 2011) or from the greater number of cells representing foveal locations in V1 (Tootell *et al.*, 1982). Taken together these results clearly show that attention alters centre-surround properties of receptive fields as early as V1.

A way to additionally increase processing capacity would be to flexibly shift receptive fields towards the attended stimulus. Early studies conducted in area V4 suggested that such alterations might occur (Connor *et al.*, 1996), and receptive fields of V4 neurons shift towards the endpoint of saccadic eye-movement, before movement

onset (Tolias *et al.*, 2001). Additionally the V4 receptive fields appear to 'shrink' around the attended stimulus (due to the biased competition) (Reynolds and Desimone, 2003), which is equivalent to RF centre shifting. Studies in macaque in the middle temporal area (MT) investigated this systematically, and showed that RFs indeed shifted towards the attended location (Womelsdorf *et al.*, 2006). While these effects were found in extrastriate cortex, they seem to be absent in V1 (McAdams and Reid, 2005), or extremely difficult to assess. This means it is important to place stimuli in an attention task so that they are centred on the V1 receptive fields, an important consideration for my study, when trying to record from partially overlapping V1 and V4 receptive fields.

Although attention has been shown by previous studies to be affecting most of the areas in the visual stream, these studies were not able to address where the origin of attentional signals may be. Some of these answers could be derived by analysis of the onset of attentional modulation in different areas, or different layers. Buffalo *et al.* (2010) showed that the onset time of attention effects in visual cortex followed a backward progression. An attentional effect in firing rates was observed first in V4, then in V2 and finally in V1, consistent with a top-down modulation of attention, but this was challenged by Pooresmaeili *et al.* (2014), who found a simultaneous onset of attentional signals in area V1 and the FEF. The authors also showed that this simultaneity was disrupted in error trials, where the FEF took the lead, arguing for an active and important role of attentional modulation signals in early sensory cortex.

Despite these results, the importance of the role of visual cortex in attention has been debated. For example, subthreshold microstimulation of V4 neurons during an attention task did not influence the monkeys' perception of contrast changes in the receptive fields of the stimulated cells (Dagnino *et al.*, 2015), while equivalent experiments performed in the FEF were able to affect the perception of contrast changes (Moore and Fallah, 2001). The authors therefore propose that V4 is more involved with visual processing and that attentional control is handled by higher cortical areas such as LIP and the FEF.

1.3.1.4 Attentional modulation of rate variability and of correlated spiking activity

Attention does not just modulate the firing rate of cells, but also the variability of their firing. In V4, the variability as measured by the Fano factor (FF) is reduced by attention to the RFs of the recorded cells (Mitchell *et al.*, 2007). This modulation was stronger in narrow spiking cells than in broad spiking cells, showing that there may be cell-type specific roles of the visual cortex in attention. Similar reductions of rate variability with attention have been reported for area V1 (Herrero *et al.*, 2013) and area MT (Niebergall *et al.*, 2011), even though neither of these studies assessed cell-type specificity. Surprisingly, attention did not reduce the FF of FEF neurons (Chang *et al.*, 2012), an area which is assumed to be one of the main sources of attentional signals (see above).

In addition, attention affects neuronal co-variability, often assessed by calculation of noise correlations (Cohen and Maunsell, 2009; Mitchell *et al.*, 2009; Herrero *et al.*, 2013). When attention was directed over the RFs of pairs of recorded neurons in V4 (or in V1) their noise correlations were reduced. Cohen and Maunsell (2009) showed that the modulation of noise correlations contributed more to the discriminability of subpopulations of cells than firing rate modulations did, showing that attention cannot be explained through single cell effects alone, but that it also alters the structure of the population code (Harris and Thiele, 2011), thereby presumably improving decoding abilities.

The aforementioned noise correlation alterations were reported for pairs of neurons with similarly tuned neurons. In contrast, when pairs of dissimilarly tuned neurons were considered, noise correlations were increased by attention (Ruff and Cohen, 2014), which could equally improve the performance of a decoder (Shadlen *et al.*, 1996; Abbott and Dayan, 1999; Ecker *et al.*, 2011). Regardless of whether noise correlations increased or decreased with attention in these studies, spike rate modulations were only increased by attention. This shows that effects in noise correlations cannot just be a consequence of spike rate modulations.

How can noise correlations be decreased, when information flow between cells (at least in different compartments/areas) should be enhanced by attention? This question was addressed in a study using combined Utah array grid recordings in V1 and single shank electrode recordings in area MT. When noise correlations were calculated between pairs of neurons in different areas, attention increased noise

correlations (Ruff and Cohen, 2016), provided that cells had overlapping RFs. The authors suggest that attention increases communication between the areas and that this is why the spike count correlations are increased. In support of this hypothesis, they showed that microstimulating V1 was more likely to affect responses in MT when attention was directed over the RF of the recorded neurons.

1.3.1.5 Attentional modulation of synchronous and of oscillatory activity

The role of oscillatory activity in sensory processing has been discussed for a long time, and various hypotheses have been proposed and often falsified. One of the early suggestions was that synchronous activity was used to achieve perceptual binding (Singer, 1999), but the most rigorous studies in task performing animals failed to support this (Thiele and Stoner, 2003; Roelfsema *et al.*, 2004). More recently, oscillatory activity was discussed in relation to cognition, whereby it enables "communication through coherence" (Fries, 2005). Specifically, it predicts that coherence between ensembles representing the attended object should be enhanced, particularly in the gamma frequency band. A seminal study investigating the effects of attention on oscillatory synchronisation in V4 was conducted by Fries *et al.* (2001). When attention was directed into the RF of V4 the spike field coherence (SFC) increased within the gamma (35-90Hz) frequency range but it decreased in the low frequency (<17Hz) range. The coherence was measured between pairs of electrodes separated by 650µm or 900µm so the effects occurred between different cortical columns. This means that the observed coherence effects could be attributed either to horizontal synchronisation within V4 or a shared synchronisation with an external source residing higher or lower in the visual stream.

Laminar differences in SFC modulation by attention have been investigated to some extent in V1, V2 and V4 (Buffalo *et al.*, 2011). Using single contact electrodes, the authors aimed to place these either into superficial or deep layers of areas V1, V2, and V4. In the superficial layers of V2 and V4 attention increased SFC in a gamma (40-60Hz) frequency range, however in the deep layers the prominent effect was a reduction in field-field coherence (FFC) at low frequencies (6-16Hz). For area V1 the effects in superficial layers were inconsistent between monkeys (an increase in SFC in the gamma range in one monkey but no significant changes in the other monkey), and no significant changes were seen in the lower layers for either gamma band

frequencies, or low SFC frequencies (6-16 Hz). The authors also investigated the laminar role of LFP power, firing rate and noise correlations but did not observe any significant layer dependent effects in the recorded areas. A potential caveat of these experiments was that they were performed using single channel electrodes so cortical layer could only be categorised as “deep” or “shallow” based on penetration depth, and only a globally referenced LFP was available, which could be contaminated by sources outside of the layers of interest.

Previous studies have also explored how attention modulates synchronisation between visual areas (Buschman and Miller, 2007; Gregoriou *et al.*, 2009; Bosman *et al.*, 2012). Bosman *et al.* (2012) recorded activity from multiple V1 and V4 locations using electrocorticography (ECoG) in macaques. Two stimuli were placed so that they were within a single V4 ECoG RF, whereby each stimulus covered one of the two V1 ECoG receptive fields (i.e. each V1 ECoG electrode represented an independent visual location (RF) which was covered by a single stimulus each). The monkeys had to switch attention between the two stimuli on alternating trials. Attention caused an increase in V1-V4 field coherence of the V1 RF that represented the attended stimulus, but not between V1 and V4 for the V1 RF that represented the unattended stimulus. This phenomenon was also observed when an additional irrelevant stimulus was placed over the V1 RF whilst the animal attended away from that location, meaning that the lack of V1-V4 coherence cannot be attributed to the stimulus not driving the V1 cells. Using Granger causality, they showed that this increase in gamma coherence was also accompanied by an increase in information flow from V1 to V4, suggesting that direction of this gamma band attention effect is from V1 to V4. These measures were taken with ECoG and they were thus not able to reveal whether these results were layer specific, or which layers were predominantly responsible for the interactions.

The synchronisation between visual cortex and higher cortical areas has also been studied. Gregoriou *et al.* (2009) used the same attention task described in Section 2.2.4 to test how attention modulates spike-field coherence (SFC) and field-field coherence (FFC) within areas V4 and within the FEF, as well as between V4 and the FEF. Attention increased coherence in the gamma (30-70Hz) frequency range both within and between these two areas. By analysing the phase and Granger causality of the oscillatory signals, they showed that attentional modulation in the FEF

occurred sooner than in V4 and therefore appears to initiate the coherence, which is consistent with a top down triggering of coherence by the FEF. After this initiation of the coherent activity, Granger causality from V4 to the FEF became stronger than from the FEF to V4, suggesting that bottom-up mechanisms came into play following the initial instigation by the FEF. In a further study (Gregoriou *et al.*, 2012), they separated the recorded FEF cells into visual, visuomovement and movement cells. This separation showed that the attentional modulation occurs predominantly in the visual and visuomovement cells, less so in movement cells.

1.3.1.6 Consistency of V1 attentional modulation in previous studies

Overall, previously studies have shown that attention consistently increases V1 and V4 firing rates. Early studies did not find changes in V1 firing rates with attention (Moran and Desimone, 1985; Luck *et al.*, 1997), however this was likely due to the low attentional demand of the tasks which were used.

The decrease of variability in spiking activity by attention was consistent across previous studies (Smith and Kohn, 2008; Cohen and Maunsell, 2009; Mitchell *et al.*, 2009; Herrero *et al.*, 2013; Smith *et al.*, 2013; Ruff and Cohen, 2016). The exception to this were two studies which demonstrated cases where noise correlations were increased by attention (Ruff and Cohen, 2014; Ruff and Cohen, 2016). However these studies both used a task which did not have the same “attend away” condition that other studies typically use (for further discussion on this see Section 6.1.4). Rather, they aimed to determine whether neurons with opposite tuning show increases in noise correlation, while same tuning neurons show decreases, which is what they indeed found.

Previous studies have largely agreed on the effects of attention on V4 oscillations, with attention increasing the power of gamma oscillations (Gregoriou *et al.*, 2009) and decreasing that of low frequency oscillations (Fries *et al.*, 2001; Buffalo *et al.*, 2011). This agreement does not extend to V1, where several differing effects have been reported. The domain in which the effects of attention varied most between previous V1 studies was gamma power. Both increases (Buffalo *et al.*, 2011; Bosman *et al.*, 2012) and decreases (Chalk *et al.*, 2010) in LFP gamma power with attention have been reported.

1.3.2 Higher cortical contributions to attention

Some of the previous descriptions have already delineated some of the areas that are likely to control the focus of attention. One area mentioned repeatedly was the FEF. The critical role of the FEF for spatial attention has been demonstrated in a microstimulation study by Moore and Fallah (2004). When regions of the FEF representing a stimulus location were microstimulated prior to a luminance change, monkeys were able to detect smaller changes (i.e. sensitivity was increased). This supports the idea that the FEF is a cortical centre for spatial attention. Moreover, when the FEF was microstimulated using subthreshold currents (i.e. no saccades were elicited) V4 neurons with matching receptive fields responded more strongly to visual stimuli, while monkeys simply passively fixated (Armstrong and Moore, 2007). Thus, microstimulation of the FEF induced feedback effects in area V4 that replicate the effects of spatial attention.

In addition to the modulation of the FEF activity, several other higher cortical areas have been implicated in attention in the primate. The lateral intraparietal cortex (LIP) is a subdivision of the macaque posterior parietal cortex (PPC). Activity in this area is modulated during spatial attention tasks (Bushnell *et al.*, 1981; Herrington and Assad, 2009), but is also affected by other spatial modalities such as spatial working memory (Pesaran *et al.*, 2002).

By recording simultaneously from the PPC and the prefrontal cortex (PFC) during both a bottom-up and top-down attention task, Buschman and Miller (2007) showed the flow of attention in higher cortical areas. When the top-down task was used the PFC was modulated by attention earliest, whereas in the bottom-up task the PPC was modulated first. This marks the PFC as being a higher area for attentional processing than the PPC. In addition, the coherence between the two areas differed depending on the task which was used. Low frequency coherence was highest in the top-down, but high frequency coherence was strongest in the bottom-up task. This highlights that top-down and bottom-up attentional processing may be mediated by these different frequency bands.

Bichot *et al.* (2015) used a feature based and spatial based attention task to try to elucidate which region provides the source of attention in these attentional domains.

Recordings were made in the FEF, the IT cortex, the ventral prearcuate (VPA) region of the prefrontal cortex and the ventral bank of the principle sulcus (VPS). In the feature based task attentional modulation occurred earliest in the VPA whereas a spatial attention effect occurred first in the FEF. Inactivating the VPA also caused the effects of feature attention in the FEF to diminish, however spatial attention effects were preserved. This once again highlights the importance of the FEF in spatial attention.

1.3.3 Subcortical contributions to attention

Although originally studied as a cortical mechanism, attention affects subcortical brain structures. Functional magnetic resonance imaging (fMRI) in human subjects showed that attention modulates responses as early in the visual stream as the LGN (O'Connor *et al.*, 2002). As with cortical studies, the effect was an increase in blood oxygenation level dependent (BOLD) activity with attention, based on which they argued that the LGN is acting either as a bottom-up controlling mechanism for attentional response gain or showing modulation due to top-down corticothalamic feedback. In more recent work by McAlonan *et al.* (2008), an attentional effect was demonstrated in the firing rate of cells in macaque LGN. This study also discovered that there were two separable effects occurring at an early and late stage of processing, again suggesting that the LGN may play a role in both bottom-up and top-down attention. Briggs *et al.* (2013) stimulated the LGN whilst recording from V1 cells receiving LGN input, whilst a monkey performed an attention task and showed that attention increased the likelihood of LGN activity influencing V1 activity. This demonstrates that either the input gain to V1 is altered by attention, or that the LGN signal reaching V1 is increased.

The superior colliculus (SC) has also been shown to play an important role in attention (Zénon and Krauzlis, 2012). In this study, the SC was inactivated whilst a monkey performed an attention task. Although the monkey had several behavioural deficits in the task, the enhancement in firing rates and rate variability of visual cortical neurons were unaffected. This shows that multiple circuits contribute to attention and attention dependent behaviours and that it cannot be explained solely by visual cortical activity.

One such subcortical circuit would include the pulvinar. Zhou *et al.* (2016) recorded simultaneously from macaque ventro-lateral pulvinar, V4 and inferior temporal (IT) cortex. Attending to a stimulus in the receptive fields (RFs) of the recorded pulvinar neurons increased their firing rates, but the attentional modulation had a longer latency than in V4 cells. This in addition to analysis of gamma phase shifts showed that V4 appears to initiate an attention modulated pulvinocortical loop between the areas. Granger causality analysis showed a causal attentional modulation of gamma oscillations from V4 to the pulvinar and IT. Deactivation of the pulvinar with injection of muscimol caused a behavioural deficit only for targets placed within the RFs of cells the injected region. Attentional modulation of pulvinar spike rates and SFC within V4 and between V4 and IT was also diminished by the injection. All of these results taken together suggest that a pulvinocortical loop is vital in the propagation of bottom-up attention to the higher cortices, but it suggests that the aforementioned effects seen after SC inactivation must yet rely on a circuit separate to the pulvinar, i.e. the pulvinar is not a main source of top-down attention.

1.4 Study aims

Based on the previous work discussed throughout Chapter 1, we separated the aims of our study into three broad questions. In the sections below, each of these questions will be stated and then several hypotheses for each put forward based on the existing literature.

1.4.1 How does attention affect spiking activity in the different cortical layers and cell types of V1 and V4?

A common finding in previous literature is that firing rates of cells in both V1 and V4 are increased by attention in their RF (Moran and Desimone, 1985; Motter, 1993; Luck *et al.*, 1997; Treue and Maunsell, 1999; McAdams and Reid, 2005; Roberts *et al.*, 2007; Herrero *et al.*, 2008), therefore we would expect to see this effect in our study. Based on a recent study performed in the FEF (Thiele *et al.*, 2016), we would expect higher firing rates in narrow-spiking cells. We would also expect to see a reduction in gain variance with attention in line with this study, and stronger effects occurring in the narrow-spiking cells. We would also expect variability as measured by the Fano factor to be reduced by attention in both areas (Mitchell *et al.*, 2007; Niebergall *et al.*, 2011; Herrero *et al.*, 2013).

Within cortical areas, we would expect noise correlations to be reduced by attention, in line with previous results (Cohen and Maunsell, 2009; Mitchell *et al.*, 2009). Since these studies did not target a specific layer and so likely recorded from different layers, we would expect that noise correlations between different layers of the same cortical area would also be decreased by attention. Although it showed an increase in noise correlations with attention between cortical areas, the study from Ruff and Cohen (2016) used multiple stimuli placed within the same RF, so we cannot predict whether noise correlations between areas will be modulated in the same way when stimuli do not occupy the same RF.

1.4.2 Does attention cause changes in the size and frequency of oscillations in V1 and V4 and are these changes specific to certain layers?

In both V1 an V4, we would expect to see a decrease in the power of low frequency theta/alpha oscillations, as has been reported in several other studies (Gieselmann and Thiele, 2008; Chalk *et al.*, 2010; Ray and Maunsell, 2010; Bosman *et al.*, 2012; Herrero *et al.*, 2013; Van Kerkoerle *et al.*, 2014).

Although an increase in the power of gamma oscillations with attention has been widely reported (Fries *et al.*, 2001; Gregoriou *et al.*, 2009; Buffalo *et al.*, 2011), studies in V1 have found either no modulation of power with attention (Bosman *et al.*, 2012) or a reduction in the power of gamma oscillations in V1 (Chalk *et al.*, 2010)

An increase in the peak frequency of gamma oscillations with attention has been reported with attention (Bosman *et al.*, 2012). Given that it is also proposed that attention increases the coherence of oscillations between areas by modulating their peak frequency (Fries, 2005; Saalmann *et al.*, 2012), we would also expect to see a change in peak frequency with attention.

1.4.3 What is the laminar “circuit” for information flow within and between V1 and V4 and how is this affected by attention?

Currently several studies support the idea that gamma oscillations represent a feedforward mechanism whereas low frequency alpha/beta oscillations are feedback (Bosman *et al.*, 2012; Van Kerkoerle *et al.*, 2014; Bastos *et al.*, 2015). Therefore we would also expect this pattern of feedforward and feedback information flow to be present in our experiments.

This idea can also be extended to consider the different layers through which information might flow. Given the canonical microcircuit (Douglas and Martin, 2004), the main input from V1 to V4 is from the V1 supragranular layers to the V4 supragranular layers. Therefore it is expected to see feedforward information flow in the gamma band moving between these layers. Projections from V4 to V1 are from the infragranular layers to layers outside of the V1 granular layers (Rockland and

Pandya, 1979), so we would expect to see low frequency feedback information flow between these layers.

Chapter 2: Methods

This chapter outlines the techniques which we used to investigate the aims set out in Section 1.4. Broadly speaking, I will describe how we recorded from areas V1 and V4 during a task of covert spatial attention as well as describing the methods used to analyse this data.

2.1 Animal subjects

We used two adult (both aged 9 years at the recording start) male rhesus macaques (macaca mulatta) for our experiments, which will be referred to as Monkey 1 and Monkey 2 in the remainder of this work. After initial chair and task training, the monkeys were implanted with a head holder and recording chambers above V1 and V4 in both hemispheres, under general anaesthesia (for details see Thiele *et al.* (2006)). All experimental animal procedures complied with the European Union Directive 2010 (2010 63 EU), the National Institutes of Health (Guidelines for Care and Use of Animals for Experimental Procedures), the Society for Neurosciences Policies on the Use of Animals and Humans in Neuroscience Research, and the UK Animals Scientific Procedures Act.

2.2 Behavioural methods

2.2.1 Training setup

The monkeys were trained to sit comfortably in the lab within purpose-built Plexiglas primate chairs, with their head held in place via the previously implanted head holder. The chair contained a touch bar which could be used in behavioural tasks. Additionally, it had a reward tube attached, through which the monkey were given a fluid of their liking upon correct task performance.

During experiments the monkeys were seated in the primate chair and placed inside a faraday cage in the laboratory. In front of the chair was a cathode ray tube (CRT) monitor, with 55cm between the monkey's eyes and the centre of the screen. The

CRT monitors used in the experiments were the Iiyama HM204DTA 22” monitor with a resolution of 1024 by 768, driven at a frame rate of 120Hz for Monkey 1 and recordings in the left hemisphere of Monkey 2 and 100Hz for recordings in the right hemisphere of Monkey 2.

Behavioural tasks were generated and controlled by the CORTEX software package (National Institute of Mental Health, USA). CORTEX allows behavioural tasks to be written in a modular fashion, whereby an individual trial is designed and then repeated for different task conditions.

Eye positions were measured using a ViewPoint EyeTracker system (Arrington Research, USA), which recorded the gaze location of the right eye using a 220 Hz monocular camera. The eye positions were then converted into a voltage between -5 and 5V and then acquired by the CORTEX hardware board. These were used to decode the current eye position into 2D screen positions (based on the eye calibration described below), used to monitor task performance and saved for post-hoc analysis.

2.2.2 Eye calibration task

Since the tasks used in the experiment required fixation by the monkey throughout each trial, the eye tracking system had to be calibrated (Figure 2-1). The task used to achieve this first required the monkey to hold onto a touch bar inside the primate chair. The monkey was then presented with a stimulus (0.1 or 0.2 degree of visual angle [DVA]) and required to hold the touch bar for 500ms to 2000ms. The monkey was cued to release the touch bar when the stimulus changed contrast, receiving a reward of a fluid of their liking, if they released the touch bar within 80ms and 500ms of the contrast change. The change in contrast was set close to the monkey’s just noticeable difference (JND), which required the monkey to fixate on the stimulus to detect the change. By repeating the task for each of the positions shown in Figure 2-1 we were able to accurately calibrate the eye tracking system on a daily basis (before commencing the main experiments).

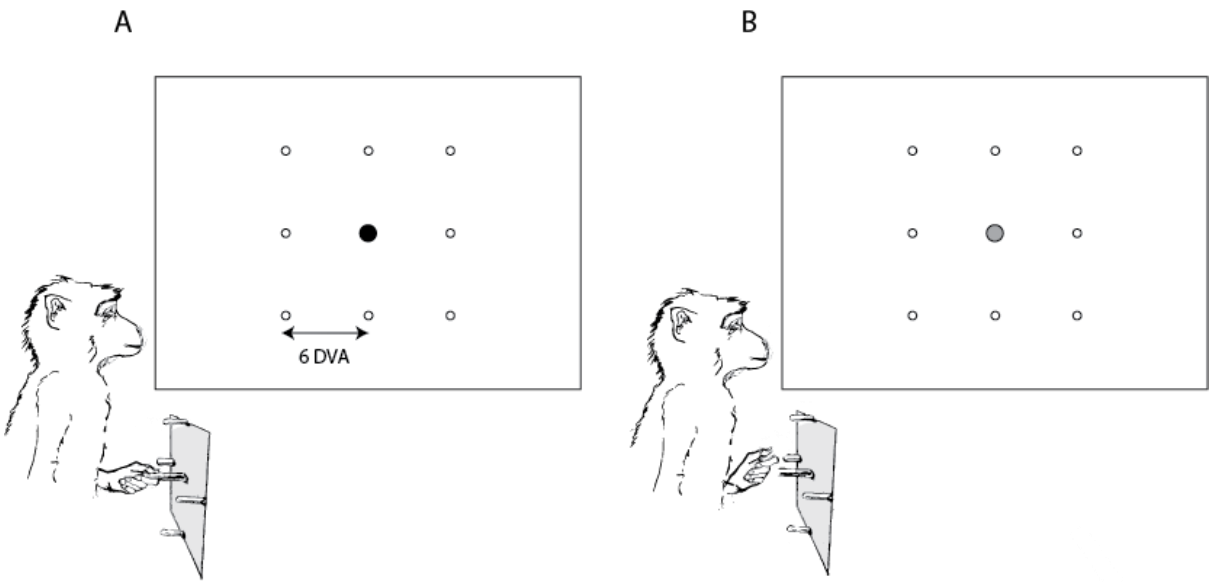

Figure 2-1: The eye calibration behavioural task. ***A***: The task is initiated by the monkey holding on to a touch bar. A black stimulus is presented, in this case centrally. Small white dots show the other stimulus locations used for calibration. ***B***: Upon a contrast change in the stimulus the monkey must release the touch bar to receive a reward.

2.2.3 Receptive field mapping task

Once electrodes had been lowered into the target areas and allowed to settle, the receptive fields (RFs) of cells were mapped. Before the attention task commenced, the approximate location of the receptive fields were estimated by the researcher. The task for RF mapping required fixation throughout the trial within 2 DVA of a central fixation spot of 0.5 DVA diameter. A stimulus was then presented at pseudorandom positions centred on an estimated RF location. The grid size for possible stimulus positions was 12 by 9, scaled so that each grid location was equal to the stimulus size and sampled such that each stimulus was presented an equal number of times. Initially the RF mapping was performed with a 2 DVA stimulus, however smaller stimuli (1 DVA, 0.5 DVA and 0.25 DVA) were used subsequently if a more detailed mapping of the RF was required, in particular for V1 recordings, where the RF size was relatively small.

The RF map was calculated by counting the number of spikes which occurred within 50ms and 130ms after each stimulus presentation for each trial. Then, by averaging these for each stimulus location, a two dimensional distribution of spiking activity was

obtained. Offline, the RFs were also calculated based on the envelope multiunit activity ($MUA_{E)}$, by taking the average rectified and filtered voltage signal occurring (for additional details regarding MUA_E analysis see Section 0) between 50ms and 130ms after each stimulus presentation.

2.2.4 Covert visuospatial attention task

In order to probe the effects of attention on neural activity, we employed a covert cued visuospatial attention task (Gregoriou *et al.*, 2009). For the remainder of this thesis, this task will be referred to as the attention task.

The task was initiated by the monkey by holding the touch bar within the primate chair (Figure 2-3A). A fixation spot of 0.1 DVA diameter was presented at the centre of the screen (Background colour: RGB = [45,45,45], Luminance = 0.8 cd/m^2, XY = [0.25,0.38]). Fixation was required to remain within 2 DVA of the fixation spot throughout the remainder of each trial. After an initial period of fixation (410ms in Monkey 1, 600ms in Monkey 2, for summary of timings in the task see Figure 2-2) three differently coloured moving gratings (colour values are given in Table 1) were presented in the periphery, with one stimulus always placed to cover the RFs of the recorded neurons. The remaining two stimuli were then placed so that the three stimuli were equidistant around an invisible circle centred on the fixation spot. The radius of the stimuli for a recording session typically varied between 1 and 3 DVA, depending on the sizes and locations of the RFs recorded. The spatial frequency of stimuli was 1.5 cycle/DVA and temporal frequency was 1 cycle/s (Note: Given the square wave nature of the stimulus, it did not really have a distinct spatial and temporal frequency in Fourier space, and the term ‘duty cycle’ would be more appropriate. However, due to the widely used convention of using spatial and temporal frequency even for square wave gratings, I will also use the terms). The orientation of the gratings was 30º for all recordings.

Table 1: Stimulus colours in the attention task. RGB values, luminance and XY coordinates in the CIE 1931 colour space are given for the undimmed and dimmed versions of the stimuli for each monkey.

	Red	Green	Blue
Monkey 1 and Monkey 2 (left)	RGB: [220, 0, 0] Luminance: 10.3 cd/m^2 XY: [0.54, 0.42]	RGB: [0, 135, 0] Luminance: 10.3 cd/m^2 XY: [0.24, 0.64]	RGB: [60, 60, 255] Luminance: 9.1 cd/m^2 XY: [0.15, 0.08]
Monkey 1 (dimmed)	RGB: [140, 0, 0] Luminance: 3.5 cd/m^2 XY: [0.54, 0.42]	RGB: [0, 90, 0] Luminance: 3.7 cd/m^2 XY: [0.23, 0.65]	RGB: [30, 30, 180] Luminance: 3.5 cd/m^2 XY = [0.14, 0.07]
Monkey 2 (right)	RGB: [255, 0, 0] Luminance: 14.5 cd/m^2 XY: [0.55, 0.41]	RGB: [0, 128, 0] Luminance: 9.1 cd/m^2 XY: [0.23, 0.65]	RGB: [60, 60, 255] Luminance: 11.5 cd/m^2 XY = [0.14, 0.07]
Monkey 2 (right, dimmed)	RGB: [100, 0, 0] Luminance: 1.4 cd/m^2 XY: [0.54, 0.43]	RGB: [0, 70, 0] Luminance: 1.9 cd/m^2 XY: [0.23, 0.64]	RGB: [10, 10, 190] Luminance: 3.7 cd/m^2 XY: [0.14, 0.07]
Monkey 2 (left, dimmed)	RGB: [180, 0, 0] Luminance: 6.3 cd/m^2 XY: [0.55, 0.42]	RGB: [0, 110, 0] Luminance: 6.1 cd/m^2 XY: [0.23, 0.65]	RGB: [40, 40, 220] Luminance: 5.8 cd/m^2 XY: [0.14, 0.08]

Following stimulus presentation, a central cue with the same colour as one of the stimuli was presented, indicating to the monkey which of the three stimuli was behaviourally relevant on that trial. The cue was presented at a random time in a window of 630-960ms after stimulus onset in Monkey 1, 630-1110ms in the right hemisphere of Monkey 2 and 620-1130ms for recordings in the left hemisphere of Monkey 2. Once the cue had been presented, the stimuli could dim in a pseudorandom order with a random dimming time between each dimming. These random dimming times could occur between 1160-1820ms after cue onset, and identical time windows again relative to the times of the first and second dimming in Monkey 1. For Monkey 2 these times differed somewhat. They were between 630-1250ms for recordings in the right hemisphere of Monkey 2 and 1160-2100ms in the left hemisphere of Monkey 2. When the cued stimulus (the target) had dimmed, the monkey was required to release the touch bar to receive a fluid reward if the trial was completed correctly.

The task above thus had three different cue colour conditions and six order of dimming conditions. In addition the stimulus could move in one of two possible

directions. This gave a total number of 36 conditions. Trials in CORTEX were grouped into blocks of 36, so that they each contained exactly one of each of these variations. The ordering of trials within a block was randomised by CORTEX so that the monkey could not learn patterns in the trial conditions. If a trial was performed incorrectly then it was reinserted ('repeat on error') into the block at a random location, meaning that the next block was only started once each condition had been performed correctly. This meant that on repeated errors, the last trial could be predictable in terms of cue colour and in terms of dimming location in the dimming series.

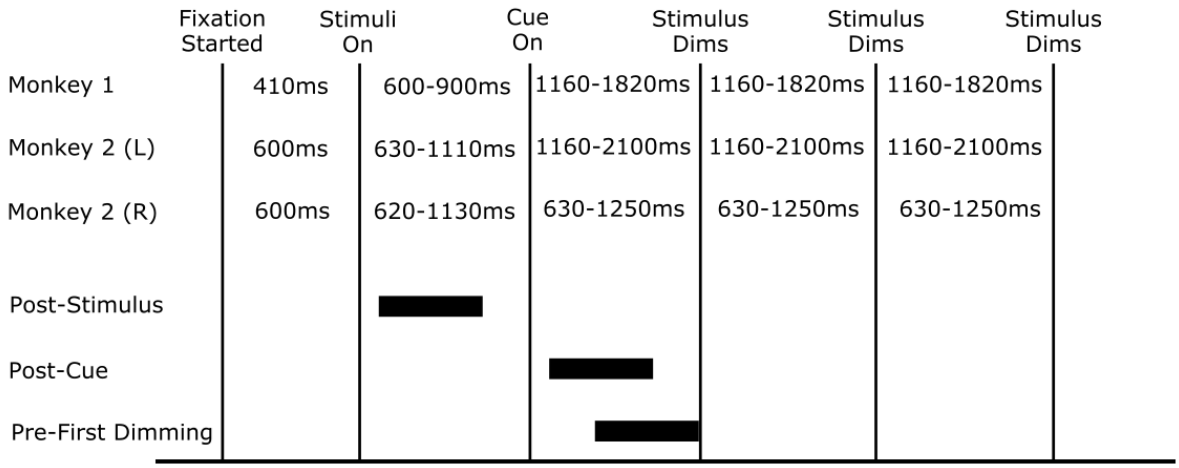

Figure 2-2: Timings between events in the attention task. Vertical lines represent task events, with the time between these given for Monkey 1 and both hemispheres of Monkey 2. The combination of events shown here occurs when the behaviourally relevant dimming in the task is the third dimming. Black rectangles give an indication of the timing of the three main analysis windows used throughout analysis. The post-stimulus and post-cue windows begin a fixed time after the event (i.e. "stimuli on" and "cue on"), whereas the end of the pre-first dimming window always occurs at the time of the first "stimulus dims" event.

Given that we performed our analysis of attention effects before the first dimming of the task, the only information which the monkey could use to predict the relevant dimming was the colour of the cue. This in combination with the monkey performing the task correctly allowed us to infer that the monkey directed its attention to the cued stimulus. A similar task has also been used in another study investigating visuospatial attention (Gregoriou *et al.*, 2009), which gives us further confidence. The

cued stimulus in our task was always the behaviourally relevant one, i.e. we had no catch trials. We cannot therefore completely rule out that the animal did not distribute attention using psychophysical data. However, the unambiguous firing rate modulations make this very unlikely.

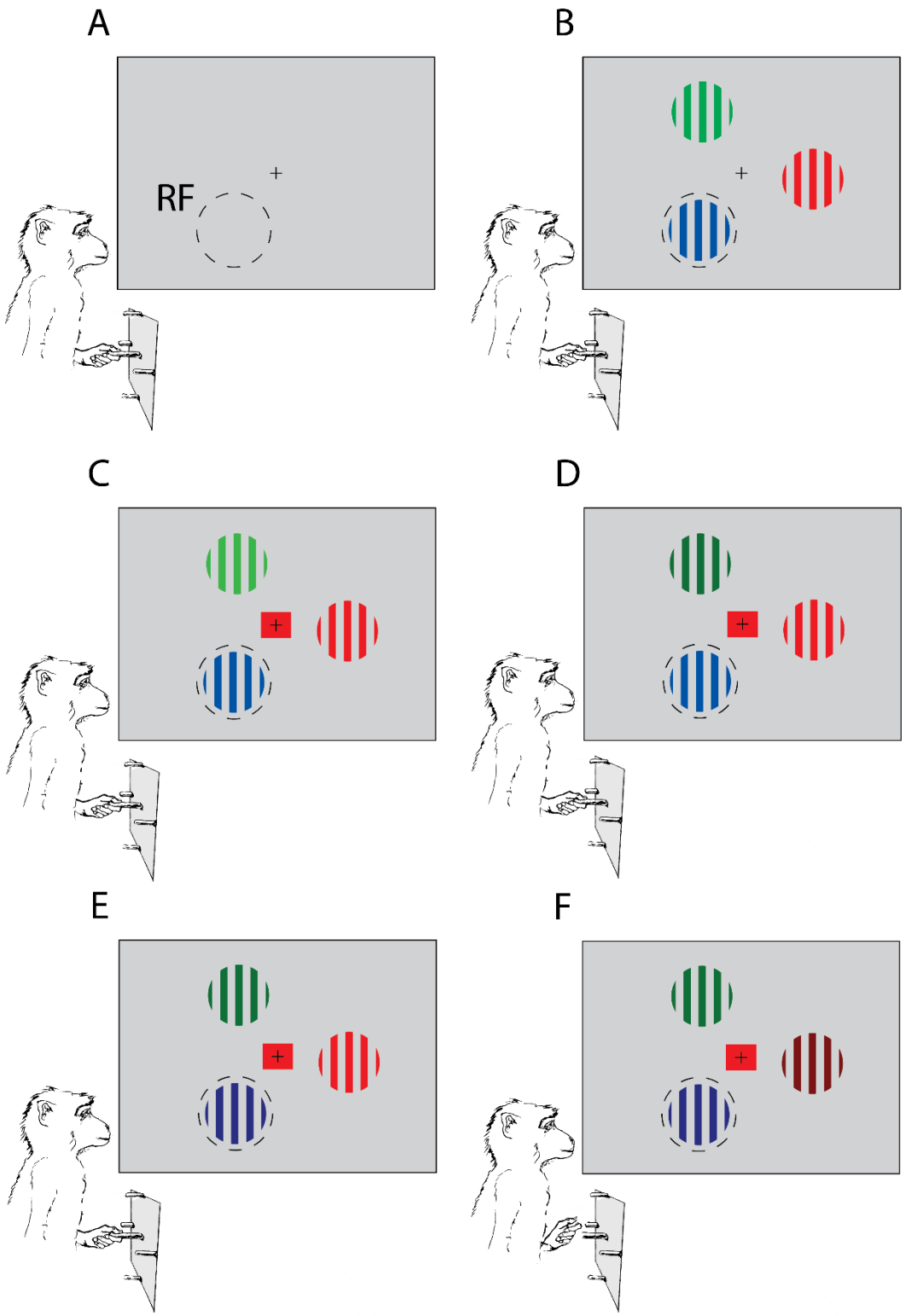

Figure 2-3: The covert visuospatial attention task. ***A***: The monkey holds a lever and fixates centrally. ***B***: Three moving grating stimuli are presented, with one always covering the RF of the recorded neurons. ***C***: A cue is presented centrally, with the colour indicating where to direct attention. ***D-F***: When the cued stimulus dims, the monkey releases the touch bar and receives a reward for a correct trial.

2.3 Electrophysiology methods

2.3.1 Data acquisition

Whilst the monkey performed the task we recorded simultaneously from neurons in V1 and V4 using extracellular electrophysiological recording techniques. Recordings were performed with three different types of 16 channel laminar electrodes. The majority of recordings were performed using 16 channel floating passive probes (ATLAS Neuroengineering, Belgium) with intercontact spacing of 150µm (E16-150-S1-L8 and E16-150-S1-L10). In addition to these, some recordings were taken using rigid passive 16 channel probes (ATLAS Neuroengineering, Belgium) with intercontact spacings of 250µm (E16-250-S1-L8) and some recordings were taken using 16 channel Plexon V-probes with intercontact spacings of 150µm. The impedances of electrodes were measured (at 1kHz) on a daily basis to identify any channels which may yield poor quality signal; electrodes were replaced if this was the case.

Table 2: Number of recordings taken with each electrode type in each monkey. Rows state the electrode type and columns the monkey and area recorded from with totals in each area given in the bottom row.

	Monkey 1 V1	Monkey 1 V4	Monkey 2 Right V1	Monkey 2 Right V4	Monkey 2 Left V4	Monkey 2 Left V4
E16-150-S1-L8	-	-	36	5		
E16-150-S1-L10	31	35	-	-	14	14
E16-250-S1-L8	-	-	-	24		
Plexon V-probe	-	-	-	2		
Total	**31**	**35**	**36**	**31**	**14**	**14**

Electrodes were mounted daily on the implanted chambers using custom made electrode holders and inserted using MO-97A Oil Hydraulic Micromanipulator (NARISHIGE, Japan). The electrodes were both referenced and grounded to a wire placed within one of the chambers (filled with saline) being recorded from. The reference was placed in the V1 chamber if possible (as this allowed the easiest access), otherwise it was placed in the V4 chamber or failing this in another chamber.

Data were acquired using a 32-channel Digital Lynx acquisition system and Cheetah 5.6.3 software (Neuralynx, USA). Electrodes were connected to the acquisition system via a preamplifier (HS36, Neuralynx, USA). The raw signal for each channel was recorded at 32556Hz (referred to as 32kHz subsequently) and digitised at a resolution of 24 bits.

2.4 Off-line analysis

The majority of analysis was performed using scripts written in Matlab 2014a (MathWorks, USA) and Matlab 2015a (MathWorks, USA). In addition, some analysis was written in C++, in particular in cases where run-time efficiency was important (e.g. handling large raw data files). The remainder of analysis was performed using third party purpose-written software, which will be detailed within the sections where it was used.

2.4.1 Data preprocessing

Raw data were post-processed after the recording sessions. In the process, the signal was multiplexed into a high frequency component filtered between 600Hz and 9kHz, stored at 32 kHz, and a low frequency component filtered between 1Hz and 300Hz which was downsampled to 1017Hz (referred to as 1kHz subsequently). Spiking activity was extracted from the high frequency 32kHz signal by thresholding above a specified value and then extracting a spike waveform of 32 samples (i.e. ~ 1ms length) for each threshold crossing, with the threshold crossing value aligned to the 8^{th} sample in the waveform. To avoid multiple occurrences of the same spike, a minimum interspike interval of 0.5ms was enforced. Envelope multiunit activity (MUA_E, Supèr and Roelfsema (2004)) was extracted from the high frequency 32kHz signal by full wave rectifying the signal, low-pass filtering at 200Hz (Butterworth 10^{th} order) and then downsampling to 1kHz.

Spikes were extracted from the high frequency 32kHz signal by setting a threshold and then extracting waveforms around the peak threshold crossing. Cells were sorted with SpikeSort3D (Neuralynx, USA), whereby each sorted cluster was assigned a semi subjective quality label. These were: 1 = absolute single unit (based on feature clustering and interspike interval histogram analysis); 2 = single unit, with good confidence in overall waveform accuracy (based on waveform selection and interspike interval histogram); 3 = decent multiunit activity (no confidence in accuracy of waveform validity, i.e. assignment to broad or narrow spiking cells, but overall quality of spikes was better than traditional ‘hash’ classification); 4 = hash (pure low threshold amplitude cut-off). All analyses pertaining to different cell types are

exclusively based on cells with quality label of at least ‘2’ or better. Recordings with spiking classification of 4 were disregarded (never used) for the spiking analysis.

All sorted clusters were then checked for stationarity by looking at the feature distribution (spike energy) over time of the recording, and by looking at the raster plots, time locked to different trial events (stimulus onset, cue onset, time of first dimming) over time. If these inspections suggested that reasonable stationarity was present (i.e. no obvious drifts [or abrupt changes] of activity levels), the sorting was accepted for further analysis (irrespective of the classification mentioned above). Cells were sorted continuously, i.e. cells recorded in V1 and V4 were sorted as recorded, with the consequence that they were sorted intermixed, without regard to their areal identity, reducing the likelihood that differences in cell classes between areas were due to biases.

Spike waveform analysis was done as described in Thiele *et al.* (2016). Recording depths assignment was based on the alignment of recording electrodes relative to the current source density signal (for additional details see Section 2.4.5). A modified Hartigan’s dip test (Ardid *et al.*, 2015; Thiele *et al.*, 2016) was used to calculate whether the distributions of peak to trough distance of the spike waveforms was unimodal (Null hypothesis). The distribution of spike peak to trough times for areas V1 and V4 is shown in Figure 2-4. We used a cut-off of 250µs for the classification of broad and narrow cells, since this was where the main “dip” in the distribution occurred. We also tested a cut-off of 200ms, as this was the next closest “dip” in the distribution. However this did not alter the cell-specific effects which we observed in the later analyses (see Section 3.2.1 and Section 4.2.1).

During spike sorting we observed occasionally that cells sorted from adjacent contacts appeared identical (e.g. waveform, PSTH shape and height, attentional modulation). It was important to only include each cell once in our analyses, otherwise the repetition could spuriously inflate the effects which we observed. We eliminated these repetitions from the analysis by calculating the noise correlations of all neighbouring contacts and only including a single channel if the correlation was below 0.5 (see Section 2.4.11).

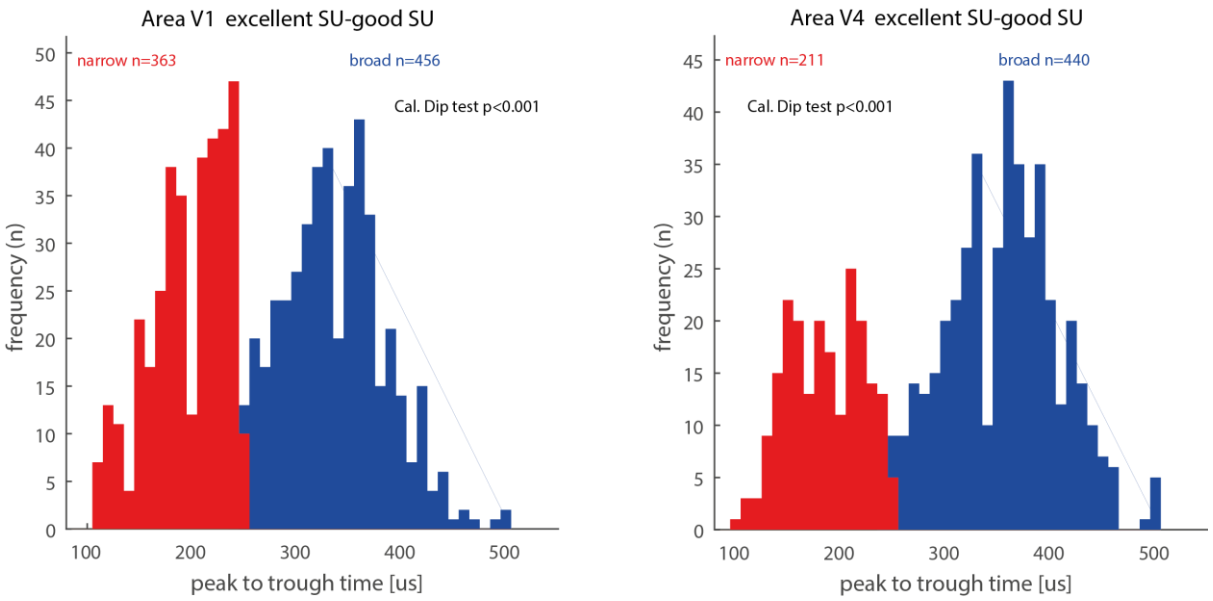

Figure 2-4: Distribution of peak to trough times in V1 and V4 cells from both monkeys. Distributions of peak to trough times were significantly non-uniform (Hartigan's modified dip test (Cal. Dip test), p<0.001 for both areas). Based on the distribution dips a cut-off of 250 µs was chosen to separate narrow (red) and broad (blue) spiking cells. Number of cells in the two classes are indicated at the top of the subplots (n). Selection was based on a sorting quality assessment of 2 (see main text for details of this quality assignment).

2.4.2 Realigning signals

In order to investigate effects in response to different task epochs in the attention task, the signals were separated into individual trials and then realigned with respect to the corresponding trial events of interest. The three task periods used for alignment were the (A) stimulus onset, (B) cue onset and (C) the time of first dimming of the stimuli.

2.4.3 Visually evoked responses

To measure the response of a continuously sampled channel to an event, the realigned signal was averaged across all of the trials in a recording. We calculated the evoked responses for both the LFP and MUA_E by first subtracting the mean signal in the period 200ms before the stimulus onset from each trial's signal. Since this epoch is at the end of the initial fixation period and not affected by direct visual

stimulation, it provides a baseline against which to compare activity from the remainder of the trial.

For each channel we then calculated an average LFP/MUA_E across all trials. These channel averages could then be averaged across channels/recordings. Before averaging the MUA_E response across channels/recordings, the average signal for each channel was normalised relative to the maximum response that occurred during any task period.

Since recordings were obtained using laminar electrodes of fixed intercontact spacing, it was not always feasible to record from the targeted cortical region on all channels, as some contacts will have been outside the tissue of interest due to the overall electrode length of 15*150µm (or in some cases 15*250µm). In addition it was not possible to optimise signal quality across all channels. This required a metric to assess the quality of a recording, allowing channels with poor signal quality to be excluded from further analysis. We used the signal to noise ratio (SNR, Equation 1), which gives a metric for how many standard deviations ($\sigma(noise)$) a signal ($\mu(signal)$) lies outside of the mean ($\mu(noise)$). The mean and standard deviation of the visually evoked MUA_E response were taken in the period 100ms prior to stimulus onset in the attention task and used as the $noise$ portion of this equation. The $signal$ in the equation was calculated by moving a 100ms sliding window and moving it between 40ms and 150ms after stimulus onset in 1ms steps and then taking the window with the maximum mean response. This means that the SNR gives a measure of the transient response to the stimuli. For a channel to be included in further analysis, it was required to have a SNR of at least +/- 3 (-3 for cells/clusters inhibited by the stimulus). We found that, after applying this inclusion criteria, we did not need to do further exclusion of channels based on the overlap between RF and stimulus. Those channels which had no overlap between their RF and the stimulus placement also had an SNR of less than 3.

$$SNR = \frac{\mu(signal) - \mu(noise)}{\sigma(noise)}$$

Equation 1: Signal to noise ratio

2.4.4 Trial sub-selection

To identify periods of stable activity (stationarity) during our recording sessions we plotted the energy of spike waveforms across the whole recording session for all channels (Figure 2-5). Any movement of the electrode (which can be induced by either slow drifts following electrode insertion, or sudden movement of the animal) could result in a change of electrode contact location. Such changes usually alter the spike waveforms or amplitudes recorded from a channel. Plotting the energy of all thresholded spikes across time, simultaneously across all channels allows detection of such events that occur in all channels simultaneously. These transition periods could then be identified by visual inspection, and periods of stable activity could be selected manually by applying adequate time boundaries for analysis. Only trials within these periods were included in further analysis. In addition to discrete changes in the electrode's position, there were also cases where the signal could be seen to change slowly throughout a recording, consistent with a slow drift of the electrode depth. In these cases, trial ranges were chosen such that the total amount of drift was minimised (by visual inspection). All trial sub-selection was performed blind to later analyses, thus avoiding any bias of results.

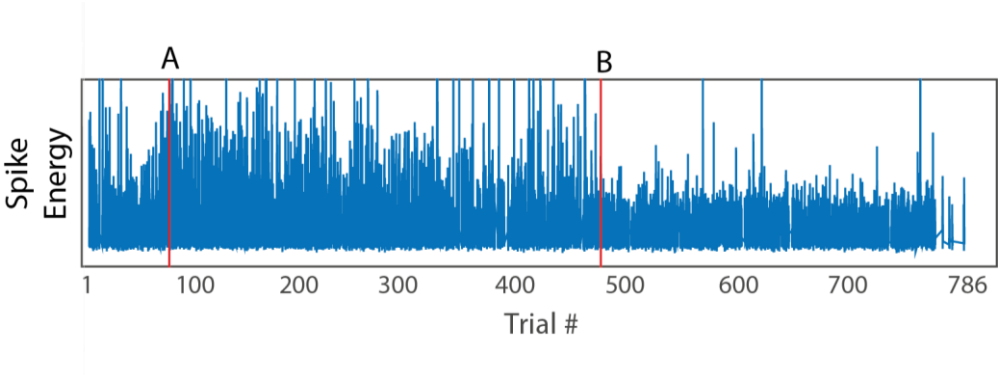

Figure 2-5: The effects of electrode drift on the energy of multi-unit spike waveforms (i.e. multiple cells) for a single channel. **A-B**: Gradual decrease in spike energy with time, consistent with a slow drift of position. **B**: Sharp change in spike waveform energy, consistent with sudden change of position. **B onwards**: Stable level of spike waveform energy, consistent with a stable electrode position.

2.4.5 Current source density analysis

We used current source density (CSD) to determine where currents entered and exited cortical cells (tissue) during the attention task (following stimulus onset). By comparing the observed patterns of current sinks and sources with the known anatomy of the cortex, inferences about the recording depth relative to different cortical layers can be made (Schroeder *et al.*, 1991). CSD can be calculated by taking the inverse of the second spatial derivative of the visually evoked potential (VEP, *φ(x)*). This is most often calculated using the finite difference approximation (Equation 2).

$$CSD(x) = \frac{2 \cdot \varphi(x) - \varphi(x + n * h) - \varphi(x - n * h)}{h^2}$$

Equation 2: Current source density finite difference method

Here, the equation is applied over the length of a laminar electrode (*x*), with the inter-electrode spacing taken as the step size (*h*). The distance between reference and recording channel was then given by *n*h* and for our analysis we used the adjacent channels (*n*=1 in Equation 2) to calculate CSD, since this meant referencing with the spatial locations closest to a given channel.

To calculate the CSD profiles in our data we used the iCSD toolbox (Pettersen *et al.*, 2006), which in addition to the above approximation for CSD, also allows calculation using a spline fitting method. This produces similar results to the traditional finite difference method, but has the advantage of being able to exclude channels from the calculation. Channel exclusion might be necessary if post experiment impedance assessment indicated that a specific contact might have been faulty. For calculation of the CSD using the toolbox's spline fitting method, we estimated tissue conductance as 0.3 Sm^{-1} (Pettersen *et al.*, 2006) and the diameter of cortical columns as 500µm (Mountcastle, 1957). Tissue conductance affected the magnitude of CSD values equally for all channels so did not affect the underlying CSD profile. We generated CSD profiles using the VEP aligned to the stimulus onset in the attention task.

2.4.6 LFP power spectra

We generated power spectra of the LFP (using the bipolar signal) for each recorded channel with sufficient SNR. For each trial in the attention task we analysed a 511ms time window (i.e. 512 data points) aligned to the stimulus onset (250-761ms), cue onset (50-561ms) and first stimulus dimming (-511-0ms). Trials in which this window overlapped with the next relevant event (e.g. trial in which cue onset was <761ms after stimulus onset) were excluded from the analysis. The activity in these windows was taken and a fast Fourier transform (FFT) was applied to determine the spectral power in different frequency bands. These single trial power spectra were then averaged across trials to give a mean single power spectrum (+/- S.E.M) for that channel.

In addition to the FFT approach, we also used the multitaper method implemented in the Chronux toolbox (Mitra and Bokil, 2007), which allows analysis of frequency bands with non-stationary peak frequencies (Mitra and Pesaran, 1999), and which performs some smoothing in the frequency domain. We used tapers with a time-half-bandwidth product of a bandwidth of 2 for this analysis, which translates to three tapers of half-bandwidth ~4Hz when using 511ms sampled at 1 kHz.

Since LFP spectra typically show a *1/f* distribution (Bedard *et al.*, 2006), it can be difficult to observe the magnitude of attention effects occurring in different (especially higher) frequency bands. We thus used a z-score to compare spectra obtained during the presence of the stimuli to those in the pre-stimulus period. Similar to the SNR, the z-score (Equation 3) is a metric for how many standard deviations (σ) a single value (x) lies above or below the mean value (μ). For each trial, the power spectra (x) were normalised to the prestimulus power spectra for all trials (μ and σ), i.e. normalisation was done separately for each frequency. Using the z-score in this way gave a measure of task/stimulus evoked spectral power.

$$z = \frac{x - \mu}{\sigma}$$

Equation 3: Z-score

2.4.7 Coherence

Interactions between different channels were measured by means of field-field coherence using the same time windows as described for the power spectrum analysis above. Coherence was calculated using the Chronux toolbox (Mitra and Bokil, 2007), again using a multitaper approach with taper bandwidth of 4Hz. This toolbox calculates the coherence based on the spectrograms of the individual channels (*S1* and *S2*) and the cross spectrogram (*S12*). The coherence (*C*) is then calculated as C = (S12^2) / (S1 * S2). We calculated coherence between channels in different layers of V1, different layers of V4, as well as the coherence of channels between different layers of V1 and of V4. Note, that coherence was calculated based on all trials, i.e. not based on single trial averages (i.e. in the code the parameter 'trialparam.ave' in Chronux was set to 1). In addition to absolute coherence at each frequency, the Chronux toolbox also gives the phase difference between the two signals at each frequency.

2.4.8 Local re-referencing

To avoid common (global) signals affecting our LFP analysis, (which would be seen on all channels due to volume conductance effects) we re-referenced our LFP signal. We used the bipolar derivation (*B(x)*, Equation 4) to locally re-reference the signal on each contact ($\varphi(x)$) to the difference between its neighbours. Using the bipolar signal to re-reference has been shown to be superior to using CSD, since the latter can inflate the noise in a signal (Trongnetrpunya *et al.*, 2015).

$$B(x) = \varphi(x + h) - \varphi(x - h)$$

Equation 4: The bipolar derivation. For description of variables see CSD paragraph (Section 2.4.5).

2.4.9 Granger causality

To measure the directionality of information flow between different channels we used Granger causality using the multivariate Granger causality (MVGC) toolbox (Barnett and Seth, 2014). We calculated Granger causality of the LFP downsampled to 254.25Hz between channels in different layers of V1, of V4 and also the Granger

causality of channels between V1 and V4. We used a model order of 10 for the multivariate regression in the toolbox. Significance of differences between Granger causal interactions for the different directions (e.g. from infragranular layer to supragranular layer in a given frequency band was calculated by using FDR corrected signed rank tests for each frequency (based on paired values for each electrode contact combination). Attentional modulation of Granger causal influences was calculated in a similar manner, but instead of taking directionality into account, we compared attend RF vs. attend away conditions (FDR corrected Wilcoxon signed rank test).

To analyse the dominant flow of information in local networks, we calculated the directional modulation index (MI) of Granger causality in each direction ($GC_{1\rightarrow2}$ and $GC_{2\rightarrow1}$) for each channel pair (Equation 5). We then represented the directional MI between each pair using an arrow, with the magnitude of the MI shown by the arrow colour. We calculated these MIs for the theta/alpha (4-12Hz), beta (13-25Hz), low gamma (30-50Hz) and high gamma (55-100Hz) frequency bands

Equation 5: Granger causal directional modulation index

$$directional\ MI_{1-2} = \frac{GC_{1\rightarrow2} - GC_{2\rightarrow1}}{GC_{1\rightarrow2} + GC_{2\rightarrow1}}$$

We also performed an equivalent analysis to show how attention affected the flow of information between channels. For each channel pair, we calculated a MI (Equation 6) of Granger causality in each attention condition ($GC_{1\rightarrow2}(in)$ and $GC_{1\rightarrow2}(out)$) in the first dimming aligned task period. Note, that the difference here is that this was done for a fixed directionality, but different attention conditions, while the previous MI was for a fixed attention condition, but different directionality. Again, we calculated these MIs for the theta/alpha (4-12Hz), beta (13-25Hz), low gamma (30-50Hz) and high gamma (55-100Hz) frequency bands

Equation 6: Granger causal attentional modulation index

$$attentional\ MI_{1\to2} = \frac{GC_{1\to2}(in) - GC_{1\to2}(out)}{GC_{1\to2}(in) + GC_{1\to2}(out)}$$

2.4.10 Cross correlations

To provide confidence in the direction of information flow which was suggested by the Granger causality analysis, cross correlations within and between V1 and V4 were also calculated. Cross correlations were calculated by following the method described by Adhikari et al. (2010). Briefly, a Hilbert transform was applied to the LFP signal and the absolute value of the result was taken, giving an instantaneous amplitude of the LFP. A cross correlation was calculated between instantaneous amplitudes of different channels, using 1ms lags between -0.1s and 0.1s. The lag with the peak cross correlation was taken for each trial and then averaged across a recording session to give a mean lag for a recording channel pair. To visualise the distribution of lags between layers, channels were grouped into layers and histograms plotted for each layer combination.

2.4.11 Noise correlations

Noise correlations measure the shared variability of spike rates between the different layers and areas we recorded from. Noise correlations were calculated using a Spearman's rank correlation coefficient (Spearman, 1904) of single trial firing rates in the stimulus, cue and first dimming aligned periods of the attention task (using the same time windows as in Section 2.4.6). A correlation coefficient of +1 represents a total positive correlation, a value of 0 means no correlation and a value of -1 represents a total negative correlation.

To avoid artificially inflated noise correlations, these were calculated separately for the two stimulus motion directions and then averaged for each attention condition. We also calculated the noise correlation separately for each attend away condition before averaging these together.

Another potential for spurious noise correlation results could be drift of firing rate over the session. If the firing rates of two channels changes over the course of the session at a roughly equal rate then this would cause a large noise correlation. We avoided

this influence by calculating a correlation coefficient for each individual channel and rejected a channel from the analysis if more than half of the conditions showed a correlation significantly different from 0 ($p < 0.001$).

2.4.12 Area under the receiver operator characteristic

Area under the receiver operator characteristic (AUROC) values were calculated as described in Thiele *et al.* (2016). They provide a measure of how well an ideal observer can determine where the monkey attends to on a single trial basis. A value of 0.5 indicates that the ideal observer can only perform at chance level while values of 1 (or 0) indicate that the ideal observer can predict the locus of attention with 100% accuracy.

2.4.13 Variability

To quantify variability of neuronal responses, we used both Fano factors and gain variance. The Fano factor (FF, Equation 7) calculates variance as the ratio between variance (σ^2) and mean (μ) spike counts in the time window of interest.

Equation 7: The Fano factor

$$FF = \frac{\sigma^2}{\mu}$$

Gain variance provides a method of quantifying variability of neuronal responses which has been proposed to better capture non linearities between the mean rate and the rate variance compared to the Fano factor (Thiele *et al.*, 2016). Gain variance was calculated as described in Thiele *et al.* (2016). Fitting a negative binomial distribution to single trial rate gives a gain variance term, which we calculated for each condition in the attention task.

2.4.14 Layer dependence of the signals of interest

To analyse layer dependency of attentional modulation of firing rates, spectral power, coherence etc., we first needed an estimate of the location of each channel relative to the cortical surface. Based on previous literature (Schroeder *et al.*, 1991) we

determined the first sink of the CSD analysis occurring after stimulus onset. This usually had a latency of 40ms and 50ms in our V1 data (e.g. Figure 2-6). Since it is well known that the early thalamic input mostly terminates in V1 layer 4Cα (Schroeder *et al.*, 1991), we used this first sink as the alignment point for our V1 recordings, and assigned it as being located in layer 4Cα. This alignment point has been used in several previous studies (Schroeder *et al.*, 1991; Givre *et al.*, 1994), however the boundary between infragranular and granular layers has also been used for alignment, which can be seen as a source/sink boundary below the early sink (Van Kerkoerle *et al.*, 2014). We found the early sink to be the most reliable feature to align to in our recordings. Based on the well described architecture of V1 (Lund, 1987; Lund *et al.*, 1988; Lund and Yoshioka, 1991; Lund and Wu, 1997), channels less than 250µm away from the first sink were treated as having been located in the granular layers, those 250-1000µm above were considered supragranular layers and those 250-700µm below as the infragranular layers.

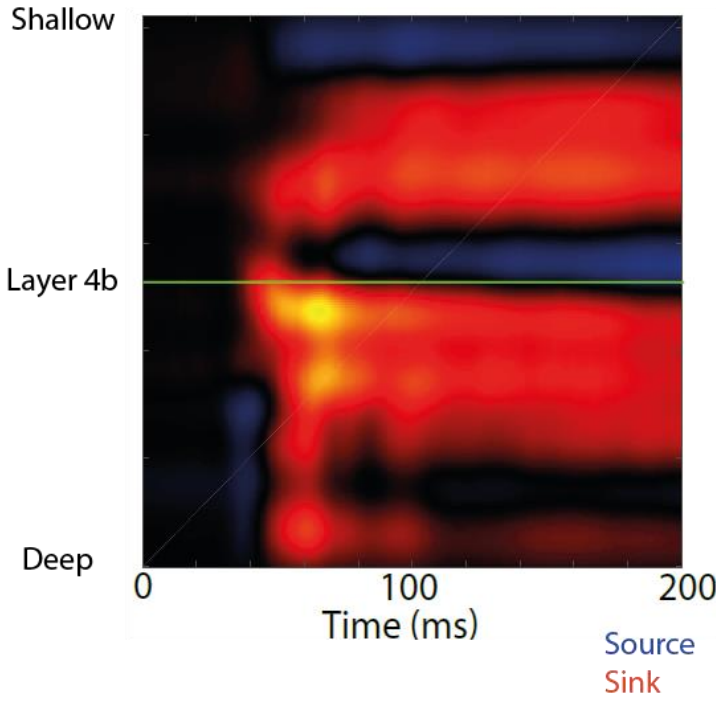

Figure 2-6: Example current source density profile. Current sinks are shown in red, current sources are shown in blue. The proposed location of layer 4cα aligned with the earliest current sink is plotted in green.

V4 has also been shown to receive granular input from the thalamus but it also receives input from other lower visual areas (Gattass *et al.*, 2014). Layer 4 in V4 only

has a width of 200µm, i.e. the V4 granular layers are narrower than those in V1 (Hof and Morrison, 1995). Therefore, a 150µm intercontact spacing of our electrodes often only had one channel located in granular V4, while with a 250µm intercontact spacing in some cases none of the contacts may have been located in layer 4 of V4. This meant that the early sink was not always as unambiguously identifiable as in V1 recordings. However, we were still able to align these recordings by comparing their overall CSD profile to those of recordings where we could be more certain of the alignment channel.

2.4.15 Attentional modulation

For the purpose of measuring the effects of attention, activity in the two 'attend away from the RF' conditions were grouped together. These conditions were given the label "attend away" condition and compared against the single condition where attention was directed to a location covered by the neuron's receptive fields.

A modulation index (Equation 8) was used as a metric for the strength of attentional modulation in the various signals. This compared the activity during trials where attention was directed into the cell's receptive field (*In*) against the activity in trials where it is was directed outside of the receptive field (*Out*). The value attained is bounded between -1 and 1, with 0 representing no attentional modulation, positive values representing an increase in activity with attention and negative values representing a decrease.

$$attMI = \frac{In - Out}{In + Out}$$

Equation 8: Attentional modulation index

We also calculated a cue response modulation index (Equation 9) of the activity when attention was directed into the cell's RF (*In*) against the average precue activity (*Precue*). As with the attentional modulation index, a positive value indicated an increase vs. precue activity, zero indicated no change and a negative value meant that activity was reduced after the cue onset. We also calculated this modulation index with respect to the attend away condition (Replace *In* for *Out* in Equation 9).

$$CueResponse(In) = \frac{In - Precue}{In + Precue}$$

Equation 9: Cue response modulation index

2.4.16 Statistical testing

To determine whether there were significant differences between the MUA_E activity for different depths and attention conditions we used one way analysis of variance (ANOVA). To determine whether the observed differences between the attention conditions in the LFP and noise correlation analyses were statistically significant, Wilcoxon signed rank tests were used.

In the population spiking analysis we used linear mixed effects (or mixed model) ANOVAs to test whether there were any effects of cell-type, task period, attention condition and cortical area/layer. These factors were defined as fixed effects. Since firing rates could randomly vary between cells, we included ‘rate’ as a random effect. If significant differences were found for the parameter of interest, we used paired t-tests to test which conditions were significantly different from each other.

Multiple comparison corrections were done using the false discovery rate (FDR) (Benjamini and Yekutieli, 2001).

Chapter 3: Results: Attentional Modulation of Neuronal Activity in the Striate Cortex

Striate cortex, also known as V1, is the gateway into the primate visual cortex. This chapter will report the main findings of how spatial attention affects the neuronal activity and communication in V1.

3.1 Multiunit activity effects of attention

The following section describes the spiking activity of different V1 layers during different epochs of the attention task and how it is modulated by attention. I will start by describing the MUA_E activity, as this is the most basic (large scale) spiking activity available, which gives an impression what V1 as a population does as a whole, while it ignores the details that are present in different cell and response types.

3.1.1 Stimulus aligned multiunit response

The stimulus response of recorded cells was obtained by aligning the signal of interest (extracted/sorted spikes or envelope multiunit activity (MUA_E)) to the onset of the stimuli in the attention task. Figure 3-1 shows the stimulus aligned response of the MUA_E signal in Monkey 1, averaged across recordings by aligning channels to the estimated location of layer 4cα. There was no attentional modulation at this stage of the task (as expected), since the cue had not yet been presented and there was therefore no information about where the monkey must attend to. The stimulus onset triggered a sharp transient response (40ms to 150ms) which was followed by a sustained response whilst the stimuli continued to be presented. The largest sustained responses occurred in the channels further from the alignment channel. This was quantified by taking the ratio of the mean response between 250ms and 500ms and the peak response for each channel. Using this metric we found that the alignment channel had the smallest sustained response (One way ANOVA, Monkey

1: $p<0.05$ against all but the next superficial channel, Monkey 2 (right): $p<0.05$ against all but the next two superficial channels and the next deeper channel). The sustained response increased with increasing distance from the alignment channel.

Recordings from the right hemisphere of Monkey 2 (Figure 3-2) showed a stimulus response and laminar profile pattern that was the largely the same as in Monkey 1, however there was an additional regular response component in the sustained stimulus aligned response in the MUA_E data. This was induced by additional (originally unintended) temporal structure in the stimulus motion characteristics used for these experiments. To put simply, the stimulus motion had additional regular 'jerky' components, and these elicited additional stimulus aligned responses in the V1 MUA_E population activity (further details are given in Appendix A). These stimuli/experiments will be referred to as 'jerky stimuli'/'jerky experiments' in the remainder of the thesis. The jerky stimuli also appeared to affect certain characteristics of the attentional modulation of the LFP power in V1, which will be described in detail later. We therefore performed addition control experiments with recordings in the left hemisphere of Monkey 2 (Figure 3-2), where we used the same stimuli which were used in recordings from Monkey 1, in addition to using the jerky stimuli. Since the stimulus in these control experiments were non-jerky, there was no persistent rhythmic component in the stimulus aligned response.

By grouping channels into supragranular, granular and infragranular cortical layers, the differences in stimulus response could be seen more clearly. In both Monkey 1 and Monkey 2 (Figure 3-2), sustained spiking activity in the granular layers was smallest relative to that in the transient period and the strongest sustained response was in the supragranular layers. Comparing the ratio of the sustained response and the peak response revealed that these differences were significant for the grouped data in each of the two monkeys (One way ANOVA, $p < 0.05$ for all pairwise comparisons in each monkey, as well as when grouped together).

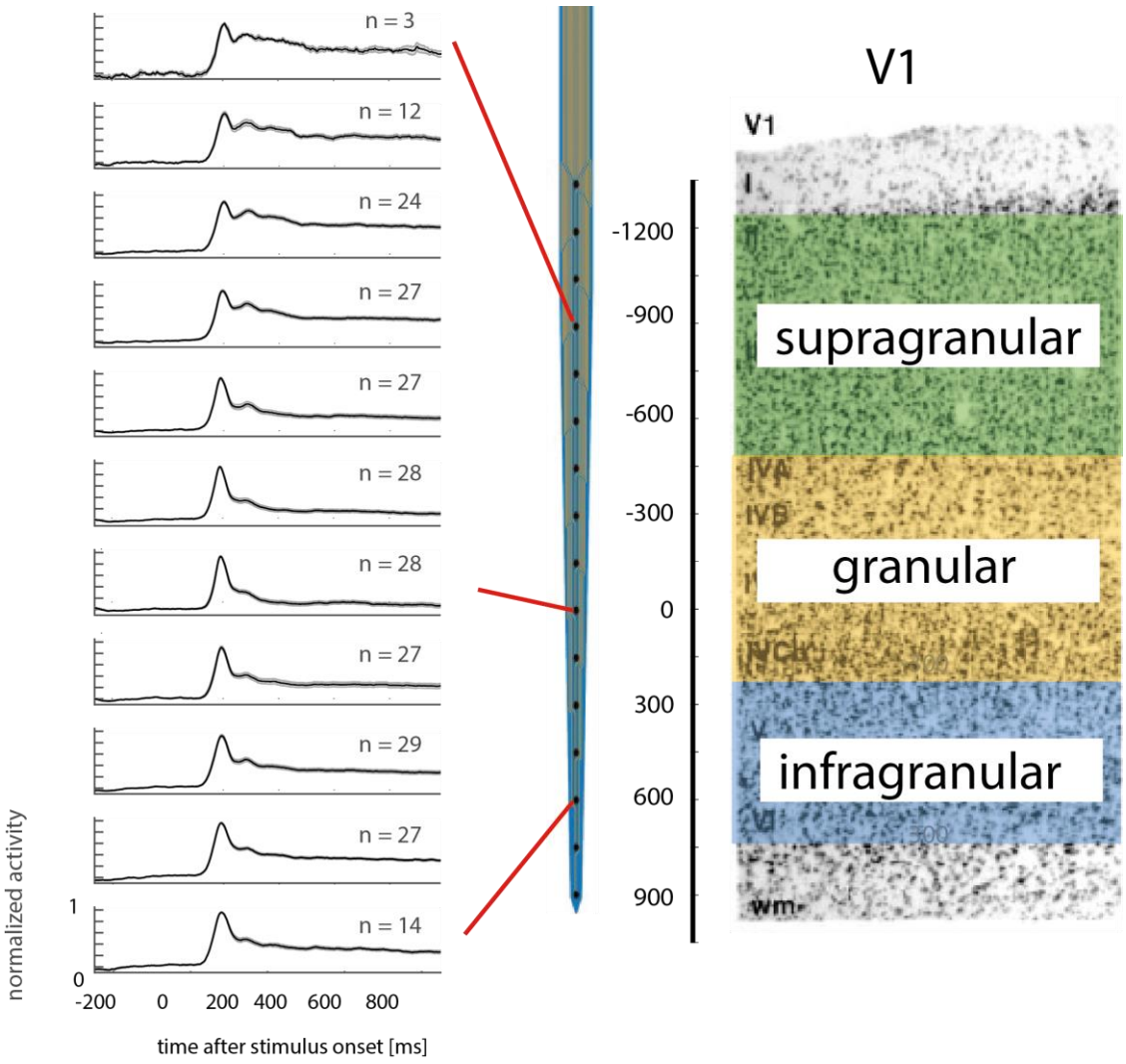

Figure 3-1- ***Left***: Monkey 1 average V1 normalised envelope multiunit activity (MUA_E) aligned to stimulus onset and spatially aligned to the layer 4cα channel (n = number of recordings in each plot). ***Centre***: Sketch of an example electrode, showing how the average MUA_E plots align with actual electrode depths. ***Right***: Illustration of V1 architecture, split into supragranular, granular and infragranular cortical layers based on distance (μm) from layer 4cα (Adapted from Stepanyants *et al.* (2002)). Solid lines show mean activity, grey shaded areas S.E.M. (often too small to be discernible).

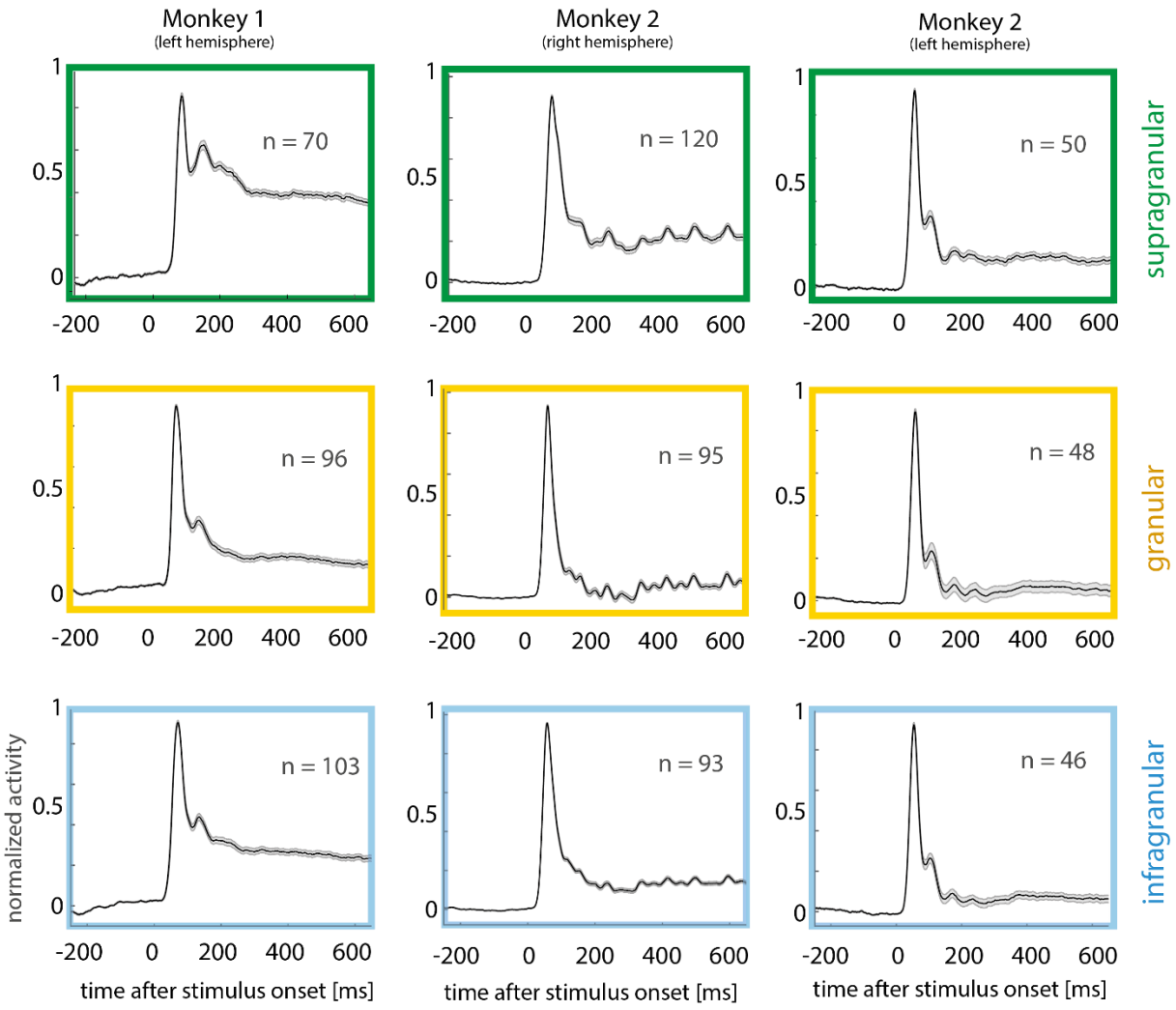

Figure 3-2 - Monkey 1 and Monkey 2 (right and left hemisphere) average V1 envelope multiunit activity (MUA_E) aligned to stimulus onset and grouped into supragranular (top, green), granular (middle, yellow) and infragranular (bottom, blue) layers (n = number of contacts in each plot). Stimuli used in the left hemispheres of Monkey 1 and Monkey 2 were moving smoothly, while those used in the right hemisphere of Monkey 2 had additional temporal structure to their motion (jerky, non-smooth). V1 structure is as defined in Figure 3-1. Solid lines show mean activity, grey shaded areas S.E.M. (often too small to be discernible).

3.1.2 Cue aligned multiunit response

Once the cue was presented in the attention task the monkey had information about where to direct attention, therefore aligning the MUA_E signal to the onset of the cue allowed the effect of attention to be probed. In both monkeys there was an initial dip in the MUA_E activity, which may have been due to the cue being presented in the suppressive surround of the RF. Alternatively it could be a change that occurs with the shifting of attention, or some other cognitive operation performed, which affects

the ongoing stimulus induced activity. MUA_E activity in both monkeys (Figure 3-3) showed a difference between attention conditions shortly after the cue had been presented, with the largest modulation occurring in the supragranular layers and smallest in the granular layers.

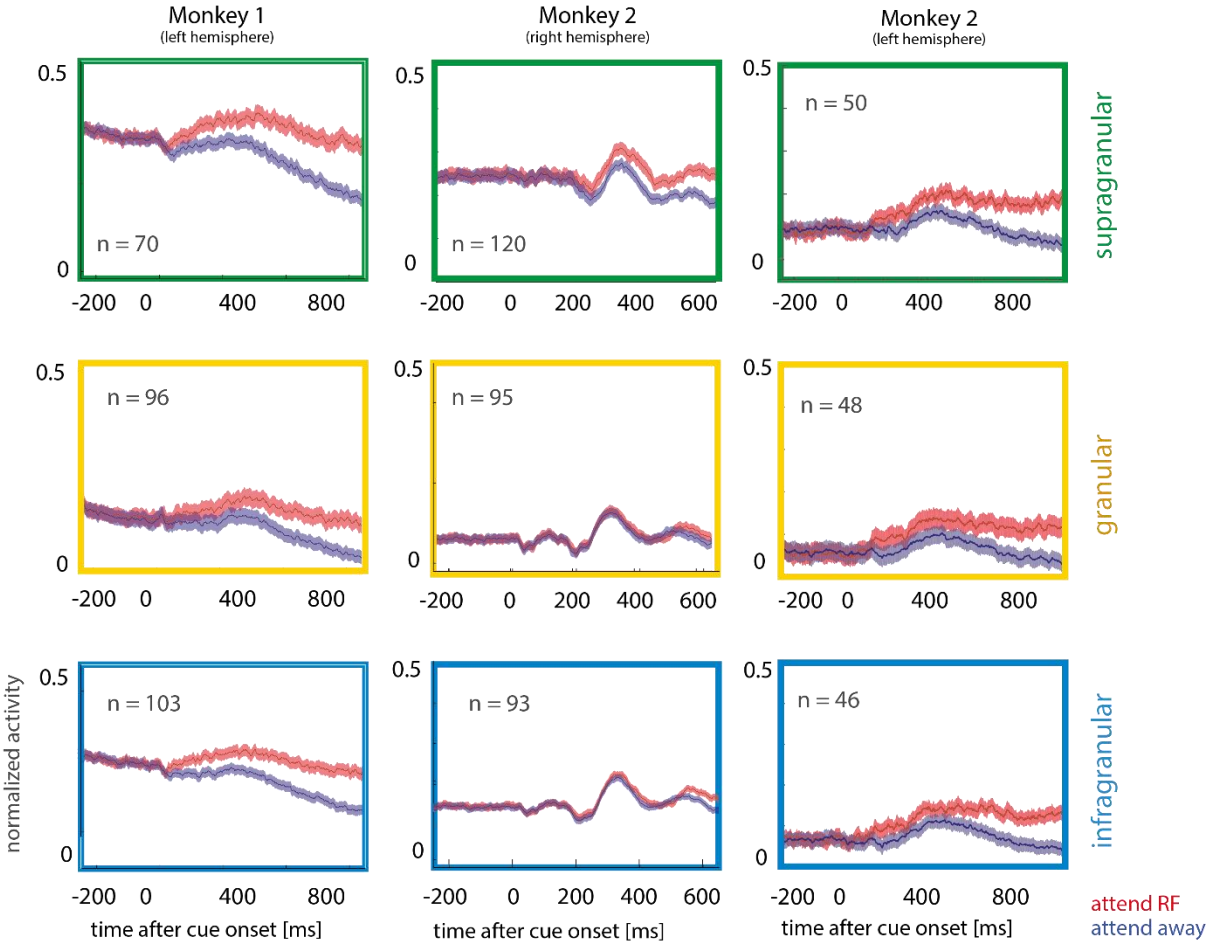

Figure 3-3 - Monkey 1 and Monkey 2 (right and left hemisphere) average V1 envelope multiunit activity (MUA_E) aligned to cue onset and grouped into supragranular (top, green), granular (middle, yellow) and infragranular (bottom, blue) layers (n = number of contacts in each plot). Plotted separately for the "attend RF" (red) and "attend away" conditions. V1 structure is as defined in Figure 3-1. Solid lines show mean activity, shaded areas S.E.M.

3.1.3 Dimming aligned multiunit response

Aligning the activity to the first dimming of the task allowed the attentional modulation of the MUA_E response to be seen more clearly, since the attentional modulation increased with time and was therefore maximal just before a dimming occurred

(Figure 3-4). As with the cue response, the attentional modulation was largest in the supragranular layers. There was also a positive deflection in the signal after the first dimming occurred. When only trials where the first dimming occurred inside the RF were analysed this effect was more pronounced for the two conditions in the same hemifield as the RF (Figure 3-5, left). Conversely, when only trials where the first dimming occurred in a location outside of the RF were analysed the deflection was only present for the attend away condition in the opposite hemifield to the RF (Figure 3-5, right), and downwards for the two conditions in the same hemifield as the RF. This shows that the deflection is mainly a response to a dimming occurring in the same hemifield as the RF of the recorded cells. This pattern of deflections was present in both monkeys so their data was averaged together for this analysis.

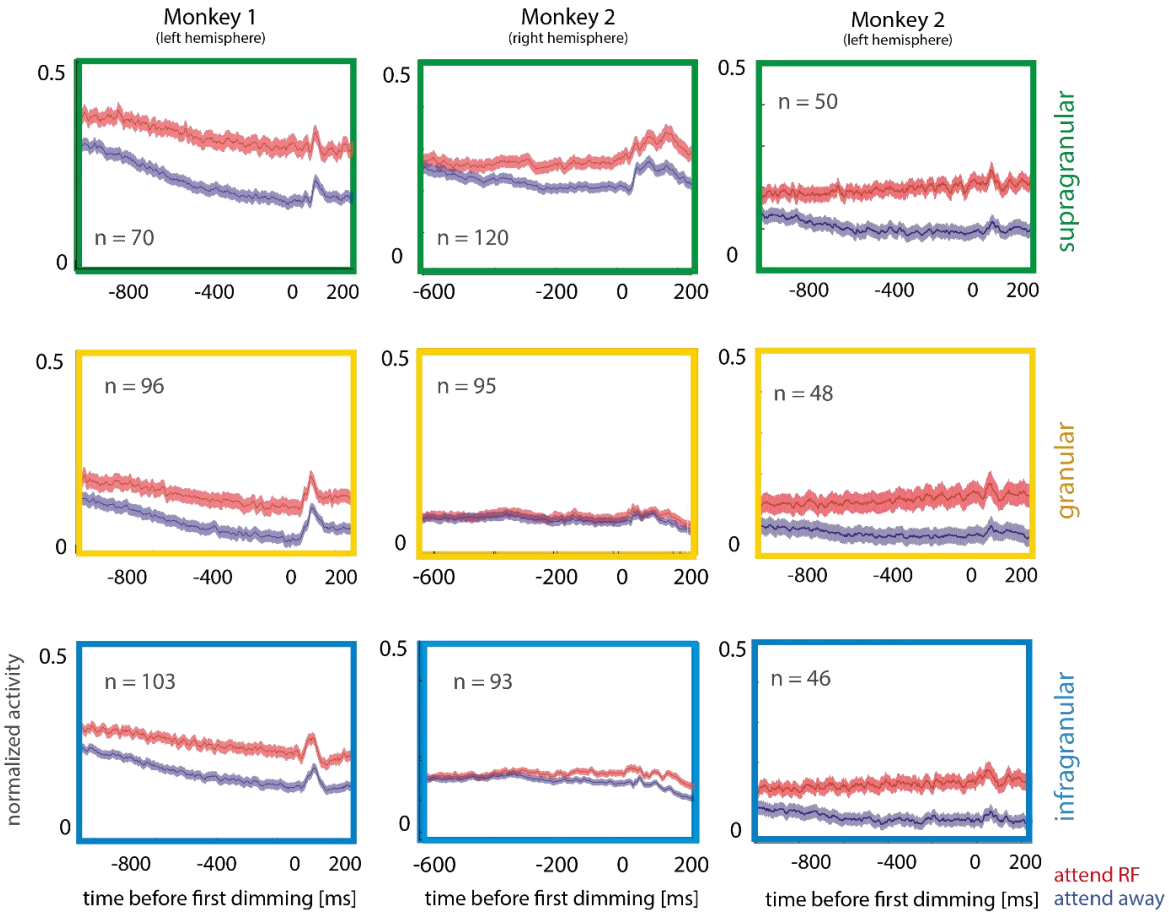

Figure 3-4: Monkey 1 and Monkey 2 (right and left hemisphere) average V1 envelope multiunit activity (MUA_E) aligned to the first stimulus dimming and grouped into supragranular (top, green), granular (middle, yellow) and infragranular (bottom, blue) layers (n = number of contacts in each plot). Attention conditions and V1 structure are as defined in Figure 3-3. Solid lines show mean activity, shaded areas S.E.M.

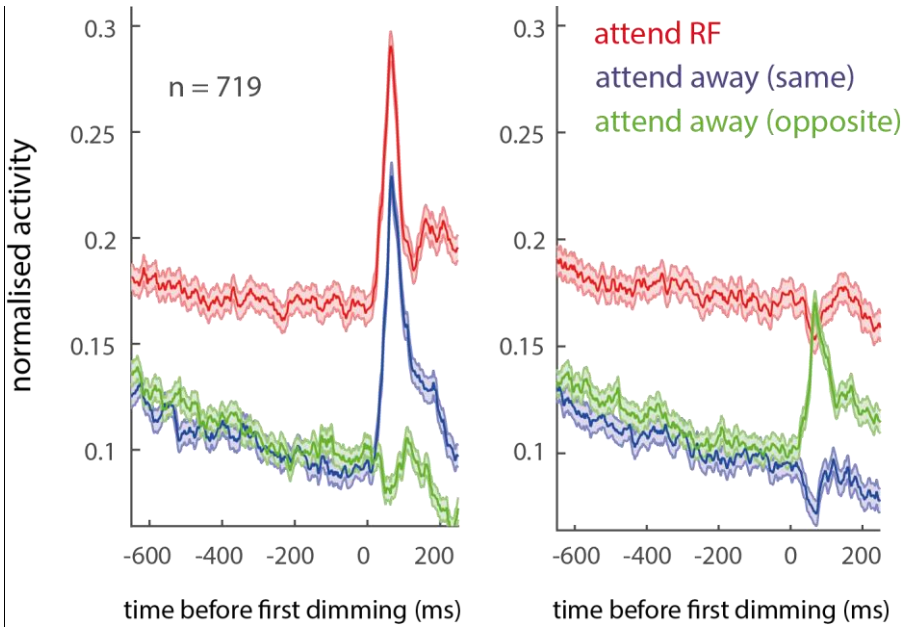

Figure 3-5: V1 envelope multiunit activity in both monkeys (pooled) aligned to the first dimming of the attention task separated based on (**left**) only trials where the first dimming occurred in the RF and (r**ight**) only trials where the first dimming occurred in one of the locations outside of the RF (n = number of contacts). Separated into the attend RF (red), attend away in the same hemifield (blue) and attend away in the opposite hemifield (green). Solid lines show mean activity, shaded areas S.E.M.

3.2 Single cell effects of attention

The previous section described the effects seen at the level of MUA_E activity, which ignores diversity between different cells, and also between different cell types. Single cell analysis allows to analyse this diversity (and analyse additional aspects of neuronal activity, such as rate variability), which is why detailed analysis of attention induced changes of neuronal spiking activity will be based on single cell data. As described in Section 2.4.1, single cell spiking activity underwent manual spike sorting with 'subjective' classification criteria ranging from 1-4, whereby classes 1 and 2 were sufficiently well isolated to have good confidence in the spike waveform grouping and to label them broadly as 'single units'. Only these cells will be analysed in the following section.

3.2.1 Classification of cell types

As described in the methods section, Figure 2-4 shows the distribution of peak to trough times in our sample of V1 single units that were recorded (n=819 [total], n=354 [Monkey 1], n=290 [Monkey 2, right], n=175 [Monkey 2, left]). The distribution was significantly non-unimodal, with a main dip in the distribution located at a peak to trough (P2T) time of about 250µs. However, the distribution suggests that there are multiple dips presents, whereby broad spiking cells can possibly be further subdivided along a P2T dip location at ~330µs, while narrow spiking cells can be subdivided into three potential classes with one P2T dip located at ~200µs, and one located at ~140µs. Many previous studies have seen a broad-narrow divide at a P2T of ~200µs, and thus the cells classified as narrow spiking with P2T times of 200-250µs might in fact be broad spiking cells. If 200µs was taken as the border to divide narrow and broad spiking cells it would yield narrow/broad ratios of 184/635 cells (not the 363/456 ratio shown in Figure 2-4), which is more in line with the distribution of interneurons/pyramidal cells found in the cortex. However, the main dip is clearly located at 250µs in our data, and the assignment of narrow spiking cells to interneurons and pyramidal cells is problematic anyway, a topic I will return to in the Discussion (Chapter 6). Importantly, a separate analysis of cells classified along a 200µs P2T divide yielded qualitatively identical results to those presented her, and

inconsistencies with the existing literature (if any), are therefore not a consequence of the divide used.

Table 3: Break down of cell types in V1. Numbers indicate whether cells were good (i.e. with a rating of 1 or 2), whether cells resided within our proposed microcolumn and whether the cells had attention effects.

Cell type	Total n from V1 placed electrodes	Good units	Good units with layer assignment	Good units with layer assignment and attention effects
broad	766	456	403	263
narrow	392	363	312	191

3.2.2 Cell types, laminar location and their relation to firing rate and rate variability

This section will address the question to what extent the overall firing rate of single units and their rate variability differs between cell types (broad vs. narrow) and between different layers. This analysis was performed on data from the stimulus aligned period (but controls were also run for the dimming aligned period). For this analysis the mean activity and the mean FFs were used across all six conditions (i.e. two direction conditions and three attention conditions). Averages of FFs were calculated from the FFs calculated for individual conditions. Averaging across all six conditions is an appropriate approach for the stimulus aligned period, as there were no attentional effects present during that period. All cells that were assigned to defined cortical layers were included. The procedures for this layer assignment were outlined in Section 2.4.14 for the MUA_E and the LFP activity, but identical steps were taken for the single cell alignment. Layer assignment reduced our sample size quite considerably. We recorded 456 broad spiking single units and 363 narrow spiking units from electrodes placed in area V1 (Table 3). 364 broad spiking cells and 262 narrow spiking cells showed an activity level of >3Hz and were recorded for >20 trials for each condition throughout all periods of interest, thus qualified for inclusion. Layer assignment according to the criteria described in Section 2.4.14 was possible for 325/364 broad spiking cells and 224/262 narrow spiking cells from area V1. These cells were then subjected to further analysis as shown in Figure 3-6.

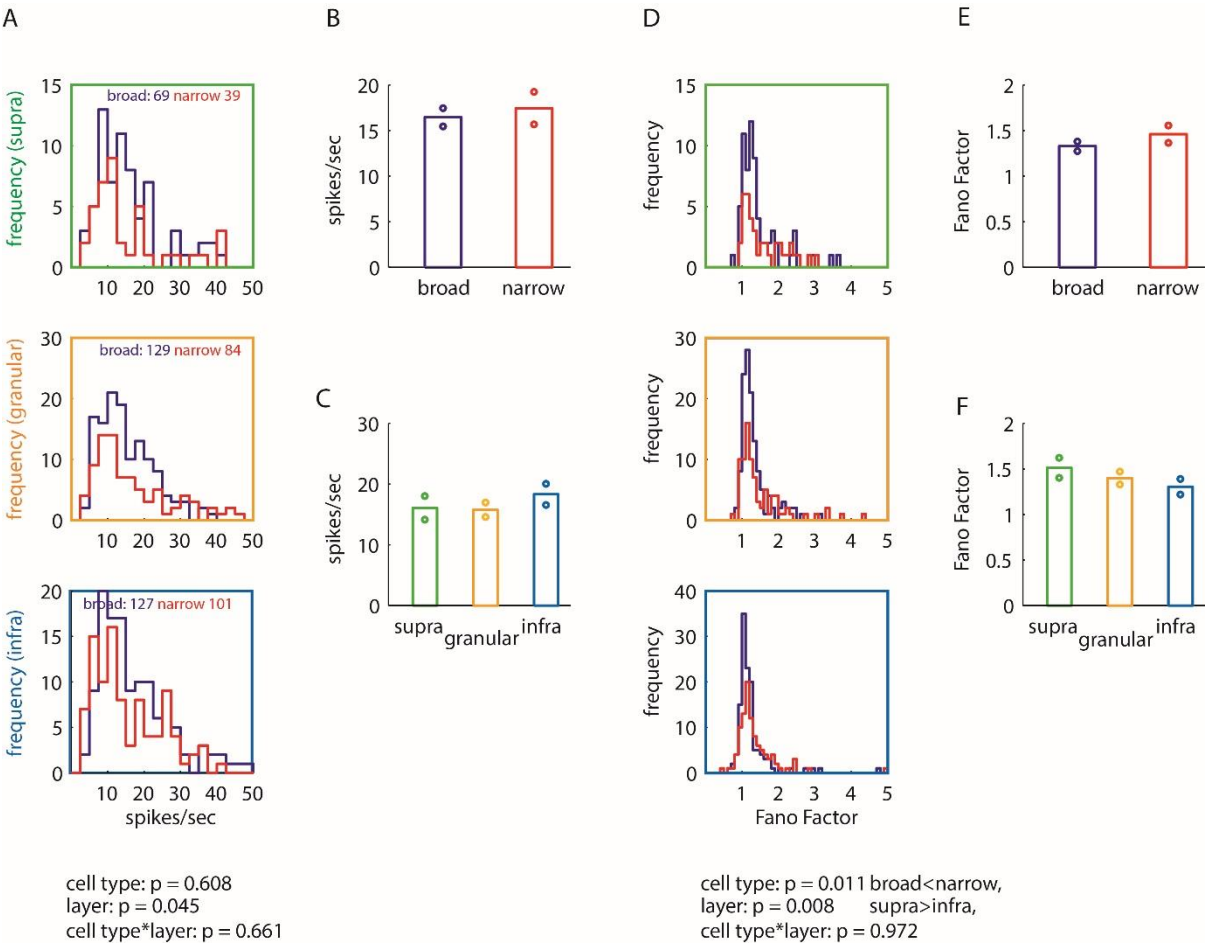

Figure 3-6: Distribution and summary statistics of firing rates and Fano-factors for broad and narrow spiking cells located in supra-, granular-, and infragranular layers respectively. A) Distribution of firing rates for narrow (red) and broad (blue) spiking cells in supra (green), granular (yellow), and infragranular (light blue) layers. Relative cell numbers recorded in each layer are given as insets. P-values below the graph show whether the factors 'celltype' or 'layer' significantly affected firing rates, and whether there was an interaction. B) Mean and 95% confidence interval of firing rates for narrow (red) and broad (blue) spiking cells. C) Mean and 95% confidence interval of firing rates for the three different layer subdivisions. D) Same as A, but with Fano-factor as the variable of interest. Statistics of differences are indicated below A and D. If differences occurred these were further investigated by post-hoc testing. Significant post-hoc test differences are indicated by quantitative comparisons, whereby the size difference is indicated by < and >, respectively. E) Same as B, but with Fano-factor as the variable of interest. F). Same as C, but with Fano-factor as the variable of interest.

3.2.3 Attention induced activity changes relative to pre-cue activity

Following cue onset the neuronal activity with attend RF conditions could increase, not change or decrease. The same is true for attend away related activity. A previous

publication showed that in FEF neurons generally increase their activity under attend RF conditions relative to pre-cue activity and decrease the activity for attend away conditions (even if there was some heterogeneity among the FEF population (Thiele *et al.*, 2016)). To investigate whether a similar pattern was present in V1 cells we calculated a cue response modulation index (cue response MI) for the attend RF and the attend away condition. The distributions of cue response MIs for both monkeys (pooled) and the different cell types (narrow vs. broad spiking) are shown in Figure 3-7. For both cell types the distributions of pre-cue MIs differed significantly for attend RF and attend away conditions ($p<0.001$, Wilcoxon signed rank test). As has been found in the FEF the distribution means for attend RF conditions were significantly positive (see Figure 3-7 insets 'P(RF/away)' for exact values). The distribution means for attend away conditions were always significantly smaller than zero (see Figure 3-7 insets 'P(RF/away)' for exact values).

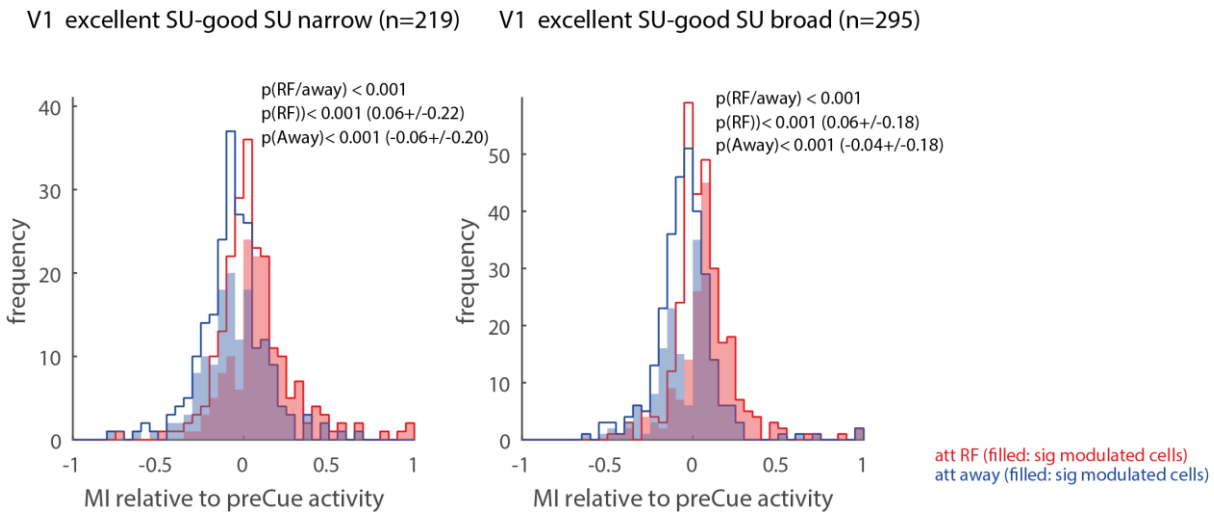

Figure 3-7: Distribution of cue response modulation indices (MI) in Monkey 1 and Monkey 2, for narrow and broad spiking cells in area V1. Blue histograms show MIs for the "attend away" condition, red histograms for the "attend RF" condition. Shaded histograms show distributions for cells that showed significant modulation relative to pre-Cue activity, outlines show distributions of all cells. N indicates sample size. Insets give significance that the respective individual distributions differed from zero [P(RF), P(away)], along with distribution means and standard deviations.

3.2.4 Effect of attention on firing rates and on rate variability

Next we analysed the effect of attention on firing rate and rate variability in area V1. This was done for the three relevant task periods, i.e. aligned to stimulus onset, aligned to cue onset and aligned to the time of the first dimming. The periods of analysis aligned to stimulus and cue onset were from 100ms after stimulus/cue onset until 400ms after stimulus/cue onset, respectively. The period aligned to the time of the first dimming was from -500ms to 0ms. The analysis of firing rates was based on 'spikes/second' to allow for comparisons between different periods (the periods had different window length). The analysis of rate variability was based on Fano-factor (FF) analysis (see Section 2.4.13). Figure 3-8 shows example raster plots of V1 spiking activity for the different layers, task periods and attention conditions used in our experiments.

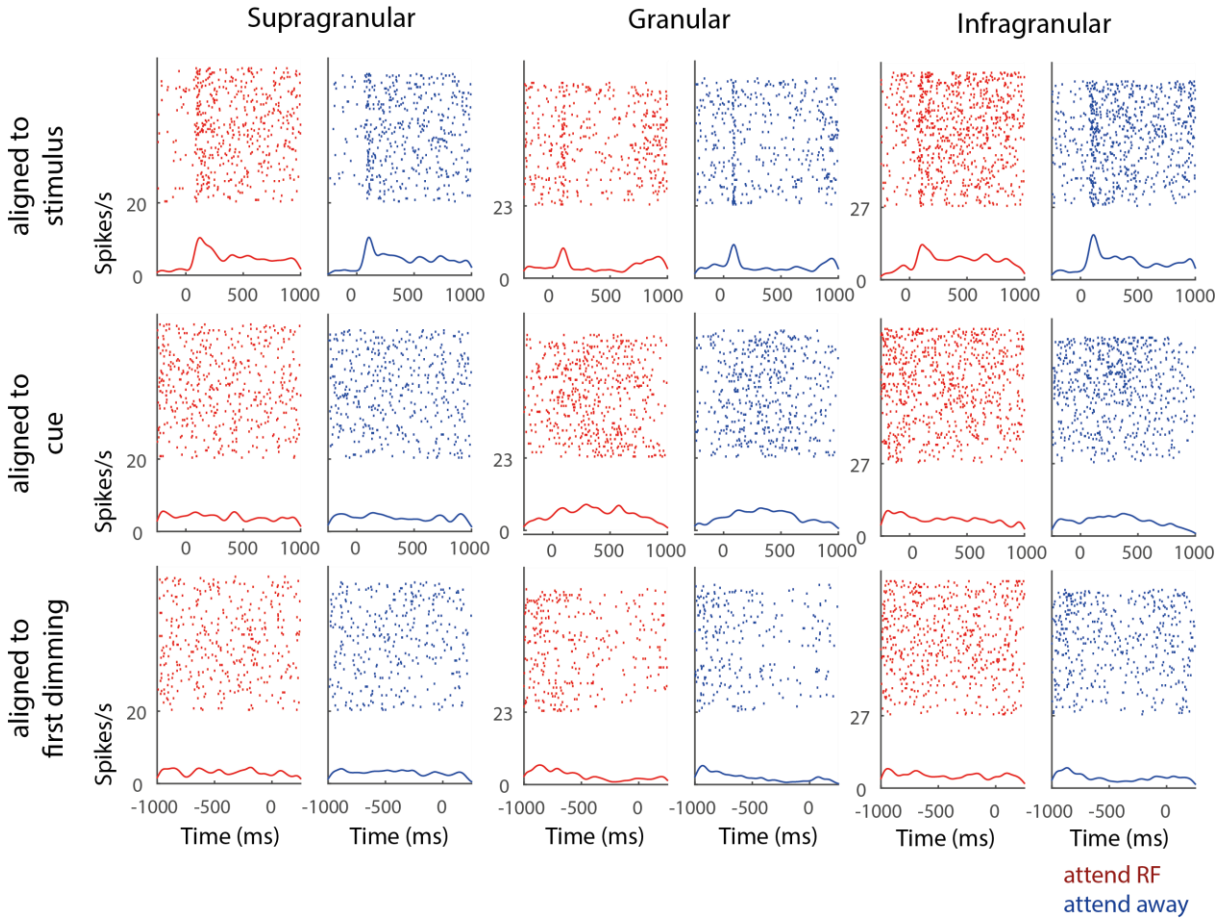

Figure 3-8: Example raster plots of spiking activity in V1, aligned to the stimulus onset, cue onset and prior to the first dimming. Data are shown for a recording channel in the supragranular, granular and infragranular layers in Monkey 1. Plotted separately for the attend RF (red) and attend away (blue) conditions. Underneath each raster plot is a histogram showing the spike rate against time throughout the task period.

Figure 3-9 shows the firing rates and the FFs of V1 neurons pooled across both monkeys (separately for broad and narrow spiking cells). Cells were included if they had at least a minimum firing rate of 3Hz in all of the relevant analyses periods and if there were at least 20 trials available for analysis in the attend RF and the attend away condition. The figure shows the effects for cells that were significantly modulated by attention during the pre-dimming period (narrow spiking cells: n=145/363, broad spiking cells: n=206/456). Note that this pre-selection is independent of the sign of attentional modulation and therefore does not bias the subsequent analysis. A Wilcoxon signed rank test was used to determine whether attention significantly (systematically) affected firing rates or FFs for the two cell types in any of the periods of interest. A mixed model ANOVA was performed to determine whether the effects seen depended on the factors: Cell type, period, attention, or layer, including any interaction between these.

Attention to the RF resulted in significantly higher firing rates in narrow and in broad spiking cells ($p<0.001$ each, Wilcoxon signed rank test) for the cue and the dimming period (Figure 3-9), but no significant effects were found for the stimulus onset aligned period ($p>0.2$ each, Wilcoxon signed rank test). The mixed model ANOVA revealed a significant main effects of attention, cell type, task period and layer on firing rates ($p<0.001$). There were also interactions between task period and attention, between cell-type and layer and between task period and layer. The ANOVA also found significant effects of all of the main factors on Fano factors, in addition to interactions between cell-type and task period and between cell-type and layer. In the dimming aligned task period, Fano factors were significantly lower for the attend RF condition than for the attend away condition for broad spiking cells ($p=0.018$, Wilcoxon signed rank test), but not for narrow spiking cells ($p=0.114$, Wilcoxon signed rank test).

Similar results were obtained, when all cells (not just those that were significantly affected by attention) were included in the study. This sample equally showed significant effects of attention on firing rate during the cue and dimming period for both cell types ($p<0.001$, Wilcoxon signed rank test, data not shown), and a significant effect of attention on the FFs of broad spiking cells in the dimming period ($p=0.03$, Wilcoxon signed rank test, data not shown).

br

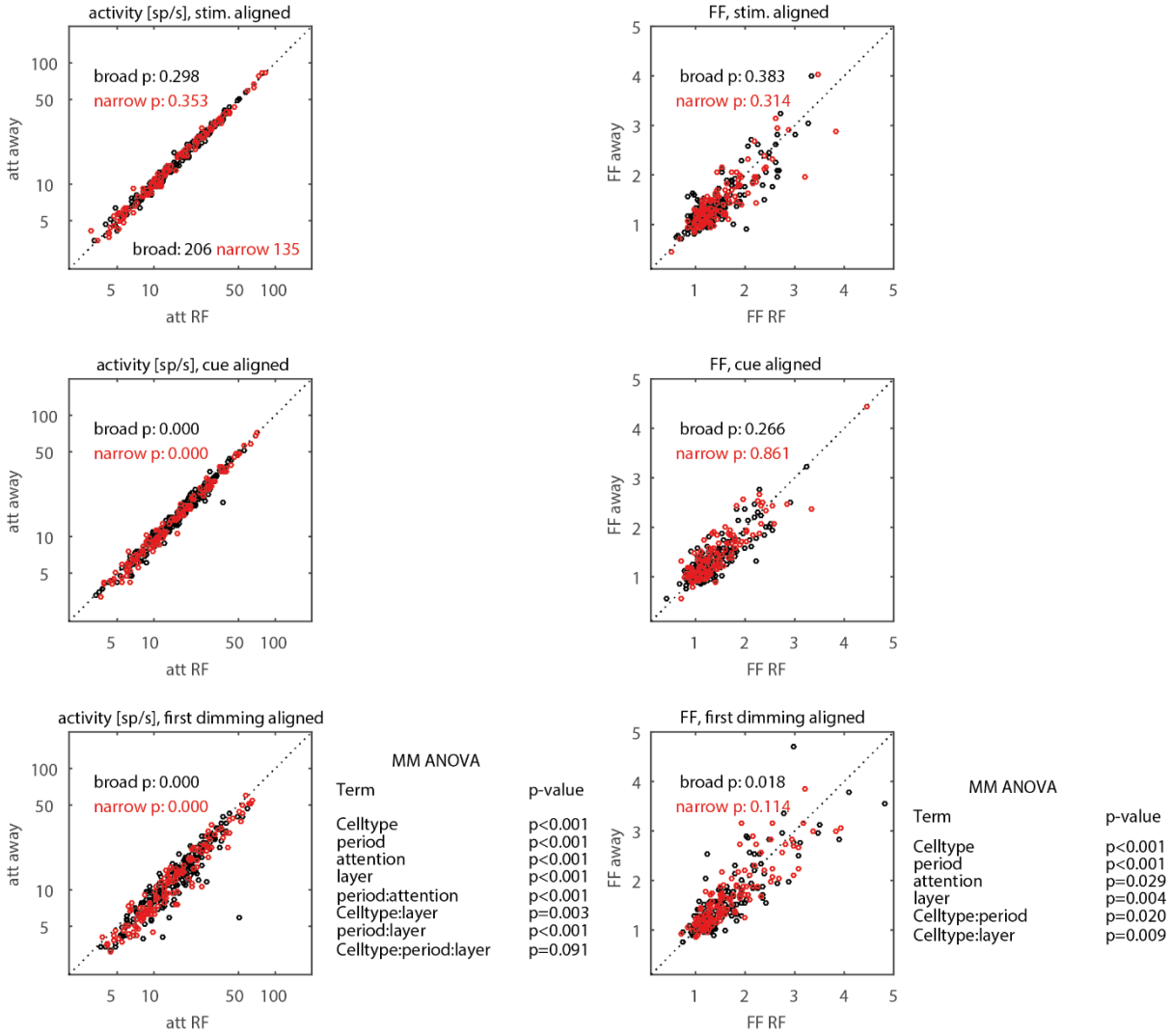

Figure 3-9: V1 firing rates (left column) and Fano-factors (FF, right column) for different task periods (top to bottom: stimulus aligned, cue onset aligned, first dim aligned), for the two cell types (narrow spiking: red, broad spiking black, sample sizes (n) are indicated in the top left subplot). Ordinate: parameter of interest during the attend RF period. Abcissae: parameter of interest during the attend away period (attend away parameters are averages across the two attend away conditions, see Section 2.2.4 for details). P-value insets indicate whether attend RF and away parameters differ significantly. The main effects of a mixed model ANOVA are shown to the right, with p-values for interaction terms shown only if they were significant.

Based on the effects which the mixed model ANOVA uncovered, we used pairwise comparisons to probe why effects arose. Figure 3-10 shows the breakdown of effects on firing rates in V1. Although we found an effect of cell-type in the ANOVA, there

was only a borderline significant difference between the two cell types upon testing with a t-test (Figure 3-10A). The effect of layer on firing rates arose because both supragranular and infragranular layers had higher firing rates than the granular layers (Figure 3-10B). Firing rates were larger in the stimulus aligned period of the task than in the first dimming aligned period (Figure 3-10C). In Figure 3-10D, no significant pairwise interactions of attention and layer were found. The interaction between layer and task period is shown in Figure 3-10E, with the p-values between the different combinations of groups denoted in Figure 3-10G. This highlights several significant differences which contribute to the interaction of layer and task period in the mixed model ANOVA. Finally, Figure 3-10F shows why the interaction between task period and attention arises, with no significant attentional modulation in the stimulus aligned period and significant modulation in both the cue and the first dim aligned task periods.

Figure 3-11 shows the pairwise comparisons between the different factors affecting the Fano factor. FFs were significantly higher for narrow spiking than broad spiking cells (Figure 3-11A). FFs were the largest in the supragranular layers and smallest in infragranular layers (Figure 3-11B). When the task periods were compared, we found the smallest FFs in the cue aligned period and largest in the dim aligned period (Figure 3-11C). The interaction of layer and attention was not significant in the mixed effect ANOVA, so it was not surprising that the pairwise comparisons between these factors did not show any effects either (Figure 3-11D). There was however an interaction between layer and task period, which is detailed in Figure 3-11E (p-values between groups in Figure 3-11G). We did not observe any pairwise interactions between task-period and attention (Figure 3-11F), which is again unsurprising given that the ANOVA did not uncover an interaction.

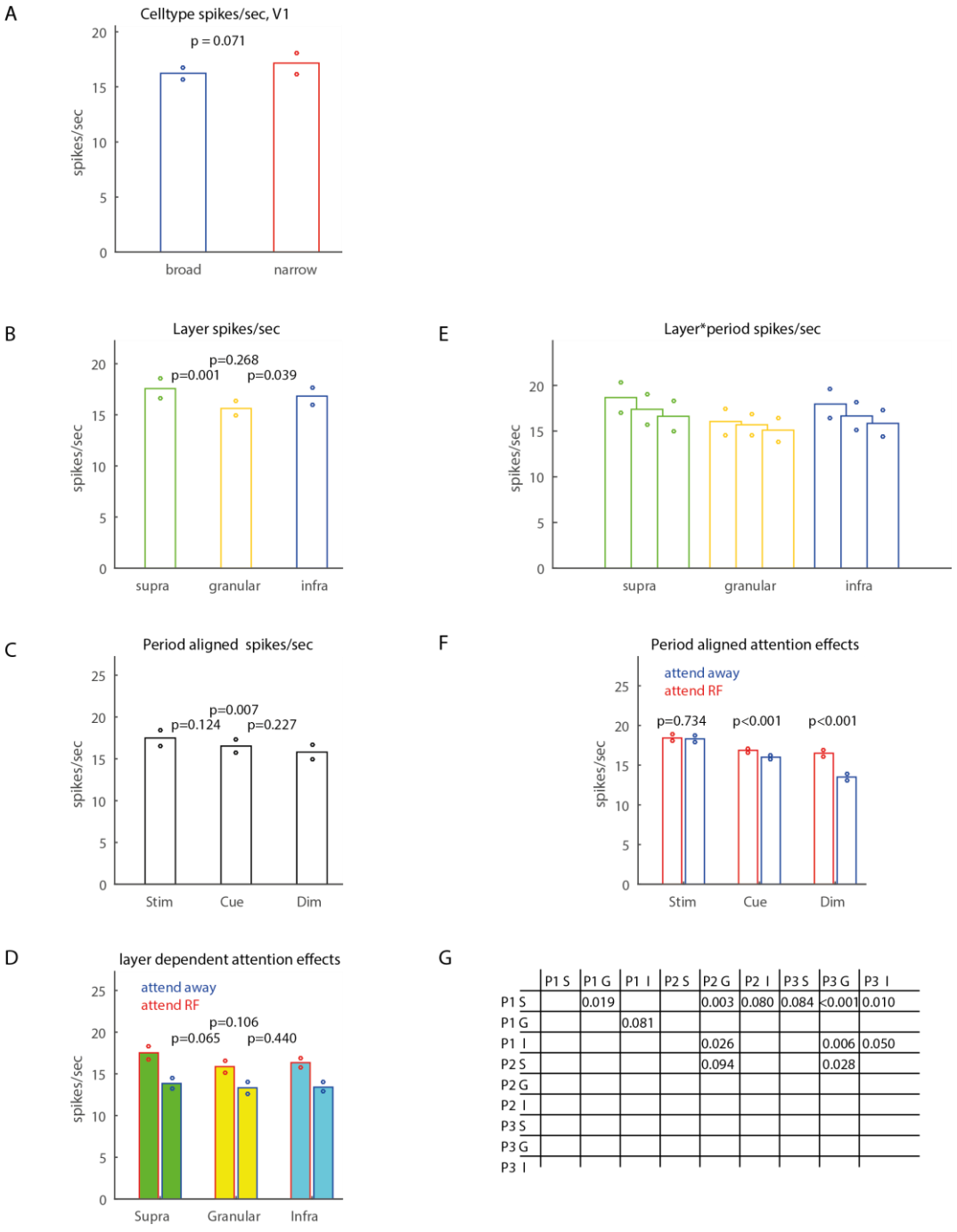

Figure 3-10: Breakdown of the effects of celltype, layer, period and attention on firing rate in V1. **A**: Firing rates for broad (blue) and narrow (red) spiking cells. **B**: Firing rates for supragranular (supra, green), granular (yellow) and infragranular (infra, blue) layers. **C**: Firing rates during the three task periods. **D**: Interaction of attention and layer on firing rates. **E**: Interaction of layer and period on firing rates. **F**: Interaction of attention and task period on firing rates. **G**: p-values for combinations of task period (P1=stim, P2=cue, P3=dim) and layer (S=supragranular, G=granular, I=infragranular), shown only for p<0.1. **All**: P-values based on t-tests (paired where possible) between the groups. Bars show means, circles around bars indicate 95% confidence intervals.

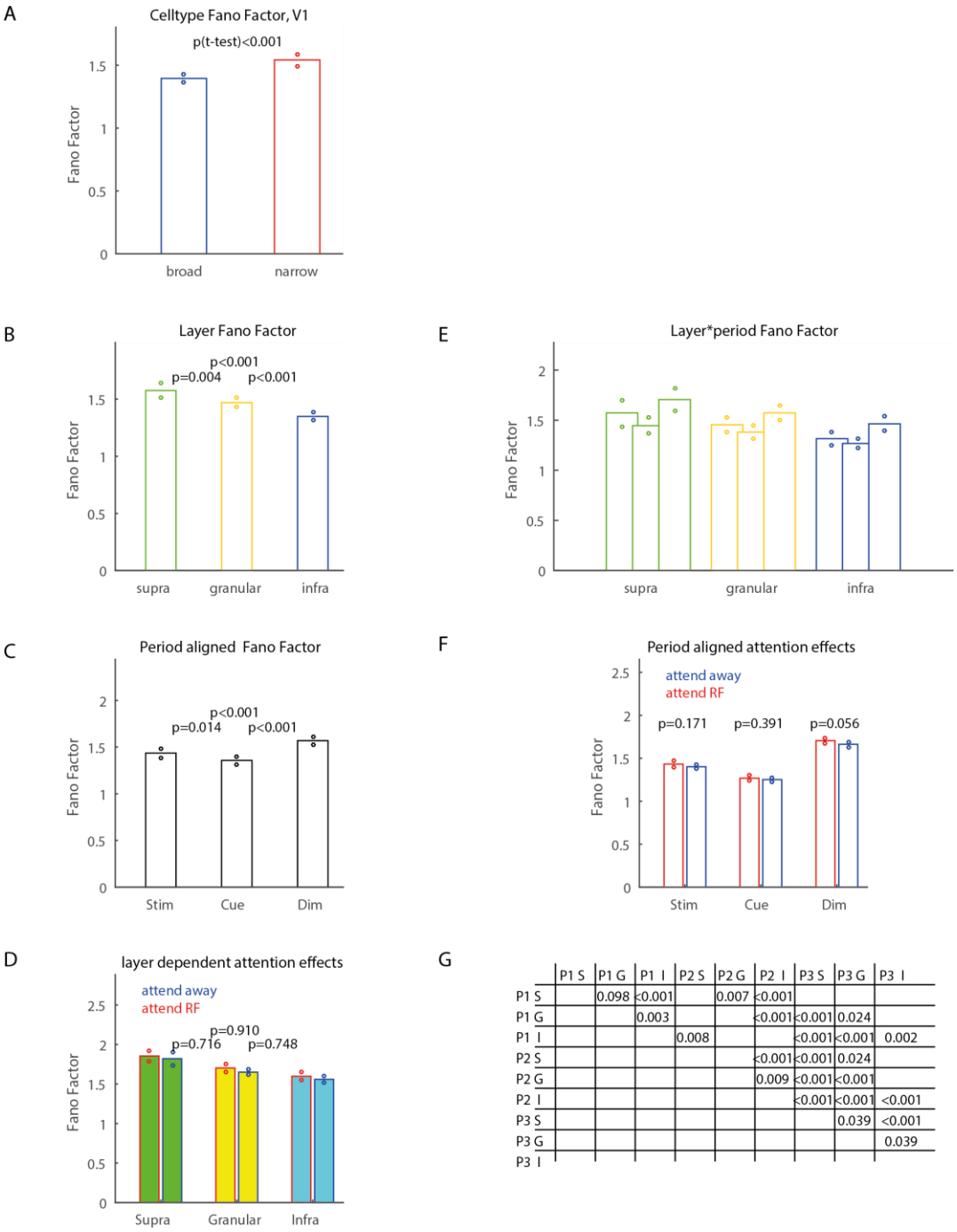

Figure 3-11: Breakdown of the effects of celltype, layer, period and attention on Fano factors in V1 cells. Subplots and statistics are as in Figure 3-10, but with Fano factor instead of firing rate.

The analysis shown in Figure 3-9 and Figure 3-11 shows that attention has only a limited effect on FFs in our study, and if anything attention to the RF resulted in higher FFs. A recent publication has argued that analysis of gain variance is more appropriate to assess changes in variability with attention than using the FF (Thiele *et al.*, 2016). We have thus analysed whether attention alters gain variance in narrow

and broad spiking cells. We found a significant reduction of gain variance with attention when pooled across narrow and broad spiking cells (Wilcoxon signed rank test, $p < 0.001$). In both cell types the effects of attention were also significant when analysed for the respective cells type alone. The exact p-values are plotted in Figure 3-12, along with the distributions of gain variance for attend RF vs. attend away conditions and the sample means and S.E.M.s.

The mixed model ANOVA showed significant effects of cell-type, attention and layer ($p<0.001$). There were also interactions between cell-type and attention, between cell-type and layer, between attention and layer and between cell-type, attention and layer.

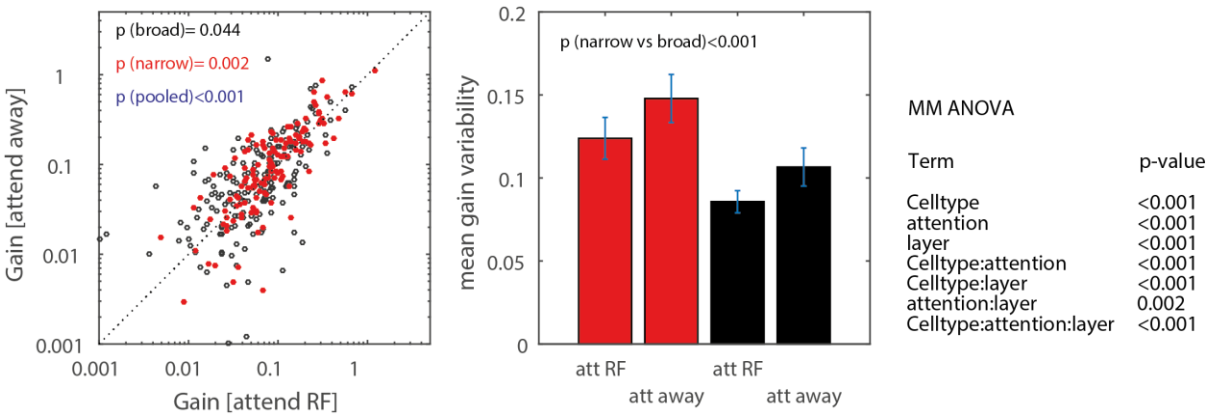

Figure 3-12*:* Effect of attention on V1 gain variance in broad and narrow spiking cells in both monkeys (pooled). Left column: Gain variance for the attend RF (x-axis) and attend away (y-axis) condition for broad (grey) and narrow (red) spiking cells. P-values indicate whether attention significantly affects gain variance (Wilcoxon signed rank test). Right column: mean and S.E.M. for gain variance distributions (p-values indicate whether gain variance differed between narrow and broad spiking cells). The main effects of a mixed model ANOVA are shown to the right, with interactions shown only if significant.

Figure 3-13 details how pairwise interactions contributed to the group effects which we observed in the mixed model ANOVA. Gain variance was significantly higher for narrow spiking cells than broad spiking cells (Figure 3-13A). Infragranular layers had the smallest gain variance. Supragranular layers had the highest gain variance (Figure 3-13B), but the difference to granular layers only showed a trend to significance. Attentional modulation of gain variance was significantly larger in

supragranular than in infragranular cells (Figure 3-13C). Figure 3-13E plots the interaction of layer, cell-type and attention.

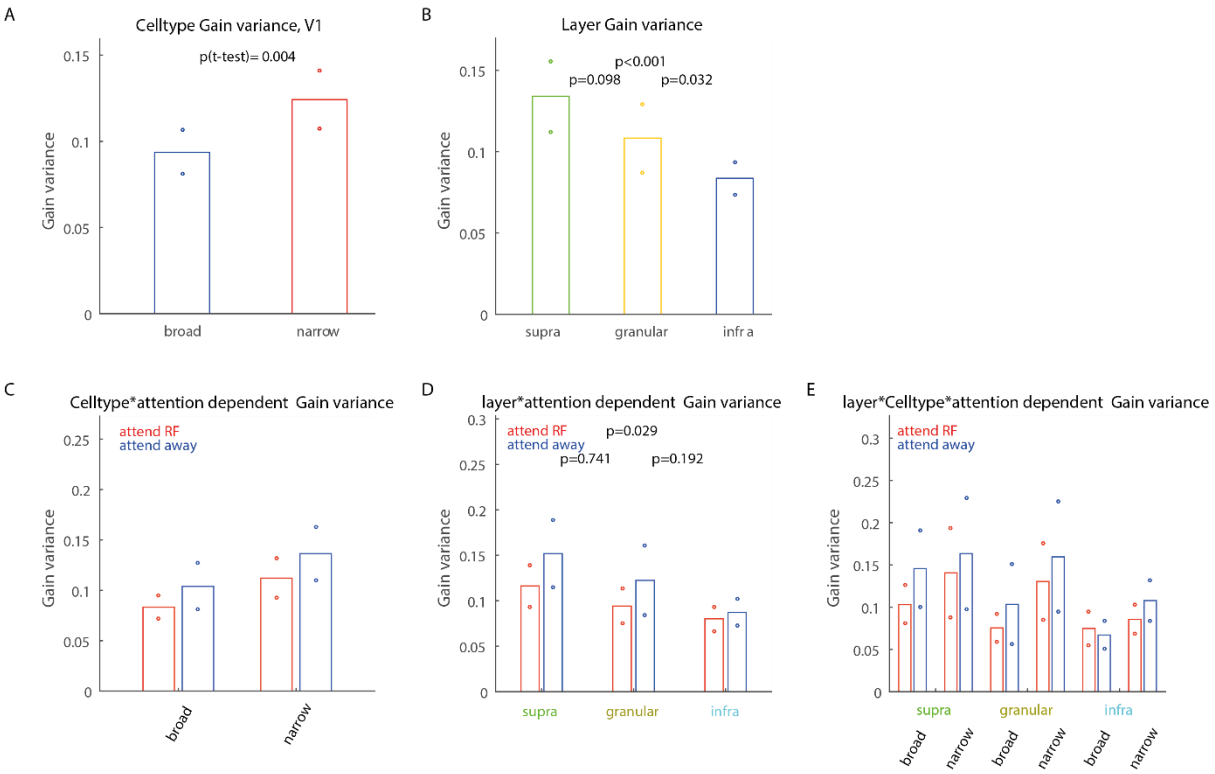

Figure 3-13: Breakdown of the effects on gain variance in V1. **A**: Gain variance for broad (blue) and narrow (red) spiking cells. **B**: Gain variance for supragranular (supra, green), granular (yellow) and infragranular (infra, blue) layers. **C**: Interaction of attention and cell type on gain variance. **D**: Interaction of layer and attention on gain variance. **E**: Interaction of layer, cell type and attention on gain variance. **All**: P-values are calculated as t-tests between the groups and circles around bars indicate 95% confidence intervals.

3.2.5 Quantification of attentional effects on spiking activity

To quantify attentional modulation we calculated two measures, the attentional modulation index (MI) and the Area Under the Receiver Operating Characteristics curve (AUROC). This was done for all three alignment periods separately. The distributions for both monkeys (pooled) are shown in Figure 3-14. MI distributions were significantly different than zero for both cell types during the cue and dim aligned periods of the task ($p<0.001$, Wilcoxon signed rank test). MIs increased when compared between stimulus aligned, cue aligned and dimming aligned periods.

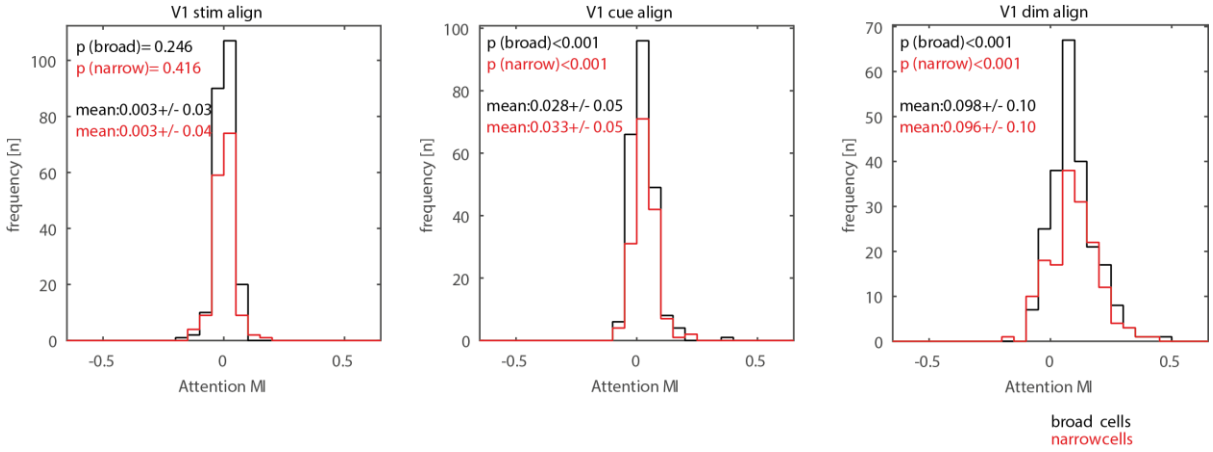

Figure 3-14: Distributions of attentional modulation indices for the 3 different alignment periods (columns) in both monkeys (pooled). Red shows narrow spiking cell MI distributions, black shows broad spiking cell MI distributions. Blue p-values indicate whether broad and narrow spiking cell MI distributions significantly differ, black and red p-value labels in subplots indicate whether respective distribution means are significantly different from zero.

Figure 3-15 shows the receiver operating characteristic (ROC) distributions of broad and narrow spiking cells plotted against the cue response MI values for area V1 recorded in both monkeys (pooled). The choice of pairwise plotting of AUROCs and MIs is done to allow for immediate comparison to data recently published for the FEF (Thiele *et al.*, 2016). The AUROC distributions for narrow and broad spiking cells did not significantly differ in area V1. Moreover, the cell types were equally unlikely (or likely) to have AUROC values <0.5 (i.e. attention induced reduction of firing rates). They also did not differ in their attend RF cue response modulation index. AUROCs were larger in supragranular layers than in granular layers ($p<0.05$, Wilcoxon rank-sum test).

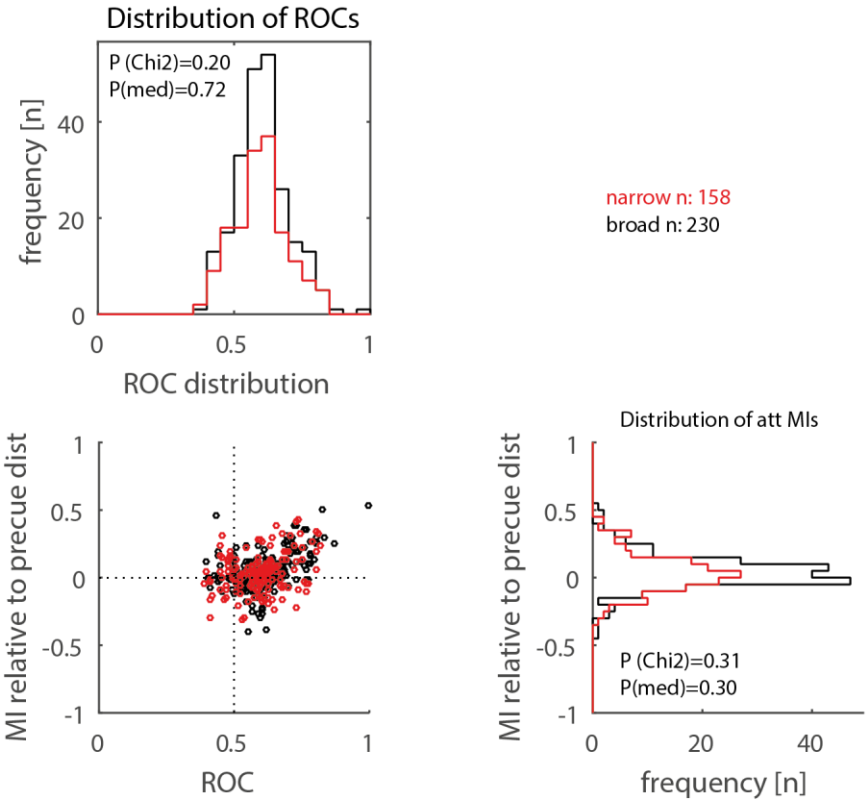

Figure 3-15: A) Area under the receiver operating characteristic (AUROC) values for broad and narrow spiking cells plotted against the cue response modulation index (MI, attend RF activity relative to pre-cue activity) in V1 of both monkeys (pooled). Black data points and histograms represent narrow spiking cells, grey data points and histograms represent broad spiking cells. B) Distribution of AUROC values for the two cell types. C) Distribution of MI values for the two cell types. P-values indicate whether the broad and narrow spiking cell AUROC or MI distributions (the medians) were significantly different (P (med)), and whether the narrow spiking cells significantly less often showed MIs<0 or AUROC values <0.5 (P (Chi2)).

3.3 The effects of attention on noise correlations

We calculated noise correlations between V1 cells, aligned to the stimulus onset, cue onset and first dimming (Figure 3-16). Noise correlations were small but positive in all three periods of the task. They were largest in Monkey 1. When aligned to the cue onset, noise correlations in Monkey 1 and in the left hemisphere of Monkey 2 were significantly lower in the attend RF condition. The same effect was also present for Monkey 1 in the dimming aligned period of the task, and a trend existed for data from the left hemisphere in Monkey 2 without being significant.

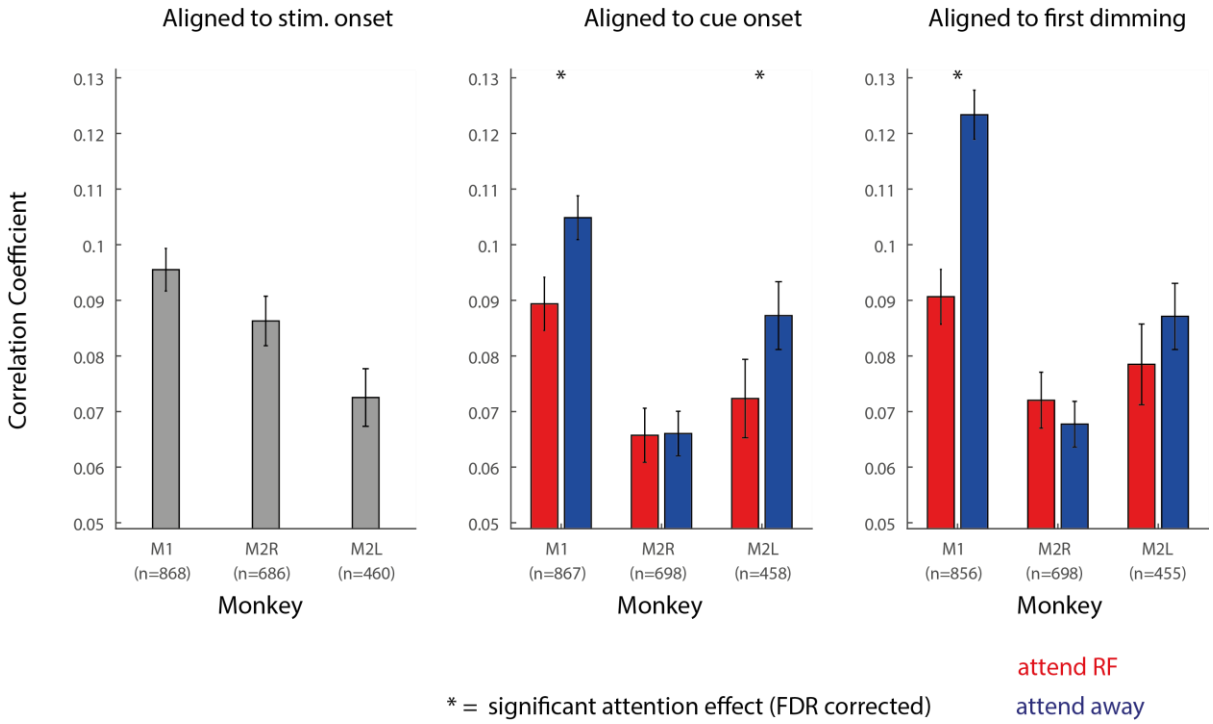

Figure 3-16: Noise correlations in V1 aligned to the stimulus onset (250-761ms, left), cue onset (50-561ms, centre) and first dimming (-511-0ms, right) in the attention task. Shown for Monkey 1 (M1) and the right and left hemispheres of Monkey 2 (M2R and M2L respectively). Asterisks indicate significant differences between the attention conditions ($p<0.05$, FDR corrected), n indicates the number of channel pairs. Attention conditions are as defined in Figure 3-1.

3.3.1 Layer dependence of noise correlations

We next investigated the effects of attention on noise correlations for the different layers in V1. For this analysis we pooled together data from Monkey 1 and the left hemisphere of Monkey 2, since both showed attention effects in the group analysis

(at least for the cue aligned period, Figure 3-16). The right hemisphere of Monkey 2 was not included in this analysis, since these recordings did not follow the same patterns as the other recordings in the group analysis. We suspect this may be due to the jerky nature of the stimuli used in these experiments (see Appendix A for more information).

When aligned to the stimulus onset (Figure 3-17, grey bars), the largest noise correlations were observed in the supragranular layers of both monkeys. The smallest noise correlations in the stimulus aligned epoch were in the infragranular layers of V1.

When aligned to the first dimming of the attention task (Figure 3-17, red and blue bars), several significant attentional modulations of V1 noise correlations were present. Noise correlations for the attend RF condition were significantly smaller between the supragranular layers and all layers and between the granular and infragranular layers. There was also a trend for this effect within the granular and infragranular layers. Within the supragranular layers, this effect occurred because noise correlations in the attend RF condition were lower than in the stimulus aligned period, however in the other layer combinations the effect arose due to an increase in noise correlations for the attend away condition.

We also performed this analysis for the cue aligned task period (not shown), but did not observe any major differences between this analysis and the first dimming aligned analysis.

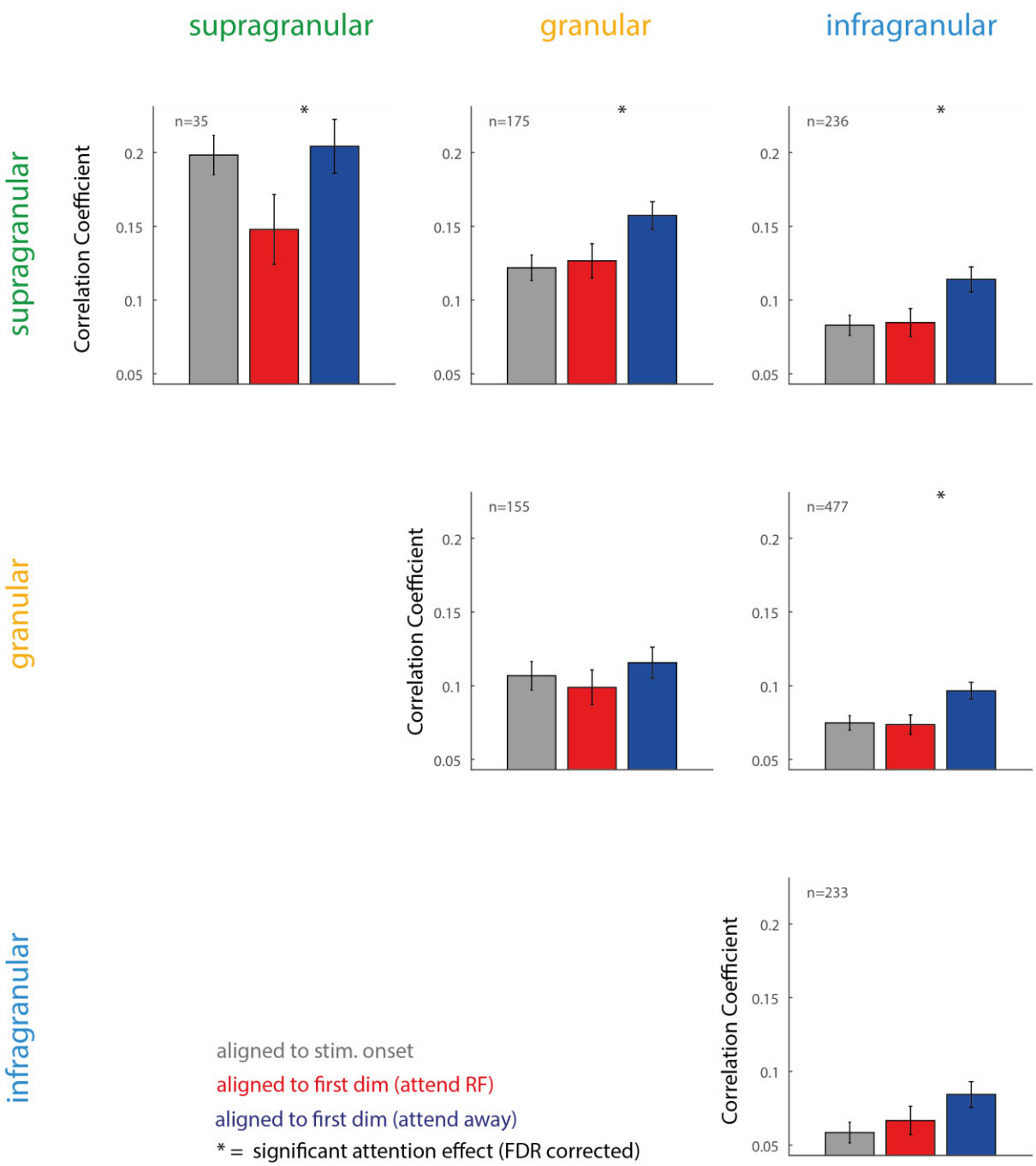

Figure 3-17: Noise correlations in V1 aligned to the stimulus onset (250-761ms, grey) and first dimming (-511-0ms, red [attend RF] and blue [attend away]) in the attention task. Pooled across recordings in Monkey 1 and the left hemisphere of Monkey 2 and grouped into pairs of supragranular (green), granular (yellow) and infragranular (blue) layers. Asterisks indicate significant differences between the attention conditions ($p<0.05$, FDR corrected), n indicates the number of channel pairs. V1 structure is as defined in Figure 3-1.

3.4 Attention induced changes to spectral power of the local field potential

We analysed the spectral power of the LFP (in the range from 1Hz to 100Hz) to explore how it was affected by the stimulus and by attention, and whether this differed between layers. The LFP signal used in all analyses was based on the bipolar derivative (see Section 2.4.8) to give a local estimate of the signal for each channel. We calculated this for the four time periods of the task; aligned to stimulus onset, cue onset and first dimming.

3.4.1 Raw LFP spectral analysis

The LFP spectral power of both monkeys (Figure 3-18) largely show a decrease of power with increasing frequency, which broadly mimics 1/f characteristics, even if some deviations thereof are present. Comparing the pre-stimulus and post-stimulus periods of the task shows that low frequency power is reduced by stimulus onset, whereas there is an increase in gamma frequency after stimulus onset. It is difficult to observe other effects of task period and attention in these plots, therefore these are analysed in more detail using normalised LFP analysis (see Section 3.4.2 and 3.4.3).

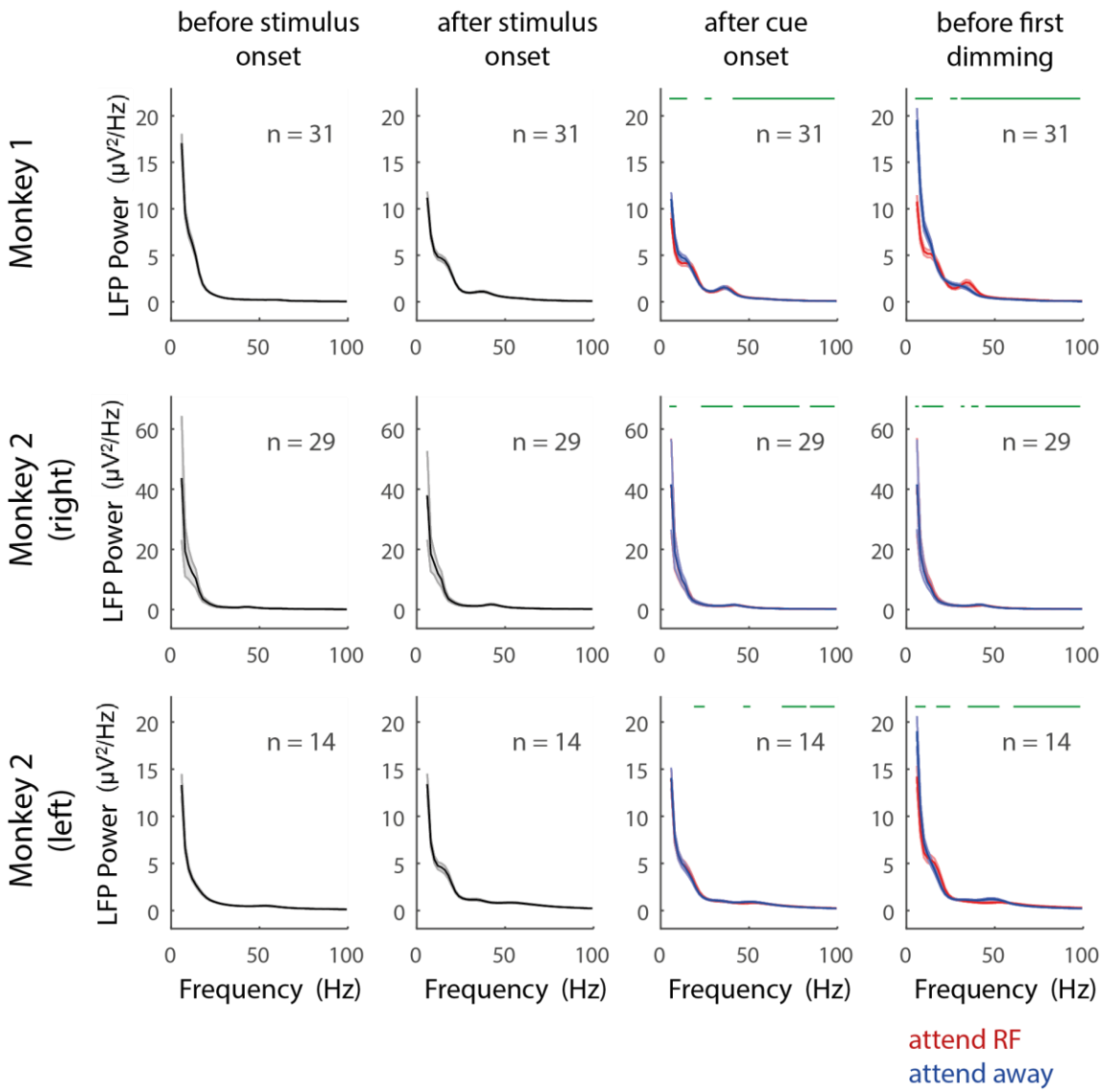

Figure 3-18: LFP power spectra in V1. Plotted for Monkey 1 and 2 (left and right hemisphere) aligned to both before and after the stimulus onset, after the cue onset and before the first dimming in the attention task (n = number of recordings per monkey). Separated into the attend RF (red) and attend away (blue) conditions for the cue and first dimming periods. Spectral power was calculated using the bipolar derivation of the local field potential, with 3 tapers of 4Hz half-bandwidth. Green bars indicate significant differences between the attention conditions (repeated measures Wilcoxon signed rank test, $p<0.05$, FDR corrected).

3.4.2 Spectral power of the LFP after stimulus onset

We used a z-score of the LFP power relative to the pre-stimulus task epoch (see Section 2.4.6) to give a measure of stimulus evoked LFP power (Figure 3-19). Stimulus presentation resulted in an increase in LFP power for frequencies above 10Hz. In both monkeys stimulus presentation resulted in frequency peaks in the low

gamma range (~38Hz in Monkey 1, ~40Hz in the right hemisphere of Monkey 2, ~36Hz in the left hemisphere of Monkey 2). Additionally a peak at lower frequencies occurred in both monkeys (~20Hz in Monkey 1, ~12Hz in the right hemisphere of Monkey 2, ~18Hz in the left hemisphere of Monkey 2). Spectral power at higher gamma frequencies (50-100Hz) were also increased when the stimuli were presented, although this did not show a distinct peak but was a broadband increase.

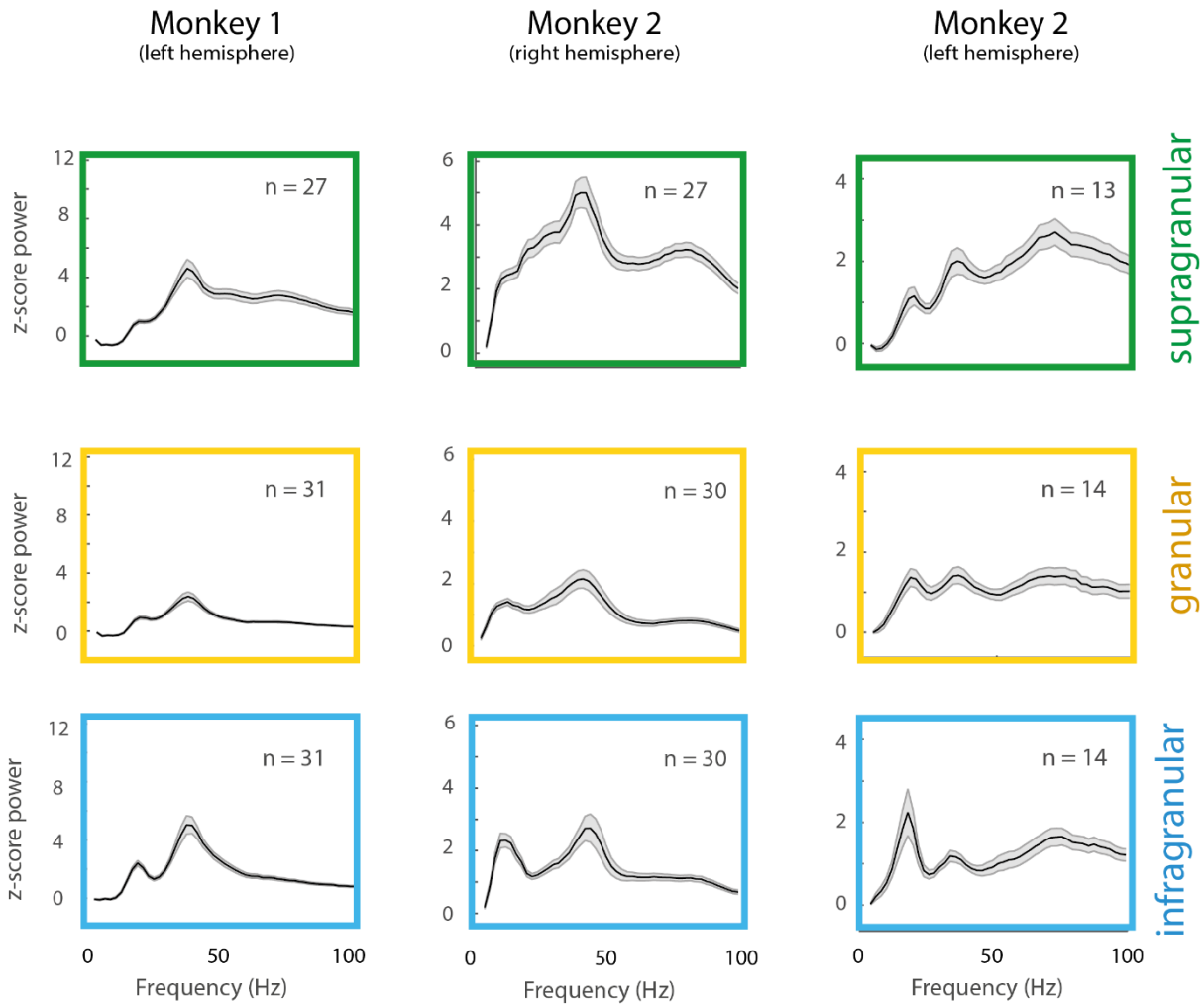

Figure 3-19: LFP spectral power in Monkey 1 and Monkey 2 (right and left hemisphere) aligned to the stimulus onset (250ms to 761ms) in the attention task (n = number of recordings in each plot). Spectral power was calculated using the bipolar derivation of the local field potential, with 3 tapers of 4Hz half-bandwidth and expressed as a z-score relative to pre-stimulus power. V1 structure is as defined in Figure 3-1.

3.4.3 Spectral power of the LFP prior to the first dimming

The effects of attention on LFP power could be observed in both the cue and first dimming periods of the attention task. However, since the analysis aligned to the cue onset always showed qualitatively the same effects as the first dimming analysis (sometimes with smaller magnitude), we only show the latter here.

The normalised power spectrum prior to the dimming period showed a distinct peak in the low gamma frequency range (~30-50 Hz) for both attention conditions in both monkeys (Figure 3-20). There was also a second higher gamma peak at roughly 60Hz to 85Hz, again in both monkeys. In Monkey 1, low frequency oscillations were most pronounced around the beta frequency range (15-25 Hz), however Monkey 2 showed low frequency peaks at a lower alpha frequency range (8-12 Hz).

In addition to the significant differences indicated by the green bars in Figure 3-20, several differences can be seen between the mean power spectra in the two attention conditions. The low gamma peak was larger and slightly shifted to higher frequencies in the attend RF condition in Monkey 1. The higher frequency gamma peak (60-85 Hz) was also increased by attention to the receptive field. The pattern of gamma power modulations for different layers showed the strongest attentional modulations in the supragranular layers and the weakest in the granular layers.

In contrast, Monkey 2 also showed attention induced spectral power modulations in the gamma frequency range, but these were a decrease in low gamma frequency power and a broadband power increase at high frequencies (>50Hz) with attention to the RF, compared to attend away conditions. This effect was significant in both hemispheres, but most prominent in the left hemisphere. A common feature between the two monkeys was a shift of the peak frequency with attention to the RF in the low gamma frequency range which was present across all three cortical layers. An important additional feature was an attention induced increase in beta band power in Monkey 2, which was present in all layers. In Monkey 1 this was also present (significant) in infragranular layers, and a trend for this effect could be observed in the granular layers. For further discussion on inter-subject differences in V1 LFP analysis in this and other studies see Section 6.2.3.

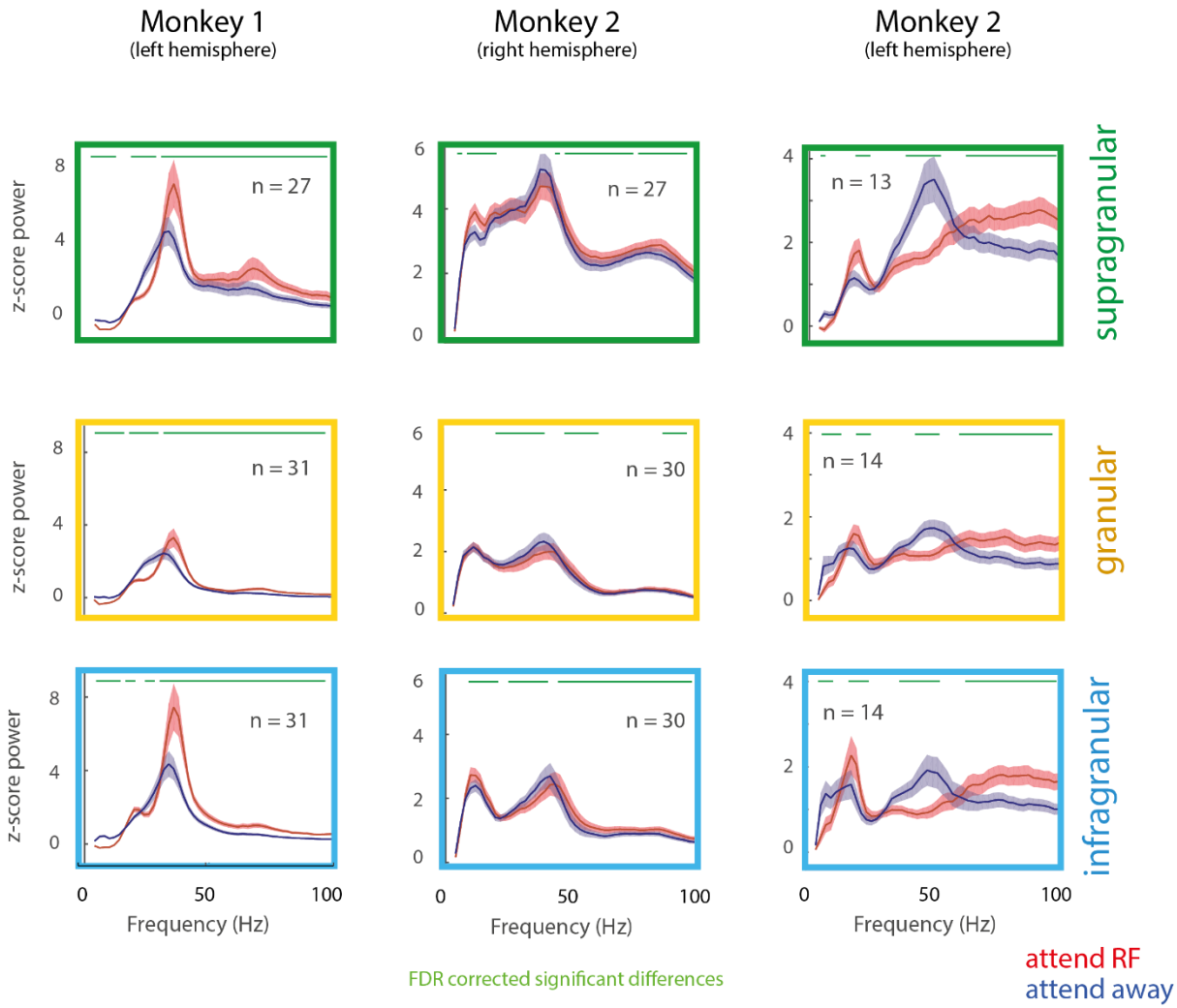

Figure 3-20: LFP spectral power in Monkey 1 and Monkey 2 (right and left hemisphere) aligned to the first dimming (-511ms to 0ms) in the attention task (n = number of recordings in each plot). Plotted separately for the attend RF (red) and attend away (blue) conditions. Green bars indicate significant differences between the attention conditions (repeated measures Wilcoxon signed rank test, $p<0.05$, FDR corrected). Power calculations and V1 structure are as defined in Figure 3-19.

3.5 Field-field coherence

We calculated the field-field coherence (referred to as field coherence subsequently) between each of the V1 electrode contacts. These were then grouped into supragranular, granular and infragranular layers and compared between attention conditions. Alignment to cue onset produced qualitatively the same effects (with smaller magnitude) as when aligned to the first dim, we only show the latter here.

3.5.1 Field coherence after the stimulus onset

The peaks we observed in the stimulus aligned field coherence occurred in the same frequencies as the stimulus aligned power analysis. In Monkey 1 (Figure 3-21), these peaks were in a beta frequency (~17Hz) and low gamma (~39Hz) frequency range. The separation of these two peaks was most refined between the infragranular layers and all other layers. The low frequency coherence was strongest within layers (i.e. supragranular-supragranular, granular-granular and infragranular-infragranular). Comparison to the coherence spectra before the stimulus onset (Appendix B, Figure B-1) showed that the gamma peak was more pronounced after the onset.

Both the beta (~12Hz) and low gamma (~42Hz) peaks were also present in the coherence spectra of the right hemisphere of Monkey 2 (Figure 3-22). In the left hemisphere (Figure 3-23), only the low frequency peak (~17Hz) was present. There was however a very broad peak in the high gamma range (50-100Hz). Again, the strongest low frequency coherence was observed within layers, regardless of the hemisphere recorded from. There were no clear differences between the coherence spectra before (Appendix B, Figure B-2) and after the stimulus onset in Monkey 2.

We also analysed the phase difference between the different layers of V1 (Appendix C.1). In Monkey 1, the phase difference of gamma coherence between deep and shallow layers (Figure C-1) was mostly negative, suggesting that the LFP in the shallow layers leads that of the deeper layers. There was also a trend for this effect in the right (Figure C-2) and left (Figure C-3) hemispheres of Monkey 2.

Since the phase is cyclic, the direction of these effects could technically have been reversed (i.e. a lag of $\pi/2$ is equivalent to a lead of $-3\pi/2$). Therefore in order to draw

conclusions on the direction of information flow we relied on other analyses, such as Granger causality and cross correlations.

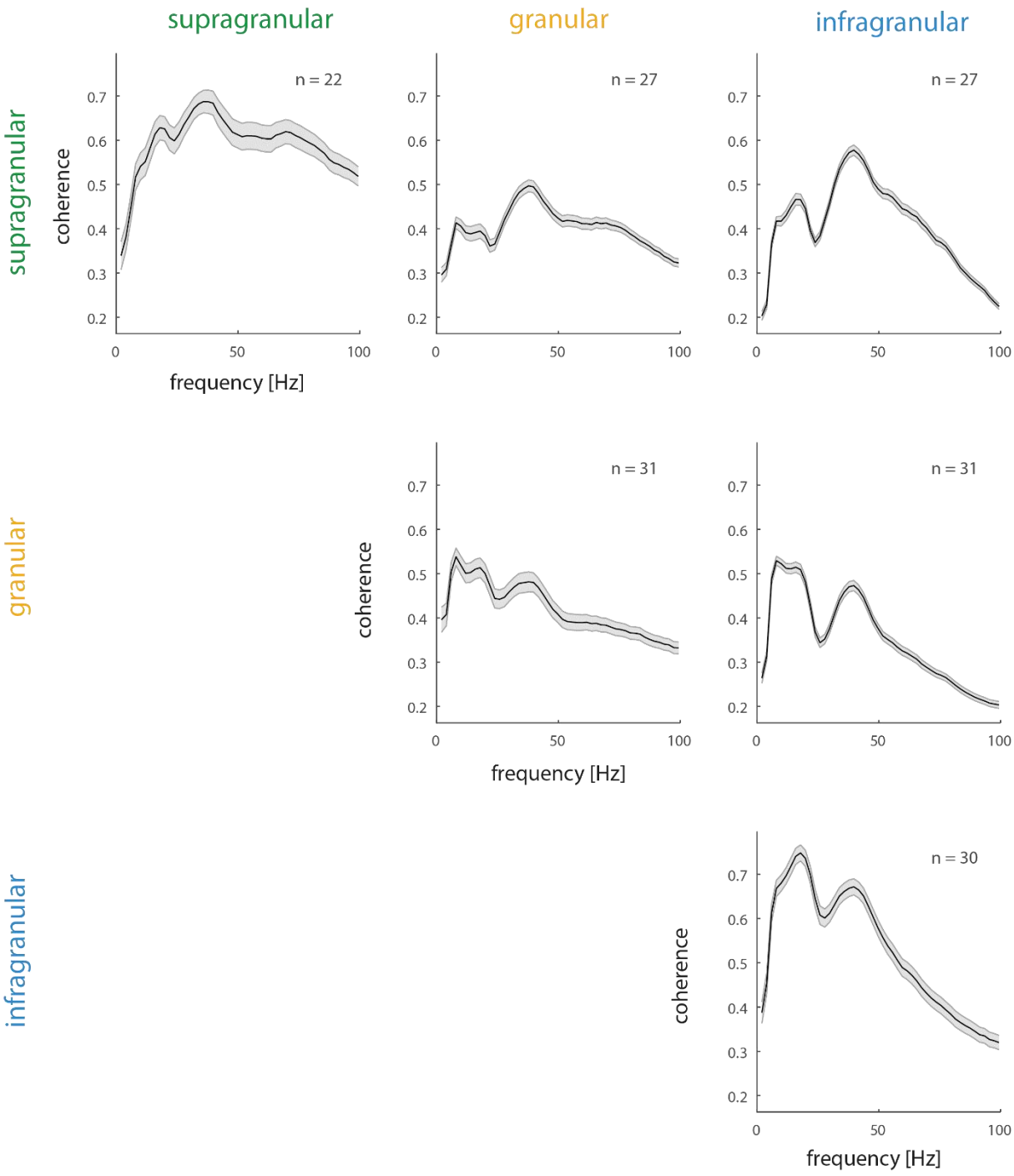

Figure 3-21: V1 field-field coherence in Monkey 1 aligned to the stimulus onset (250ms to 761ms) in the attention task. Shown are all possible combinations of supragranular, granular and infragranular layer comparisons, averaged across the channels contributing to the respective sections (n = number of recordings in each plot). Coherence was calculated using the bipolar derivation of the local field potential and 3 tapers of 4Hz half-bandwidth. V1 structure is as defined in Figure 3-19.

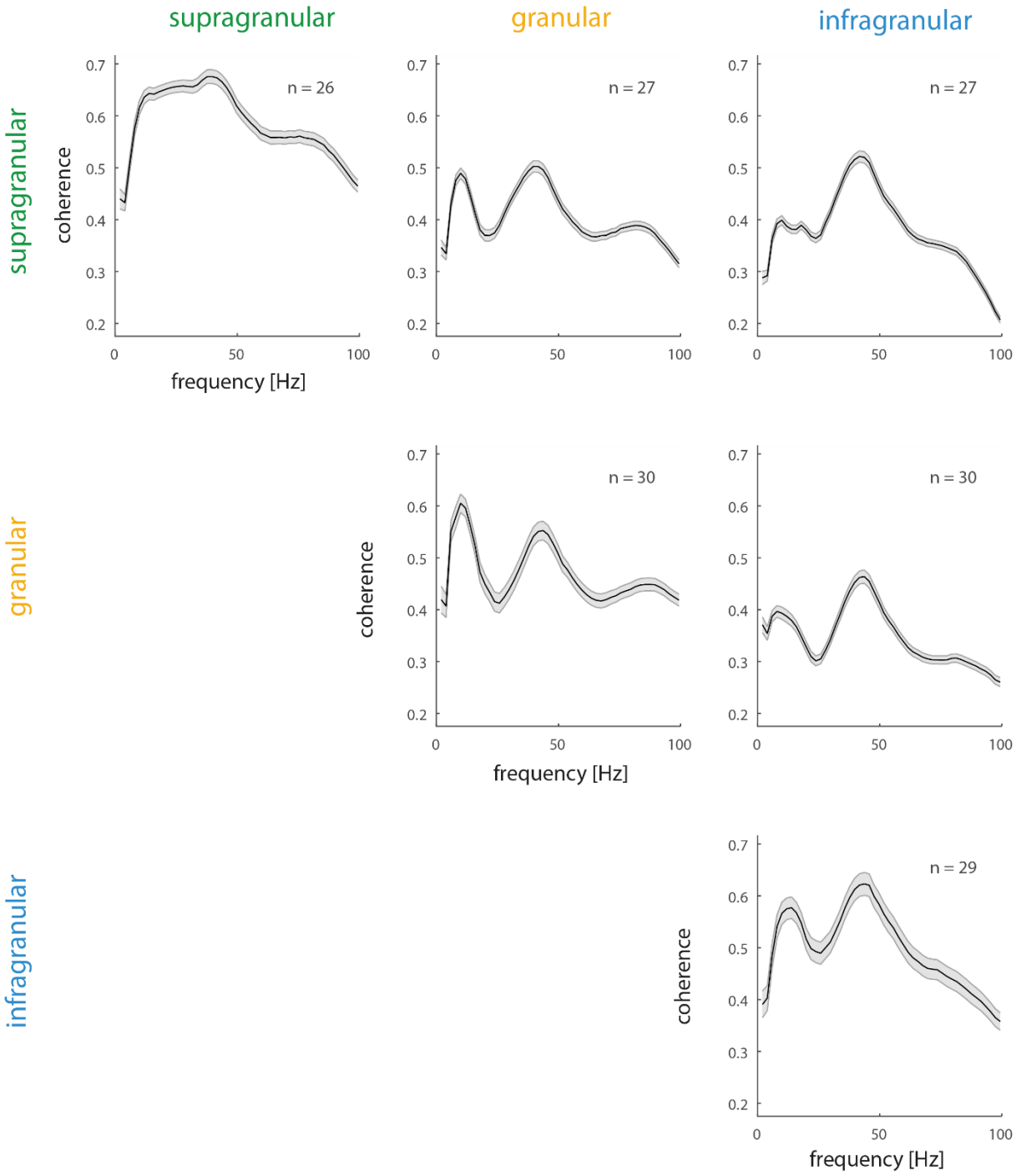

Figure 3-22: V1 field-field coherence in Monkey 2 (right hemisphere) aligned to the stimulus onset (250ms to 761ms) in the attention task. Shown are all possible combinations of supragranular, granular and infragranular layer comparisons, averaged across the channels contributing to the respective sections (n = number of recordings in each plot). Coherence calculation and V1 structure are as defined in Figure 3-21.

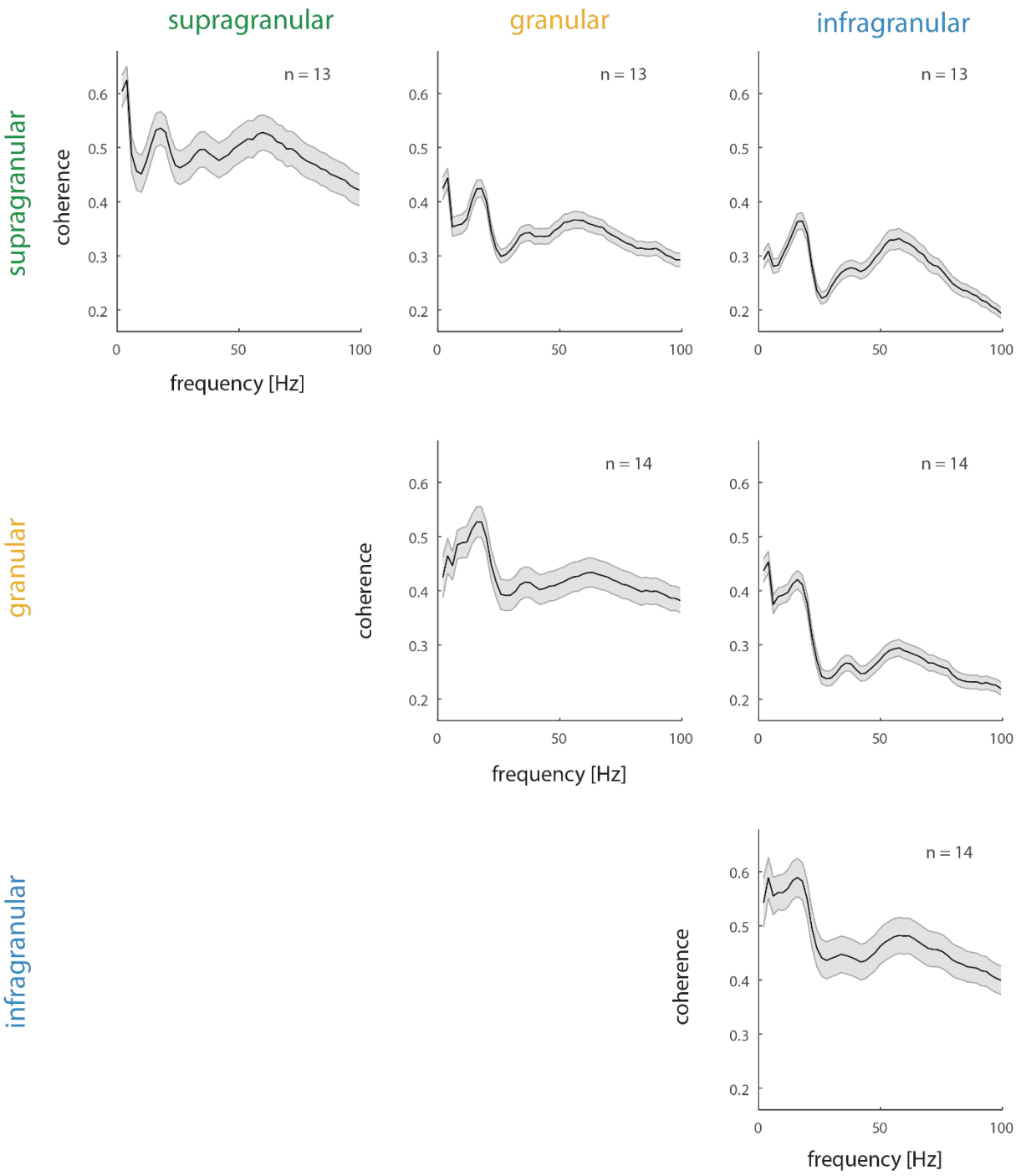

Figure 3-23: V1 field-field coherence in Monkey 2 (left hemisphere) aligned to the stimulus onset (250ms to 761ms) in the attention task. Shown are all possible combinations of supragranular, granular and infragranular layer comparisons, averaged across the channels contributing to the respective sections (n = number of recordings in each plot). Coherence calculation and V1 structure are as defined in Figure 3-21.

3.5.2 Field coherence prior to the first dimming

In Monkey 1 attention increased the peak frequency of low frequency and low gamma coherence, which was also accompanied by a tightening of the low gamma peak (Figure 3-24).

In the low frequency range the attention effects were not consistent between monkeys. In the left hemisphere of both monkeys, attention decreased the coherence at low frequencies throughout the layers in both monkeys (Figure 3-24 and Figure 3-26). However in the right hemisphere of Monkey 2 there were a combination of increases and decreases in this frequency range (Figure 3-25).

In the left hemisphere of Monkey 2, low gamma coherence was significantly increased when the monkey attended away from the receptive field of the recorded cells (Figure 3-26). This effect was most pronounced when coherence was calculated between different layers of the cortex.

Having described the effects in this way, there is equally a different description possible, which highlights similarities between monkeys rather than differences. In both monkeys the attend RF coherence could be interpreted as a frequency shifted and in parts amplitude scaled version of the attend away coherence, whereby attention shifts the frequency peaks (across the board) to higher frequencies, and the magnitude of the shift depends on starting frequency. In both monkeys this results in increased beta band coherence for most layer combinations and decreased alpha band coherence. Given this description, the main difference between monkeys is the power in the mid frequency gamma coherence.

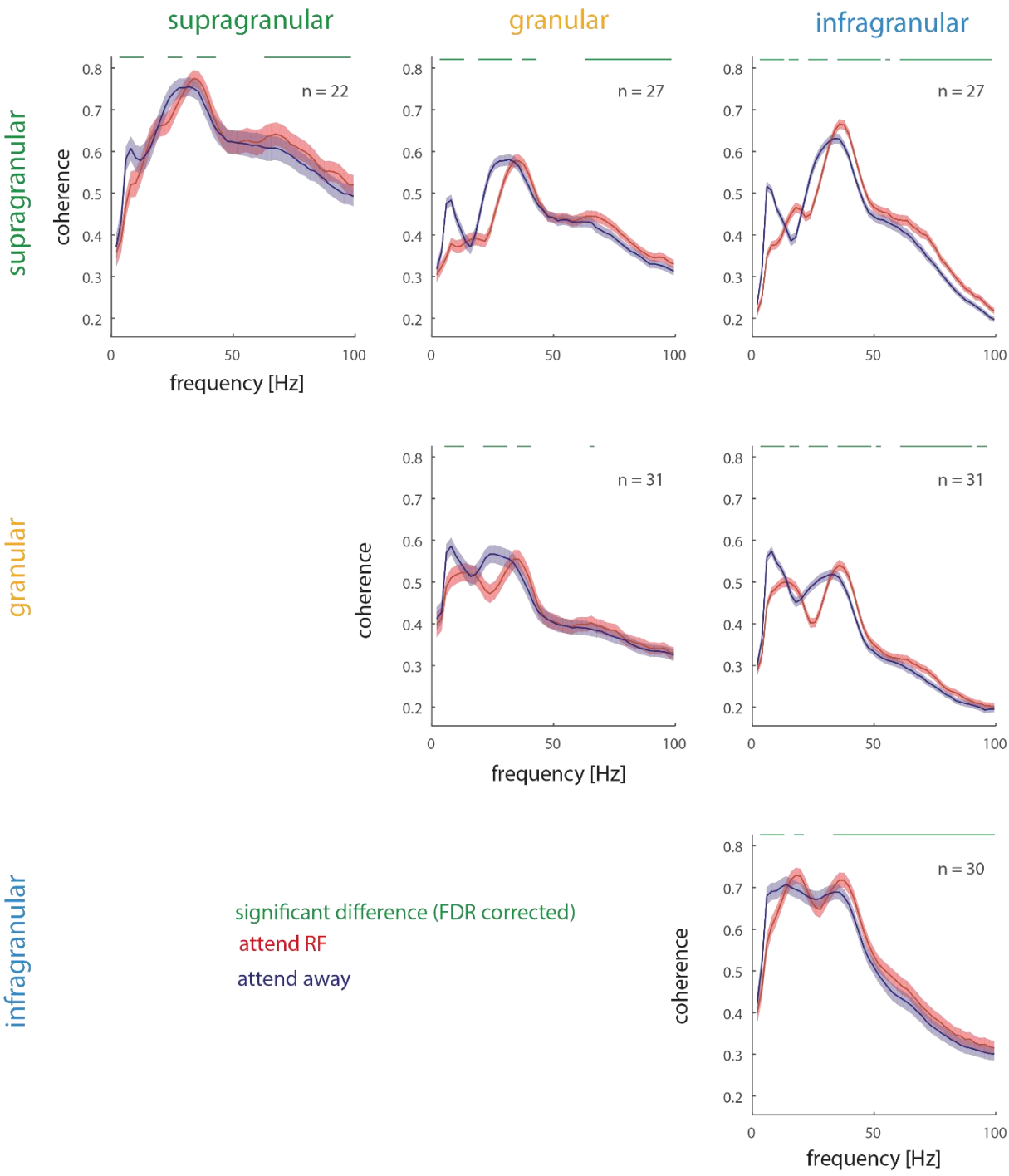

Figure 3-24: V1 field-field coherence in Monkey 1 aligned to the first dimming (-511ms to 0ms) in the attention task. Shown are all possible combinations of supragranular, granular and infragranular layer comparisons, averaged across the channels contributing to the respective sections (n = number of recordings in each plot). Plotted separately for the attend RF (red) and attend away (blue) conditions. Green bars indicate significant differences between the attention conditions (repeated measures Wilcoxon signed rank test, $p<0.05$, FDR corrected). Coherence calculation and V1 structure are as defined in Figure 3-21.

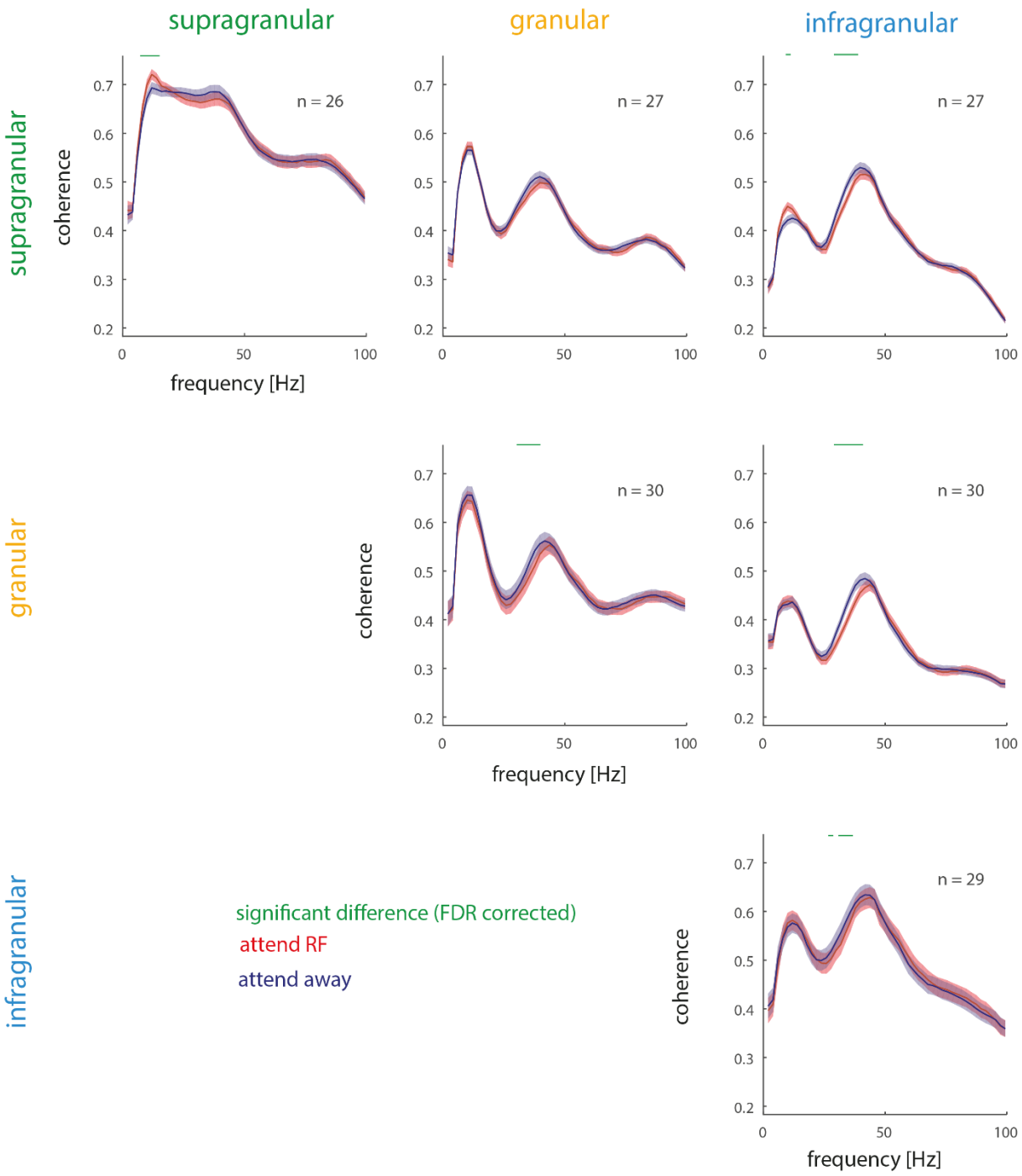

Figure 3-25: V1 field-field coherence in Monkey 2 (right hemisphere) aligned to the first dimming (-511ms to 0ms) in the attention task. Shown are all possible combinations of supragranular, granular and infragranular layer comparisons, averaged across the channels contributing to the respective sections (n = number of recordings in each plot). Coherence calculation, significance bars, attention conditions and V1 structure are as defined in Figure 3-24.

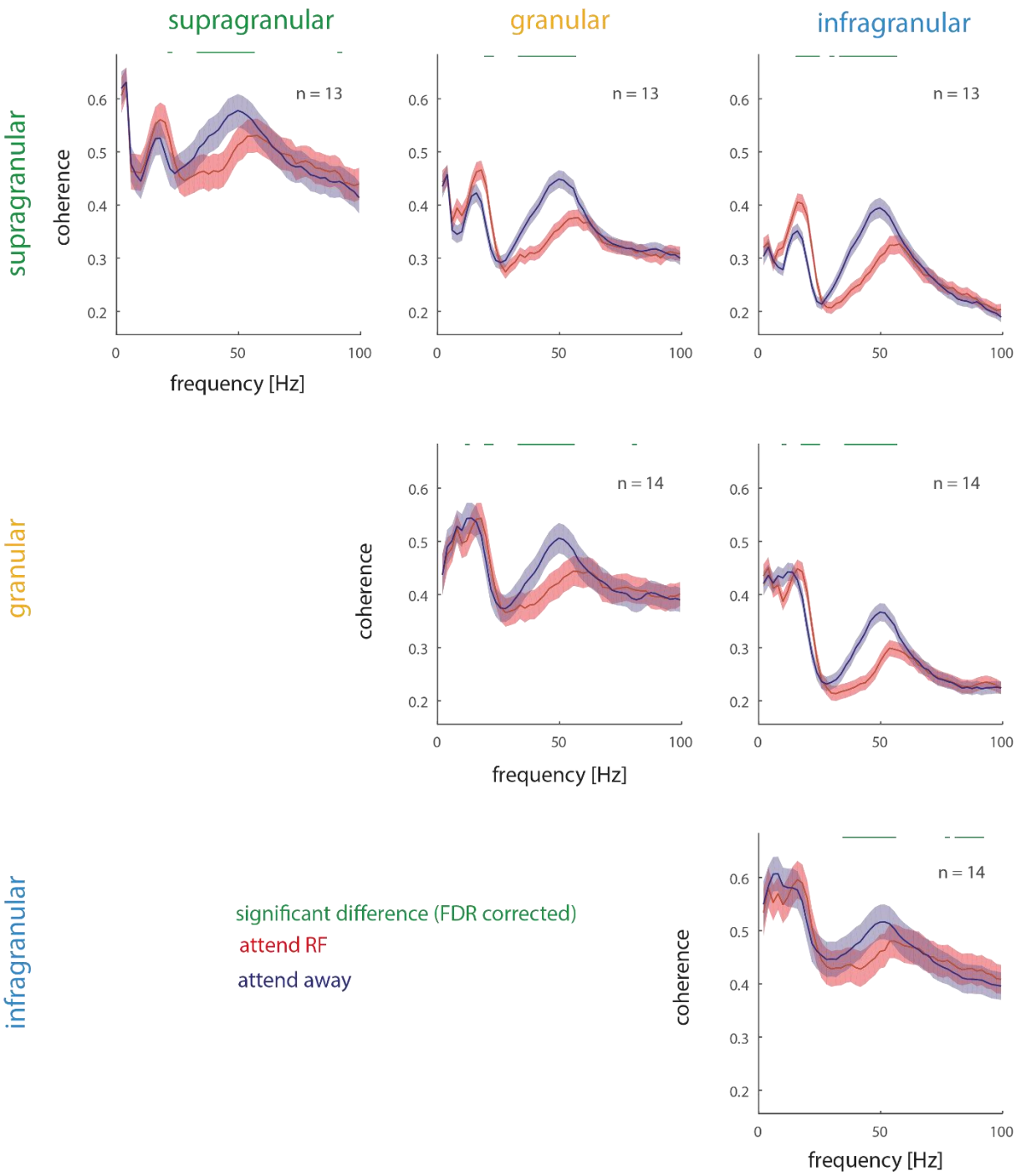

Figure 3-26: V1 field-field coherence in Monkey 2 (left hemisphere) aligned to the first dimming (-511ms to 0ms) in the attention task. Shown are all possible combinations of supragranular, granular and infragranular layer comparisons, averaged across the channels contributing to the respective sections (n = number of recordings in each plot). Coherence calculation, significance bars, attention conditions and V1 structure are as defined in Figure 3-24.

3.6 Granger causality

Coherence measures show to what extend two signals co-fluctuate, but do not yield insight whether one of the two signals causes the co-fluctuations in the other signal. To assess the latter, we calculated Granger causality between the bipolar derived LFPs of different layers of V1, giving a measure of the directionality of information flow in different frequency ranges. As in the other LFP analyses, aligning to the cue onset produced qualitatively the same attention effects which we observe prior to the first dimming period (albeit often smaller in magnitude). Given these similarities we do not show this time period separately in this section.

3.6.1 Granger causality after the stimulus onset

Granger causality is plotted in a slightly different manner than coherence was. Given the directionality of Granger causality, I decided to plot the two possible directions of influence in the same subplot (where different layers are involved). Thus, the (changed) colour code does not represent attentional modulation, but directionality. This is stated here explicitly at the outset, as it can otherwise easily cause confusion.

In Monkey 1 (Figure 3-27), the largest peak in the stimulus aligned V1 Granger causal spectrum was from the infragranular layers to the supragranular layers in the low-mid frequency range (~20Hz). This peak was not present in the opposite direction (supragranular to infragranular). This peak was also present in the infragranular to granular and infragranular to infragranular spectra. From supragranular to infragranular layers, there was a peak in Granger causality in the low gamma frequency range (~35Hz). In the other layer combinations, this peak occurred at a slightly higher frequency (35-65Hz). While the ‘downward’ Granger causality direction (down within a columns from higher to lower layers) clearly showed this pattern, it is noteworthy that the upward Granger causality equally showed a peak in the gamma range (~40Hz), which was even stronger than the downward Granger causality for the infra- to supra-, and the granular to supragranular comparisons.

In the recordings in the right hemisphere of Monkey 2 (Figure 3-28), the most prominent feature in the stimulus aligned Granger causality spectra was the

dominance of very low frequency components (peaking at close to 4 Hz or below), and a peak in the low gamma frequency range (30-50Hz). The former showed an ‘upwards’ directionality, while the directionality of the latter was dominant from supragranular sources. . There were also small peaks in the low frequency range (~8-10 Hz) which were mostly present in the downward direction, and probably reflect the ‘jitter’ component.

In the left hemisphere of Monkey 2 (Figure 3-29), the dominant Granger causality was in the low beta frequency range, whereby this was pronounced mostly for the upward direction. There were small peaks (or plateaus) of Granger causal interactions in the gamma frequency range (30-70Hz). The Granger causal interactions in this frequency band was also, generally stronger in the upward than in the downward direction, similar to what was found in Monkey 1, even if peak frequency locations do not match.

We also performed a separate cross correlation analysis (Appendix D.1) of V1 LFP signals to confirm the direction of information flow which was indicated by the Granger causal analysis.

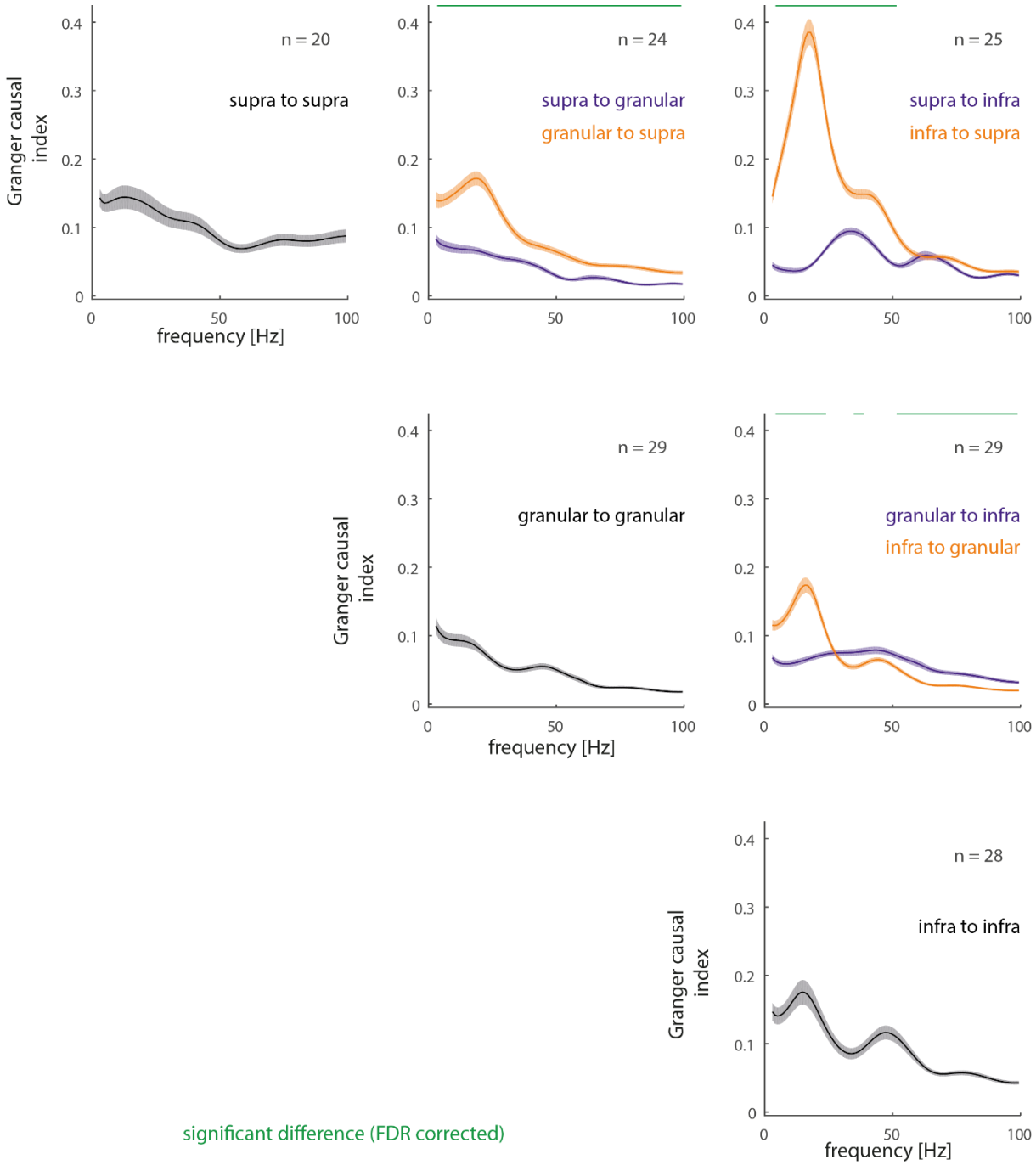

Figure 3-27: Granger causality in Monkey 1 V1 aligned to the stimulus onset (250ms to 761ms) in the attention task. Shown between all possible combinations of supragranular ("supra"), granular and infragranular ("infra") layers (n = number of recordings in each plot). Directionality of Granger causality spectra is indicated by the figure legends. Granger causality was calculated based on the bipolar derivation of the local field potential. Significance bars and V1 structure are as defined in Figure 3-24.

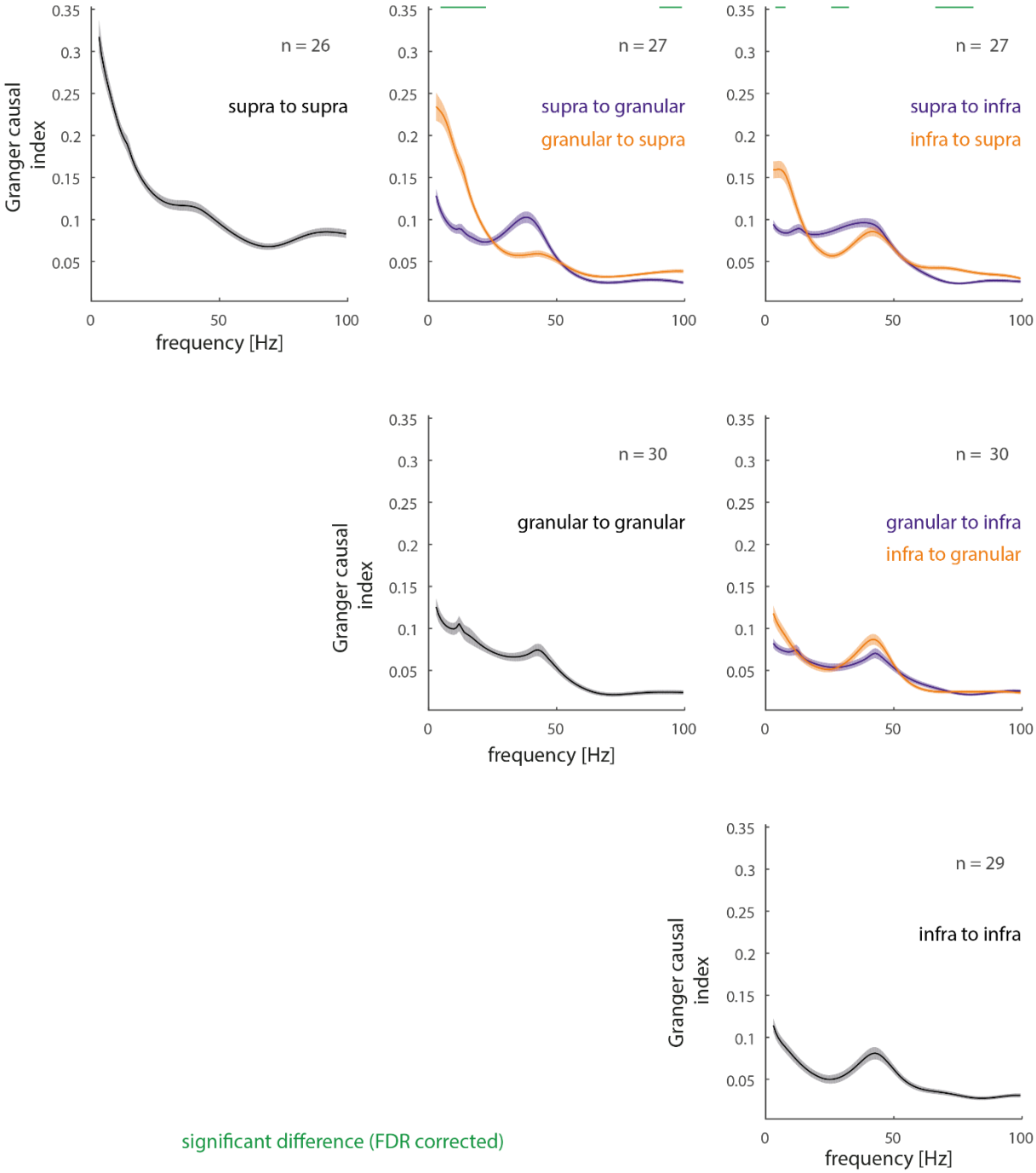

Figure 3-28: Granger causality in Monkey 2 (right hemisphere) V1 aligned to the stimulus onset (250ms to 761ms) in the attention task. Shown between all possible combinations of supragranular ("supra"), granular and infragranular ("infra") layers (n = number of recordings in each plot). Granger causality calculation, significance bars, directionality and V1 structure are as defined in Figure 3-27.

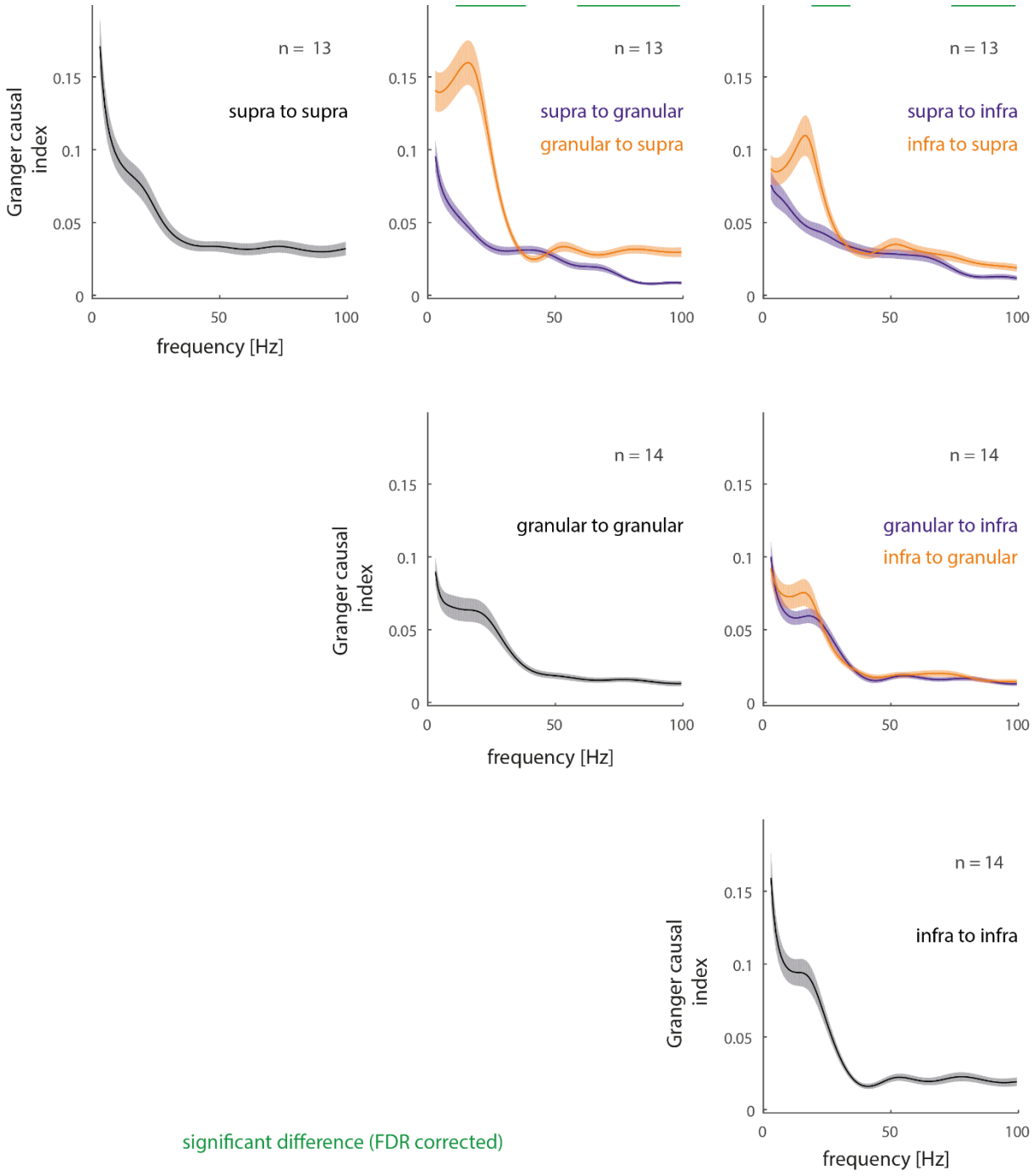

Figure 3-29: Granger causality in Monkey 2 (left hemisphere) V1 aligned to the stimulus onset (250ms to 761ms) in the attention task. Shown between all possible combinations of supragranular ("supra"), granular and infragranular ("infra") layers (n = number of recordings in each plot). Granger causality calculation, significance bars, directionality and V1 structure are as defined in Figure 3-27.

3.6.2 Granger causality prior to the first dimming

In Monkey 1 (Figure 3-30) there was a strong effect of attention on Granger causal influences from infragranular layers to supragranular layers, whereby attention to the RF shifted the Granger causal profile to higher frequencies, and increased the influence in the beta and gamma frequency range (at the same time reducing the influence in the theta/alpha frequency range (4-12 Hz). From supragranular to infragranular and from supragranular to granular layers there was a prominent effect of attention on Granger causal influences, whereby attention to the RF resulted in reduced Granger causal influence in the beta/low gamma frequency range (12-30 Hz) along with a small shift in peak frequency influence towards higher frequencies. Overall it appears that attention increases the influence of infragranular layers on supragranular layers in the beta and gamma frequency range, while the influence of supragranular on infragranular layers is reduced by attention.

In the right hemisphere of Monkey 2 (Figure 3-31), there was a significant decrease in low gamma Granger causality with attention between all layer combinations. However this decrease was smallest from the infragranular to supragranular layers, which may be in line with what was observed in Monkey 1. As with the previous power and coherence analyses, attention increased the peak frequency of low gamma Granger causality for all layer combinations in both monkeys.

Granger causality in the low gamma frequency range was lower in the attend RF condition for all layer combinations in the left hemisphere of Monkey 2 (Figure 3-32). The peak frequency in the attend RF condition was also higher than when attention was direction away. Low frequency Granger causality was increased with attention to the RF, however this was only significant from supragranular/infragranular to infragranular layers.

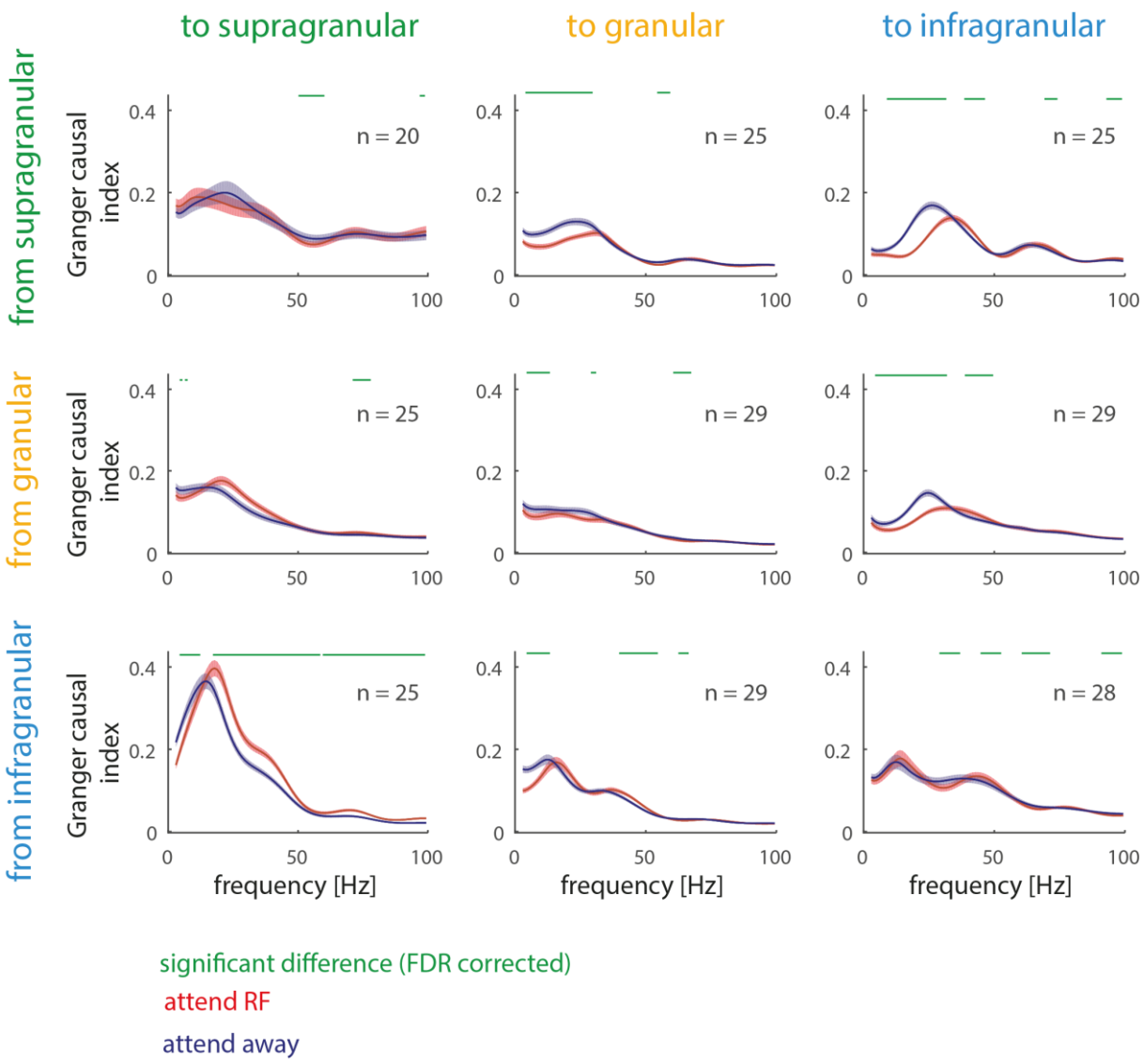

Figure 3-30: Granger causality in Monkey 1 V1 aligned to the first dimming (-511ms to 0ms) in the attention task. Shown are all possible combinations of supragranular, granular and infragranular layers (n = number of recordings in each plot). Plotted separately for the attend RF (red) and attend away (blue) conditions. Granger causality calculation, significance bars and V1 structure are as defined in Figure 3-27.

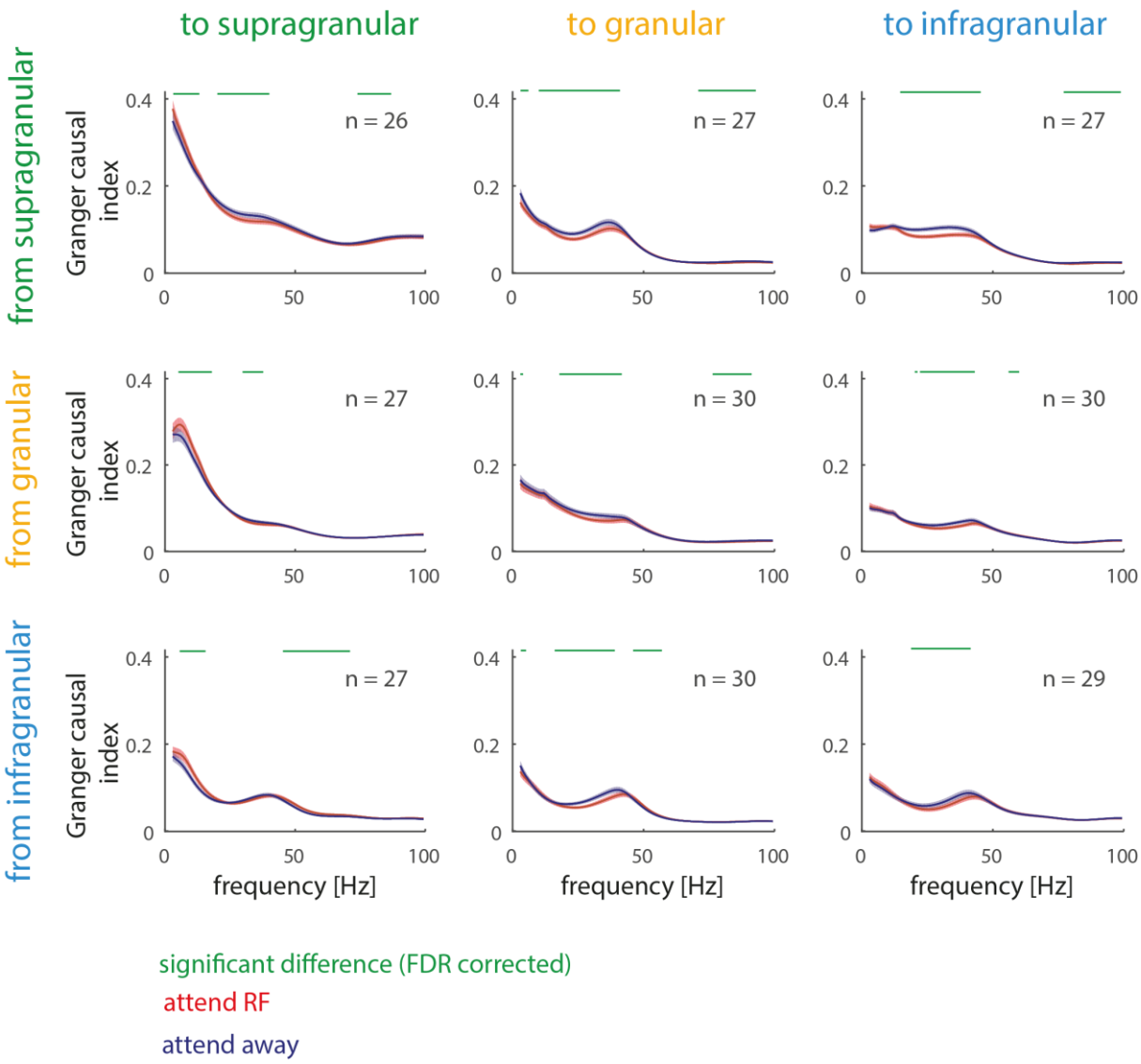

Figure 3-31: Granger causality in Monkey 2 (right hemisphere) V1 aligned to the first dimming (-511ms to 0ms) in the attention task. Shown between all possible combinations of supragranular, granular and infragranular layers (n = number of recordings in each plot). Granger causality calculation, significance bars, attention conditions and V1 structure are as defined in Figure 3-28.

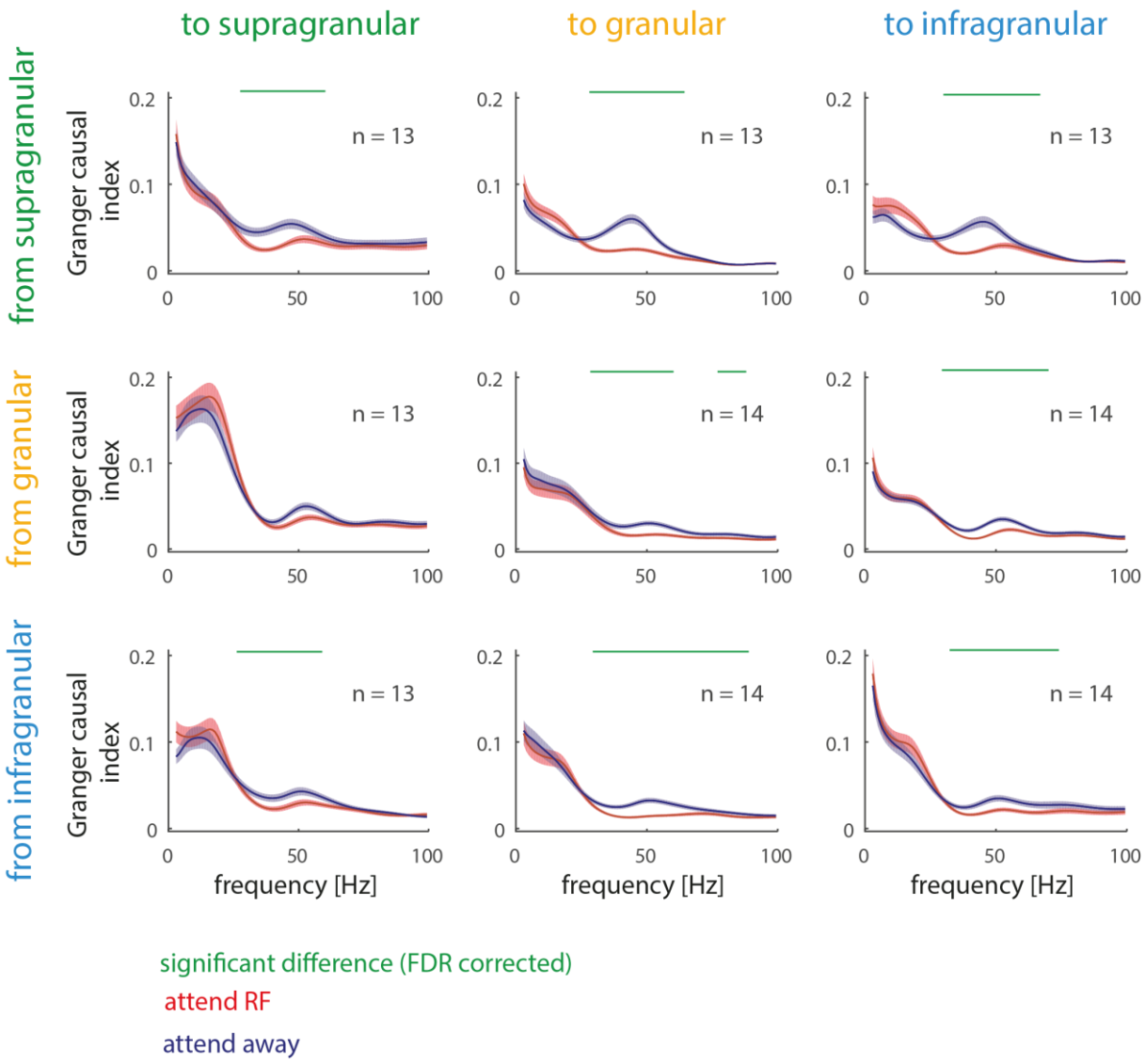

Figure 3-32: Granger causality in Monkey 2 (left hemisphere) V1 aligned to the first dimming (-511ms to 0ms) in the attention task. Shown between all possible combinations of supragranular, granular and infragranular layers (n = number of recordings in each plot). Granger causality calculation, significance bars, attention conditions and V1 structure are as defined in Figure 3-28.

3.6.3 Granger causal local networks

Next we analysed potential local networks of information flow in V1 based on the Granger causality (GC). For this we calculated modulation indices of Granger causal directionality (see Section 2.4.8). We calculated these MIs for the theta/alpha (4-12Hz), beta (13-25Hz), low gamma (30-50Hz) and high gamma (55-100Hz) frequency bands. The MIs are plotted in Figure 3-33. If the upward direction was more Granger causal influential, then MIs for a given contact pair are plotted in warm colours to the right of the electrode sketch. If the downward direction was more Granger causal influential, the MIs for a given contact pair is plotted in cold colours to the left of the electrode sketch. Only MIs where the upwards directionality was significantly different to the downwards directionality are shown in these figures. In the left hemisphere of Monkey 2 this meant that no channel pairs survived, so these analyses are not shown here.

Figure 3-33 (top) shows the stimulus aligned MI directionality of GC between each contact (relative to the alignment channel) in Monkey 1. In the theta/alpha and beta frequency ranges Granger causality was generally much stronger from deep to superficial channels than from superficial to deep channels (note that most arrows are upward pointing and show large positive MIs (red/dark red colours). This was the case for stimulus induced (stimulus aligned) directionality (top row of Figure 3-33), as well as for the directionality that was present before the first dimming (bottom rows of Figure 3-33). In the beta range, this directionality was stronger for the attend RF condition when aligned to the first dimming of the task. In the low gamma range GC directionality was also largely upwards from the deep layers to the superficial layers, but the strength of the directionality difference (MI) was reduced, when compared to lower frequency bands (note the reduction in red/dark red colours). Moreover, there was also downwards directionality from upper granular to infragranular. For the high gamma frequency range, significant directionalities were mostly short range and originated mainly in the granular layers.

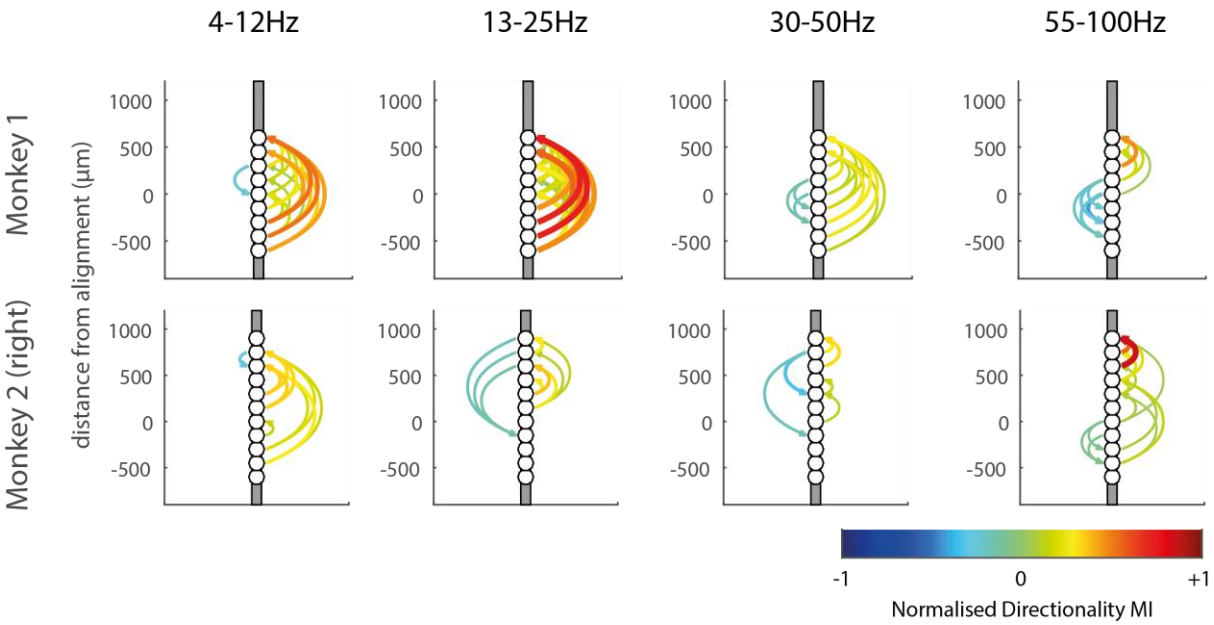

Figure 3-33: Granger causal directional dominance networks of V1 in Monkey 1 and Monkey 2 (right hemisphere) between electrode contacts relative to the alignment channel, aligned to the stimulus onset (250-761ms) task period. Calculated are Modulation indices for granger causal interactions based on downwards and upwards influences for any two contact pairs. These were calculated for the theta/alpha (4-12Hz), beta (13-25Hz), low gamma (30-50Hz) and high gamma (55-100Hz) frequency. Directionalities are calculated as a modulation index (MI) based on the Granger causality in each direction between all possible electrode contacts. Upwards (i.e. deep to superficial) directionalities are represented by positive MIs (yellow/red arrows) and drawn on the right hand side of the subplots. Downwards (i.e. superficial to deep) directionalities are represented by negative MIs (cyan/blue arrows) and drawn on the left hand side of the subplots. Only directionalities which were significantly different to zero are shown in these plots (Wilcoxon signed rank test, $p<0.05$ FDR corrected).

In the right hemisphere of Monkey 2 (Figure 3-33, bottom), upwards directionality in the theta/alpha band was prominent from the deep to the superficial layers, as well as within superficial layers. Downwards directionality dominated from the lower supragranular and from the granular layers to the infragranular layers, as well as within infragranular layers. In the beta frequency there was upwards directionality from the granular layers to the supragranular layers and a downwards component from the supragranular layers to the infragranular layers. Granger causal influences in the high gamma frequency range were more strongly upwards from infragranular layers to supragranular layers. Dominant downwards directionality originated in upper supragranular to lower supragranular, granular, and lower infragranular layers as well as from lower granular/upper infragranular to lower infragranular layers.

In the theta/alpha and beta ranges, upwards directionality was stronger for the attend RF condition (Figure 3-34, middle). There were no obvious attention effects on dominant directionality in the gamma frequency ranges.

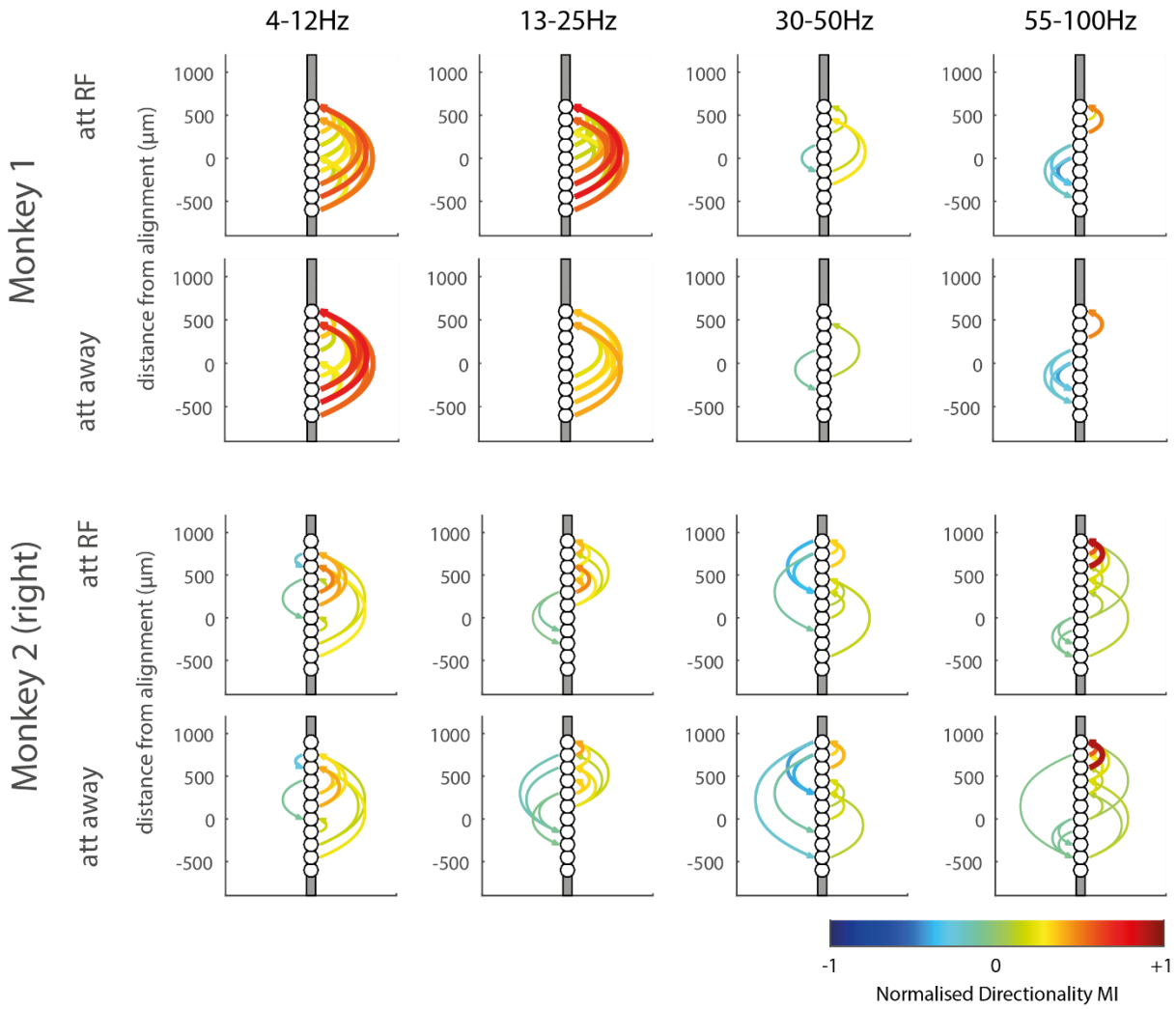

Figure 3-34: Granger causal local networks of V1 in Monkey 1 and Monkey 2 (right hemisphere) between electrode contacts relative to the alignment channel aligned to the first dimming (-511-0ms, separately for the attend RF [“att RF”] and attend away [‘att away”] conditions) period. Calculated for the theta/alpha (4-12Hz), beta (13-25Hz), low gamma (30-50Hz) and high gamma (55-100Hz) frequency bands. Directionality MI calculation and plotting as in Figure 3-33. Only directionalities which were significantly different to zero are shown in these plots (Wilcoxon signed rank test, $p<0.05$ FDR corrected).

3.6.4 Granger causal attentional networks

The previous analysis showed the dominant directions of Granger causal influences between V1 contacts for given stimulus or attention conditions, but it did not explicitly show how attention affected the strength of a given Granger causal interaction. To do the latter, we calculated attentional MIs of Granger causality (Figure 3-35). Attentional modulation of GC influences, was almost opposite in all frequency bands between the two monkeys. In Monkey 1, attention to the RF decreased CG for both directions in the theta/alpha frequency band, while in Monkey 2 GC increased in the upwards direction. In Monkey 1 upward GC increased with attention in the beta frequency band, with no significant effect on downwards GC. In Monkey 2 the downward GC decreased with attention. In Monkey 1 upward GC increased for the low gamma frequency range, while in Monkey 2 there was largely a decrease. A similar pattern (even is somewhat reduced) was present for the high gamma frequency range.

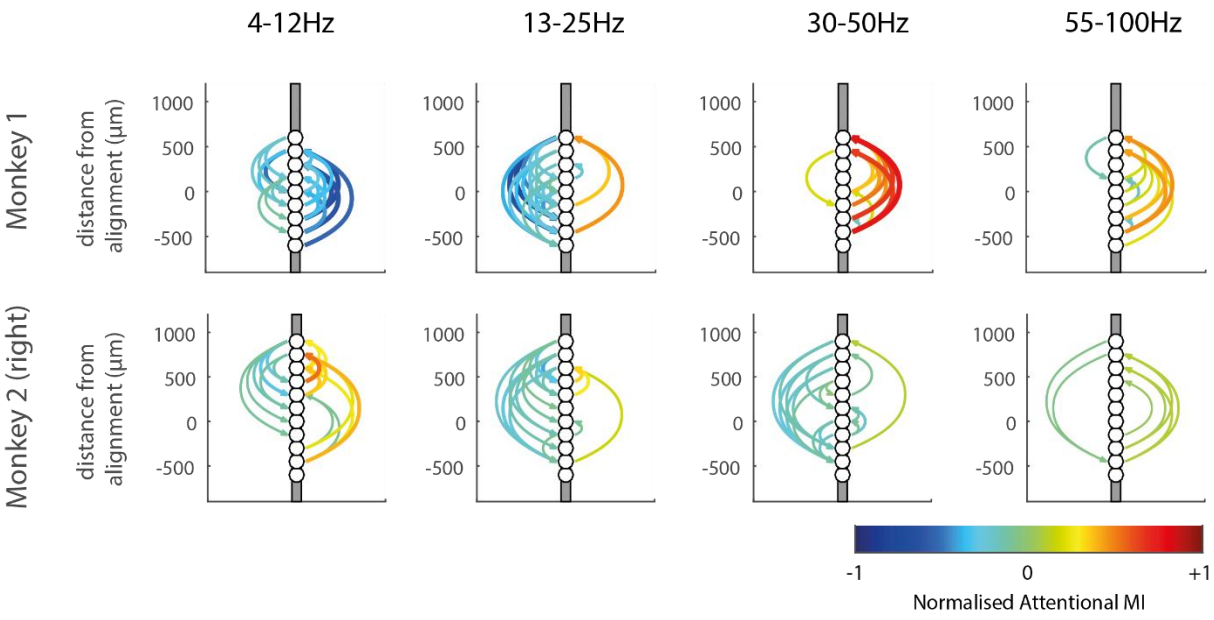

Figure 3-35: Attentional granger causal local networks of V1 in Monkey 1 and Monkey 2 (right hemisphere) between electrode contacts relative to the alignment channel. Calculated for the theta/alpha (4-12Hz), beta (13-25Hz), low gamma (30-50Hz) and high gamma (55-100Hz) in the first dimming aligned (-511-0ms) period. Attentional modulation index (MI) calculated from the Granger causality in each attention condition between all possible electrode contacts and normalised across the frequency ranges separately for each monkey/hemisphere. Attentional MIs for upwards (i.e. deep to superficial) directionalities are drawn on the right hand side of the subplots and downwards (i.e.

superficial to deep) directionalities are drawn on the left hand side of the subplots. Only modulation indices which were significantly different to zero are shown in these plots (Wilcoxon signed rank test, $p<0.05$ FDR corrected).

3.7 Summary

In this chapter, the behaviour of V1 activity during the attention task has been described. This was studied at the levels of multiunit activity, single cells, noise correlations and LFP power, coherence and Granger causality.

Attention to the RFs of V1 cells increased their multiunit activity, as well as increasing the firing rates of single cells. The variability of V1 responses was also reduced by attention, as measured by the Fano factor and gain variance. Variability between V1 cells was also reduced by attention, with noise correlations significantly lower when attention was directed into the RF of the recorded cells.

There was a discrepancy between subjects in the effects of attention on V1 LFP gamma power and coherence, with one monkey showing an increase and the other a decrease. Despite this discrepancy, both subjects showed an increase of the peak gamma frequency with attention.

Granger causality analysis suggested that the flow of information within V1 was upwards within cortical microcolumns, moving from deep layers to more superficial layers. It also showed that attention modulates the flow of information in V1, altering both the peak frequencies and magnitude of Granger causality.

Chapter 4: Results: Attentional Modulation of Neuronal Activity in the Extrastriate Cortex

4.1 Multiunit activity effects of attention

The following section describes the spiking activity of different V4 layers during different epochs of the attention task and how it is modulated by attention. As for the V1 analysis first the MUA_E activity will be described.

4.1.1 Stimulus aligned multiunit response

When aligned to the stimulus onset (Figure 4-1), we observed a similar response in the V4 envelope multiunit activity (MUA_E) as seen in the V1 MUA_E (Figure 3-1). There was an initial transient response occurring at around 50ms. After the transient peak there was small reduction of activity (not present in the V1 data) followed by a second increase in firing rate at roughly 250ms. The firing rate then stabilised to a persistent level which was higher than the initial baseline activity. Unlike in the V1 responses, we did not observe the lowest persistent firing rate to occur in the alignment channel. In Monkey 1 there was a difference between deep and superficial channels (One way ANOVA, $p<0.05$ between channels 2-5 and 9-12, counting from the lowest plot in Figure 4-1), with the superficial channels having a higher mean persistent firing rate relative to their transient response. In Monkey 2 there were no channel dependent differences in the persistent activity levels (One way ANOVA, $p>0.05$ between all channels for both stimulus types).

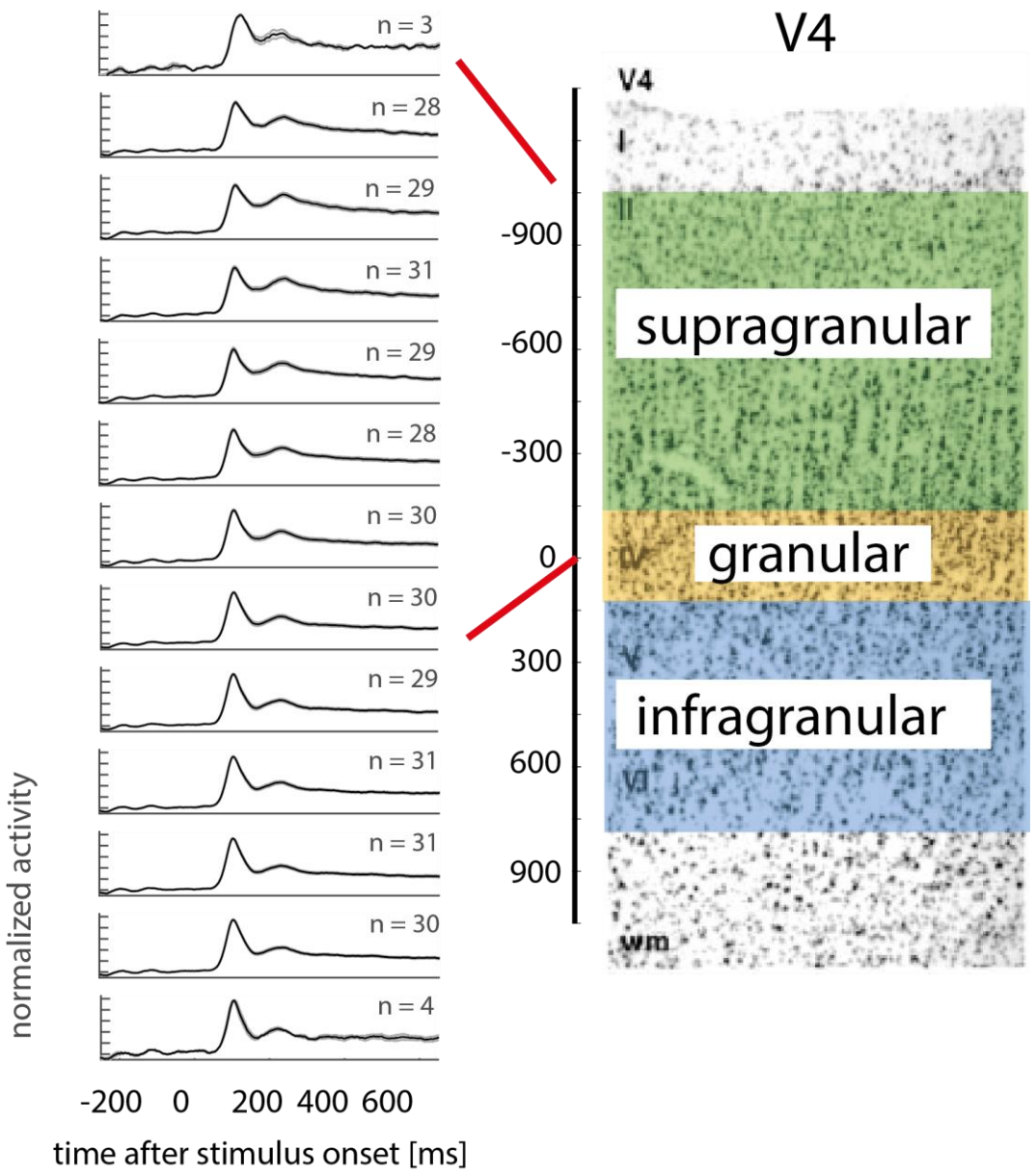

Figure 4-1- ***Left***: Monkey 1 average V4 normalised envelope multiunit activity (MUA_E) aligned to stimulus onset and spatially aligned to the layer 4 channel (n = number of recordings in each plot). ***Centre***: Sketch of an example electrode, showing how the average MUA_E plots align with actual electrode depths. ***Right***: Illustration of V4 architecture, split into supragranular, granular and infragranular cortical layers based on distance (µm) from layer 4 (Adapted from (Stepanyants *et al.* (2002))).

The MUA_E responses were then grouped based on the estimated cortical layer which they resided in (Figure 4-2). The difference between sustained response in the supragranular and infragranular layers of Monkey 1 was also significant after this grouping (One way ANOVA, $p<0.05$). For Monkey 2 right hemisphere, the supragranular sustained response was significantly larger than in both the granular and infragranular layers (One way ANOVA, $p<0.05$). No layer dependent differences were present in the left hemisphere (One way ANOVA, $p>0.05$). The non-smooth stimuli used in the right hemisphere recordings did not invoke a rhythmic artefact in the V4 recordings as they did in V1 (see Appendix A for more details).

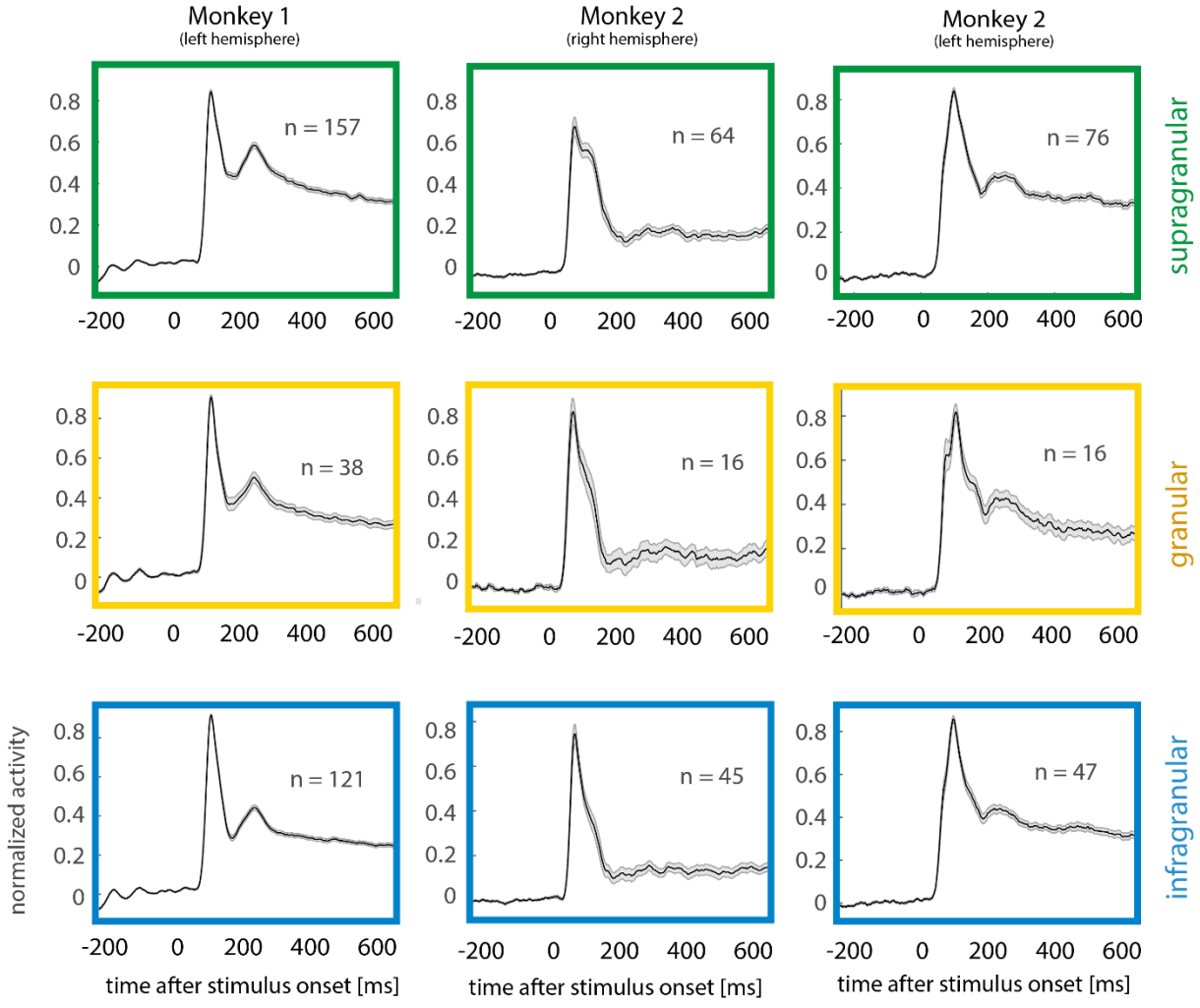

Figure 4-2 - Monkey 1 and Monkey 2 (right and left hemisphere) average V4 envelope multiunit activity (MUA_E) aligned to stimulus onset and grouped into supragranular (top, green), granular (middle, yellow) and infragranular (bottom, blue) layers (n = number of contacts in each plot). Normalisation and V4 structure are as defined in Figure 4-1.

4.1.2 Cue aligned multiunit response

In the left hemispheres of Monkey 1 and 2 there was an initial downwards deflection in the cue aligned MUA_E activity (Figure 4-3) shortly after the cue was presented. In the recordings in the right hemisphere of Monkey 2, this deflection was positive, indicating an excitatory response to the cue. The RFs of recorded V4 cells in the right hemisphere of Monkey 2 were typically more foveal than in the other recordings, which is consistent with an excitatory response to the cue. The downwards deflection in the other recordings could be due to the cue overlapping with the inhibitory surround of the recorded cells. Attentional modulation of the MUA_E activity was present in both monkeys, however in the right hemisphere of Monkey 2, this was mainly restricted to the supragranular layers.

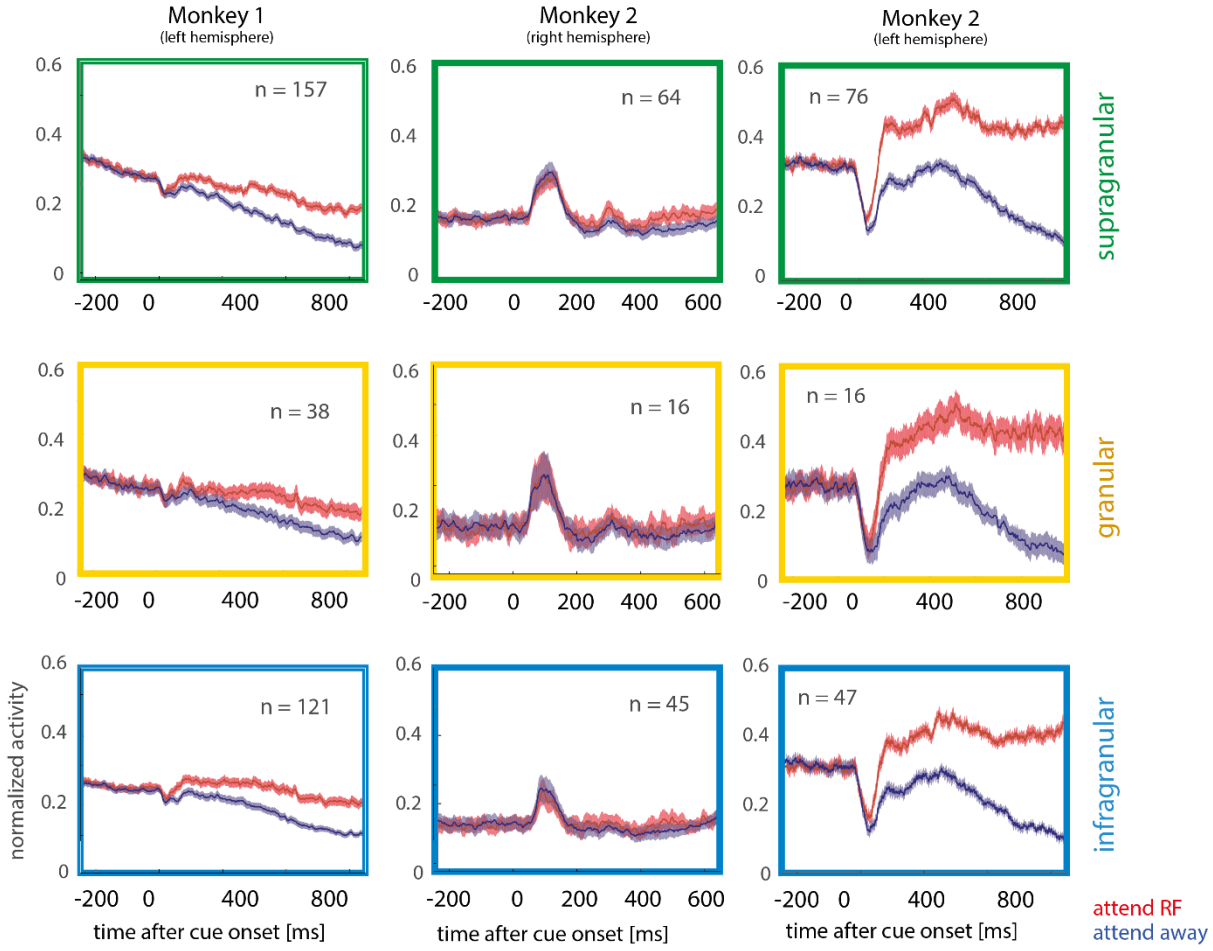

Figure 4-3 - Monkey 1 and Monkey 2 (right and left hemisphere) average V4 envelope multiunit activity (MUA_E) aligned to cue onset and grouped into supragranular (top, green), granular (middle, yellow) and infragranular (bottom, blue) layers (n = number of contacts in each plot). Plotted separately for the attend RF (red) and attend away (blue) conditions. Normalisation and V4 structure are as defined in Figure 4-2.

4.1.3 Dimming aligned multiunit response

As in V1, V4 attentional modulation was stronger when aligned to the first dimming Figure 4-4) than when aligned to the cue onset. Attentional modulation was stronger in the supragranular layers of the right hemisphere of Monkey 2, otherwise no layer dependent differences were found for the MUA_E analysis. After the first dimming occurred there was a positive deflection in the V4 MUA_E response, which was largest in the right hemisphere of Monkey 2.

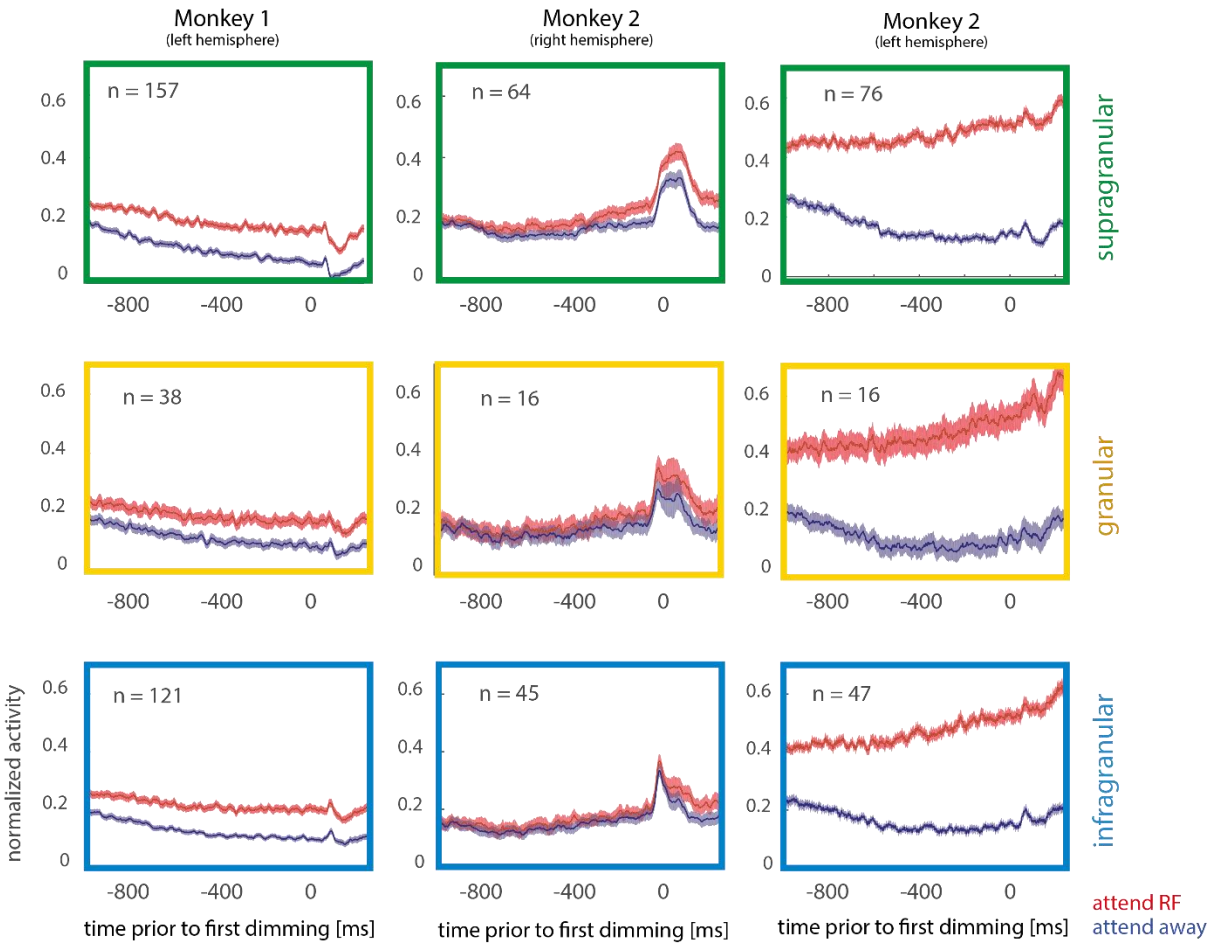

Figure 4-4: Monkey 1 and Monkey 2 (right and left hemisphere) average V4 envelope multiunit activity (MUA_E) aligned to the first stimulus dimming and grouped into supragranular (top, green), granular (middle, yellow) and infragranular (bottom, blue) layers (n = number of contacts in each plot). Normalisation, attention conditions and V4 structure are as defined in Figure 4-3.

4.2 Single cell effects of attention

We next performed a single cell analysis. This allowed us to investigate the diversity between different cells and different cell types. It also allowed us to analyse different aspects of neuronal activity, such as rate variability, which could not be calculated from the MUA_E activity. As described in the methods section, single cell spiking activity was derived from manual spike sorting with 'subjective' classification criteria ranging from 1-4, whereby classes 1 and 2 were sufficiently well isolated cells, to have good confidence in the spike waveform grouping and to label them as 'single units'. Only these cells will be analysed in the following section.

4.2.1 Classification of cell types

The distribution of peak to trough times in our sample of V4 single units has been shown in Figure 2-4. We recorded n=651 [total] cells (n=406 [Monkey 1], n=119 [Monkey 2, right], n=126 [Monkey 2, left]). The distribution was significantly non-unimodal, with a main dip in the distribution located at a peak to trough (P2T) time of about 250µs. As in the V1 distribution, the distribution of V4 P2T times suggests that there are multiple dips present, whereby broad spiking cells can possibly be further subdivided along a P2T dip location at ~330µs, while narrow spiking cells can be subdivided into three potential classes with one P2T dip located at ~200µs, and one located at ~160µs. The main dip is clearly located at 250µs in our data, so we used this as our separation point for cell type classification. Using a separation at 200µs yielded qualitatively identical results.

Table 4: Break down of cell types in V4. Numbers indicate whether cells were good (i.e. with a rating of 1 or 2), whether cells resided within our proposed microcolumn and whether the cells had attention effects.

Cell type	Total from V4 placed electrode	Good units	Good units with layer assignment	Good units with layer assignment and attention effects
broad	700	440	304	217
narrow	230	211	120	73

4.2.2 Cell types, laminar location and their relation to firing rate and rate variability

As already described for area V1 data, for this analysis all cells that were assigned to defined cortical layers were included. The procedures for this assignment were outlined in Section 2.4.14 for the MUA_E and the LFP activity, but identical steps were taken for the single cell alignment. This reduced our sample size quite considerably. We recorded 440 broad spiking single units and 211 narrow spiking units from area V4 (Table 4). Of these 346 broad spiking cells and 142 narrow spiking cells showed an activity level of >3Hz and were recorded for >20 trials for each condition throughout all periods of interest. Layer assignment according to the criteria described was possible for 296/346 broad spiking cells and 118/142 narrow spiking cells from area V4. These cells were then subjected to further analysis as shown in e.g. in Figure 4-5.

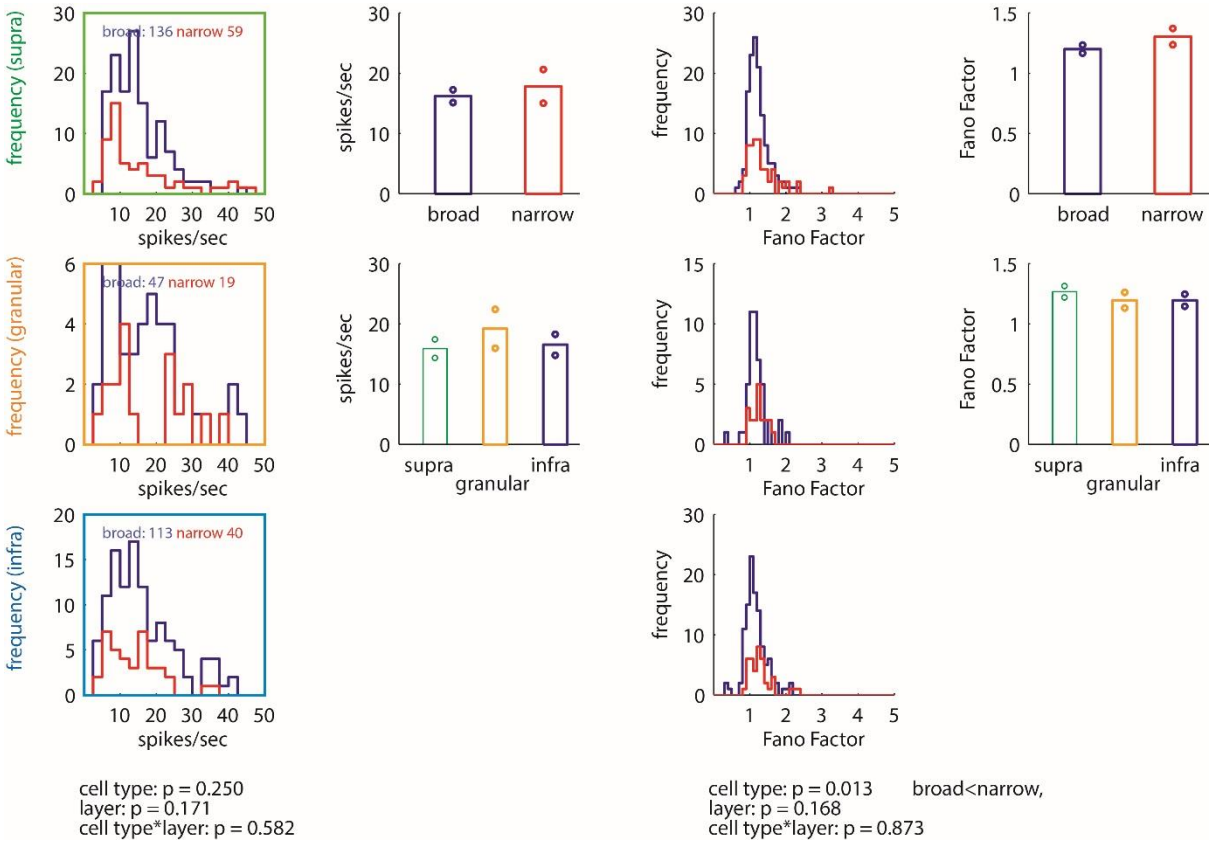

Figure 4-5: Distribution and summary statistics of firing rates and Fano-factors for broad and narrow spiking V4 cells located in supra, granular, and infragranular layers respectively. A) Distribution of firing rates for narrow (red) and broad (blue) spiking cells in supra (green), granular (yellow), and

infragranular (light blue) layers. Relative cell numbers recorded in each layer are given as insets. P-values below the graph show whether the factors 'celltype' or 'layer' significantly affected firing rates, and whether there was an interaction. B) Mean and 95% confidence interval of firing rates for narrow (red) and broad (blue) spiking cells. C) Mean and 95% confidence interval of firing rates for the three different layer subdivisions. D) Same as A, but with Fano-factor as the variable of interest. Where post-hoc testing revealed significant differences these are indicated by quantitative comparisons, whereby the size difference is indicated by < and >, respectively. E) Same as B, but with Fano-factor as the variable of interest. F) Same as C, but with Fano-factor as the variable of interest.

4.2.3 Attention induced activity changes relative to pre-cue activity

We calculated a cue response modulation index (cue response MI) for the attend RF and the attend away conditions in V4 cells. The distributions of precue MIs for both monkeys (pooled) for the two areas and the different cell types (narrow vs. broad spiking) are shown in Figure 4-6. For both cell types the distributions of pre-cue MIs differed significantly for attend RF and attend away conditions ($p<0.001$, Wilcoxon signed rank test). The distribution means for attend RF conditions were significantly positive (see Figure 4-6 insets 'p(RF)' for exact values). The distribution means for attend away conditions were significantly smaller than zero (see Figure 4-6 insets 'p(away)' for exact values). There was a significant difference ($p<0.001$, Wilcoxon signed rank test) between the two attention conditions in both narrow and broad spiking cells.

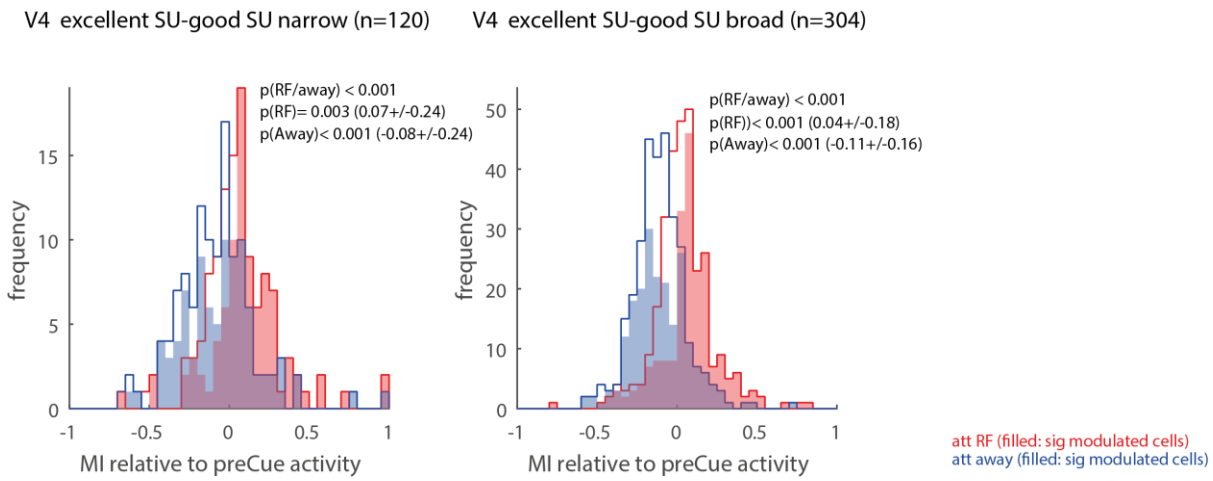

Figure 4-6: Distribution of cue response modulation indices (MI) in both monkeys (pooled), for narrow and broad spiking cells in area V4. Cell sorting quality was '2' or better. Blue histograms show MIs for the "attend away" condition, red histograms for the "attend RF" condition. Shaded histograms show distributions for cells that showed

significant modulation relative to pre-Cue activity, outlines show distributions of all cells. N indicates sample sizes. Insets give significance that attend RF and attend away conditions differed significantly [P(RF/away)], and significance that the respective individual distributions significantly differed from zero [P(RF), P(away)], along with distribution means and standard deviations.

4.2.4 Effect of attention of firing rates and on rate variability

We next calculated the effects of attention on firings rates on V4 cells in different layers and task periods. Figure 4-7 shows example raster plots of V4 cells in different layers of V4, plotted separately for the different attention conditions and epochs in the attention task.

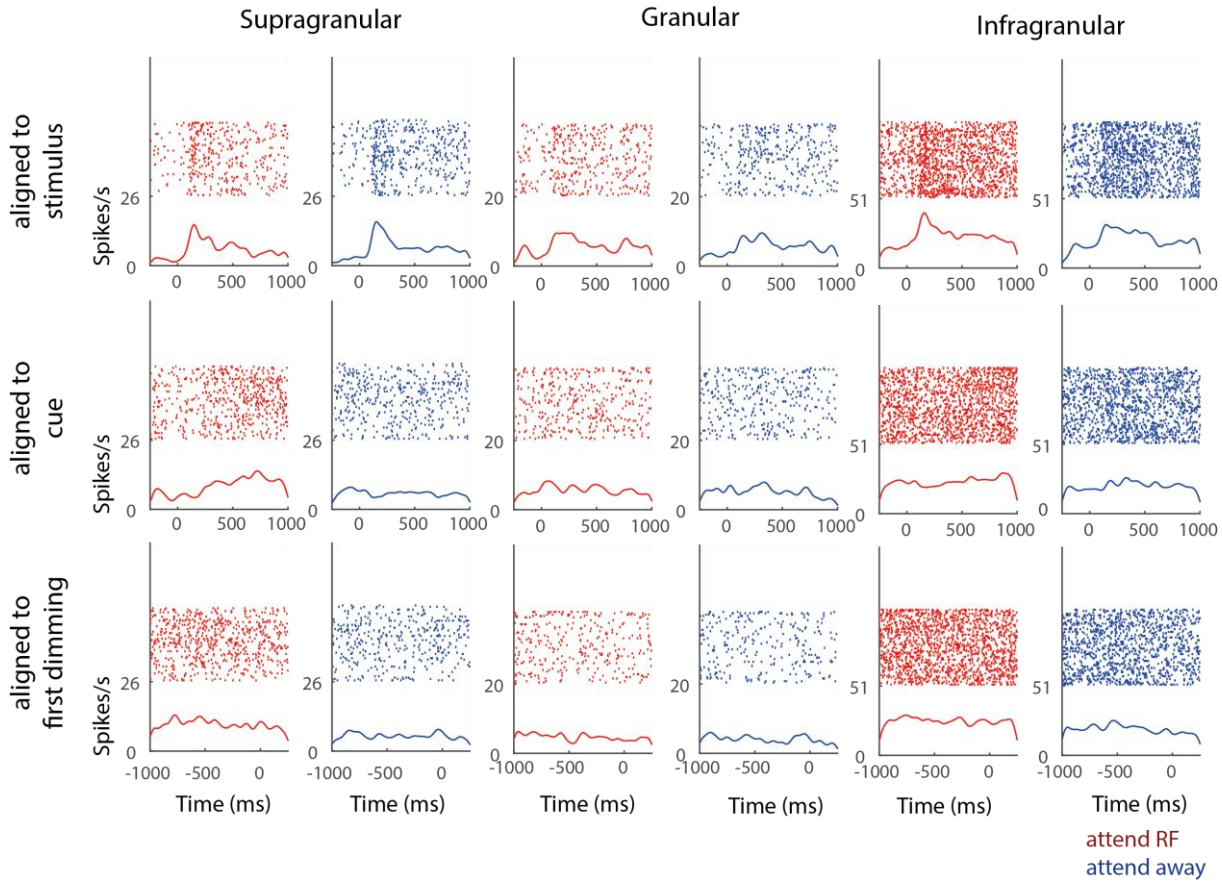

Figure 4-7: Example raster plots of spiking activity in V4, aligned to the stimulus onset, cue onset and prior to the first dimming. Data are shown for a recording channel in the supragranular, granular and infragranular layers in Monkey 1. Plotted separately for the attend RF (red) and attend away (blue) conditions. Underneath each raster plot is a histogram showing the spike rate against time throughout the task period.

The effects of attention on firing rates and rate variability were calculated for area V4. Figure 4-8 shows the firing rates and the FF of V4 neurons (separately for broad and narrow spiking cells). Inclusion criteria and statistical tests performed were identical to those described above for V1 cells. The figure shows the effects for cells that were significantly modulated by attention during the pre-dimming period (narrow spiking cells: n=73/211, broad spiking cells: n=217/440).

Attention to the RF resulted in significantly higher firing rates in narrow and in broad spiking cells ($p<0.001$ each, Wilcoxon signed rank test) for the cue and the dimming period (Figure 4-8, cue period not shown), but no significant effects for the stimulus onset aligned period ($p>0.4$ each, Wilcoxon signed rank test, not shown). The mixed model ANOVA revealed significant main effects of attention, layer, task period and cell-type. There were significant interactions between cell-type and layer, between cell-type and task period and between task period and attention.

Attention did not significantly affect the FFs in our study in any of the periods of interest ($p>0.2$, Wilcoxon signed rank test). The mixed model ANOVA revealed significant main effects of analysis period, cell-type and layer on FFs ($p<0.001$). There were also interactions between cell-type and period and between cell-type and layer.

Similar results were obtained, when all cells (not just those that were significantly affected by attention) were included in the study. This sample equally showed significant effects of attention on firing rate during the cue and dimming period for both cell types ($p<0.001$, Wilcoxon signed rank test, data not shown), but no effects of attention on the FF ($p>0.1$, Wilcoxon signed rank test, data not shown).

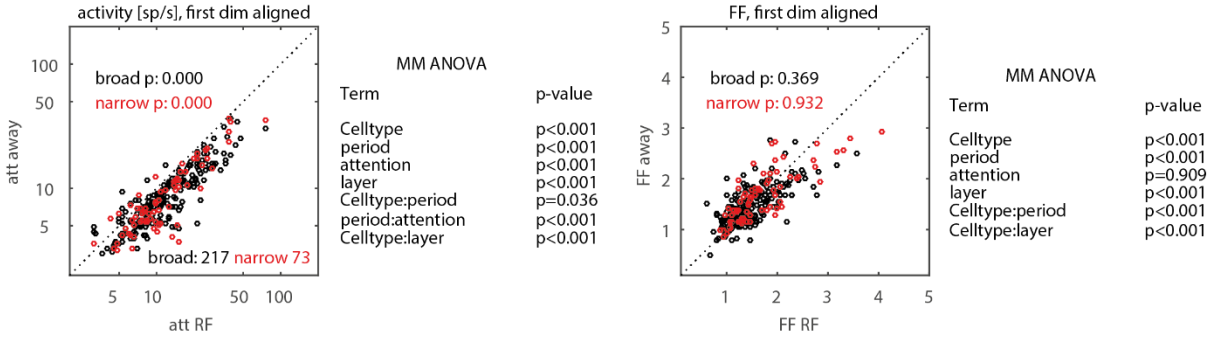

Figure 4-8: V4 firing rates (left column) and Fano-factors (FF, right column) in both monkeys (pooled) for the first dim aligned task period, for the two cell types (narrow spiking: red, broad spiking black, sample sizes (n) are indicated in the top left subplot). Ordinate: parameter of interest during the "attend RF" period. Abcissae: parameter of interest during the "attend away" period (attend away parameters are averages across the two attend away conditions, see methods for details). P-value insets indicate whether attend RF and away parameters differ significantly. The main effects of mixed model ANOVAs are shown to the right of plots, with interactions shown only if significant.

To understand which subconditions differed, and the directionality of the differences, we used paired t-tests. We found that firing rates were higher in narrow spiking cells than in broad spiking cells (Figure 4-9A). Infragranular layers had significantly higher firing rates than supragranular layers, but there were no significant differences with the granular layers (Figure 4-9B). The firing rate was also higher in the stimulus aligned period than in the rest of the task (Figure 4-9C). We did not see any differences in attentional modulation between the different layers (Figure 4-9D), which is consistent with the absence of an interaction in the ANOVA. The largest difference between the stimulus aligned period and the rest of the task was in the supragranular layers (Figure 4-9E and p-values in Figure 4-9G). There was no attentional modulation in the stimulus aligned period, but there were significant modulations in the cue and dim aligned periods (Figure 4-9F).

Fano factors were larger for narrow spiking cells than for broad spiking cells (Figure 4-10A). We also found significantly higher FFs in the supragranular than in the infragranular layers (Figure 4-10B). We saw the largest FFs in the dim aligned period of the task, with the smallest in the stimulus aligned period (Figure 4-10C). There were no pairwise differences between layer and attention (Figure 4-10D). The interaction between FF for layer and task period, revealed by the ANOVA, occurred because FFs in the granular layer were essentially identical for the stimulus aligned and cue aligned

periods, while they differed for the other layers (Figure 4-10E and Figure 4-10G). There were no pairwise interactions between attention and task period (Figure 4-10F).

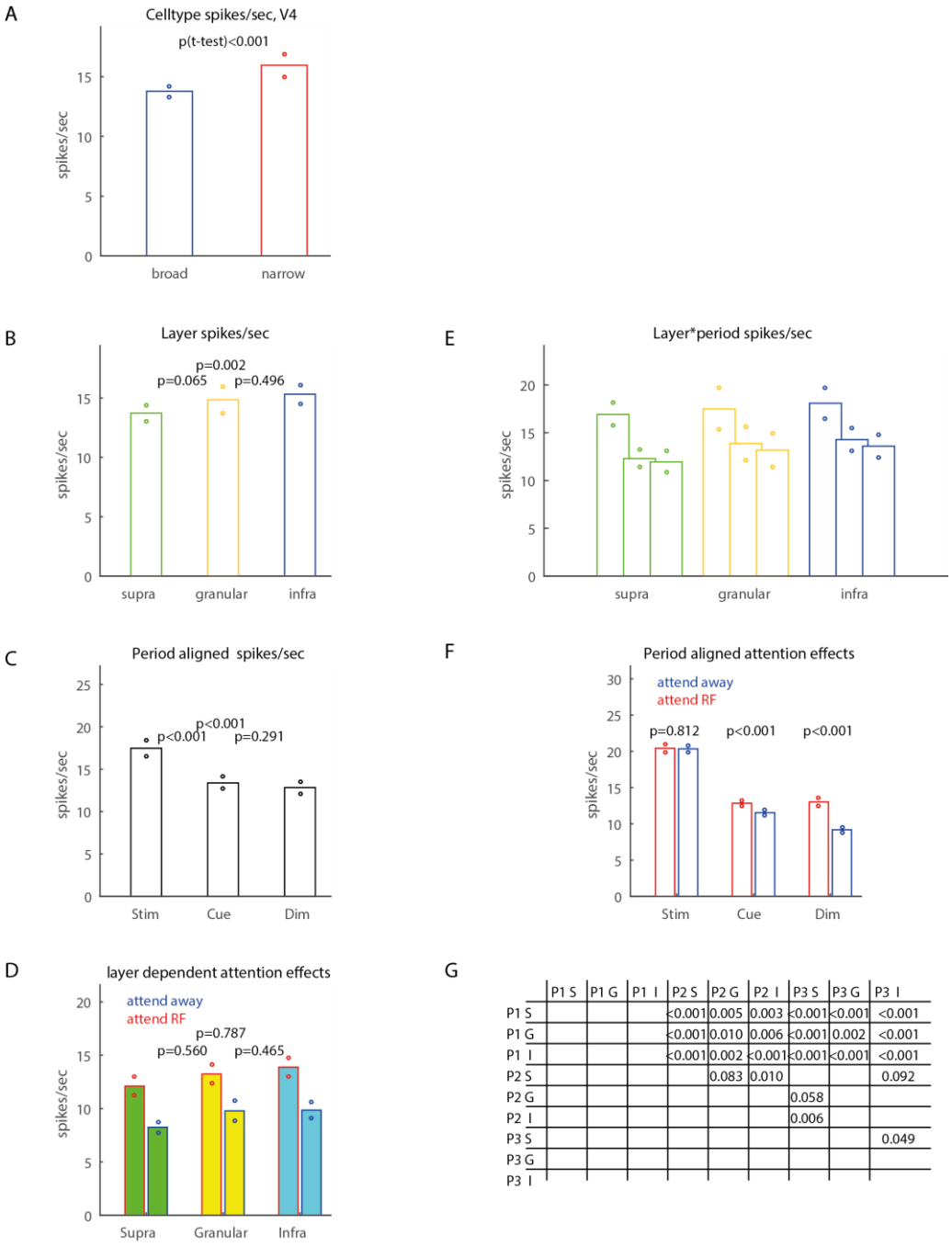

Figure 4-9: Breakdown of the effects of attention, celltype, period and task on firing rate in V4. **A**: Firing rates for broad (blue) and narrow (red) spiking cells. **B**: Firing rates for supragranular (supra, green), granular (yellow) and infragranular (infra, blue) layers. **C**: Firing rates during the three task periods. **D**: Interaction of attention and layer on firing rates. **E**: Interaction of layer and period on firing rates. **F**: Interaction of attention and task period on firing rates. **G**: p-values for combinations of task period (P1=stim, P2=cue, P3=dim) and layer (S=supragranular, G=granular, I=infragranular), shown only for p<0.1. **All**: P-values are calculated as t-tests between the groups and circles around bars indicate 95% confidence intervals.

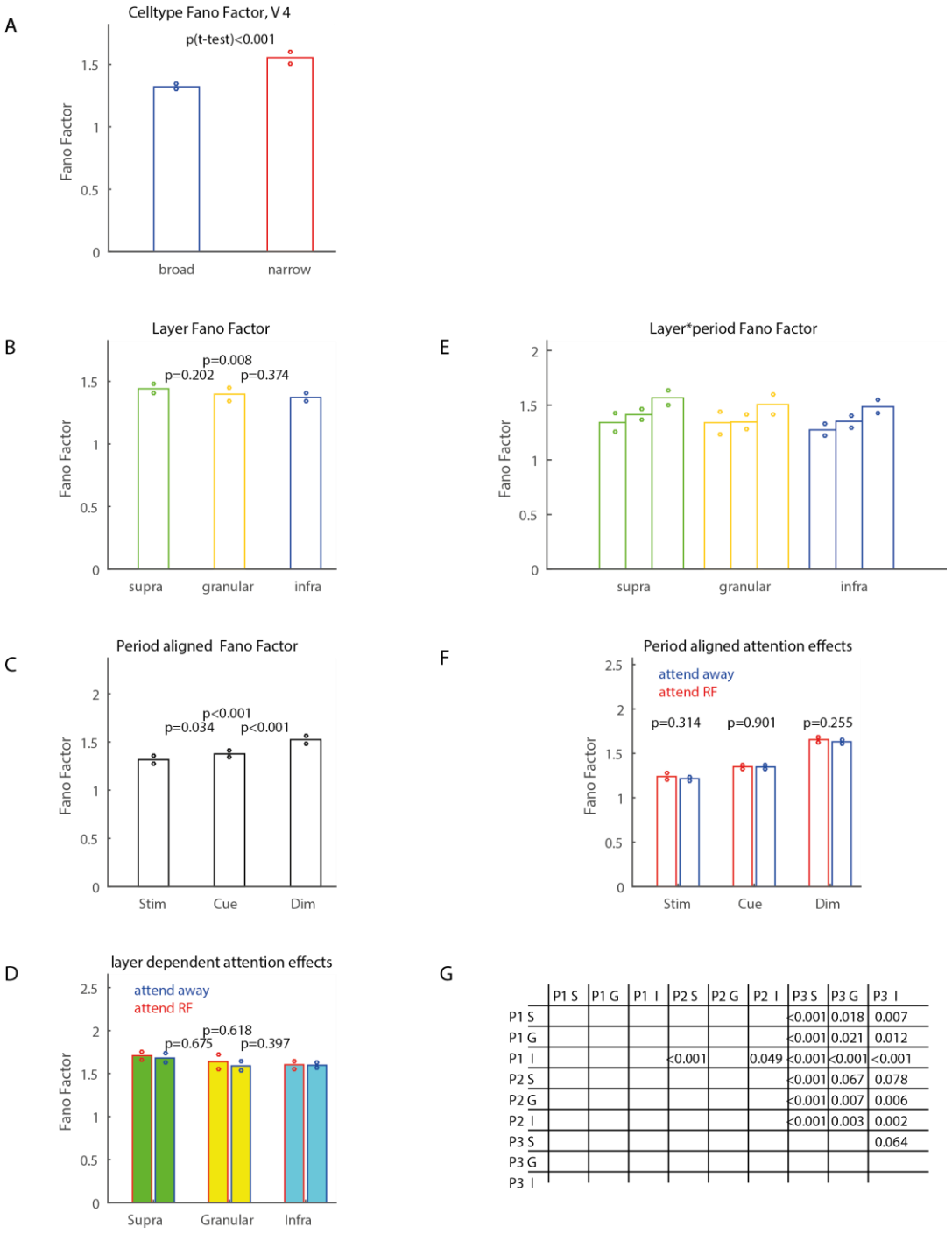

Figure 4-10: Breakdown of the effects of attention, celltype, period and task on Fano factor in V4. Subplots and statistics are as in Figure 4-9, but with rate substituted for Fano factor.

We next analysed whether gain variance was affected by attention in V4, as it may be the more sensitive parameter to measure rate variability (in comparison to FF). In V4 there was a significant reduction of gain variance with attention when pooled across

narrow and broad spiking cells (Wilcoxon signed rank test, p<0.001). In both cell types the effects of attention were also significant (Wilcoxon signed rank test, p<0.001). The exact p-values are plotted in Figure 4-11, along with the distributions of Gain variance for attend RF vs. attend away conditions and the sample means and S.E.M.s. In area V4, there was also a significant difference between gain variance in narrow vs. broad spiking cells (p<0.001, Wilcoxon signed rank test).

A mixed model ANOVA uncovered significant main effects of cell-type, attention and layer. There were also interactions of cell-type and attention and between cell-type and layer.

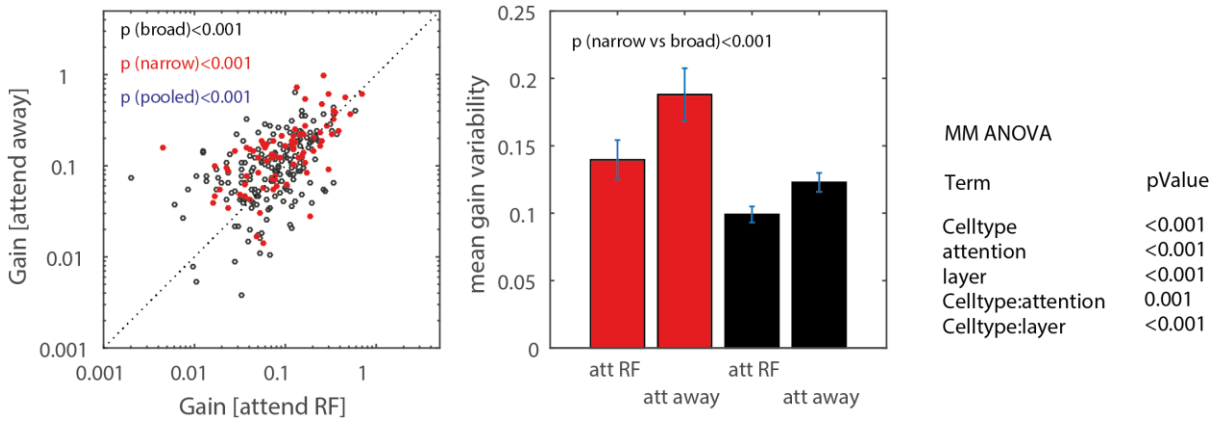

Figure 4-11: Effect of attention on gain variance in broad and narrow spiking cells in both monkeys (pooled). Left: Gain variance for the attend RF (x-axis) and attend away (y-axis) condition for broad (grey) and narrow (red) spiking cells. P-values indicate whether attention significantly affects gain variance (Wilcoxon signed rank test). Right: mean and S.E.M. for gain variance distributions (p-values indicate whether gain variance differed between narrow and broad spiking cells. The main effects of a mixed model ANOVA are shown to the right, with interactions shown only if significant.

Gain variance was significantly higher in narrow spiking cells than in broad spiking cells (Figure 4-12A). Supragranular layers had significantly higher gain variance than both granular and infragranular layers (Figure 4-12B). Attentional modulation of gain variance was larger for narrow spiking cells than broad spiking cells (Figure 4-12C). There were no differences between gain variance when we looked at pairwise interactions of layer and attention and layer, cell-type and attention (Figure 4-12D and Figure 4-12E).

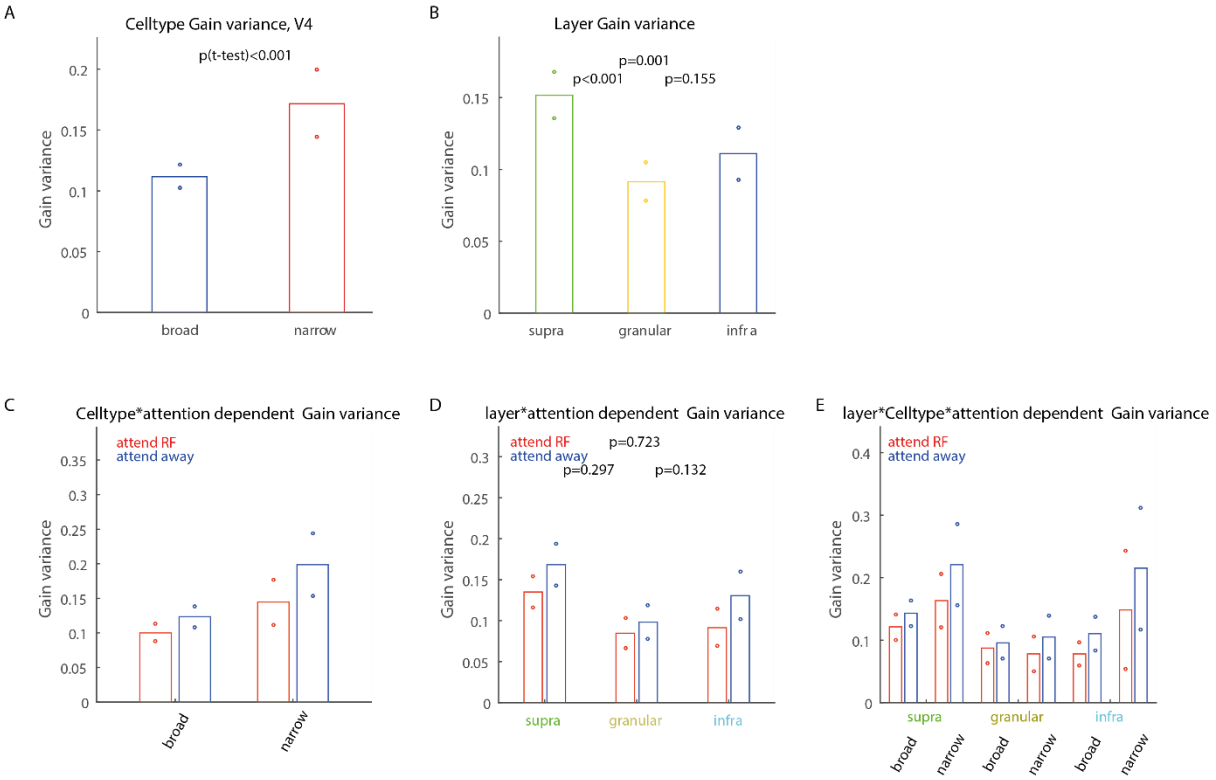

Figure 4-12: Breakdown of the effects of celltype, layer, and task on gain variance in V4. **A**: Gain variance for broad (blue) and narrow (red) spiking cells. **B**: Gain variance for supragranular (supra, green), granular (yellow) and infragranular (infra, blue) layers. **C**: Interaction of attention and cell type on gain variance. **D**: Interaction of layer and attention on gain variance. **E**: Interaction of layer, cell type and attention on gain variance. **All**: P-values are calculated as t-tests between the groups and circles around bars indicate 95% confidence intervals.

4.2.5 Quantification of attentional effects on spiking activity

To quantify attentional modulation we calculates two measures, the attentional modulation index (MI and the Area under the Receiver Operating Characteristics curve (AUROC). The distributions for both monkeys (pooled) are shown in Figure 4-13. The cue and dimming aligned distributions of both broad and narrow cells were significantly different from zero for both cell types ($p<0.001$, Wilcoxon signed rank test).

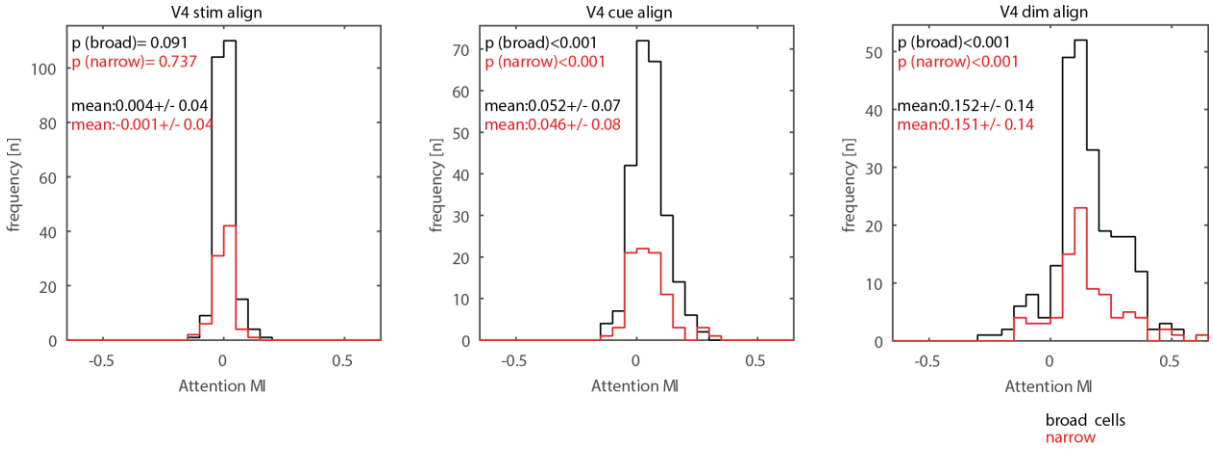

Figure 4-13: Distributions of attentional modulation indices for the 3 different alignment periods (columns) in V4 of both monkeys (pooled). Red shows narrow spiking cell MI distributions, black shows broad spiking cell MI distributions. Blue p-values indicate whether broad and narrow spiking cell MI distributions significantly differ, black and red p-value labels in subplots indicate whether respective distribution means are significantly different from zero.

Figure 4-14 shows the ROC distributions of broad and narrow spiking cells plotted against the cue response MI values for area V4 recorded in both monkeys (pooled). As for area V1, the cell types were equally likely (or equally unlikely really) to have AUROC values <0.5 (i.e. attention induced reduction of firing rates). They also did not differ in their attend RF pre-Cue modulation index.

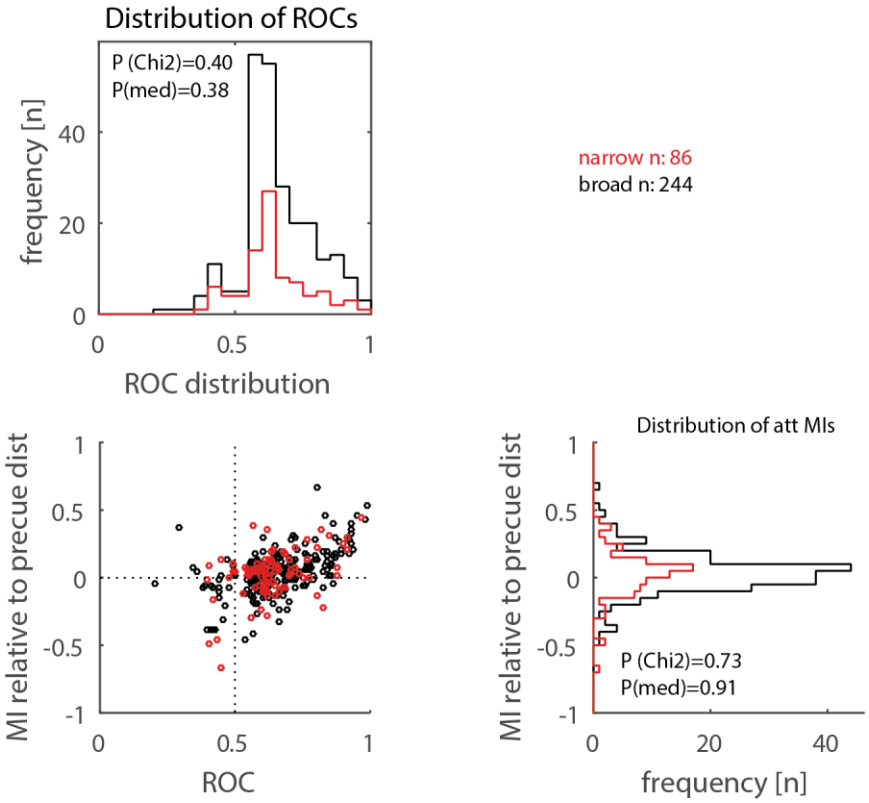

Figure 4-14*:* A) Area under the receiver operating characteristic (AUROC) values for broad and narrow spiking cells plotted against the cue response modulation index (MI, attend RF activity relative to precue activity) in V4 of both monkeys (pooled). Black data points and histograms represent broad spiking cells, red data points and histograms represent narrow spiking cells. B) Distribution of AUROC values for the two cell types. C) Distribution of MI values for the two cell types. P-values indicate whether the broad and narrow spiking cell AUROC or MI distributions (the medians) were significantly different (P (med)), and whether the narrow spiking cells significantly less often showed MIs<0 or AUROC values <0.5 (P (Chi2)) compared against broad spiking cells.

4.3 The effects of attention on noise correlations

We calculated noise correlations between V4 cells, aligned to the stimulus onset, cue onset and first dimming (Figure 4-15). As in V1, V4 noise correlations were positive in all periods of the attention task. In Monkey 1, noise correlations were lower for the attend RF condition when aligned to the first dimming of the task. Attention was significantly lower for the attend RF condition when noise correlations for the left hemisphere of Monkey 2 were aligned to both the cue onset. In the right hemisphere of Monkey 2 we did not find any attentional modulation of noise correlations however there was a trend for lower noise correlations in the attend RF condition in both the cue aligned and first dim aligned task periods.

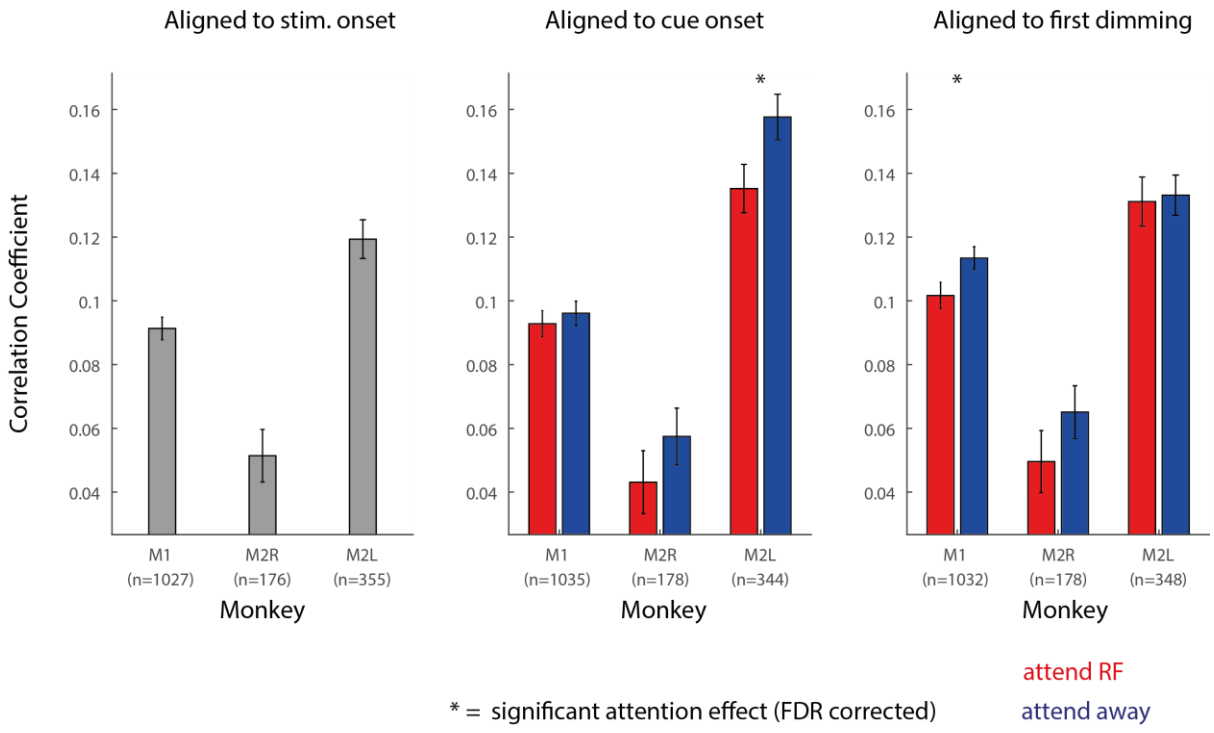

Figure 4-15: Noise correlations in V4 aligned to the stimulus onset (250-761ms, left), cue onset (50-561ms, centre) and first dimming (-511-0ms, right) in the attention task. Shown for Monkey 1 (M1) and the right and left hemispheres of Monkey 2 (M2R and M2L respectively). Asterisks indicate significant differences between the attention conditions ($p<0.05$, FDR corrected), n indicates number of channel pairs. Plotted separately for the attend RF (red) and attend away (blue) conditions.

4.3.1 Layer dependence of noise correlations

We compared noise correlations between the different V4 layers when aligned to the stimulus onset and first dimming of the attention task (Figure 4-16). For this analysis we pooled recordings from Monkey 1 and the left hemisphere of Monkey 2 together. We did not include recordings from the right hemisphere of Monkey 2, since these were recorded using the jerky stimuli (see Appendix A for more information).

When aligned to the stimulus onset (Figure 4-16, grey bars) noise correlations were highest when neurons were compared from within layers (e.g. supragranular-supragranular etc.).

Aligning to the first dimming of the task (Figure 4-16, red and blue bars) uncovered no significant effect of attention on noise correlations, however there was a trend for lower noise correlations in the attend RF condition between the infragranular layers and supragranular/infragranular layers. Within the supragranular layers and between the supragranular and granular layers, noise correlations were higher than in the stimulus aligned period of the task for both attention conditions.

We also repeated this analysis for the cue aligned period of the task (not shown), but this analysis did not uncover any effects of attention either.

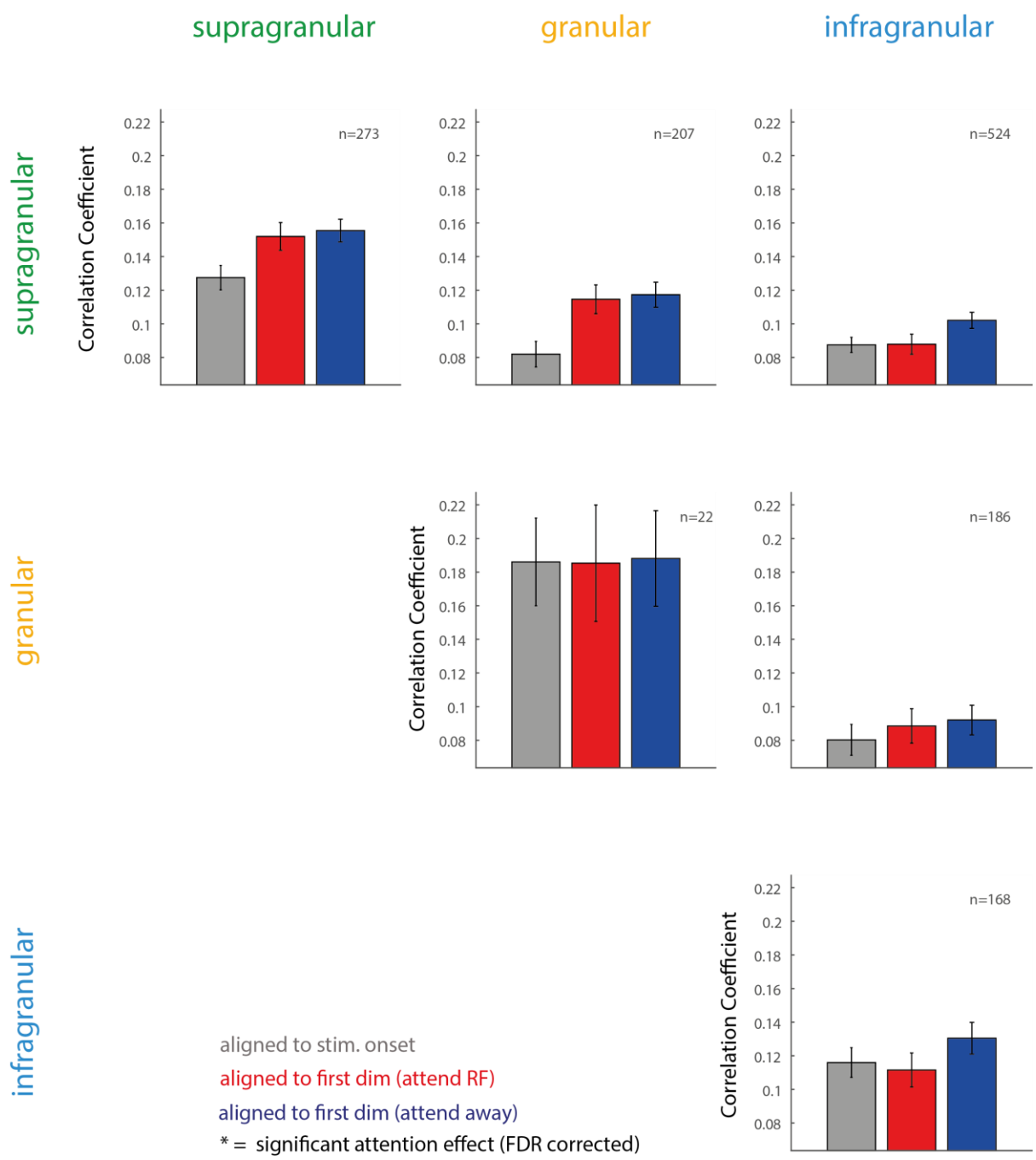

Figure 4-16: Noise correlations in V4 aligned to the stimulus onset (250-761ms, grey) and first dimming (-511-0ms, red and blue) in the attention task. Pooled across recordings in Monkey 1 and the left hemisphere of Monkey 2 and grouped into pairs of supragranular (green), granular (yellow) and infragranular (blue) layers. Asterisks indicate significant differences between the attention conditions ($p<0.05$, FDR corrected), n indicates number of channel pairs. Plotted separately for the attend RF (red) and attend away (blue) conditions. V4 structure is as defined in Figure 4-1.

4.4 Attention induced changes to spectral power of the local field potential

The LFP signal used in all analyses was based on the bipolar derivative (see Section 2.4.8) to give a local estimate of the signal for each channel. We calculated the LFP spectra aligned to the stimulus, cue and first dimming aligned periods of the attention task.

4.4.1 Raw LFP spectral analysis

The LFP spectral power of both monkeys (Figure 4-17) had the highest power at low frequencies and lowest power at higher frequencies. Comparing the pre-stimulus and post-stimulus periods of the task shows that low frequency power is reduced by stimulus onset. It is difficult to observe other effects of task period and attention in these plots, therefore these are analysed in more detail using normalised LFP analysis (see Section 4.4.2 and 4.4.3).

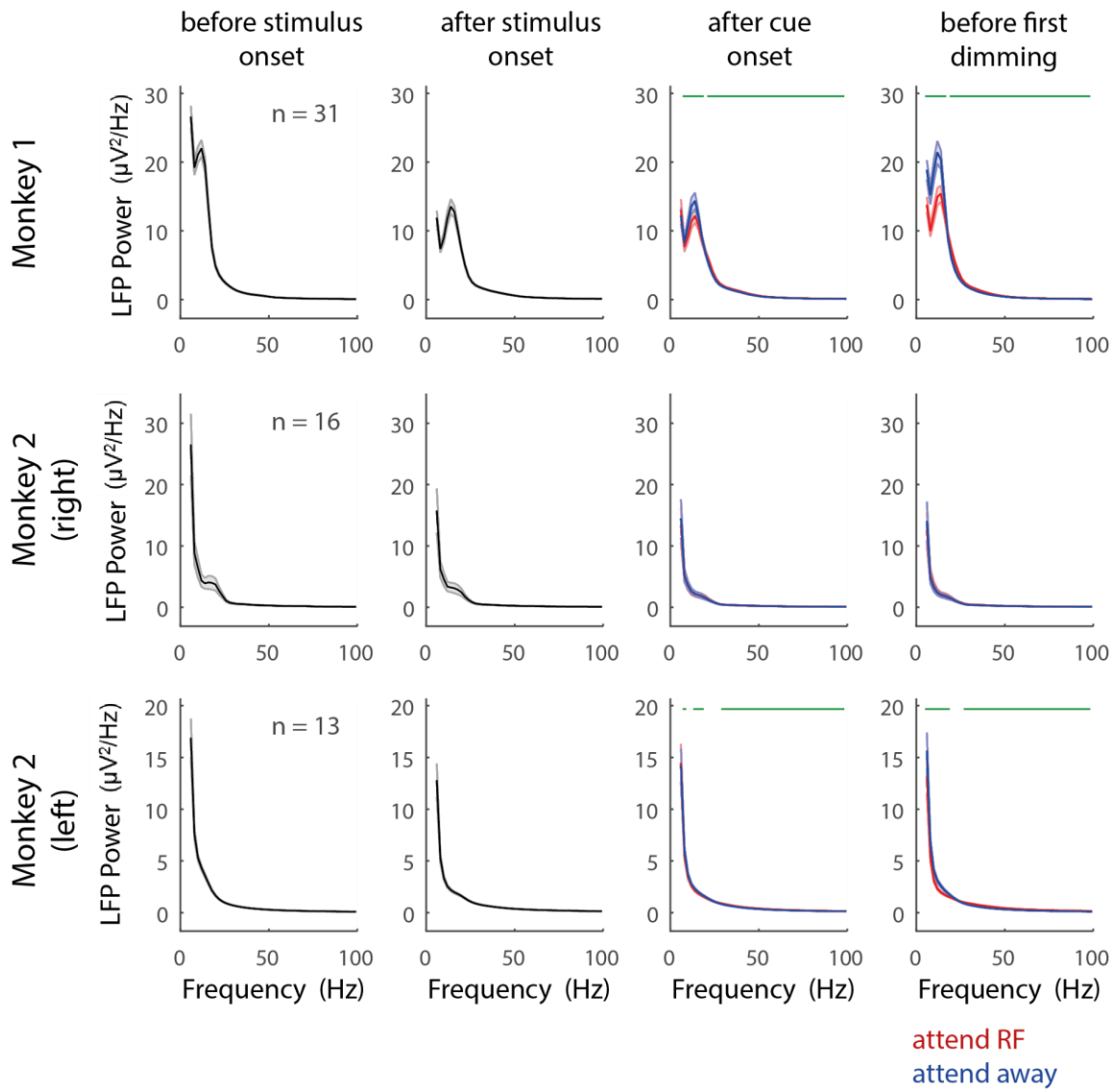

Figure 4-17: LFP power spectra in V4. Plotted for Monkey 1 and 2 (left and right hemisphere) aligned to both before and after the stimulus onset, after the cue onset and before the first dimming in the attention task (n = number of recordings per monkey). Separated into the attend RF (red) and attend away (blue) conditions for the cue and first dimming periods. Spectral power was calculated using the bipolar derivation of the local field potential, with 3 tapers of 4Hz half-bandwidth. Green bars indicate significant differences between the attention conditions (repeated measures Wilcoxon signed rank test, $p<0.05$, FDR corrected).

4.4.2 Spectral power of the LFP after stimulus onset

In the low frequency range (<13Hz), the stimulus invoked a reduction in V4 LFP spectral power (Figure 4-18). This was most pronounced in the left hemispheres of Monkey 1 and 2, but there was also a broader reduction in the right hemisphere of Monkey 2. In Monkey 1, a peak centred on a beta frequency (~20Hz) and a broadband

increase across the gamma frequency range (30-100Hz) occurred. In both hemispheres of Monkey 2 there was also an increase in beta/gamma power, however this was a broadband increase without distinguishable beta peaks.

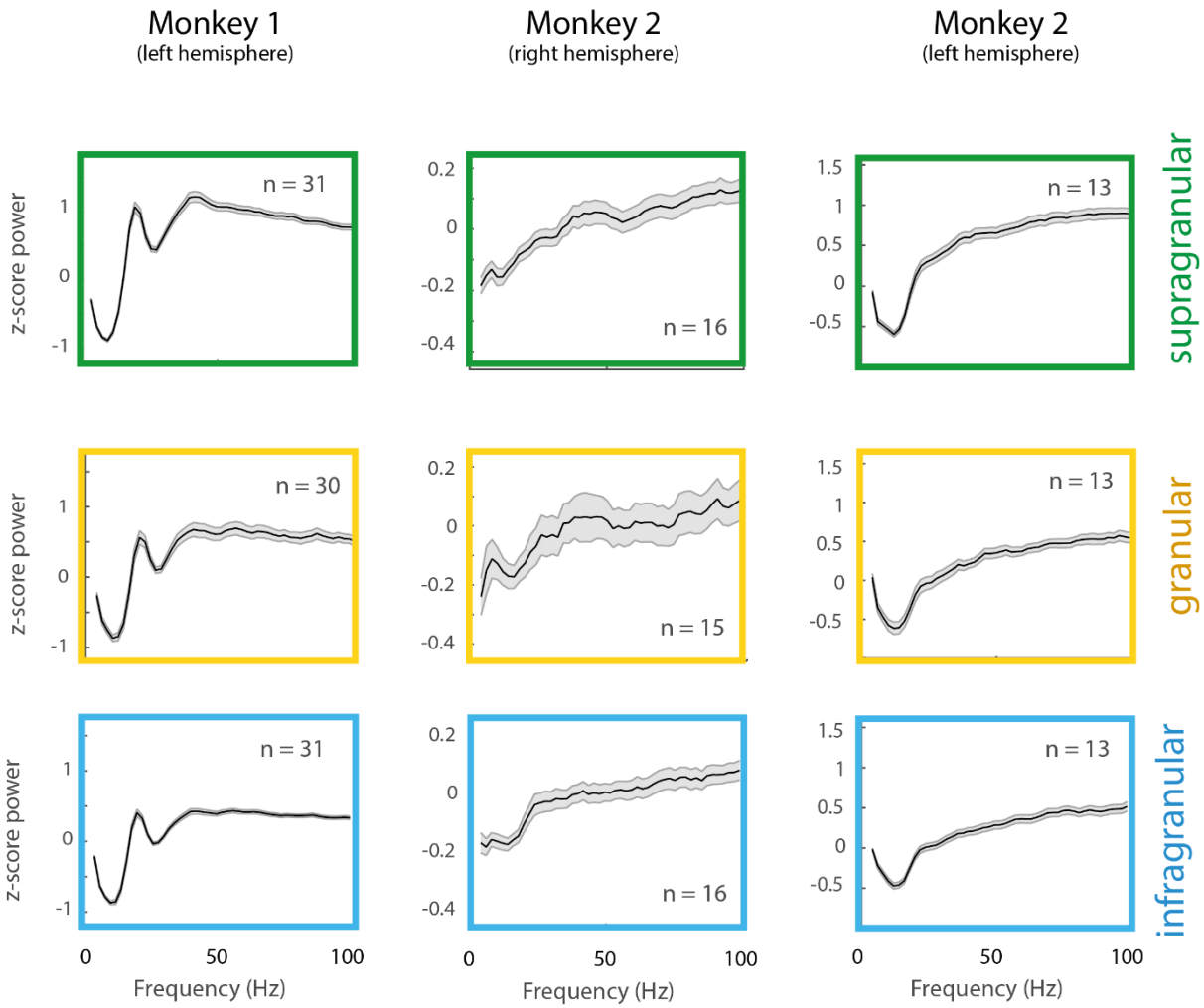

Figure 4-18: V4 LFP spectral power in Monkey 1 and Monkey 2 (right and left hemisphere) aligned to the stimulus onset (250ms to 761ms) in the attention task. Spectral power calculated using the bipolar derivation of the local field potential, 3 tapers of 4Hz half-bandwidth and expressed as a z-score relative to pre-stimulus power (n = number of recordings in each plot). V4 structure is as defined in Figure 4-1.

4.4.3 Spectral power of the LFP prior to the first dimming

Attentional modulation of the LFP spectral power in V4 was profound when aligned to the first dimming of the attention task (Figure 4-19). The effects of attention were similar between Monkey 1 and the left hemisphere of Monkey 2. Attention decreased alpha power whilst increasing beta/gamma power in a broadband manner. In the right hemisphere of Monkey 2 there was little attentional modulation of V4 LFP power.

Attention also increased the peak frequency of beta band oscillations in Monkey 1 slightly (Figure 4-19).

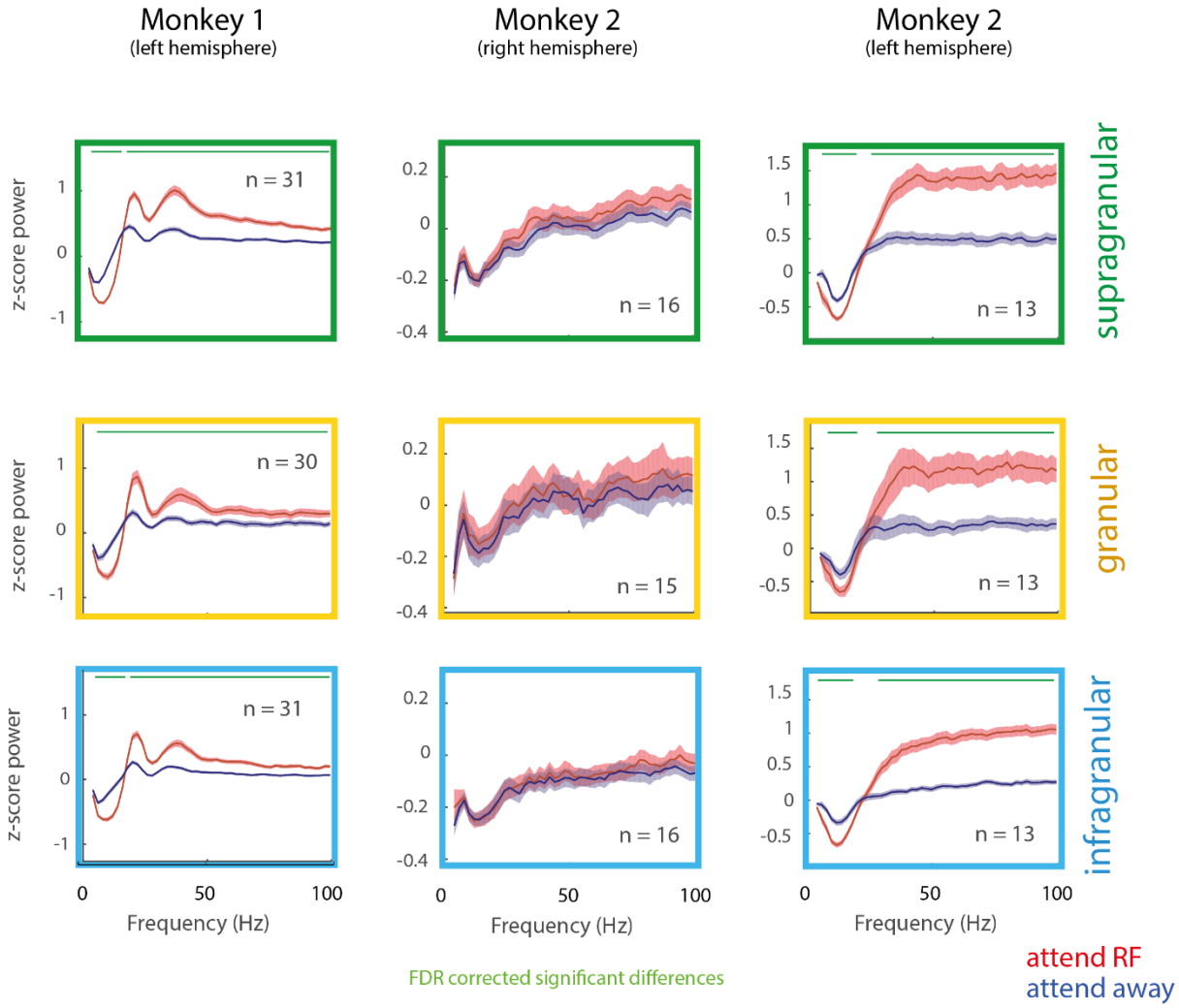

Figure 4-19: V4 LFP spectral power in Monkey 1 and Monkey 2 (right and left hemisphere) aligned to the first dimming (-511ms to 0ms) in the attention task. Power is plotted separately for the attend RF (red) and attend away (blue) conditions. Green bars indicate significant differences between the attention conditions (Wilcoxon signed rank test, $p<0.05$, FDR corrected, n = number of recordings in each plot). Power calculations and V4 structure are as defined in Figure 4-18.

4.5 Field-field coherence

We next calculated the field-field coherence (referred to as field coherence subsequently) between each of the electrode contacts during a V4 recording. This was done for the stimulus aligned activity (not dissociating between attention conditions), separately for contacts located in supragranular, granular and infragranular layers. For cue and first dimming aligned periods of the task the coherence was calculated separately for the two attention conditions. As in the LFP power spectra analysis, the cue aligned period produced qualitatively the same effects as the first dimming aligned analysis, so we show only the first dimming analysis here.

4.5.1 Field coherence after the stimulus onset

As in V1, coherence between contacts in V4 was higher within the same layers than between different layers (Figure 4-20, Figure 4-21 and Figure 4-22). In Monkey 1, the V4 field coherence (Figure 4-20) showed a distinct peak in the low frequency range (~16Hz). The coherence then decreased as the frequency increased, with a slight peak/bump in the low gamma frequency range (~42Hz). As in V1, stimulus onset increased the V4 gamma coherence compared that observed before the stimulus onset (Appendix B, Figure B-4).

In the left hemisphere of Monkey 2, there was a similar pattern of coherence (Figure 4-22), with a peak in the low frequency range (~20Hz) followed by a decrease of the coherence through the gamma frequency range (30-100Hz). The main difference between these recordings and those in Monkey 1 was a main peak in the low frequency range (<5Hz).

In the recordings in the right hemisphere of Monkey 2 (Figure 4-21), the coherence spectra also showed a decrease in coherence magnitude as frequency increased. There were also frequency peaks in the low frequency range (<5Hz and ~20Hz) and low gamma frequency range (~35Hz).

There were no clear differences between the coherence spectra before (Appendix B, Figure B-5 and Figure B-6) and after the stimulus onset in Monkey 2.

As in the analysis of V1 phase differences, the most prominent effect which we observed in phase differences of V4 coherence (Appendix C.2) was a negative phase

difference for gamma frequencies, indicating that the LFP in the shallow layers leads that in the deep layers. This could be seen in analysis of both monkeys (Figure C-4, Figure C-5 and Figure C-6), however as noted previously, it could not be used to confirm which direction signals propagated due the cyclic nature of phase differences.

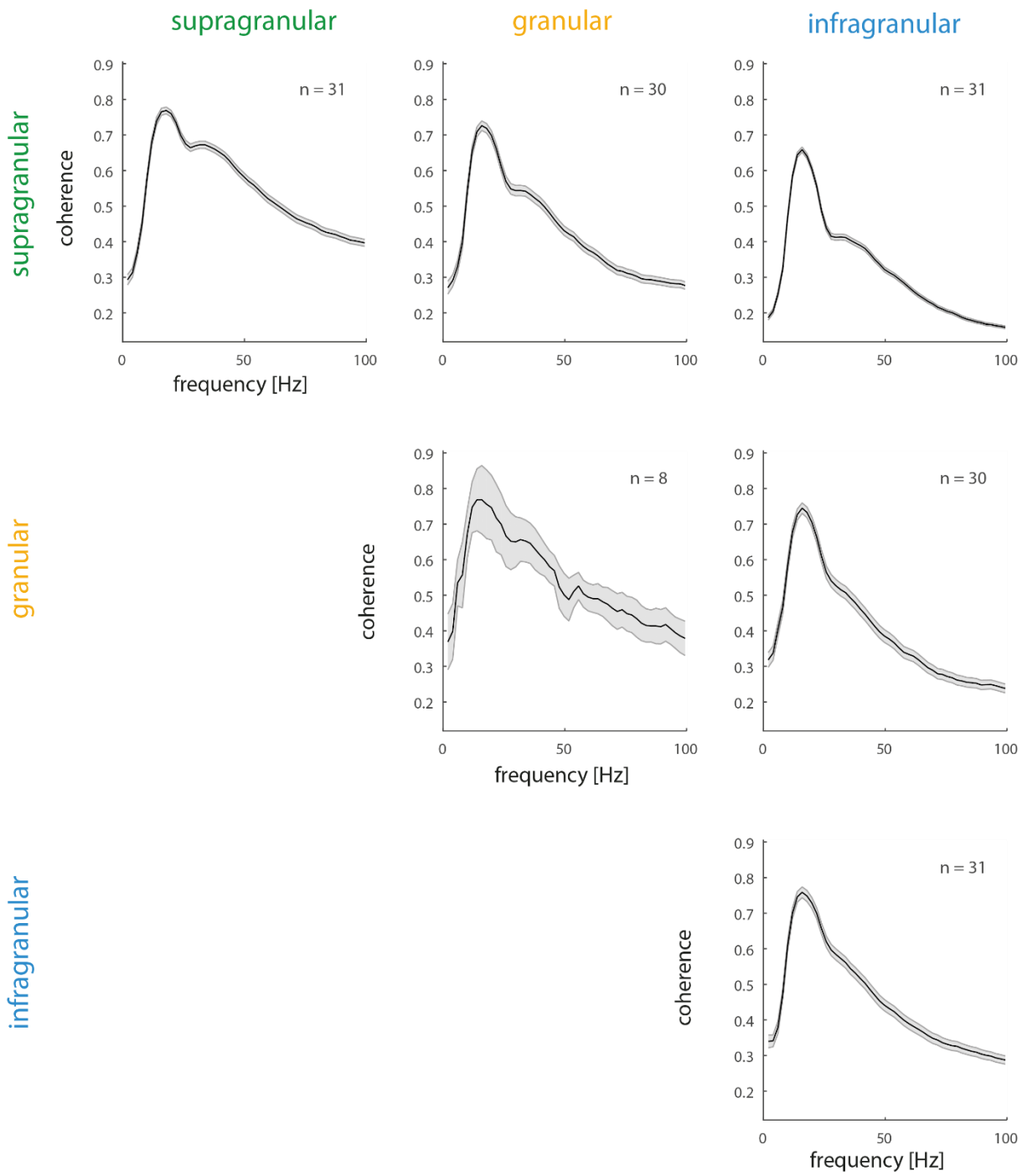

Figure 4-20: V4 field-field coherence in Monkey 1 aligned to the stimulus onset (250ms to 761ms) in the attention task. Shown are all possible combinations of supragranular, granular and infragranular layer comparisons, averaged across the channels contributing to the respective sections (n = number of recordings in each plot). Coherence was calculated using the bipolar derivation of the local field potential and 3 tapers of 4Hz half-bandwidth. V4 structure is as defined in Figure 4-1.

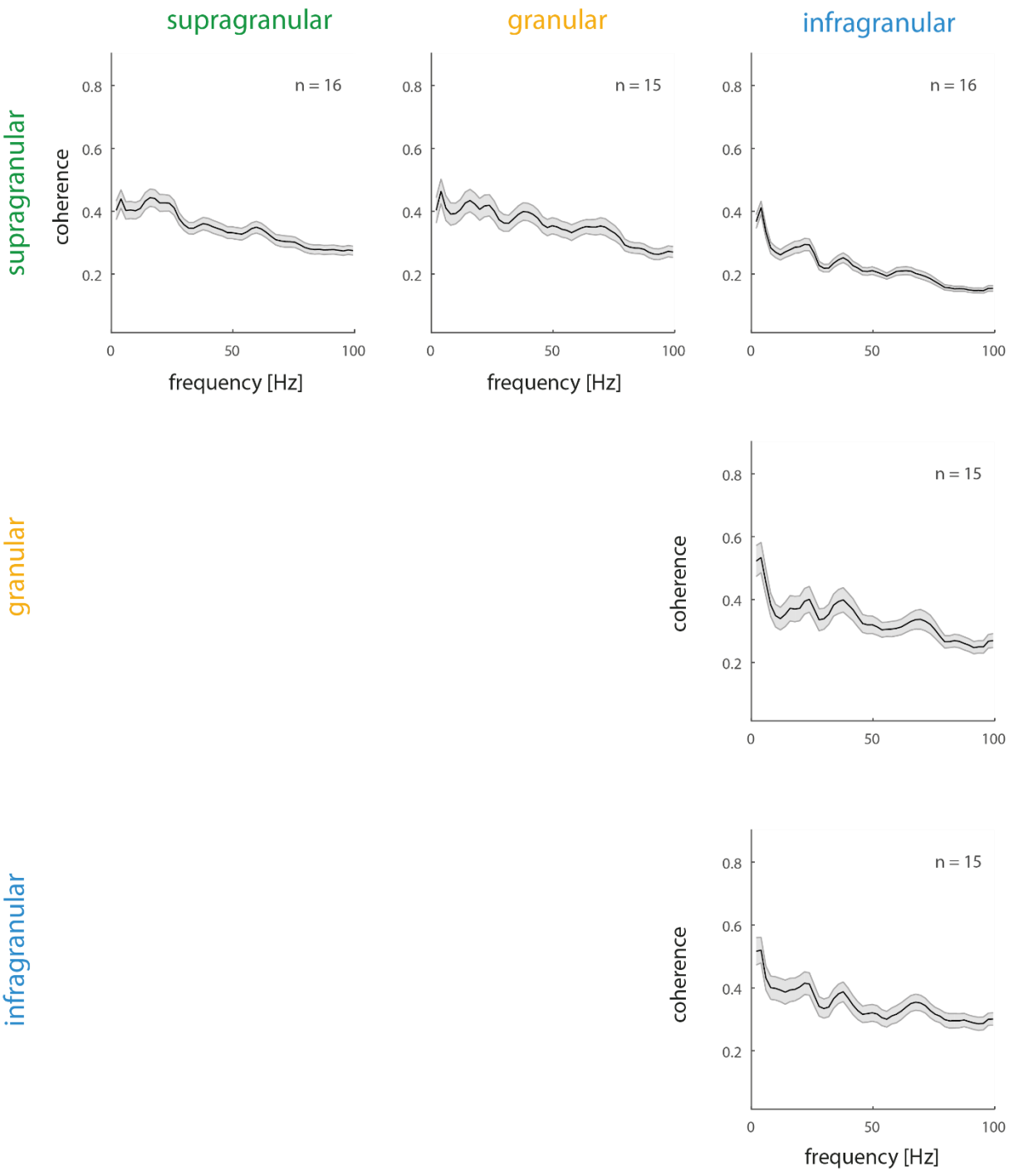

Figure 4-21: V4 field-field coherence in Monkey 2 (right hemisphere) aligned to the stimulus onset (250ms to 761ms) in the attention task. Shown are all possible combinations of supragranular, granular

and infragranular layer comparisons, averaged across the channels contributing to the respective sections (n = number of recordings in each plot). Coherence calculation and V4 structure are as defined in Figure 4-20.

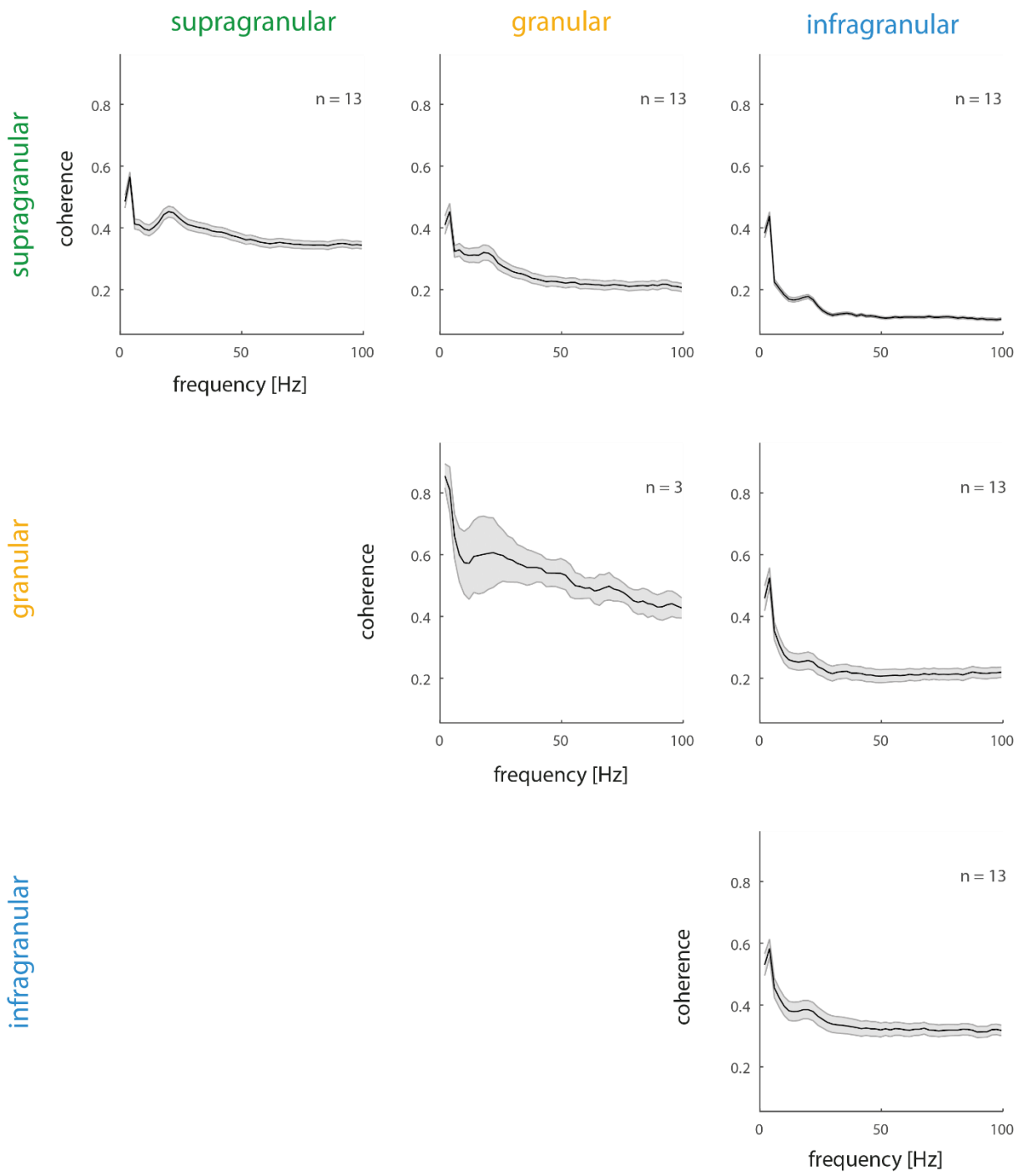

Figure 4-22: V4 field-field coherence in Monkey 2 (left hemisphere) aligned to the stimulus onset (250ms to 761ms) in the attention task. Shown are all possible combinations of supragranular, granular and infragranular layer comparisons, averaged across the channels contributing to the respective

sections (n = number of recordings in each plot). Coherence calculation and V4 structure are as defined in Figure 4-20.

4.5.2 Field coherence prior to the first dimming

When aligned to the first dimming of the attention task, V4 coherence in Monkey 1 (Figure 4-23) showed a reduction with attention in the magnitude of low frequency coherence peaks (<16Hz) and an increase in low gamma peaks throughout the different layer combinations. The increase in gamma coherence with attention also extended to higher frequencies, in particularly between supragranular channels, where there was a broadband increase for the whole gamma band.

In the left hemisphere of Monkey 2 (Figure 4-24), there was also a decrease in the magnitude of the low frequency (<25Hz) coherence with attention. In the gamma range there was a broadband increase in coherence with attention. However, these effects were mostly significant between supragranular and all other layers. The reduction in low frequency coherence with attention was also significant between infragranular and granular layers.

In the right hemisphere recordings in Monkey 2 there was no significant attentional modulation in this task period (Figure 4-25).

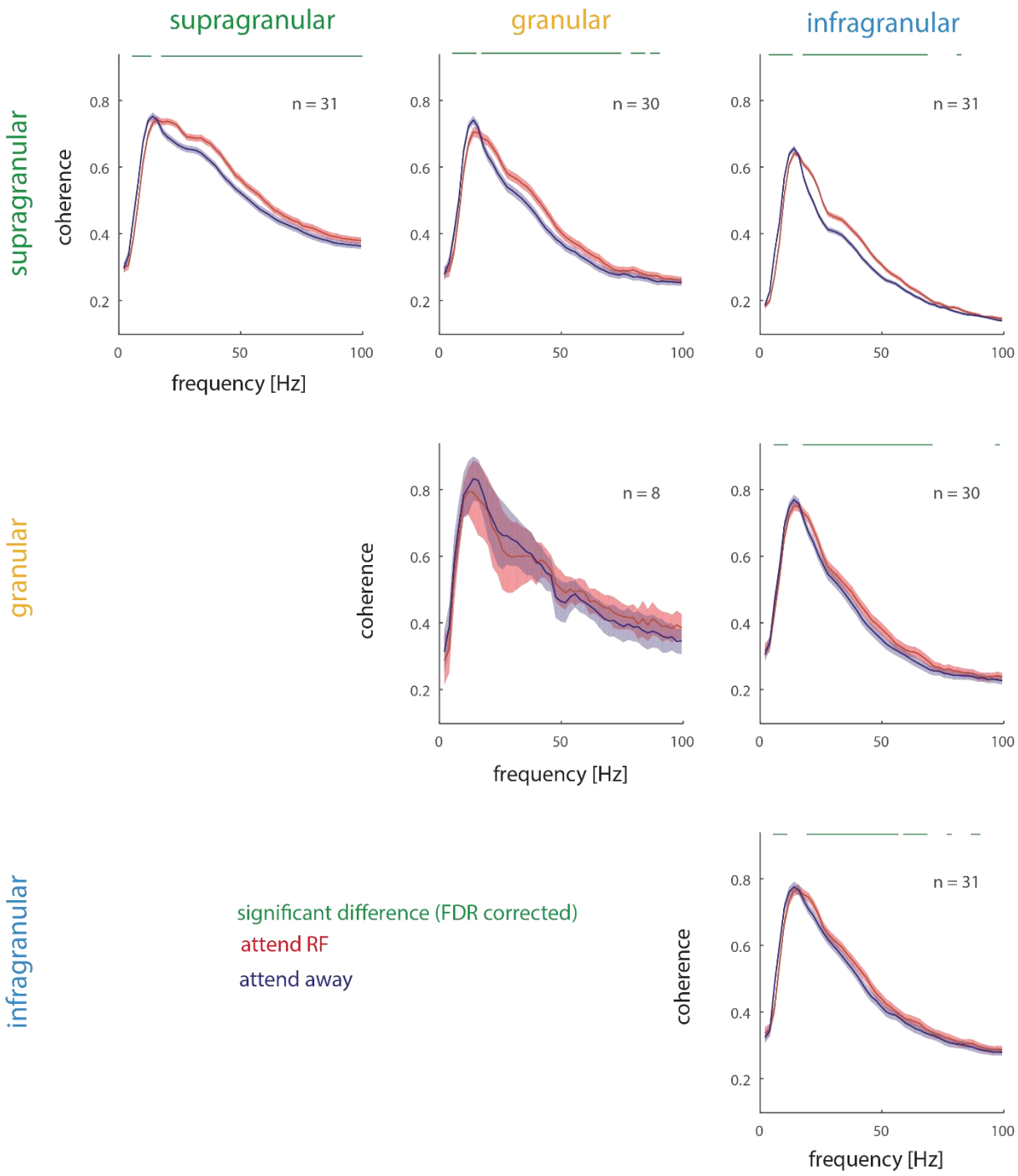

Figure 4-23: V4 field-field coherence in Monkey 1 aligned to the first dimming (-511ms to 0ms) in the attention task. Shown are all possible combinations of supragranular, granular and infragranular layer comparisons, averaged across the channel contributions (n = number of recordings in each plot). Coherence is plotted separately for the attend RF (red) and attend away (conditions). Green bars indicate significant differences between the attention conditions (repeated measures Wilcoxon signed rank test, $p<0.05$, FDR corrected). Coherence calculation and V4 structure are as defined in Figure 4-20.

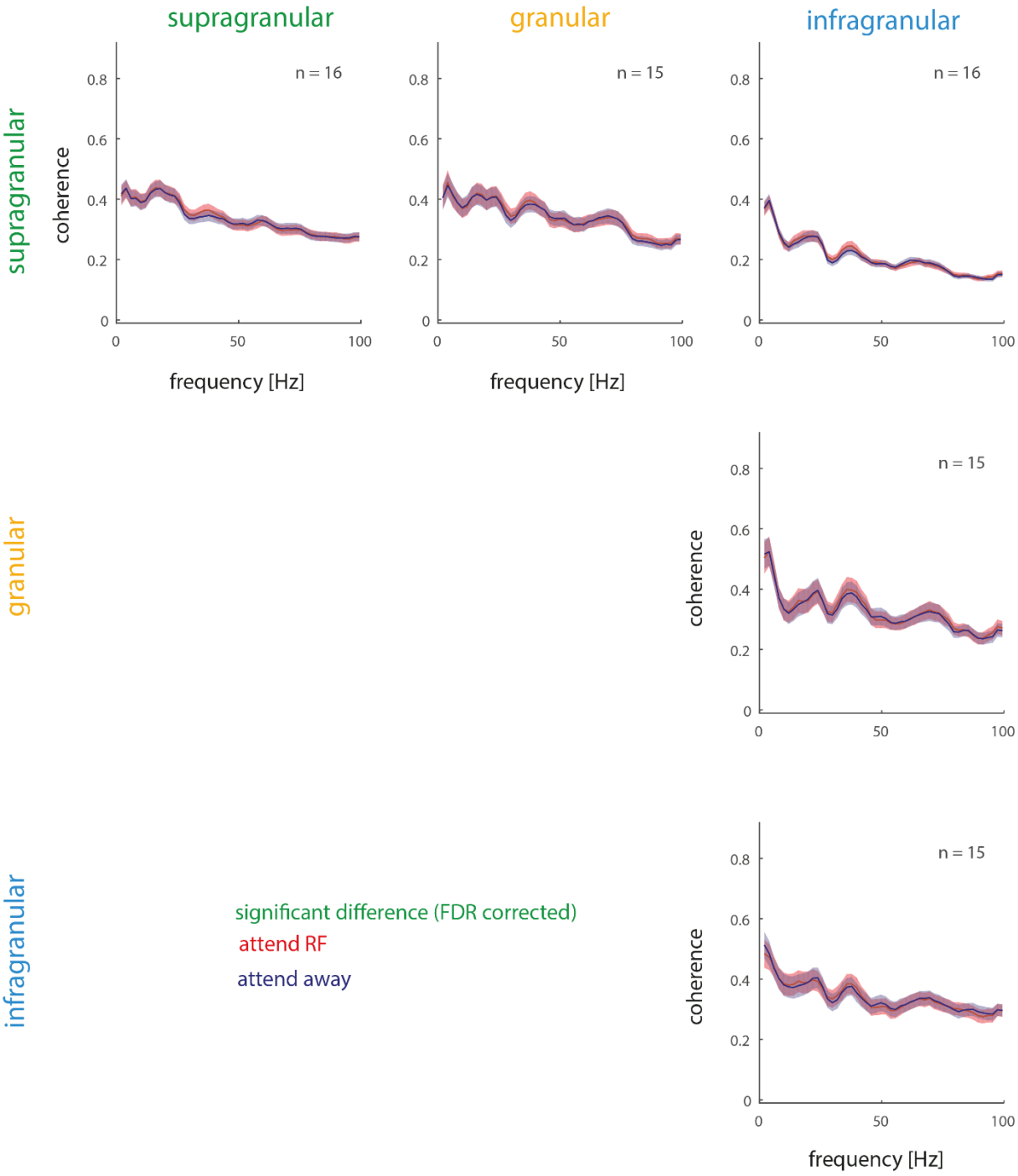

Figure 4-24: V4 field-field coherence in Monkey 2 (right hemisphere) aligned to the first dimming (-511ms to 0ms) in the attention task. Shown are all possible combinations of supragranular, granular and infragranular layer comparisons, averaged across the channel contributions (n = number of recordings in each plot). Coherence calculation, significance bars, attention conditions and V4 structure are as defined in Figure 4-23.

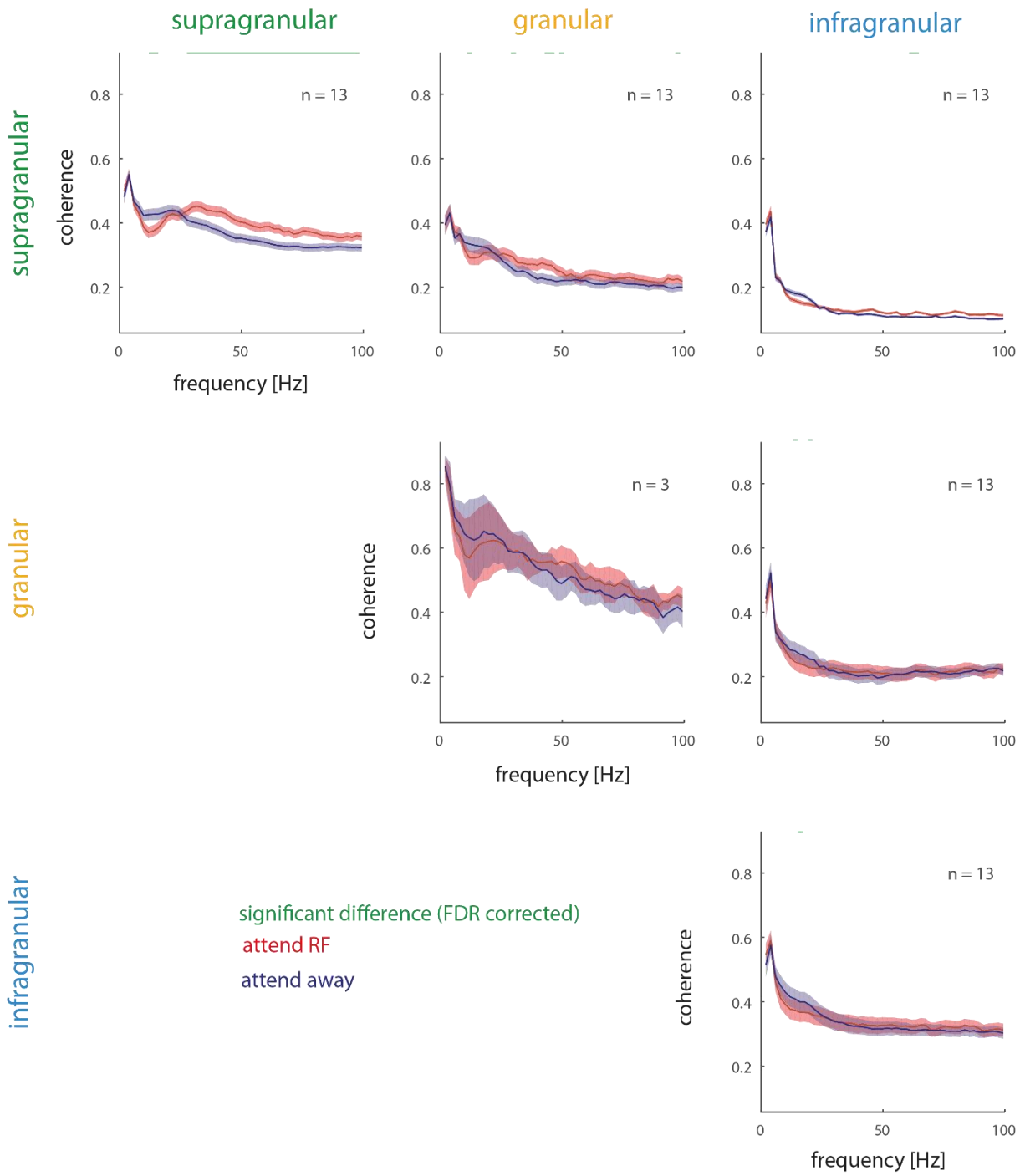

Figure 4-25: V4 field-field coherence in Monkey 2 (left hemisphere) aligned to the first dimming (-511ms to 0ms) in the attention task. Shown are all possible combinations of supragranular, granular and infragranular layer comparisons, averaged across the channel contributions (n = number of recordings in each plot). Coherence calculation, significance bars, attention conditions and V4 structure are as defined in Figure 4-23.

4.6 Granger causality

We calculated Granger causality between the bipolar derived LFPs of different layers of V4, giving a measure of the directionality of information flow in different frequency ranges. This was calculated for the stimulus, cue and first dimming aligned periods of the attention task. We do not show the cue aligned analysis here, as it showed qualitatively similar, but weaker versions of the effects seen the dimming aligned analysis.

4.6.1 Granger causality after the stimulus onset

The stimulus aligned Granger causality spectra in V4 of Monkey 1 (Figure 4-26) showed two frequency peaks. The first was in the low frequency range (~17Hz), which was most prominent from the granular to the supragranular layers, but also present in all other layer combinations to a lesser extent. The second peak was in the low gamma range (~45Hz) for all layer combinations, however this peak was relatively small in comparison. Overall, the Granger causal influences were stronger in the upward direction than in the downward direction. This was the case for the entire frequency band analysed, but most profound for the beta band peak.

In the right hemisphere of Monkey 2 (Figure 4-27) similar low frequency peaks (~20Hz) were present, however there were no clear laminar differences in the size or peak frequency of these. There were also subtle peaks in the gamma frequency range, however these occurred in a range of 60-70Hz rather than the low gamma range observed in Monkey 1.

The Granger causality in the left hemisphere of Monkey 2 (Figure 4-28) were more similar to Monkey 1 than those in the right hemisphere. There were low frequency peaks (~22Hz) in the spectra which were also strongest from the granular to supragranular layers. In the gamma frequency range, slight peaks were present that were centred around 60Hz. As in Monkey 1, the GC influences were more pronounced in the upward direction, than in the downward direction.

We also performed a separate cross correlation analysis (Appendix D.2) of V4 LFP signals to confirm the direction of information flow which was indicated by the Granger causal analysis.

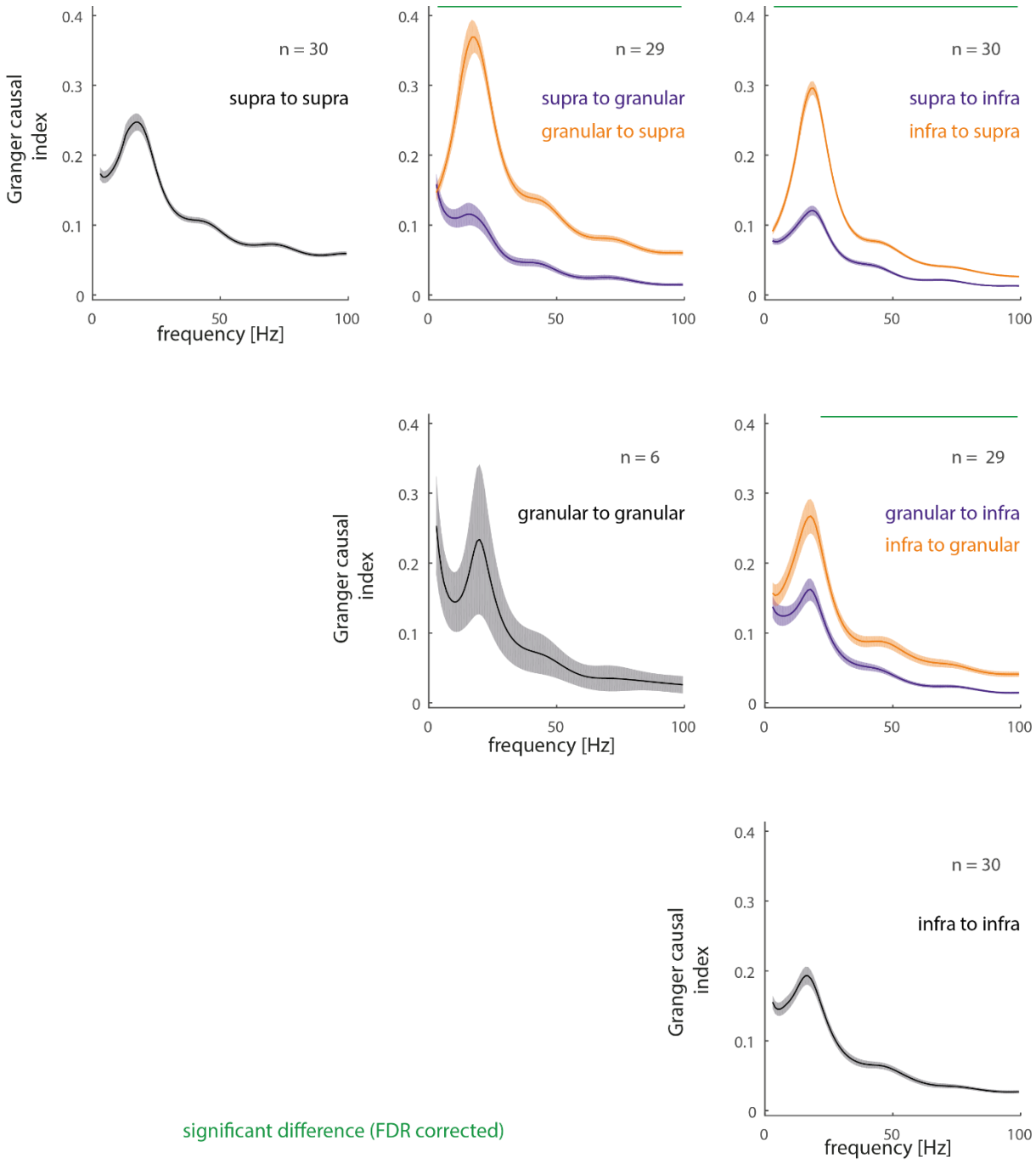

Figure 4-26: Granger causality in Monkey 1 V4 aligned to the stimulus onset (250ms to 761ms) in the attention task. Shown between all possible combinations of supragranular ("supra"), granular and infragranular ("infra") layers (n = number of recordings in each plot). Directionality of Granger causality spectra is indicated by the figure legends. Granger causality was calculated based on the bipolar derivation of the local field potential. Significance bars and V4 structure are as defined in Figure 4-19.

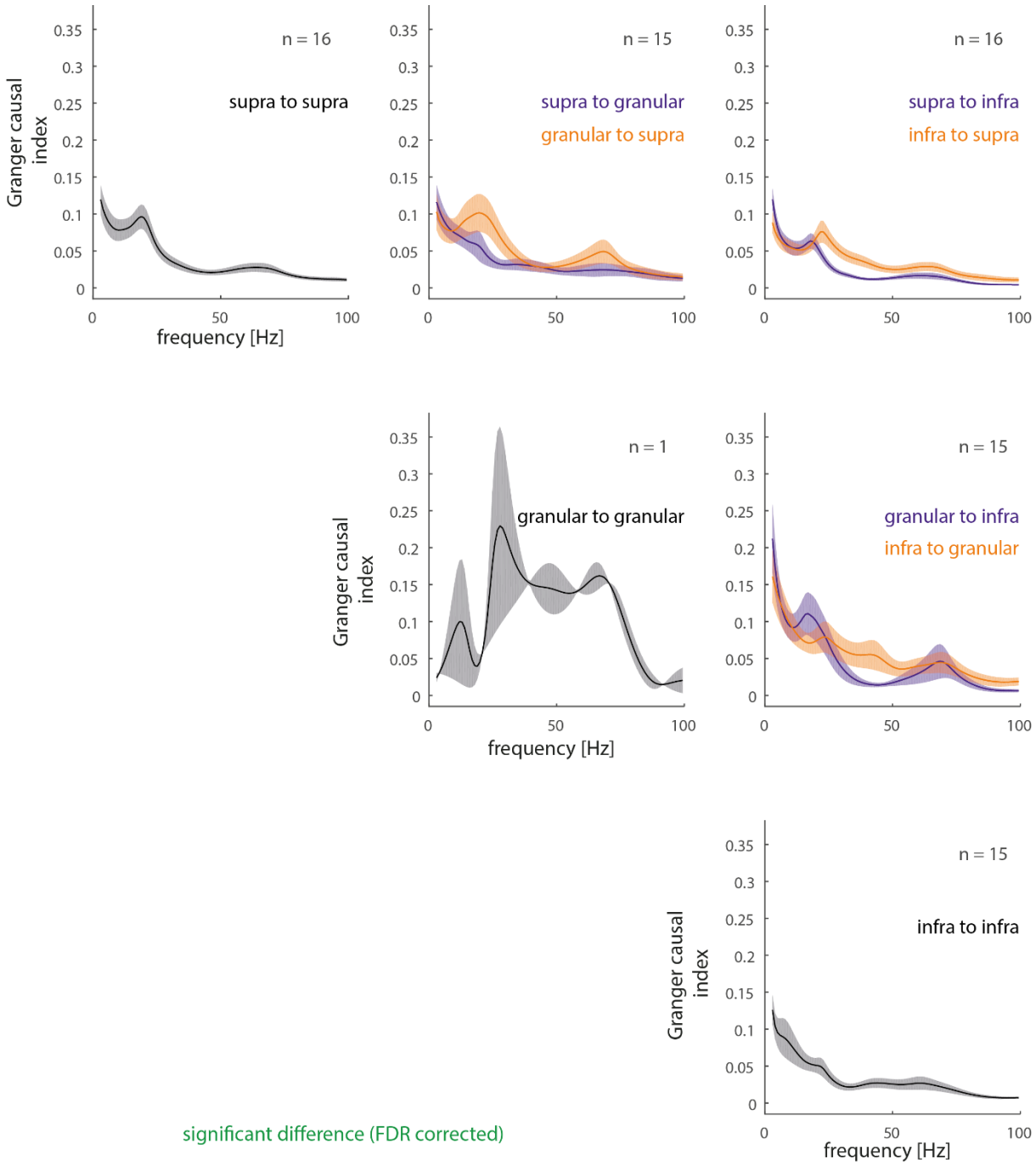

Figure 4-27: Granger causality in Monkey 2 (right hemisphere) V4 aligned to the stimulus onset (250ms to 761ms) in the attention task. Shown between all possible combinations of supragranular ("supra"), granular and infragranular ("infra") layers (n = number of recordings in each plot). Granger causality calculation, significance bars, directionality and V4 structure are as defined in Figure 4-26.

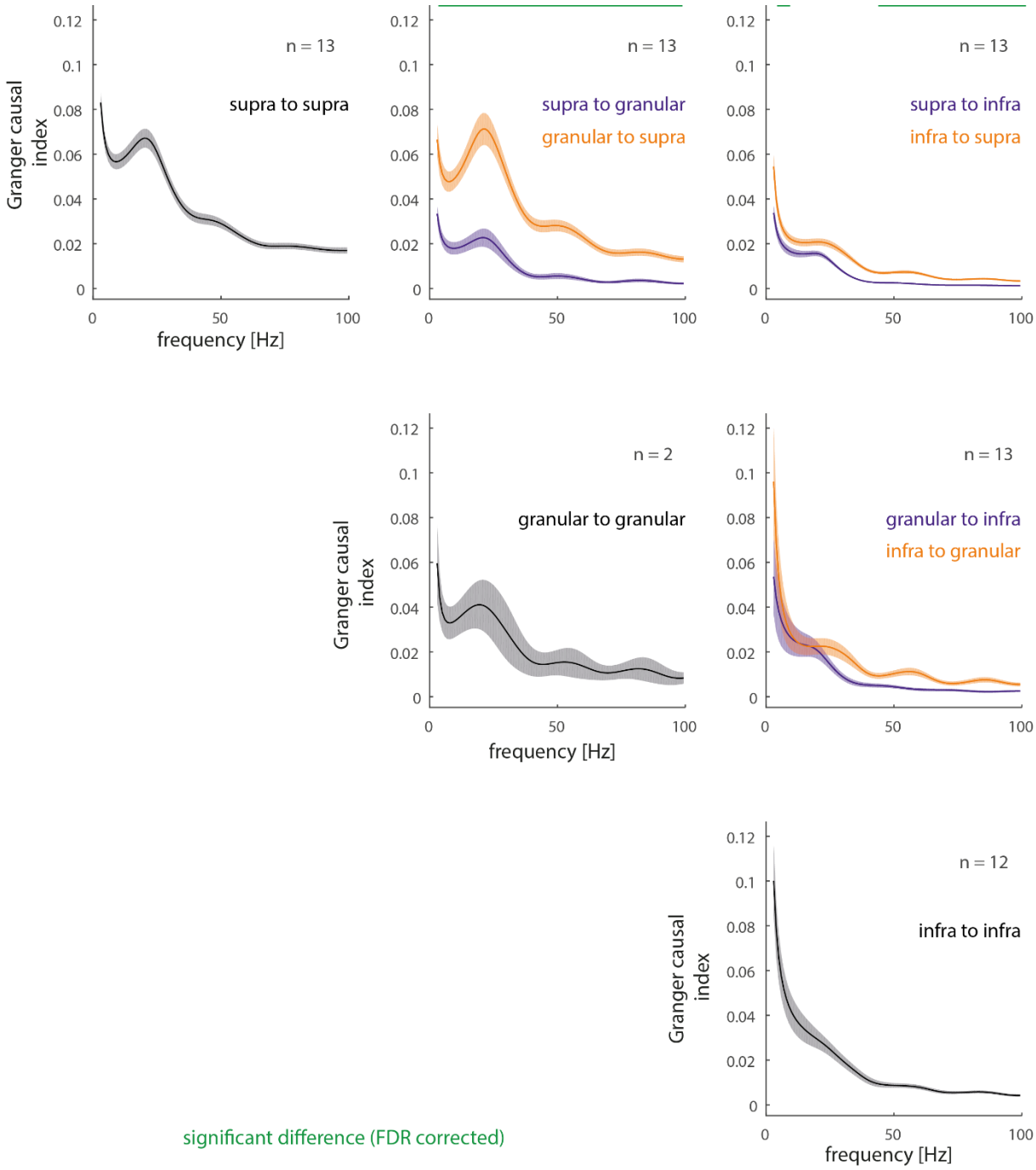

Figure 4-28: Granger causality in Monkey 2 (left hemisphere) V4 aligned to the stimulus onset (250ms to 761ms) in the attention task. Shown between all possible combinations of supragranular ("supra"), granular and infragranular ("infra") layers (n = number of recordings in each plot). Granger causality calculation, significance bars, directionality and V4 structure are as defined in Figure 4-26.

4.6.2 Granger causality prior to the first dimming

Aligning to the first dimming of the attention task showed a significant reduction in of GC influences in the theta/alpha frequency range (i.e. <15Hz) with attention in V4 of Monkey 1 (Figure 4-29). This reduction was significant from infragranular to supragranular, from granular to both granular and supragranular layers and from the supragranular layers to both the granular and supragranular layers.

Granger causal influences for higher frequencies (>15Hz) generally increased with attention. This was profound from infragranular layers to supragranular layers, but also within e.g. supragranular layers (for details see Figure 4-29). In the lower frequency ranges (low beta band) the attention induced changes were mostly due to a frequency shift of the GC to higher frequencies, as the peak magnitude themselves did not seem to increase. Changes in higher frequencies ranges were due to GC amplitude changes.

No attentional modulation of the Granger causality was observed in the right hemisphere of Monkey 2 when aligned to the first dimming of the task (Figure 4-30).

Unlike in Monkey 1, the attentional modulation of low frequency (alpha and low beta band) GC in the left V4 of Monkey 2 (Figure 4-31) was a reduction with attention. Although there was a trend for this effect between all layers, it was significant within the supragranular layers and between the infragranular layers and all layers. A broadband increase in for higher frequency GC with attention was significant from all V4 layers to the supragranular layers, while a decrease was found within infragranular layers.

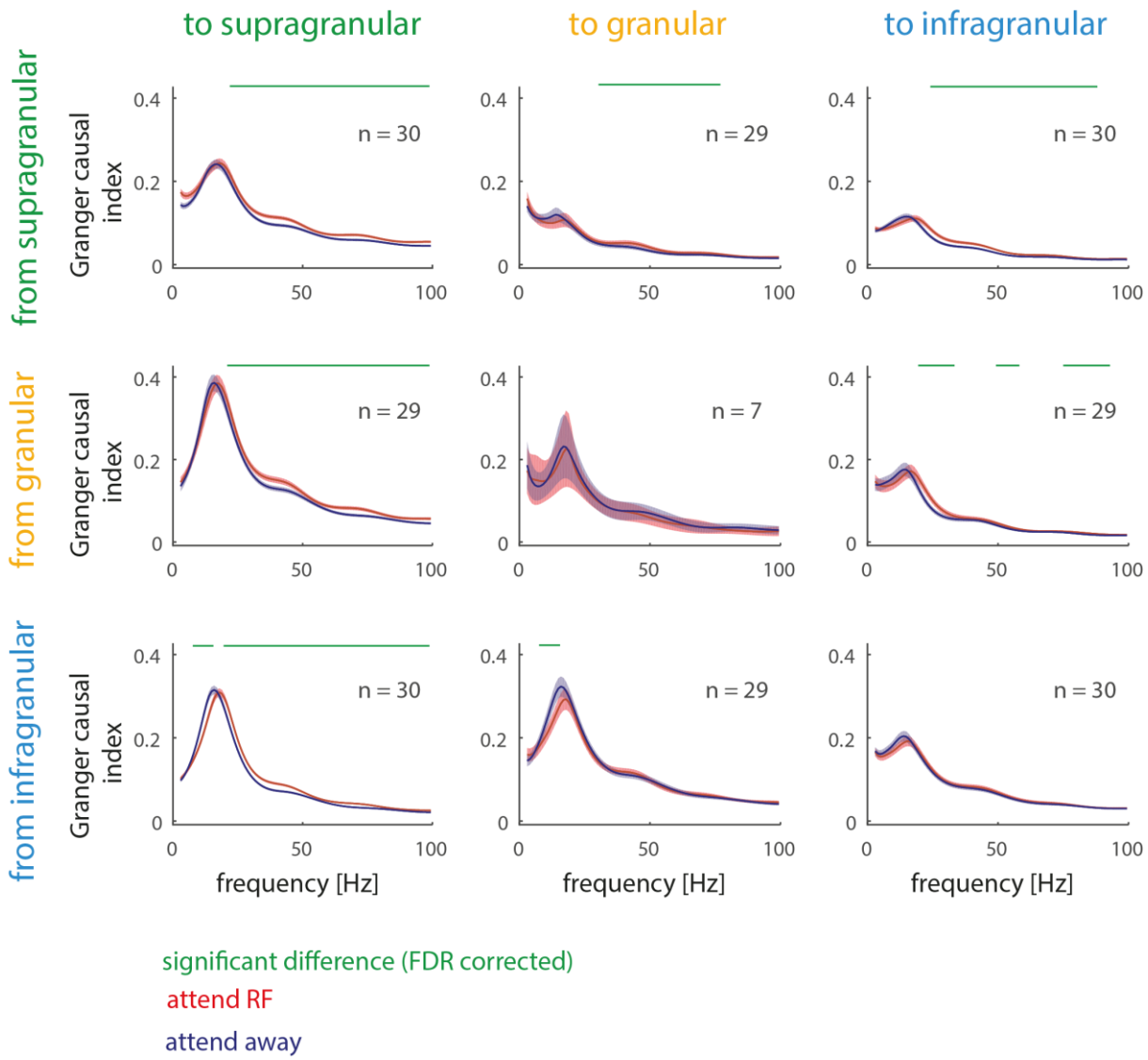

Figure 4-29: Granger causal influences between electrode contacts in Monkey 1 V4 aligned to the first dimming (-511ms to 0ms) in the attention task. These are shown between all possible combinations of supragranular, granular and infragranular layers (n = number of recordings in each plot), and plotted separately for the attend RF (red) and attend away (blue) conditions V4 structure as defined in Figure 4-26.

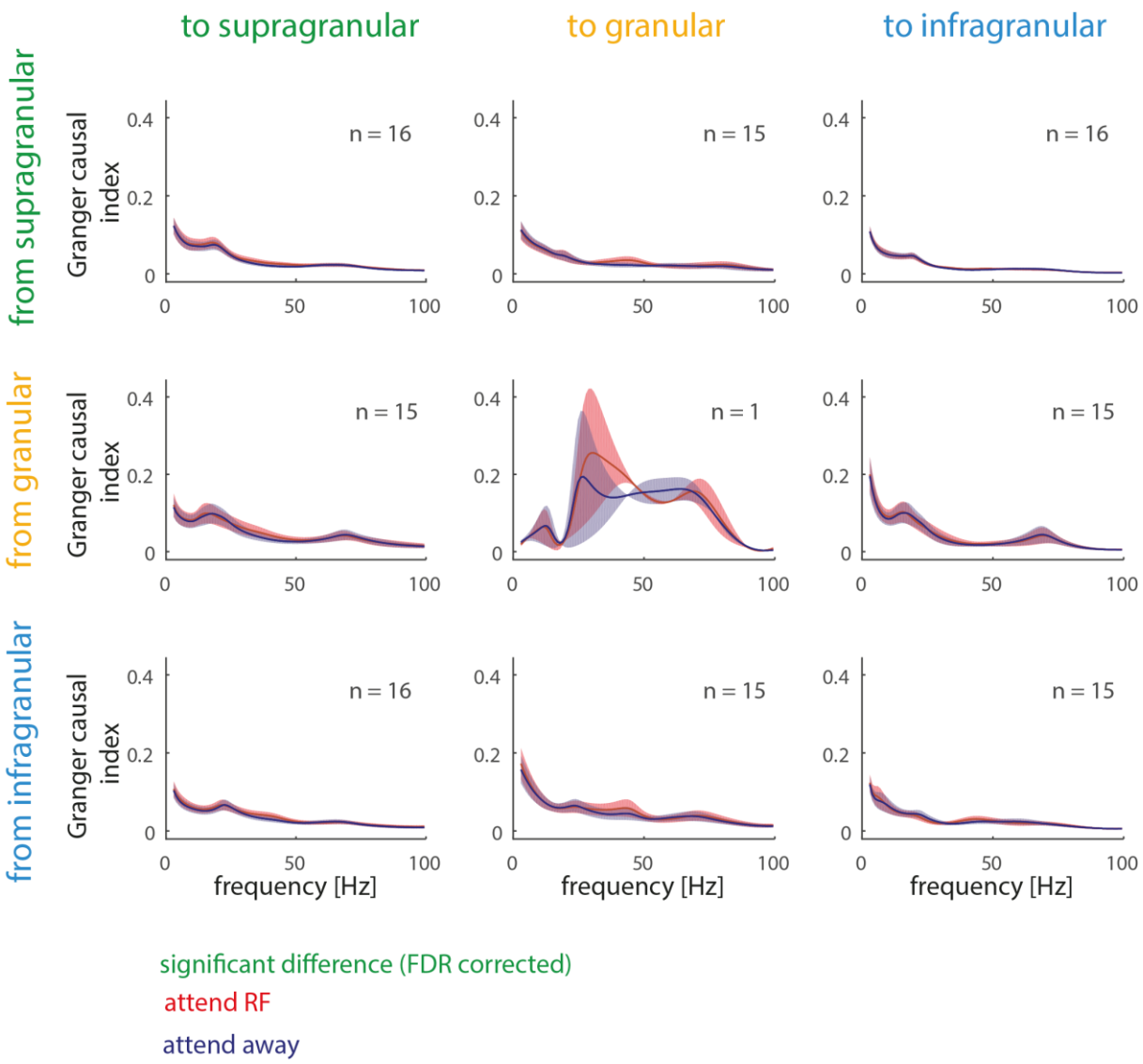

Figure 4-30: Granger causal influences between contacts in Monkey 2 (right hemisphere) V4 aligned to the first dimming (-511ms to 0ms) in the attention task. These are shown between all possible combinations of supragranular, granular and infragranular layers (n = number of recordings in each plot). V4 structure as defined in Figure 4-29.

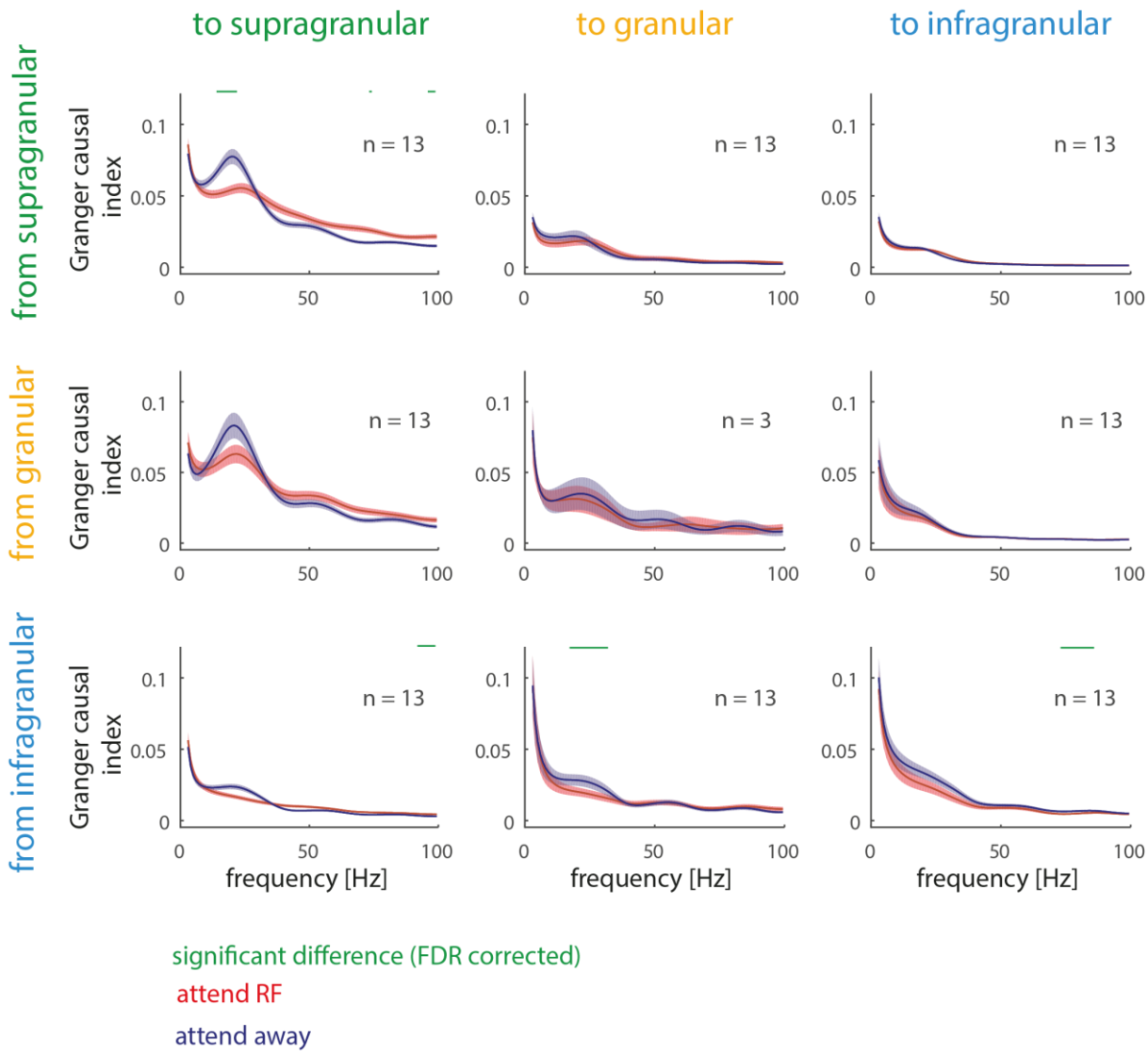

Figure 4-31: Granger causal influences between contacts in Monkey 2 (left hemisphere) V4 aligned to the first dimming (-511ms to 0ms) in the attention task. These are shown between all possible combinations of supragranular, granular and infragranular layers (n = number of recordings in each plot). V4 structure as defined in Figure 4-29.

4.6.3 Granger causal local networks

Next we analysed potential local networks of information flow in V4 based on the Granger causality (see Section 2.4.8). We calculated these networks based on GC influences in the theta/alpha (4-12Hz), beta (13-25Hz), low gamma (30-50Hz) and high gamma (55-100Hz) frequency bands.

The local networks in Monkey 1 (Figure 4-32, top) showed larger upwards than downwards GC influences in all frequency bands. In the theta/alpha range (and to a lesser extent in the beta band) there were also a few contacts where downwards GC influences were stronger than upwards influences. These predominantly originated in lower supragranular layers and targeted lower infragranular layers, or there were very local influences (between neighbouring contacts). In the gamma frequency range there was also some limited downwards directionality from the supragranular layers to the infragranular layers, however, in the low gamma band this was only present when aligned to the stimulus onset in the task.

In the recordings in the left hemisphere of Monkey 2 (Figure 4-32, top) the predominant GC influence directionality was also upwards for all frequency bands. There was also limited downwards directionality of GC influences between the supragranular layers and the infragranular layers in all frequency bands. When aligned to the first stimulus dimming, there were no obvious differences between the different attention conditions in these plots (Figure 4-33, bottom).

Since the recordings in the right hemisphere of Monkey 2 were taken using electrodes with a mixture of 150µm and 250µm intercontact spacings, it was not possible to generate channel aligned local networks in these recordings.

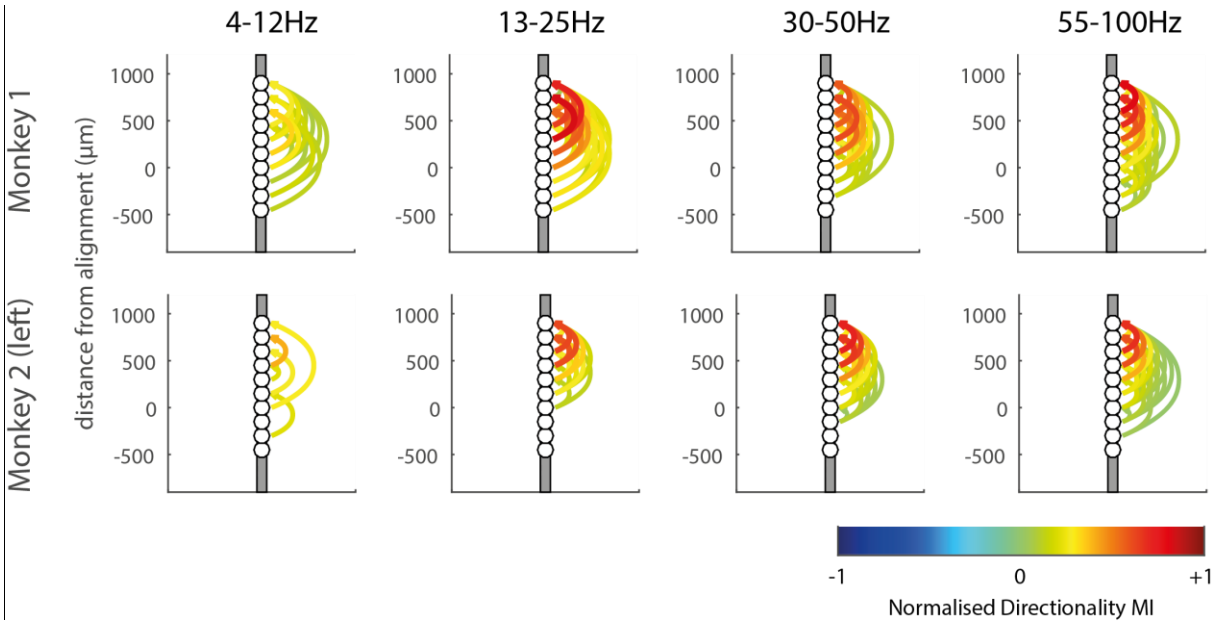

Figure 4-32: Granger causal local networks of V4 in Monkey 1 and Monkey 2 (left hemisphere) between electrode contacts relative to the alignment channel aligned to the stimulus onset (250-761ms). Calculated for the theta/alpha (4-12Hz), beta (13-25Hz), low gamma (30-50Hz) and high gamma (55-100Hz) frequency bands. Directionalities are calculated as a modulation index (MI) based on the Granger causality in each direction between all possible electrode contacts. Upwards (i.e. deep to superficial) directionalities are represented by positive MIs (yellow/red arrows) and drawn on the right hand side of the subplots. Downwards (i.e. superficial to deep) directionalities are represented by negative MIs (cyan/blue arrows) and drawn on the left hand side of the subplots. Only directionalities which were significantly different to zero are shown in these plots (Wilcoxon signed rank test, $p<0.05$ FDR corrected).

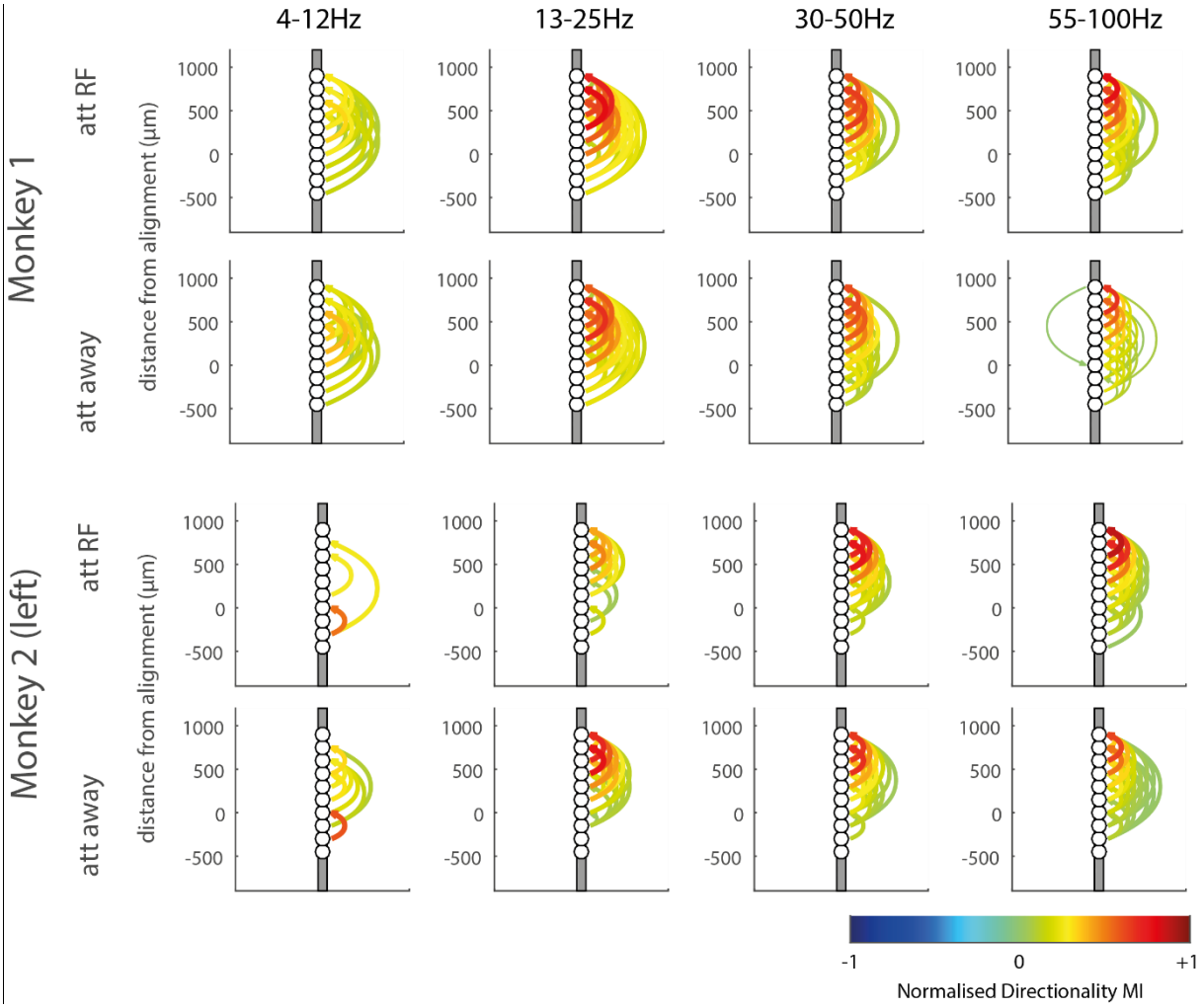

Figure 4-33: Granger causal local networks of V4 in Monkey 1 and Monkey 2 (left hemisphere) between electrode contacts relative to the alignment channel aligned to the first dimming (-511-0ms, separately for the attend RF [“att RF”] and attend away [‘att away”] conditions). Calculated for the theta/alpha (4-12Hz), beta (13-25Hz), low gamma (30-50Hz) and high gamma (55-100Hz) frequency bands and for the stimulus aligned (250-761ms) and first dimming aligned (-511-0ms, separately for the attend RF [“att RF”] and attend away [‘att away”] conditions) periods. Directionality MI calculation and plotting as in Figure 4-32. Only directionalities which were significantly different to zero are shown in these plots (Wilcoxon signed rank test, $p<0.05$ FDR corrected).

4.6.4 Granger causal attentional networks

We used attentional GC MIs to generate Granger causal attentional networks, specifically how GC influences between contacts are altered by attention. As for the V1 analysis, changes in GC influences in the downward direction are shown to the left of the electrode sketches in (Figure 4-34), while changes for the upward direction are

shown to the right of each electrode sketch. No channel pairs survived significance testing in either hemisphere of Monkey 2, so these are not shown here.

There was little effect of attention on the GC of the alpha/theta and beta frequency bands. In the low and high gamma frequency ranges attention increased GC, but there was no clear layer specificity to this.

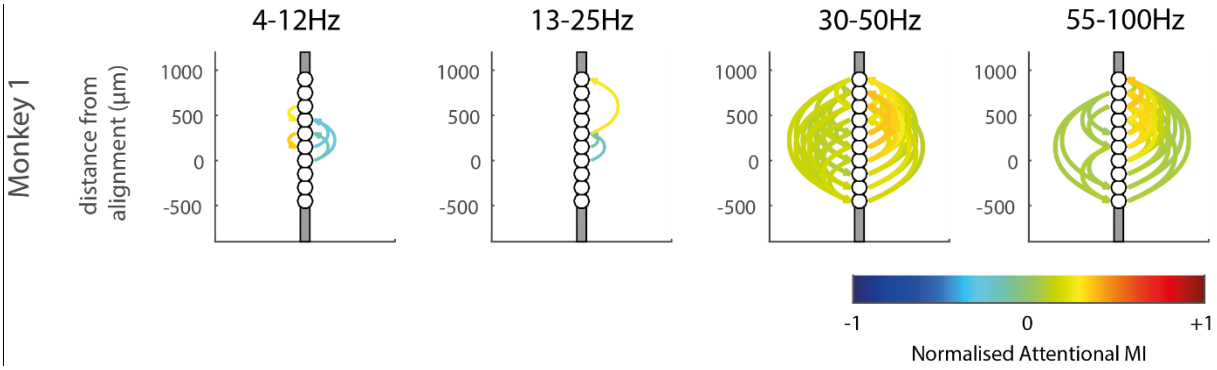

Figure 4-34: Attentional granger causal local networks of V4 in Monkey 1 between electrode contacts relative to the alignment channel. Calculated for the theta/alpha (4-12Hz), beta (13-25Hz), low gamma (30-50Hz) and high gamma (55-100Hz) in the first dimming aligned (-511-0ms) period. Shown are attentional modulation index (MI) calculated from the Granger causality in each attention condition between all possible electrode contacts separately for each monkey/hemisphere. Attentional MIs for upwards (i.e. deep to superficial) directionalities are drawn on the right hand side of the electrode sketches in each subplot and downwards (i.e. superficial to deep) directionalities are drawn on the left hand side of the electrode sketches in each subplot. Only directionalities which were significantly different to zero are shown in these plots (Wilcoxon signed rank test, $p<0.05$ FDR corrected).

4.7 Summary

This chapter described the behaviour of V4 cells whilst a monkey performed a covert visuospatial attention task. As in the analysis of V1 activity, this was at the levels of multiunit activity, single cells, noise correlations and LFP power, coherence and Granger causality.

In V4, attention into the RF of the recorded cells increased firing rates, which was observed in both multiunit and single cell activity. Although there was no effect of attention on Fano factor, there was a reduction in gain variability and noise correlations with attention.

Unlike in V1, the effects of attention on LFP power in V4 were similar between subjects. Attention into the recorded cell's RF reduced low frequency theta/alpha power whilst increasing gamma power. This pattern of attentional modulation was also present in the analysis of V4 field coherence.

The flow of information within cortical microcolumns of V4 was shown to be upwards, from deeper layers to more superficial layers. Information flow was also affected by attention, with Granger causality reduced in the theta/alpha frequency range and increased in the gamma frequency range.

Chapter 5: Effects of Attention on Interactions between Striate and Extrastriate Cortical Neurons

Now that the effects within V1 and V4 have been described, I will now analyse how attention (and stimulus presentation) affects interactions between the two areas. This analysis was focused on how activity in the areas is correlated and the direction of information flow between them. In addition I provide a brief analysis whether the effects of attention differ between areas.

5.1 Differences between V1 and V4 single cell effects

We compared the AUROC distributions of V1 and V4 cells (Figure 5-1) for both broad and narrow spiking cells. For both cell types the AUROCs were higher in V4 cells than in V1 cells ($p<0.05$, Wilcoxon rank-sum test).

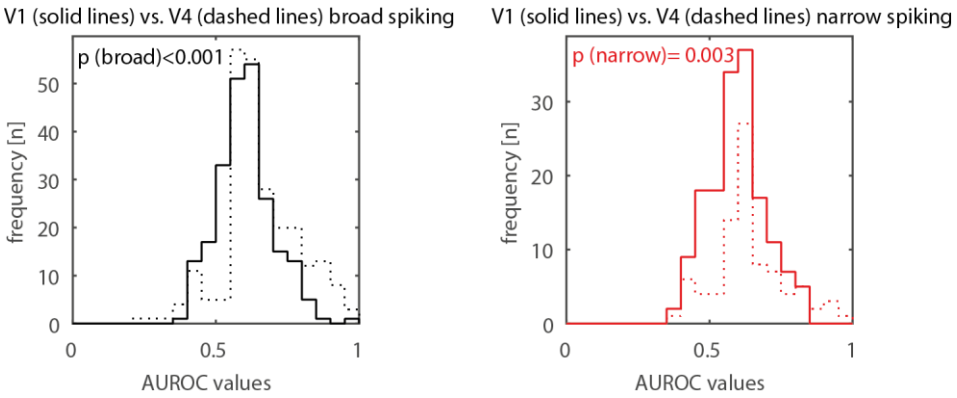

Figure 5-1: Area under the receiver operating characteristic (AUROC) values for broad (black) and narrow (red) spiking cells in areas V1 (solid line histograms) and V4 (dashed line histograms), respectively.

5.2 The effects of attention on noise correlations

We calculated noise correlations between V1 and V4 cells, aligned to the stimulus onset, cue onset and first dimming (Figure 5-2). When aligned to the stimulus onset of the attention task, noise correlations were positive for both Monkeys. Aligning to the cue onset showed significantly lower noise correlations in the attend RF condition than the attend away condition in Monkey 1 and the left hemisphere of Monkey 2. These differences were also significant when aligned to the first dimming of the task.

When noise correlations between V1 and V4 of the right hemisphere of Monkey 2 were aligned to the cue onset and the first dimming, they were not significantly different between attention conditions.

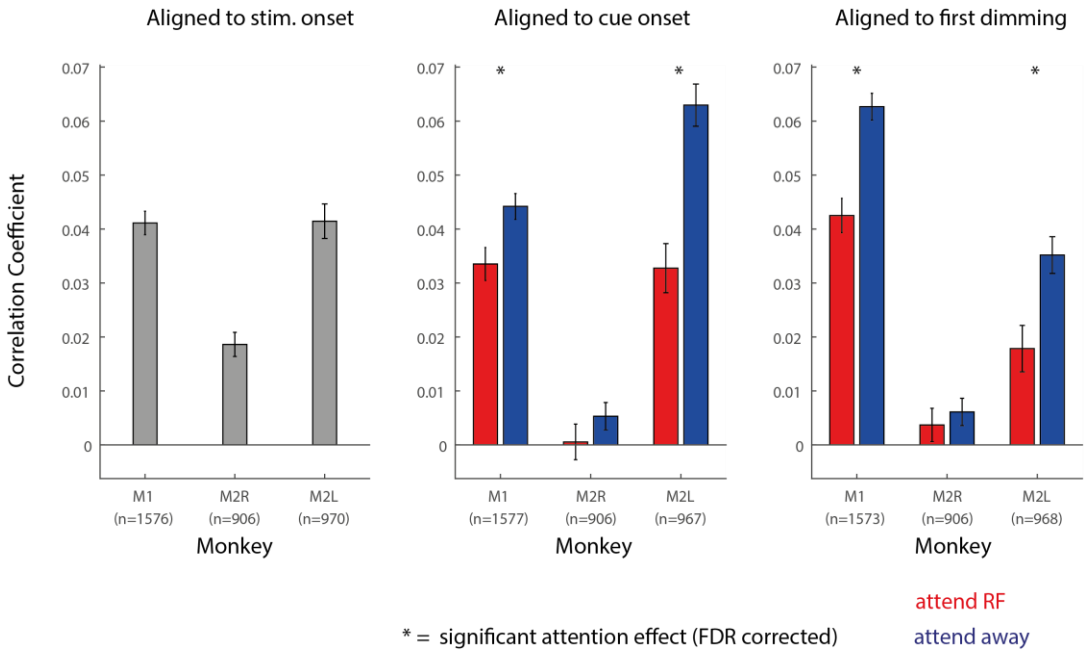

Figure 5-2: Noise correlations between V1 and V4 neurons, aligned to the stimulus onset (250-761ms, left), cue onset (50-561ms, centre) and first dimming (-511-0ms, right) in the attention task. These are shown for Monkey 1 (M1) and the right and left hemispheres of Monkey 2 (M2R and M2L respectively). Asterisks indicate significant differences between the attention conditions ($p<0.05$, FDR corrected), n indicates number of channel pairs. Correlations are shown separately for trials where the monkey attended into the receptive field (RF, red) and away from it (blue).

5.2.1 Layer dependence of noise correlations

We next separated noise correlations into different V1-V4 layers combinations for the stimulus aligned and first dimming aligned periods of the attention task (Figure 5-3). These were calculated by pooling across recordings in Monkey 1 and the left hemisphere of Monkey 2. The right hemisphere of Monkey 2 was excluded from this analysis because it did not show any effects of attention in the grouped analysis and because the jerky stimulus was used (see Appendix A for details).

As in the previous grouped analysis, stimulus aligned noise correlations were positive for the different layer combinations (Figure 5-3, grey bars). There were no clear layer differences in the magnitude of noise correlations in the stimulus aligned period of the task.

When aligned to the dimming period of the task (Figure 5-3, red and blue bars), we observed significantly lower noise correlations in the attend RF condition than the attend away condition for most layer combinations, and lower means in the attend RF condition for all layer combinations. The largest noise correlations (in the attend away condition) were between the V1 supragranular layers and the V4 granular/infragranular layers. Judging by eye, noise correlations increased for attend away conditions over the ‘non-attentional’ stimulus onset aligned condition, while attend RF conditions were largely similar to the latter (even if possibly slightly decreased overall).

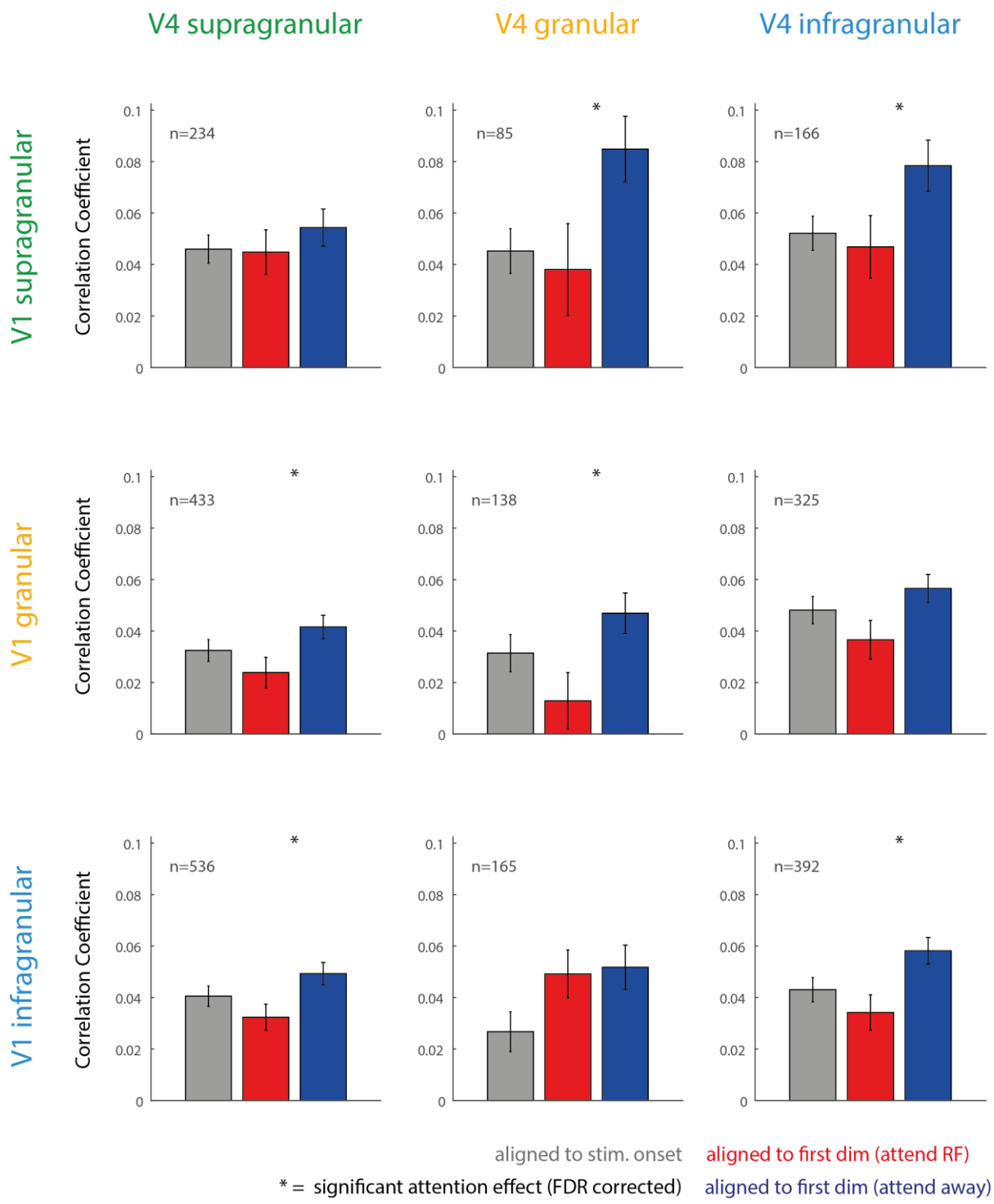

Figure 5-3: Noise correlations between V1 and V4 aligned to the stimulus onset (250-761ms, grey) and first dimming (-511-0ms, red and blue) in the attention task. Pooled across recordings in Monkey 1 and the left hemisphere of Monkey 2 and grouped into pairs of supragranular (green), granular (yellow) and infragranular (blue) layers (n = number of channel pairs in each plot). Statistical testing and attention conditions are as defined in Figure 5-2.

5.3 Field-field coherence

5.3.1 Field coherence after the stimulus onset

We next analysed field-field coherence between electrode contacts in V1 and V4 respectively. When aligned to the stimulus onset, V1-V4 field coherence in Monkey 1 (Figure 5-4) had similar spectra for all layer combinations. In the low frequency range there were two peaks, one at ~18Hz and the other at ~6Hz. There were also peaks in the low gamma frequency range (~43Hz) for all layer combinations.

In all layer combinations of the right hemisphere of Monkey 2 there was a single low frequency (~13Hz) peak present in the V1-V4 field coherence (Figure 5-5). In the gamma range, there were two separate peaks, one at ~42Hz and the other at ~64Hz. Coherence was smallest between V1 supragranular layers and all V4 layers.

V1-V4 field coherence in the left hemisphere of Monkey 2 (Figure 5-6) also showed a peak in the low frequency range (~18Hz). There were no obvious peaks in the V1-V4 coherence in the gamma frequency range for these recordings.

We also analysed V1-V4 field-field coherence prior to the stimulus onset (Appendix B.3), however these spectra did not present any clear differences to those after the stimulus onset.

In addition to absolute coherence values, we also analysed the phase difference between V1 and V4 (Appendix C.3). In Monkey 1 (Figure C.7), there were several distinct peaks in the phase difference plots. For low frequencies (<30Hz), phase differences were positive, indicating that the V4 signal leads the V1 signal. For gamma frequencies, phase differences varied depending on the V4 layer involved. Between all V1 and supragranular V4 layers, there was a negative phase difference in the low gamma (~40Hz) frequency range. This peak occurred at a higher frequencies for granular (~45Hz) and infragranular (~50Hz) V4 layers. There was also a positive phase difference for frequencies higher than 50Hz between all V1 layers and supragranular V4 layers. Although it is tempting to interpret these phase differences as equivalent to the direction which information flows from one area to the other, this cannot be done, since phase differences are cyclic.

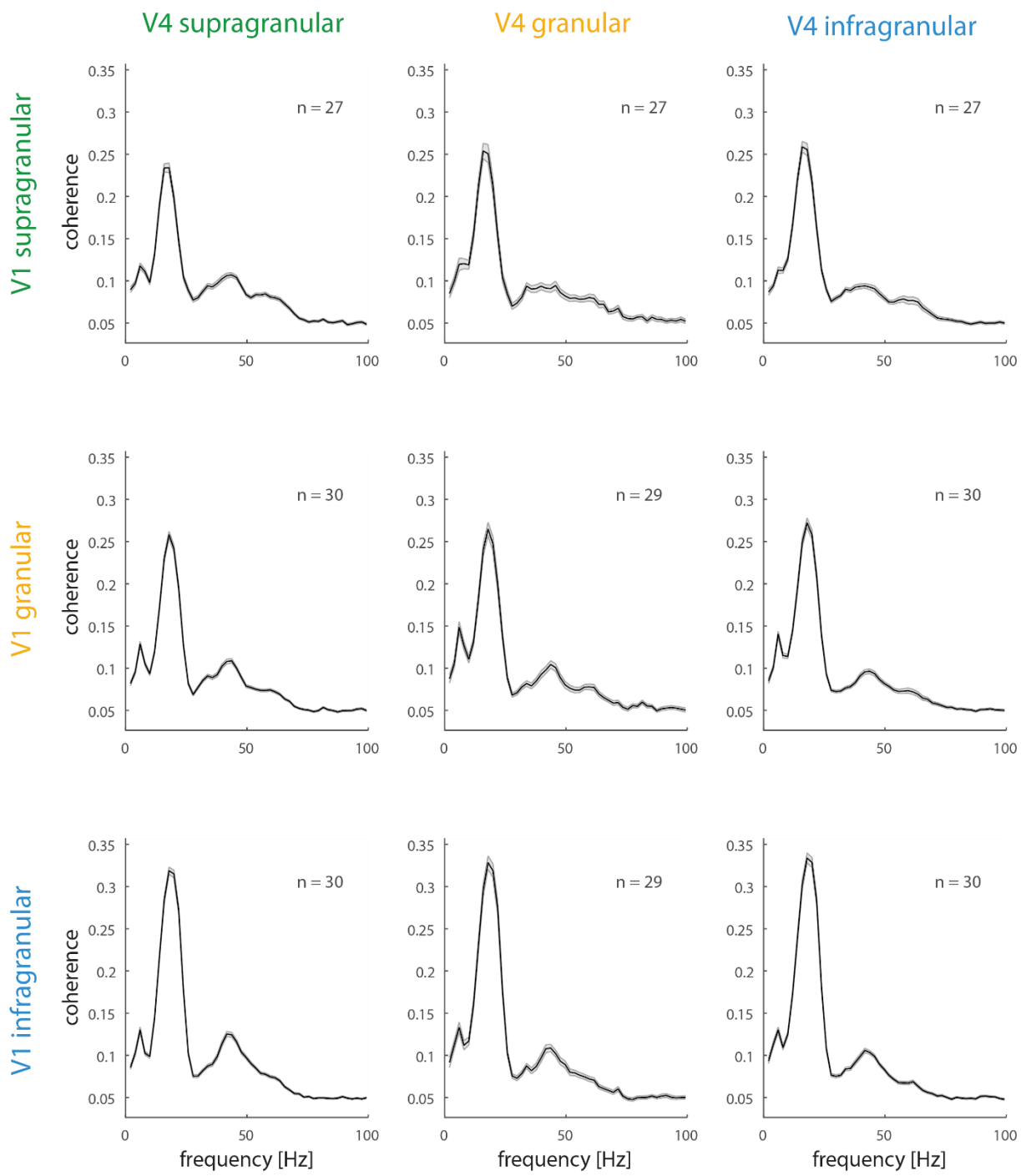

Figure 5-4: V1-V4 field-field coherence in Monkey 1 aligned to the stimulus onset (250ms to 761ms) in the attention task. Shown are all possible combinations of supragranular, granular and infragranular layer comparisons, averaged across the channels contribution (n = number of recordings in each plot). Coherence was calculated using the bipolar derivation of the local field potential and 3 tapers of 4Hz half-bandwidth. V1 and V4 structure are as defined in Figure 3-1 and Figure 4-1.

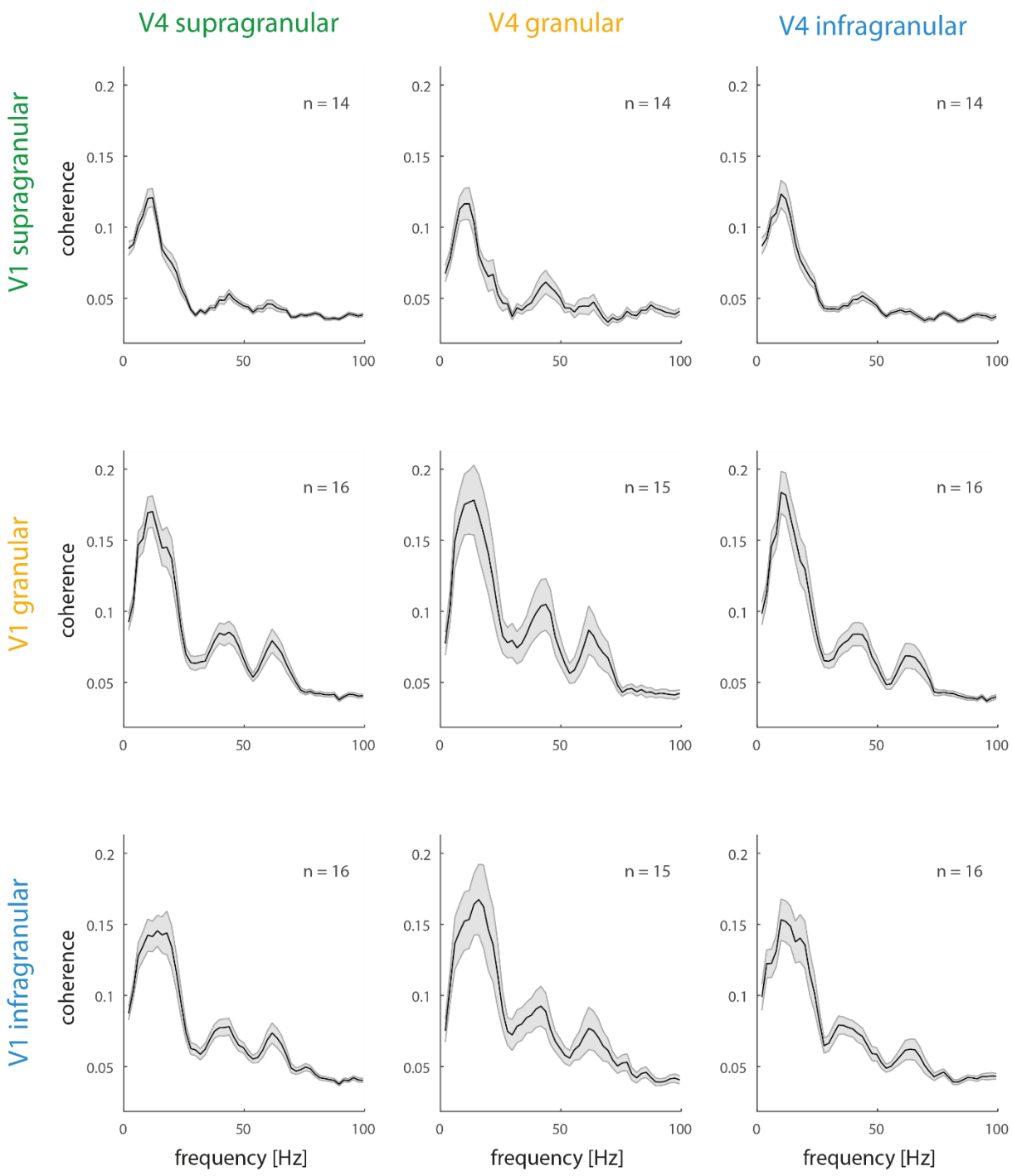

Figure 5-5: V1-V4 field-field coherence in Monkey 2 (right hemisphere) aligned to the stimulus onset (250ms to 761ms) in the attention task. Shown are all possible combinations of supragranular, granular and infragranular layer comparisons, averaged across the channels contributing to the respective sections (n = number of recordings in each plot). Coherence calculation and V1/V4 structure are as defined in Figure 5-4.

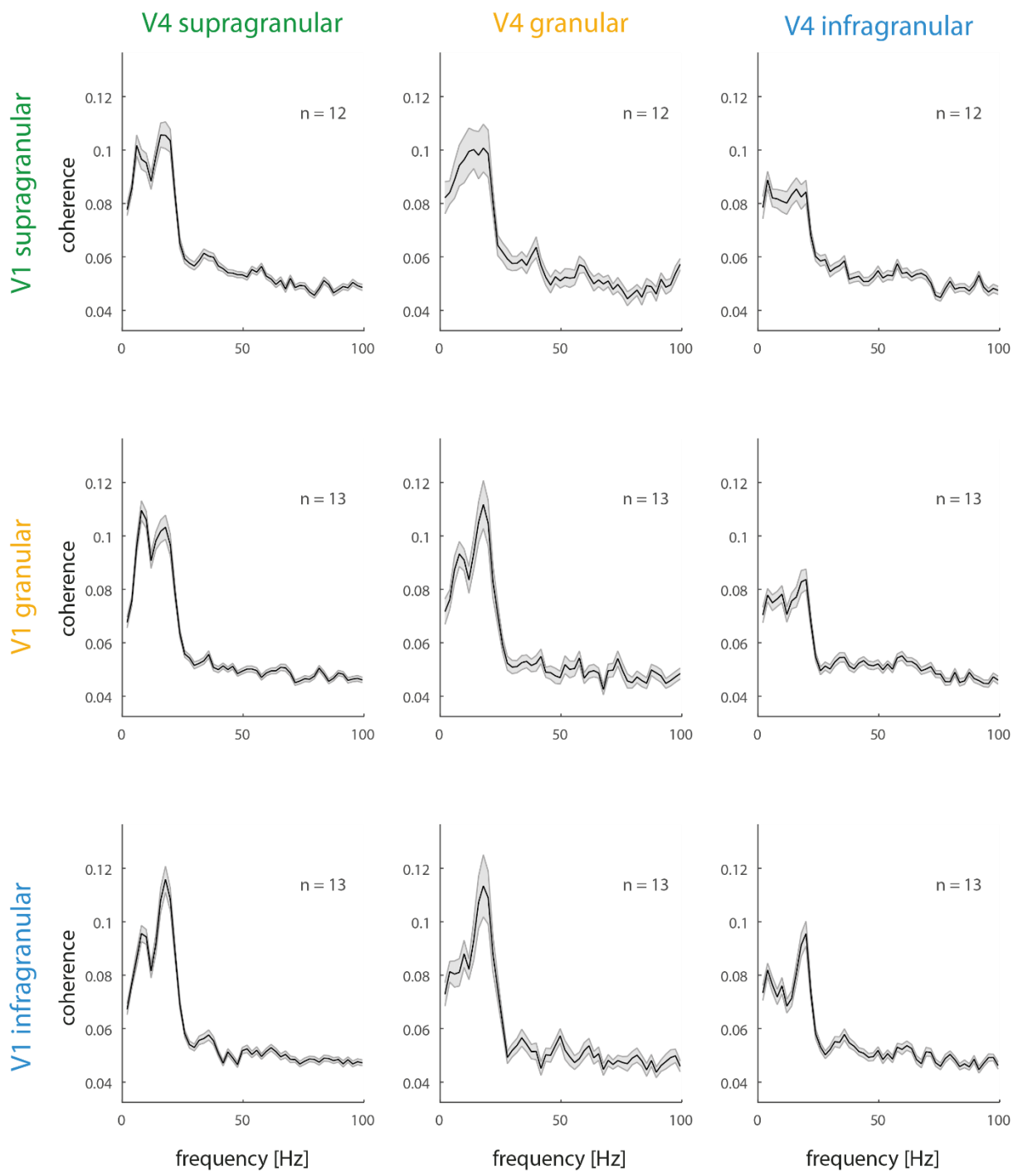

Figure 5-6: V1-V4 field-field coherence in Monkey 2 (left hemisphere) aligned to the stimulus onset (250ms to 761ms) in the attention task. Shown are all possible combinations of supragranular, granular and infragranular layer comparisons, averaged across the channels contributing to the respective sections (n = number of recordings in each plot). Coherence calculation and V1/V4 structure are as defined in Figure 5-4.

5.3.2 Field coherence prior to the first dimming

The field coherence between V1 and V4 of Monkey 1 showed similar patterns of attentional modulation whether aligned to the cue onset or the first dimming of the attention task (Figure 5-7, cue period not shown). It can be seen that the magnitude and peak frequency of low gamma coherence is significantly increased with attention. Attention also affected the main V1-V4 coherence peak. Attention to the RF resulted in a frequency shift across all layers, combined with an amplitude reduction when comparing coherence between V1 supragranular with all V4 subcompartments, and an amplitude increase when comparing V1 infragranular layers with all V4 subcompartments. Attention also reduced the magnitude of the lowest (<10Hz) coherence frequency peak for all comparisons.

In the right hemisphere of Monkey 2 (Figure 5-8) there was a slight trend for incresed V1-V4 field coherence with attention bewteen the V1 supragranular layers and V4, however this was only significant for a small portion of the frequency peak between supragranular V1 and V4 layers.

While more noisy, attentional modulation of coherence between V1 and V4 in the left hemisphere of Monkey 2 (Figure 5-9) showed a pattern similar to that seen in Monkey 1. Specifically attention to the RF resulted in a frequency shift of the peak located at ~10Hz in the attend away condition, to a peak location at ~18-20 Hz in the attend RF condition. For the comparison of V1 supragranular with all V4 subcompartments this was associated with a reduction in coherence maximum. For the comparison of V1 infragranular layers with all V4 subcompartments it was associated with an amplitude increase. In the gamma frequency range, there were suprious signs of increased coherence with attention, again, similar to what had been seen for Monkey 1.

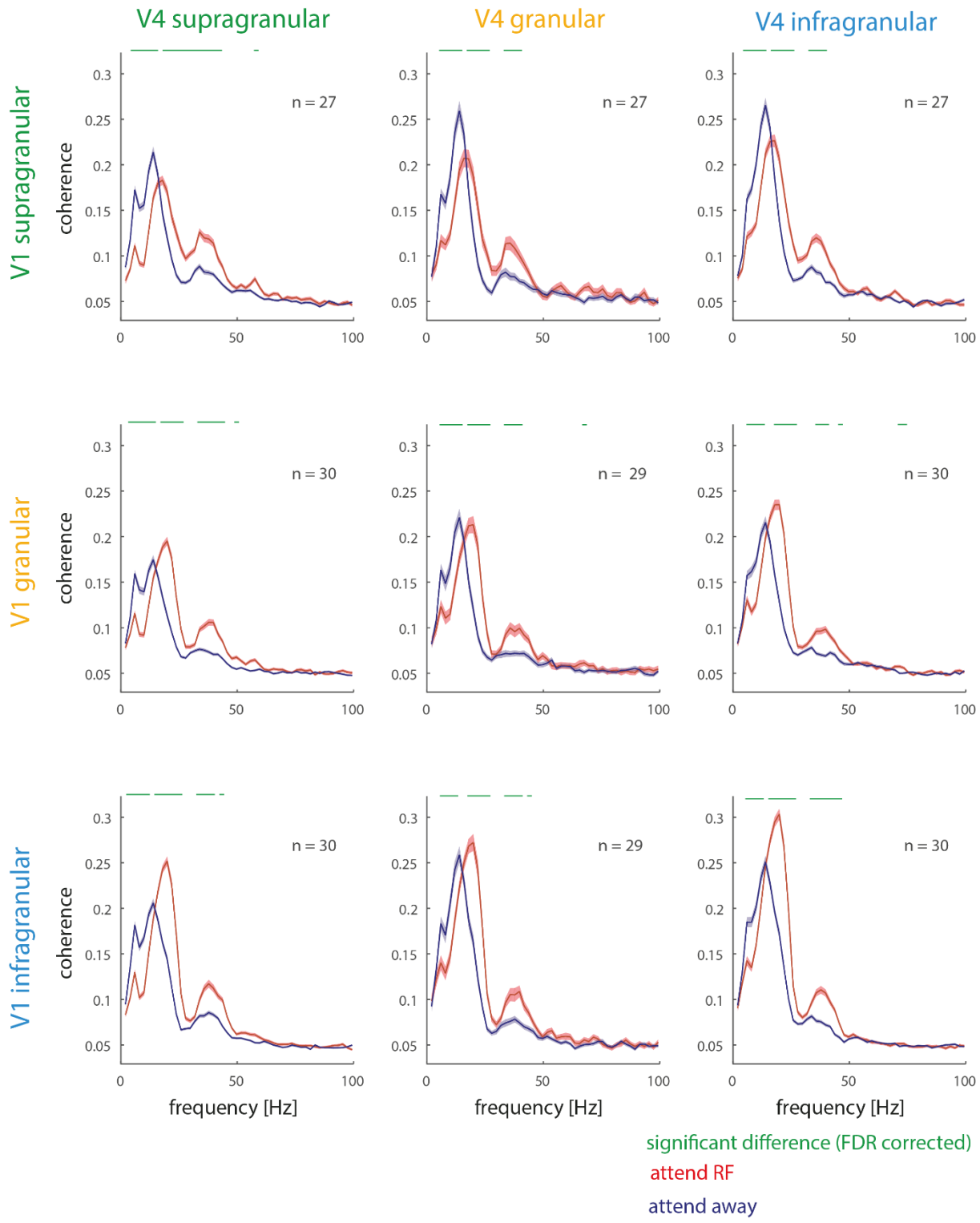

Figure 5-7: V1-V4 field-field coherence in Monkey 1 aligned to the first dimming (-511ms to 0ms) in the attention task. Shown are all possible combinations of supragranular, granular and infragranular layer comparisons, averaged across the channels contributing to the respective sections (n = number of recordings in each plot). Plotted separately for the attend RF (red) and attend away (blue) conditions. Green bars indicate a significant difference between the attention conditions (Wilcoxon signed rank test, $p<0.05$, FDR corrected). Coherence calculation and V1/V4 structure are as defined in Figure 5-4.

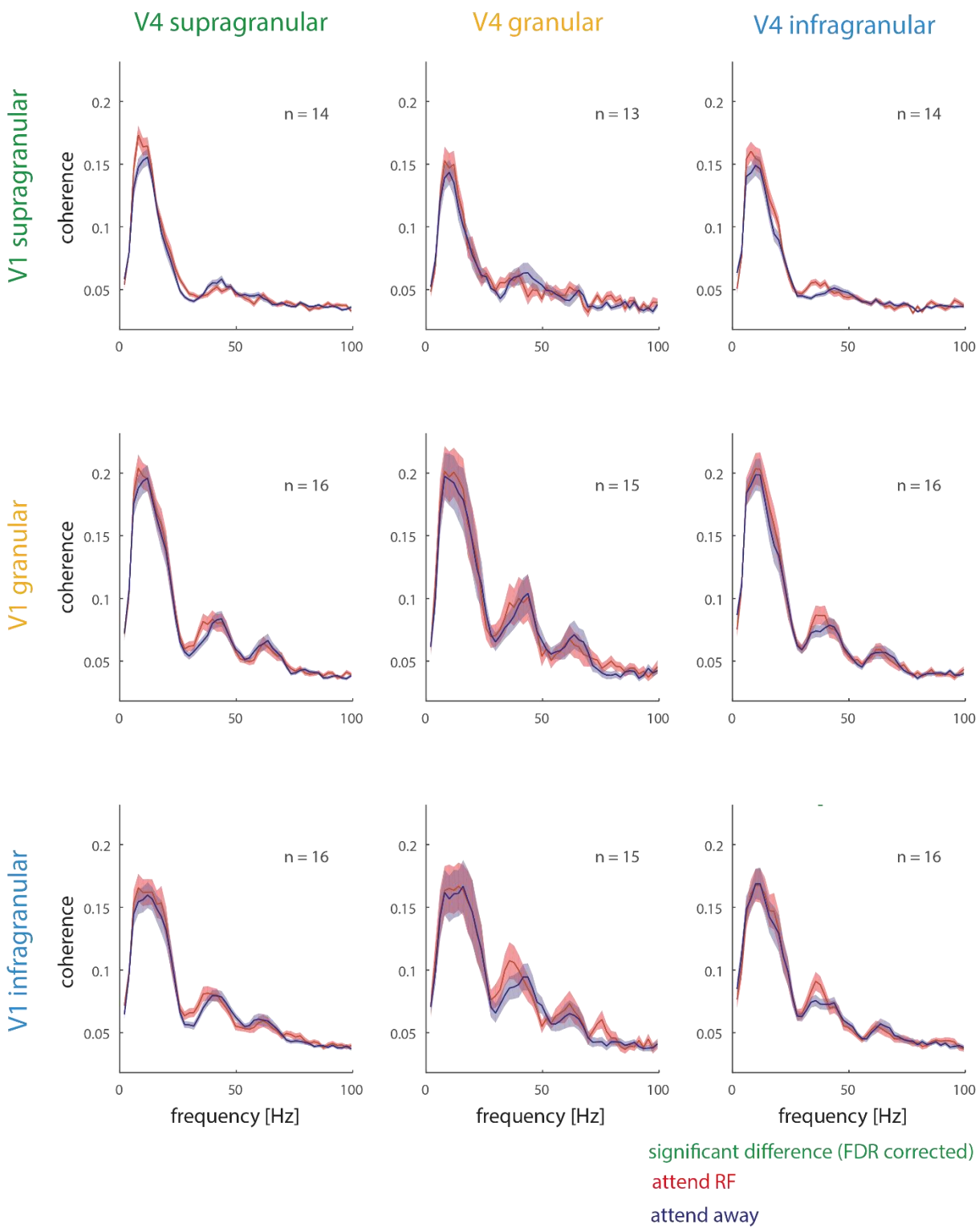

Figure 5-8: V1-V4 field-field coherence in Monkey 2 (right hemisphere) aligned to the first dimming (-511ms to 0ms) in the attention task. Shown are all possible combinations of supragranular, granular and infragranular layer comparisons, averaged across the channels contributing to the respective sections (n = number of recordings in each plot). Coherence calculation, significance bars, attention conditions and V1/V4 structure are as defined in Figure 5-7.

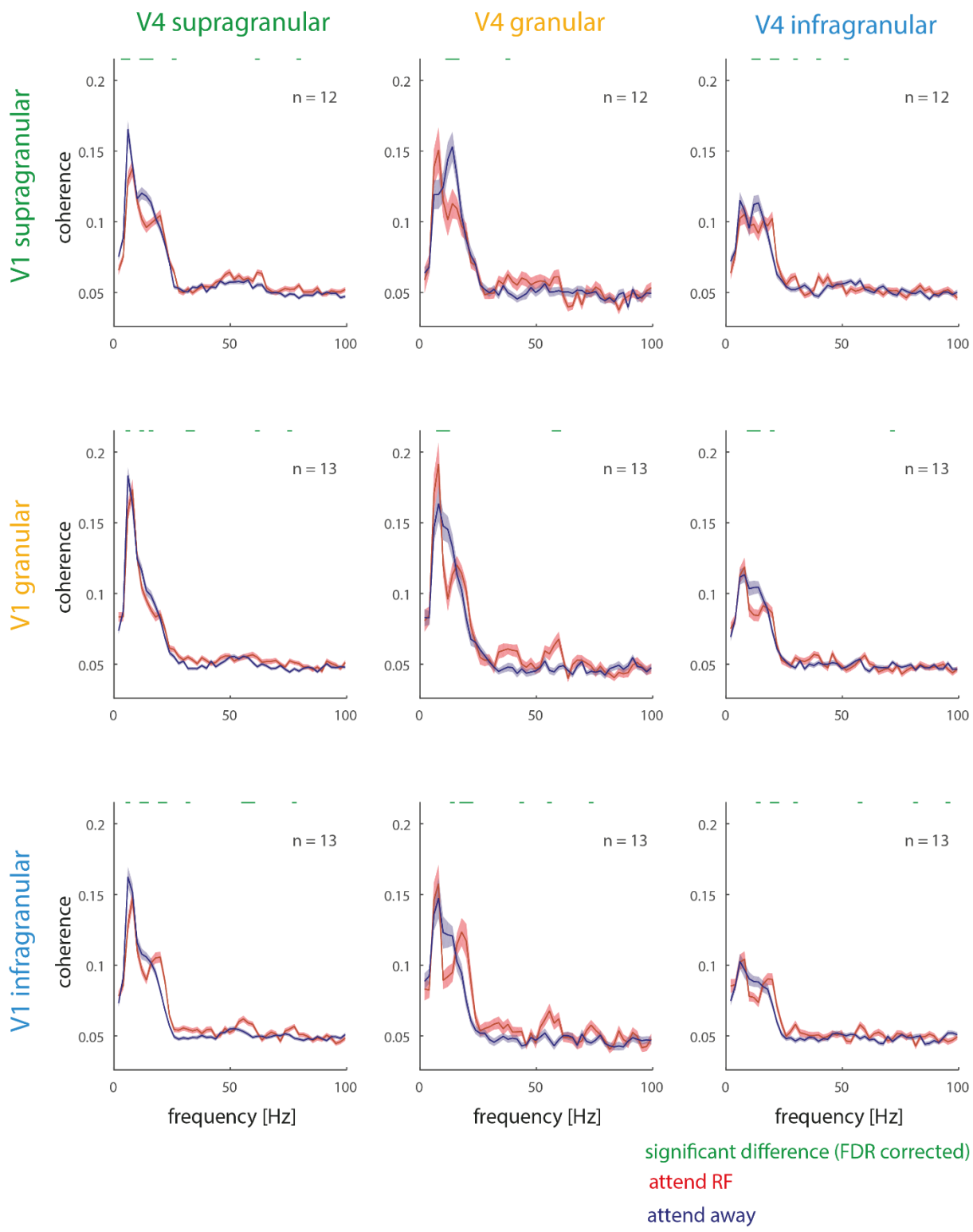

Figure 5-9: V1-V4 field-field coherence in Monkey 2 (left hemisphere) aligned to the first dimming (-511ms to 0ms) in the attention task. Shown are all possible combinations of supragranular, granular and infragranular layer comparisons, averaged across the channels contributing to the respective sections (n = number of recordings in each plot). Coherence calculation, significance bars, attention conditions and V1/V4 structure are as defined in Figure 5-7.

5.4 Granger causality

We used Granger causality to determine the direction of information flow in different frequency bands between V1 and V4. Granger causality was calculated separately for the feedforward direction from V1 to V4 and for the feedback direction from V4 to V1. We do not show the cue aligned Granger causality here, since in both monkeys it showed the same effects as in the dimming aligned period, but with a lesser magnitude.

5.4.1 Granger causality aligned to the stimulus onset

Aligning the Granger causality analysis to the stimulus onset of the task shows how information flows prior to any attentional context. In Monkey 1 (Figure 5-10) low frequency Granger causality peaks (~17Hz) were larger from V4 to V1 than from V1 to V4. The strongest causal influence in this frequency band was from V4 infragranular to V1 infragranular layers. From the V1 infragranular layers to all layers of V4 there was also a small peak in this frequency range. In the gamma frequency range Granger causality peaks (~46Hz) were significantly higher from V1 to V4 than from V4 to V1. GC peaks in the gamma frequency range from V1 to V4 were clearest from the V1 infragranular to all V4 layers, however there was also a clear peak from the V1 supragranular to V4 supragranular layers. In general the GC influence from V1 is strongest to V4 supragranular layers and decreases towards V4 infragranular layers.

The Granger causal spectra for the right hemisphere of Monkey 2 (Figure 5-11) also showed their strongest low frequency gamma (~44Hz) in feedforward connections (i.e. from V1 to V4). In addition, there was also a trend for a second, higher gamma peak (~68Hz) which was stronger in the feedback (V4 to V1) direction, but this difference was not significant for any of the layer combinations. Low frequency (12-25Hz) Granger causality was higher in the feedback direction between all layers of V4 and the V1 granular/infragranular layers. In addition this data set showed a peak of feedforward (V1 to V4) GC influence at ~8-10 Hz, which may have been triggered by the ‘jerkiness’ of the stimulus used.

The left hemisphere of Monkey 2 (Figure 5-12) also showed significantly higher feedforward than feedback Granger causality throughout the gamma frequency range

(30-100Hz). Unlike in the previous two figures, low frequency (~20Hz) Granger causality was highest in the feedforward direction and highest from V1 infragranular layers to the supragranular/granular layers of V4.

We also performed a separate cross correlation analysis (Appendix D.3) of the V1 and V4 LFP signals to confirm the direction of information flow which was indicated by the Granger causal analysis.

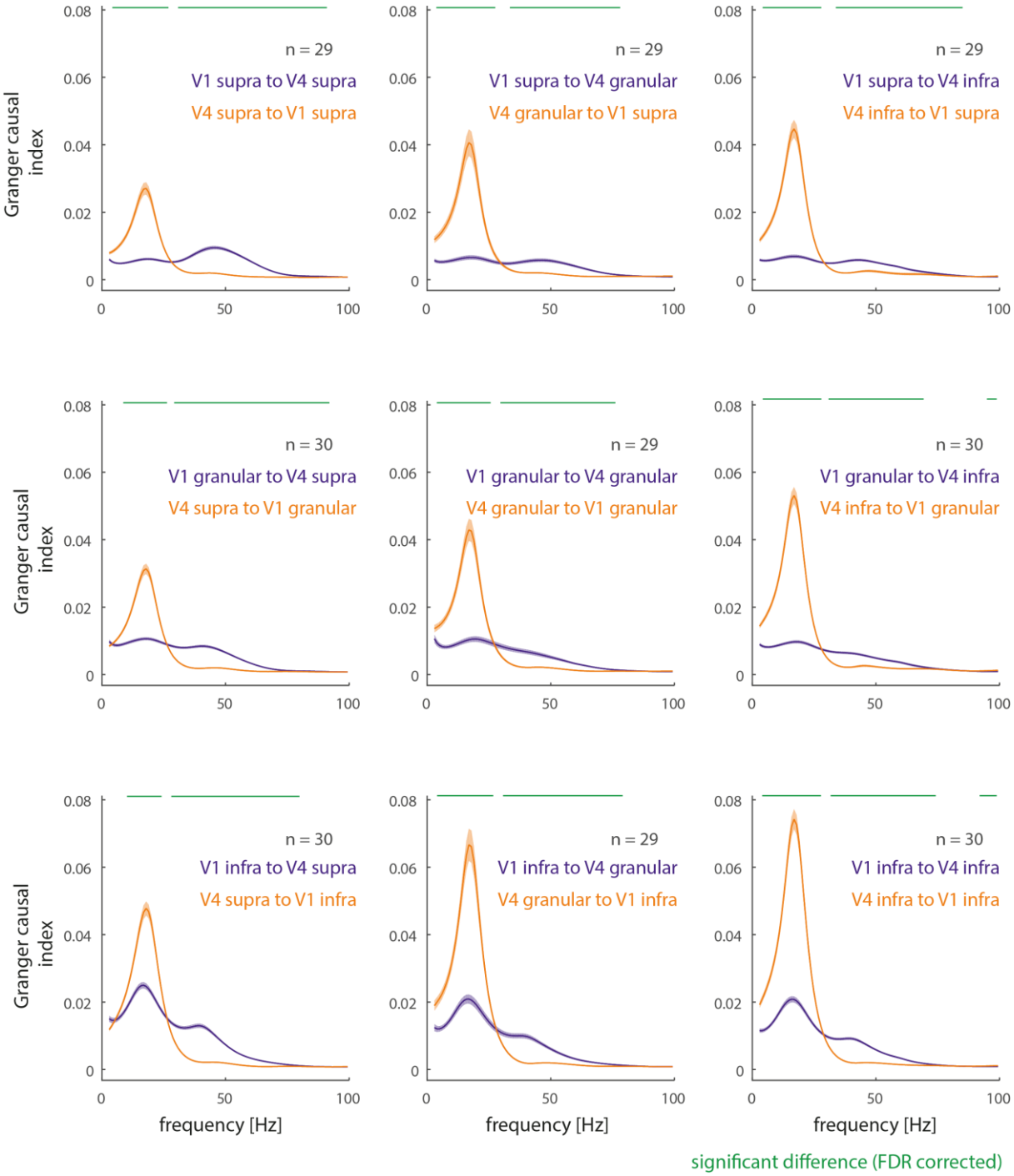

Figure 5-10: Granger causality between Monkey 1 V1 and V4 aligned to the stimulus onset (250ms to 761ms) in the attention task. Shown between all possible combinations of supragranular ("supra"), granular and infragranular ("infra") layers (n = number of recordings in each plot). Directionality of Granger causality spectra is indicated by the figure legends. Granger causality was calculated based on the bipolar derivation of the local field potential. Significance bars and V1/V4 structure are as defined in Figure 5-7.

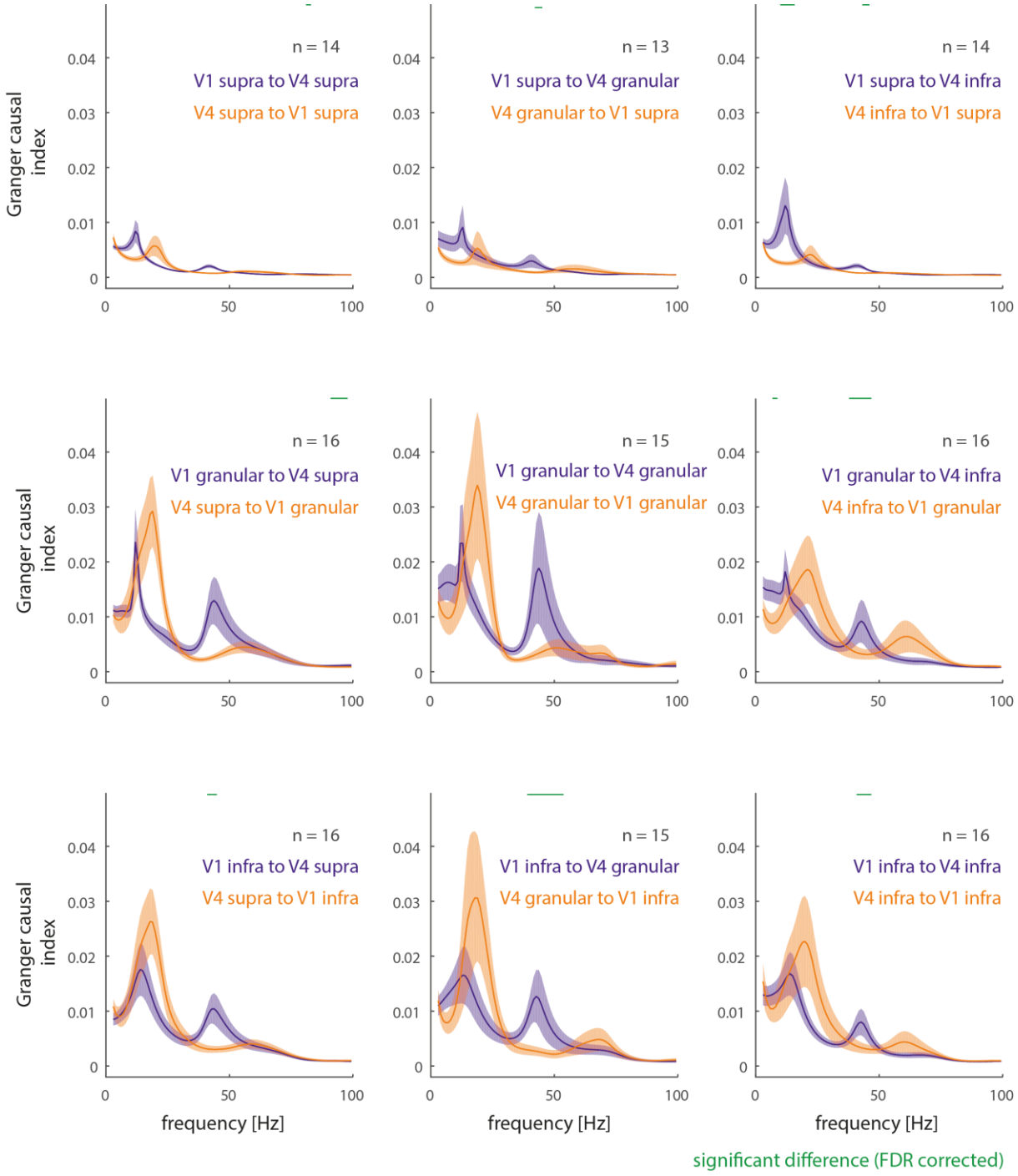

Figure 5-11: Granger causality between Monkey 2 (right hemisphere) V1 and V4 aligned to the stimulus onset (250ms to 761ms) in the attention task. Shown between all possible combinations of supragranular ("supra"), granular and infragranular ("infra") layers (n = number of recordings in each plot). Granger causality calculation, significance bars, directionality and V1/V4 structure are as defined in Figure 5-10.

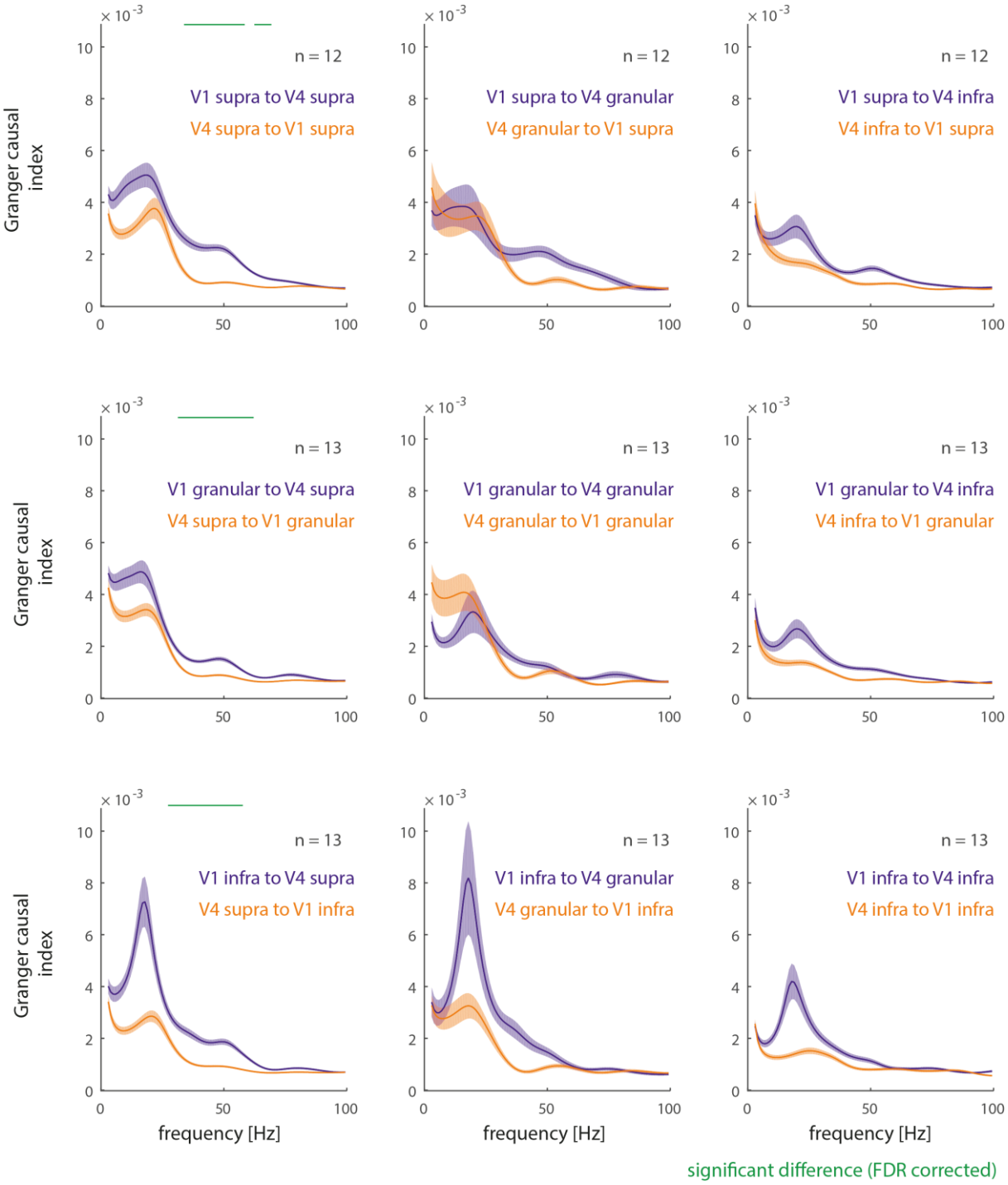

Figure 5-12: Granger causality between Monkey 2 (left hemisphere) V1 and V4 aligned to the stimulus onset (250ms to 761ms) in the attention task. Shown between all possible combinations of supragranular ("supra"), granular and infragranular ("infra") layers (n = number of recordings in each plot). Granger causality calculation, significance bars, directionality and V1/V4 structure are as defined in Figure 5-10.

5.4.2 Granger causality aligned to the first dimming (V1 to V4)

We calculated Granger causality between the LFPs of V1 and V4 aligned to the first dimming of the attention task. These are plotted separately for the feedforward (V1 to V4) and feedback (V4 to V1) directions so that the effects of attention in each direction can be seen clearly.

In the feedforward direction, low frequency GC influences in Monkey 1 (Figure 5-13) were significantly decreased by attention to the RF. This was also accompanied by an increase in the peak frequency, which can be seen clearly between the V1 infragranular layers and all V4 layers in the figure. The magnitude of gamma frequency Granger causality peaks was increased with attention in all layer combinations, again combined with an increase in the peak frequency.

In the right hemisphere of Monkey 2 there was little significant modulation of feedforward GC influence with attention (Figure 5-14). There was however a trend for the frequency of peaks in the low gamma range to be increased with attention to the RF.

Recordings in the left hemisphere of Monkey 2 (Figure 5-15) showed effects more akin to those observed in Monkey 1. The magnitude and peak frequency of gamma Granger causality were both increased with attention into the RFs of the recorded cells. A significant reduction in low frequency Granger causality was also observed between the granular and infragranular layers of V1 and all V4 layers.

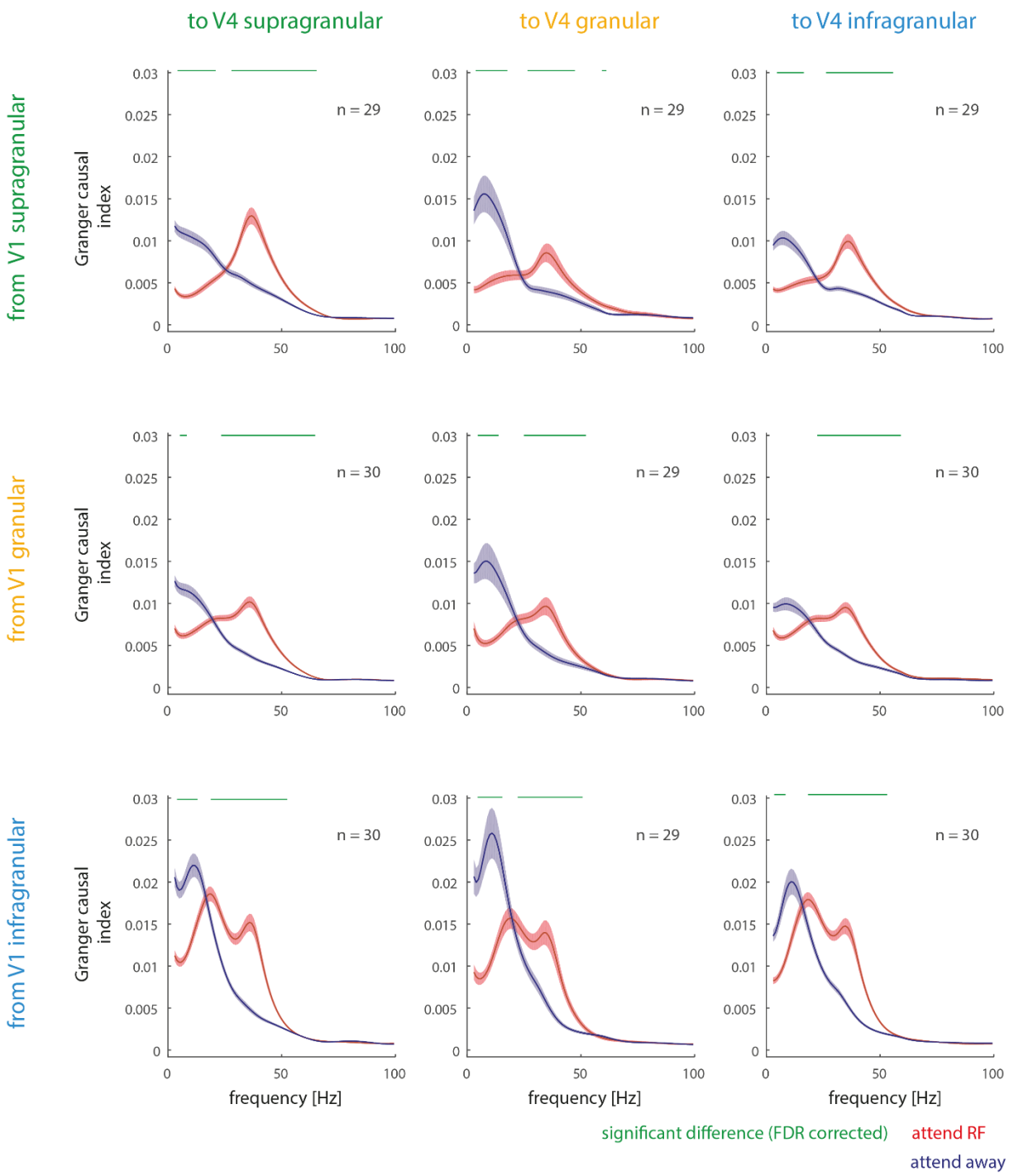

Figure 5-13: Granger causality between Monkey 1 V1 and V4 aligned to the first dimming (-511ms to 0ms) in the attention task. Shown are all possible combinations of supragranular, granular and infragranular layers (n = number of recordings in each plot). Plotted separately for the attend RF (red) and attend away (blue) conditions. Granger causality calculation, significance bars and V1/V4 structure are as defined in Figure 5-7.

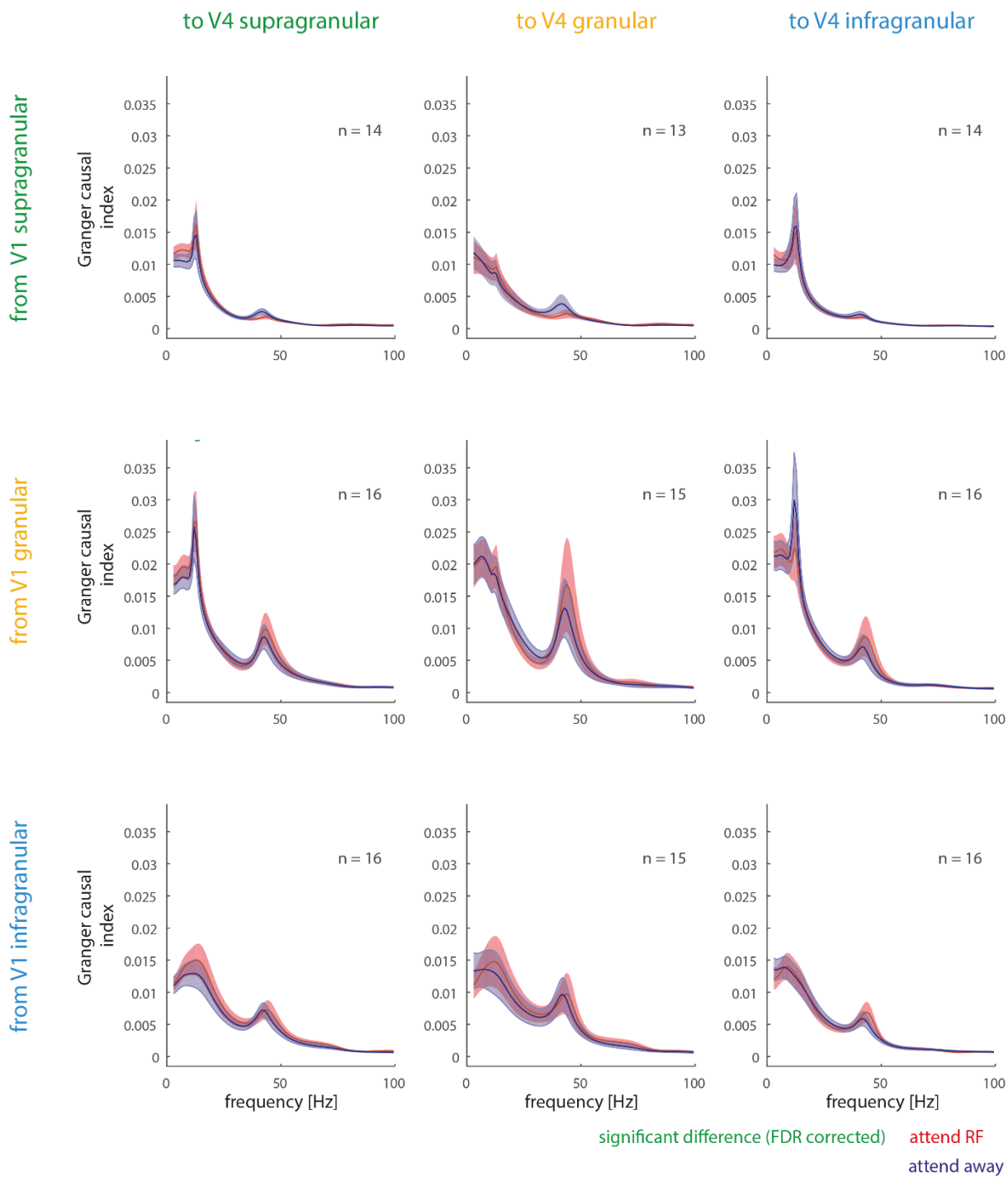

Figure 5-14: Granger causality between Monkey 2 (right hemisphere) V1 and V4 aligned to the first dimming (-511ms to 0ms) in the attention task. Shown between all possible combinations of supragranular, granular and infragranular layers (n = number of recordings in each plot). Granger causality calculation, significance bars, attention conditions and V1/V4 structure are as defined in Figure 5-13.

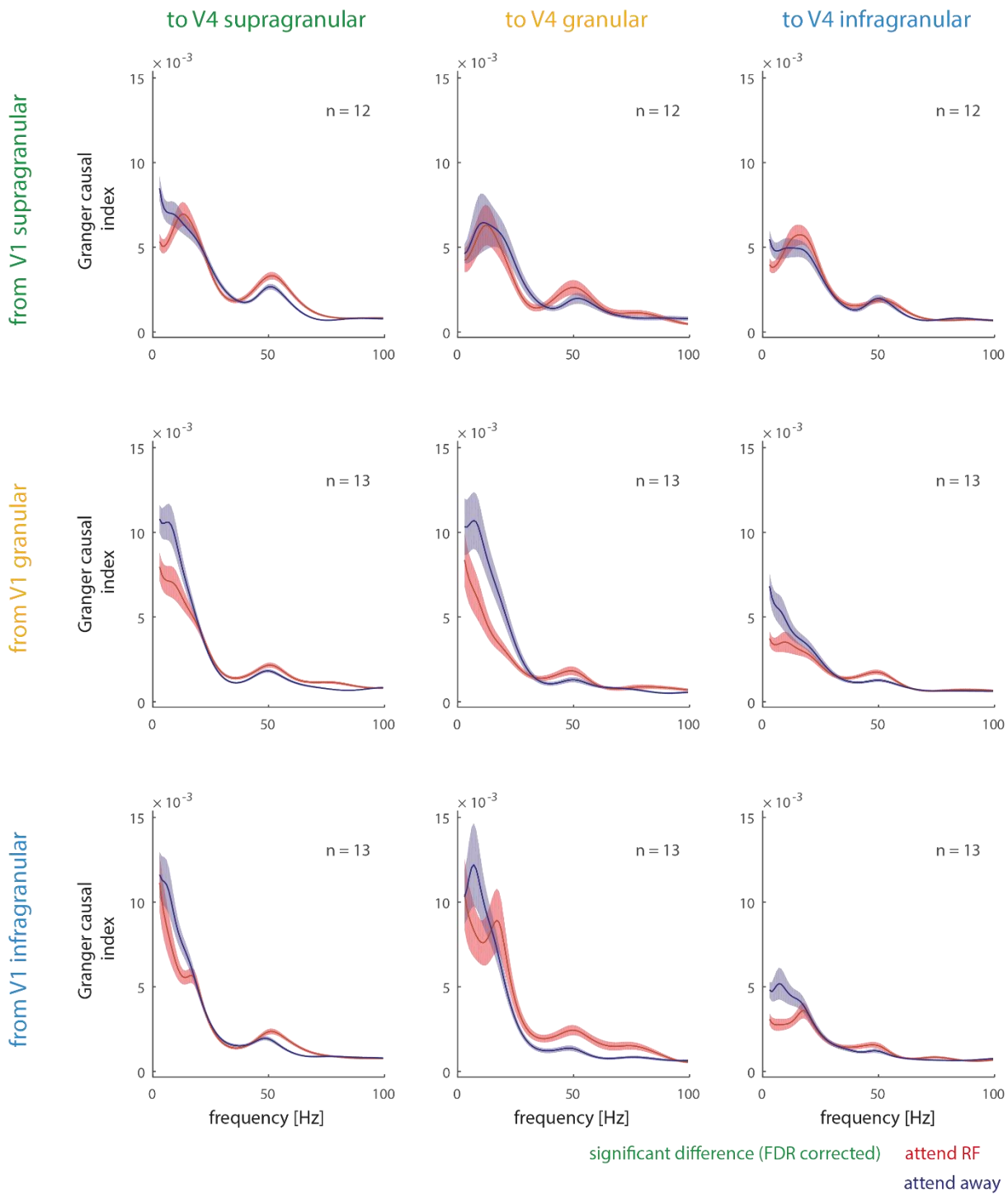

Figure 5-15: Granger causality between Monkey 2 (left hemisphere) V1 and V4 aligned to the first dimming (-511ms to 0ms) in the attention task. Shown between all possible combinations of supragranular, granular and infragranular layers (n = number of recordings in each plot). Granger causality calculation, significance bars, attention conditions and V1/V4 structure are as defined in Figure 5-13.

5.4.3 Granger causality aligned to the first dimming (V4 to V1)

The attention effects observed in the feedback (V4 to V1) Granger causality analysis were typically restricted to low frequencies. In Monkey 1 (Figure 5-16), attention to the RF increased the peak frequency of low frequency Granger causality. In addition the magnitude of GC influences increased for connections from V4 (all layers) to the granular/infragranular layers of V1 with attention to the RF.

Feedback GC influence in the right hemisphere of Monkey 2 (Figure 5-17) showed a significant increase with attention in a theta/alpha frequency range (4-12Hz) between all V4 layers and V1 supragranular layers. There was also a trend for an increase with attention in the gamma frequency band between all V4 layers and the granular/supragranular V1 layers, but this was only significant from the V4 supragranular layers.

The main effect of attention to the RF seen in the feedback Granger causality analysis in the left hemisphere of Monkey 2 (Figure 5-18) was a decrease of GC influence in the low frequency range (<25Hz). This difference was significant from V4 supragranular layers to all V1 layers and from the V4 infragranular layers to V1 supragranular layers.

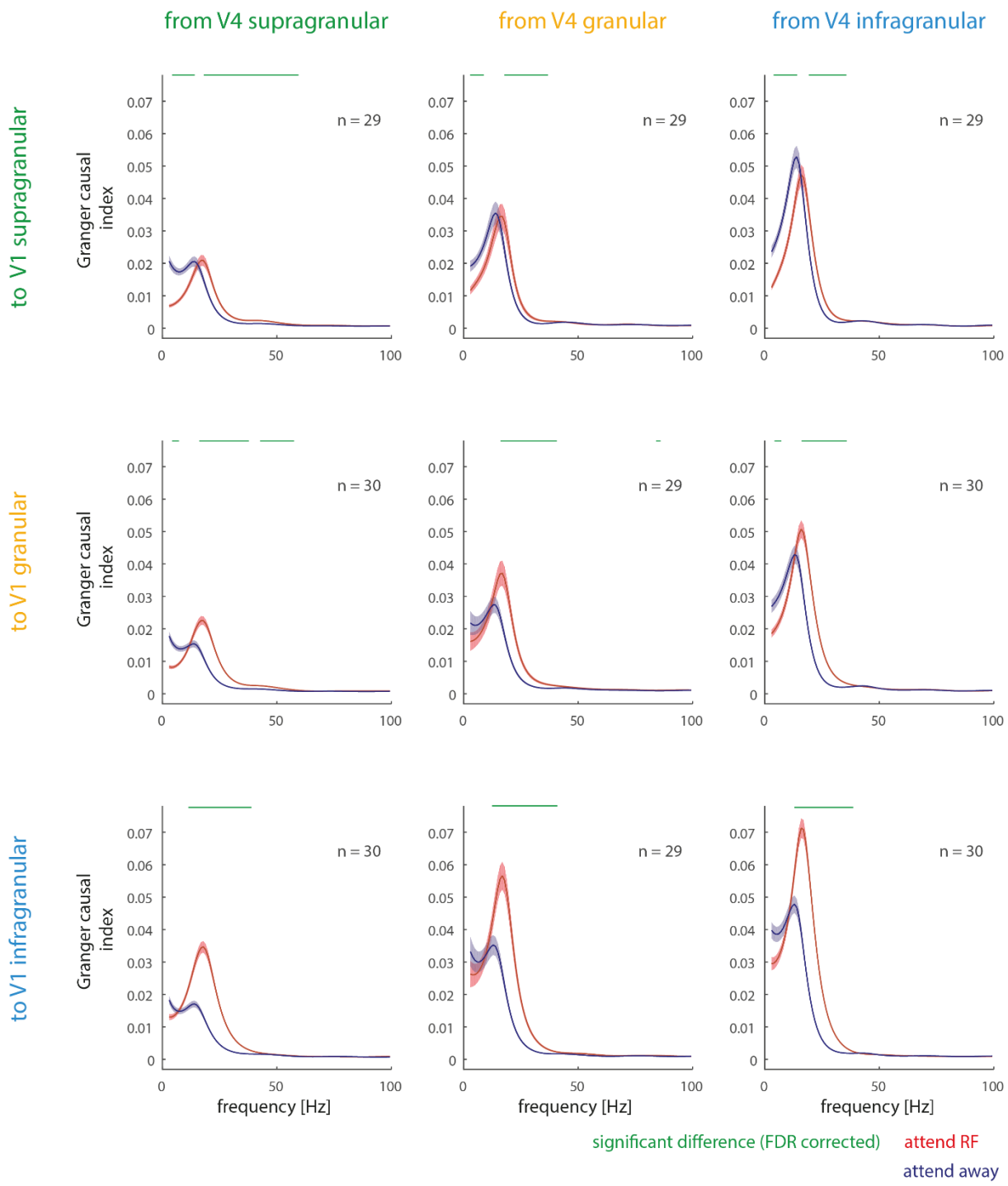

Figure 5-16: Granger causality between Monkey 1 V4 and V1 aligned to the first dimming (-511ms to 0ms) in the attention task. Shown between all possible combinations of supragranular, granular and infragranular layers (n = number of recordings in each plot). Plotted separately for the attend RF (red) and attend away (blue) conditions. Granger causality calculation, significance bars, and V1/V4 structure are as defined in Figure 5-10.

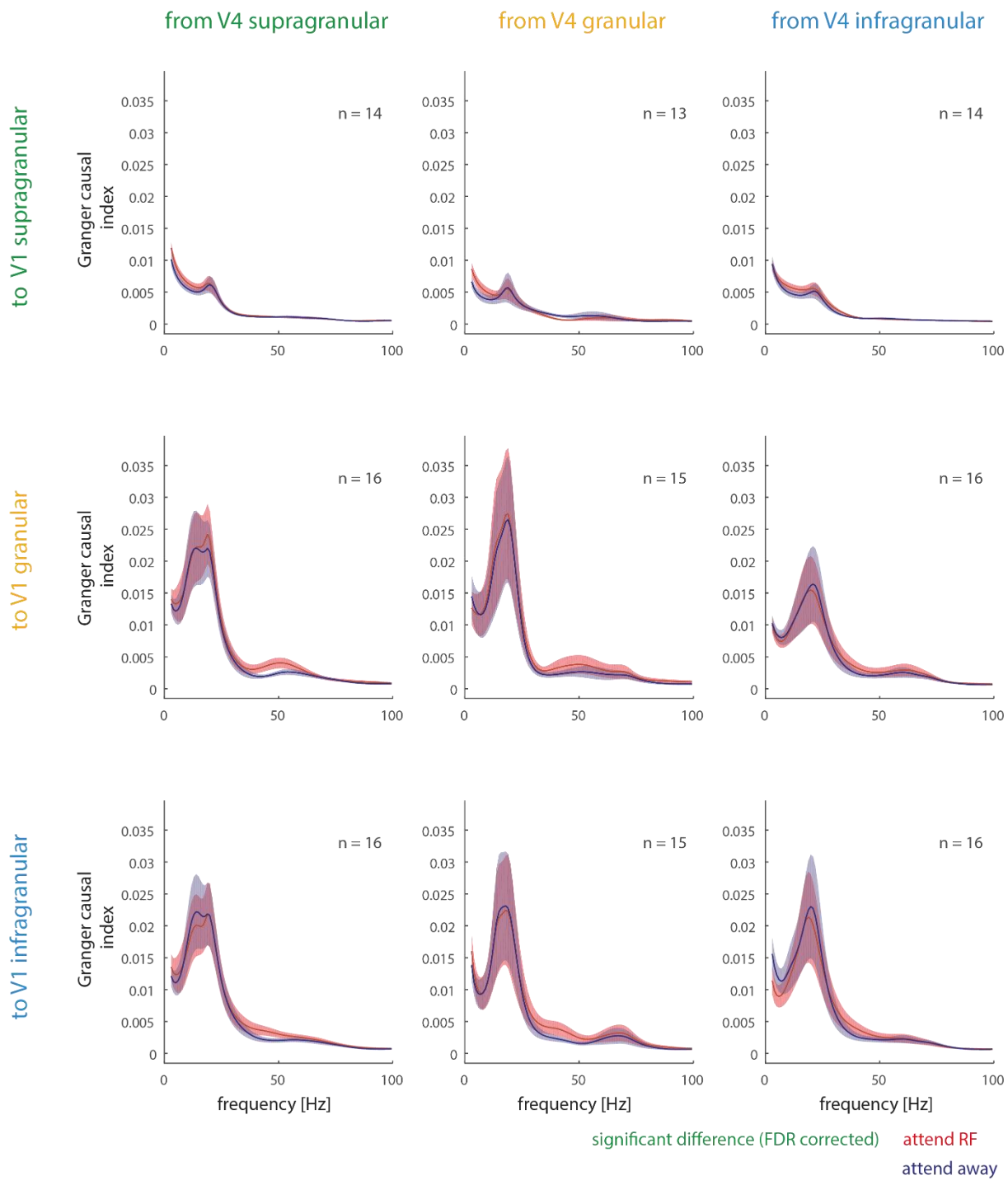

Figure 5-17: Granger causality between Monkey 2 (right hemisphere) V4 and V1 aligned to the first dimming (-511ms to 0ms) in the attention task. Shown between all possible combinations of supragranular, granular and infragranular layers (n = number of recordings in each plot). Granger causality calculation, significance bars, attention conditions and V1/V4 structure are as defined in Figure 5-16.

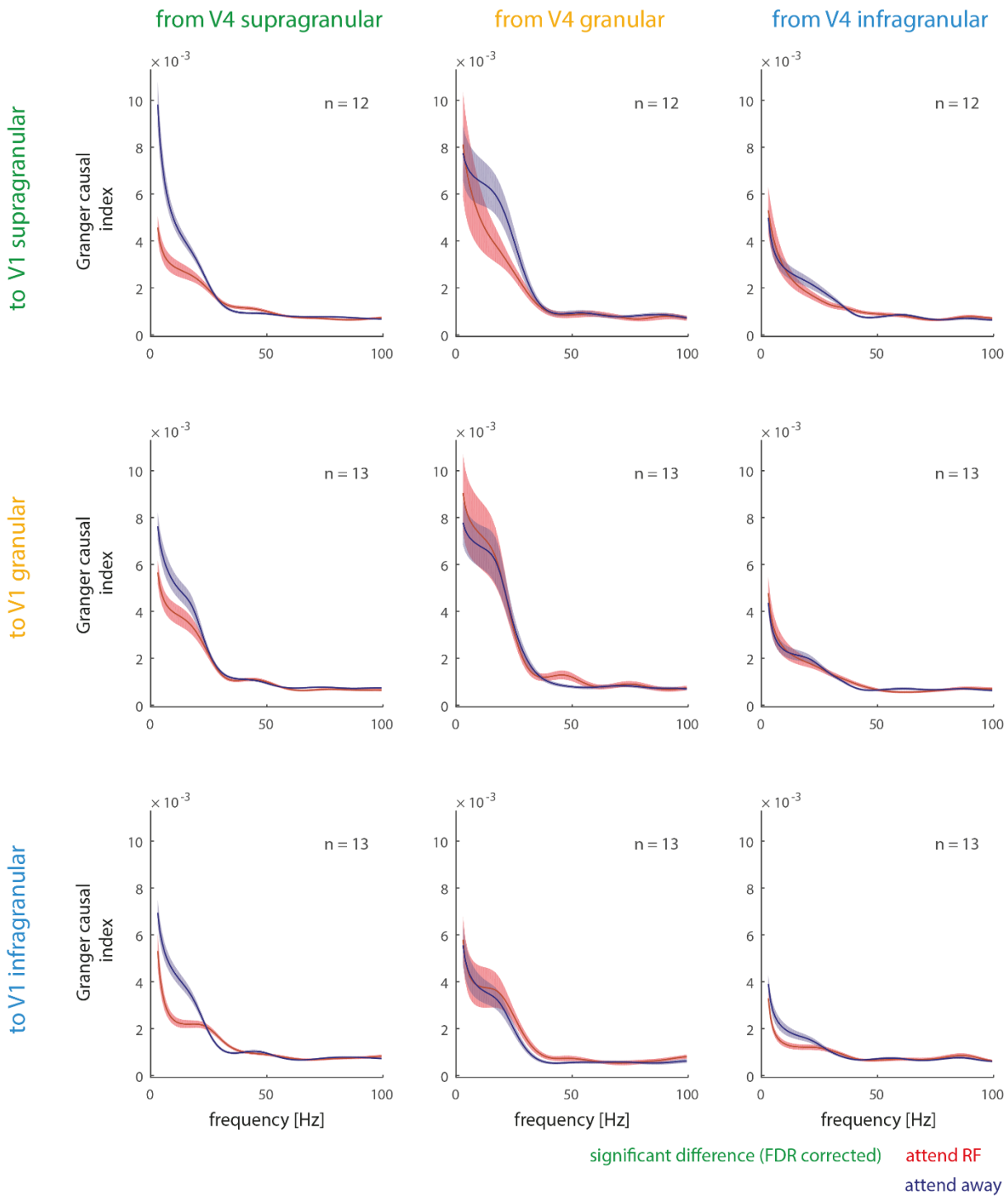

Figure 5-18: Granger causality between Monkey 2 (left hemisphere) V4 and V1 aligned to the first dimming (-511ms to 0ms) in the attention task. Shown between all possible combinations of supragranular, granular and infragranular layers (n = number of recordings in each plot). Granger causality calculation, significance bars, attention conditions and V1/V4 structure are as defined in Figure 5-16.

5.4.4 Granger causal networks

Next we generated potential networks of information flow between V1 and V4 based on the GC influences observed. We calculated these networks in the theta/alpha (4-12Hz), beta (13-25Hz), low gamma (30-50Hz) and high gamma (55-100Hz) frequency bands. Recordings in the left and right hemispheres of Monkey 2 are not shown here, since they did not survive the significance testing in these analyses.

We again calculated GC MIs as described in Section 2.4.8. Given the calculation, GC influences that are dominant from V1 to V4 (than the opposite direction) will yield positive MIs, while negative MIs will be obtained if the influence is stronger from V4 to V1. In Figure 5-19 and Figure 5-20, these directionalities are shown in two ways. Firstly the colour coding indicates the strength and the direction of the MI (warm colours show V1 to V4 influences, cold colours the opposite), and the location of the connecting line equally indicates directionality (left of electrode connecting lines show V1 to V4 dominant influences, right of electrode connecting lines show V4 to V1 dominant influences). Figure 5-19 (top) shows the dominant flow of information between V1 and V4 of Monkey 1 during the stimulus and first dimming aligned periods of the attention task. In both the theta/alpha and beta frequency bands, the dominant directionality was from V4 to V1. This was the case for most contacts along the entire V4 depths. There were a few V1 to V4 contacts where GC influences were more dominant in the feedforward direction. These terminated mostly on supragranular layers in V4 to connections from V1 (all but the uppermost supragranular channels) to the supragranular layers of V4. In the attend way conditions for both of the low frequency bands there was greater feedforward directionality to the V4 infragranular layers than for the attend RF condition (Figure 5-20, top).

In both of the gamma frequency bands stimulus aligned GC influences dominated in the feedforward direction from V1 to V4 and were strongest between the supragranular layers of V1 and supragranular layers of V4. When aligned to the first dimming of the task, low gamma directionality was higher for the attend RF condition. There was no clear difference between the attention conditions in the high gamma band, however both conditions.

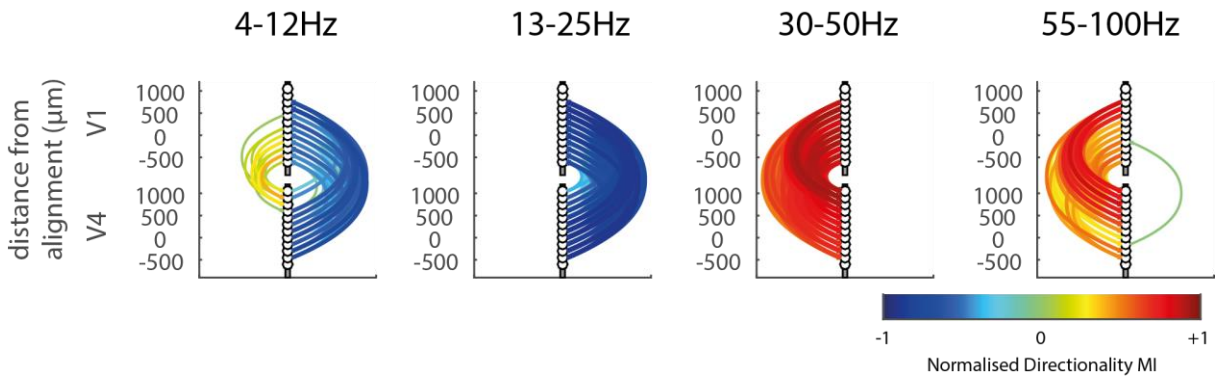

Figure 5-19: Granger causal local networks between V1 (upper contacts in plots) and V4 (lower contacts in plots) in Monkey 1 between electrode contacts relative to the alignment channel aligned to the stimulus onset (250-761ms). Calculated for the theta/alpha (4-12Hz), beta (13-25Hz), low gamma (30-50Hz) and high gamma (55-100Hz) frequency. Directionalities are calculated as a modulation index (MI) based on the Granger causality in each direction between all possible electrode contacts. Feedforward (i.e. V1 to V4) directionalities are represented by positive MIs (yellow/red arrows) and drawn on the left hand side of the subplots. Feedback (i.e. V4 to V1) directionalities are represented by negative MIs (cyan/blue arrows) and drawn on the right hand side of the subplots. Only directionalities which were significantly different to zero are shown in these plots (Wilcoxon signed rank test, $p<0.05$ FDR corrected).

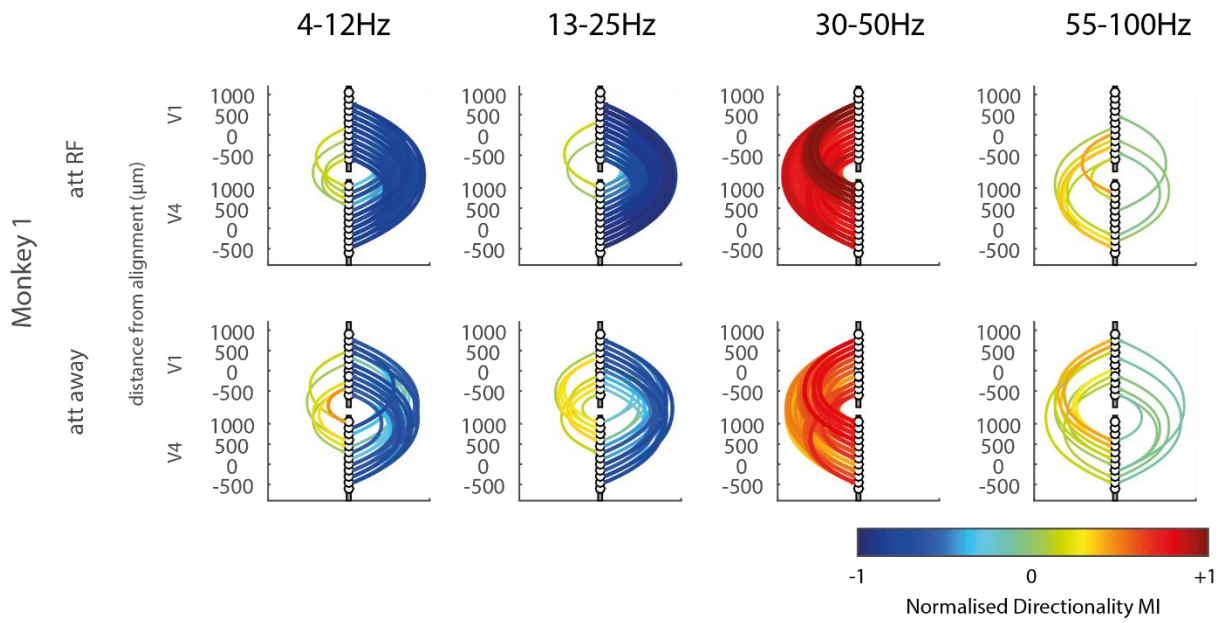

Figure 5-20: Granger causal local networks between V1 (upper contacts in plots) and V4 (lower contacts in plots) in Monkey 1 between electrode contacts relative to the alignment channel aligned to the first dimming (-511-0ms, separately for the attend RF ["att RF"] and attend away ['att away"] conditions). Calculated for the theta/alpha (4-12Hz), beta (13-25Hz), low gamma (30-50Hz) and high gamma (55-100Hz) frequency bands. Directionality MI calculation and plotting as in Figure 5-19. Only directionalities which were significantly different to zero are shown in these plots (Wilcoxon signed rank test, $p<0.05$ FDR corrected).

5.4.5 Granger causal attentional networks

We calculated attentional MIs of GC influences to determine how attention affected the information flow between V1 and V4 for both Monkeys (Figure 5-21). Since the analysis in Monkey 2 did not survive significance testing, we do not show those results here.

In the theta/alpha frequency range attention to the RF reduced GC influences in the feedforward and feedback directions for both monkeys. The strongest reduction of feedback GC influences occurred between the V4 supragranular and V1 supragranular layers. There was no clear layer specificity for feedforward modulation. The attentional network in the beta range showed both increases and decreases of Granger causality with attention. Feedback was increased by attention and feedforward causality was decreased by attention.

In the low gamma frequency ranges, there was increased feedforward and feedback GC influences with attention even if these seemed somewhat more pronounced in the feedforward direction. In the high gamma frequency range GC there were a small number of significant attentional modulations from V1 to V4 which terminated in the V4 supragranular layers.

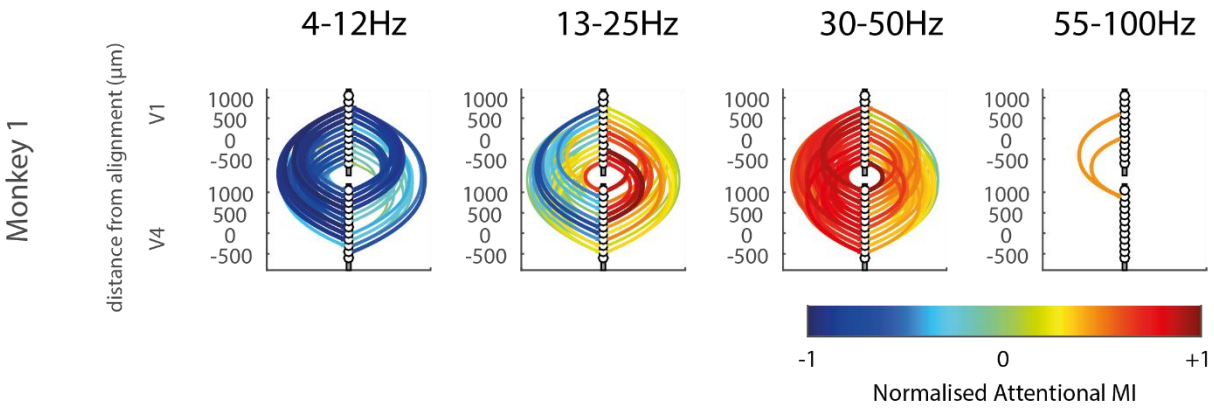

Figure 5-21: Attentional modulation of Granger causal influences between V1 (upper contacts in plots) and V4 (lower contacts in each subplot) in Monkey 1 and Monkey 2 (left hemisphere). Attentional GC MIs were calculated for the theta/alpha (4-12Hz), beta (13-25Hz), low gamma (30-50Hz) and high gamma (55-100Hz) during the first dimming aligned (-511-0ms) period. Feedforward (i.e. V1 to V4) directionalities are represented drawn on the left hand side of the subplots. Feedback (i.e. V4 to V1) directionalities are drawn on the right hand side of the subplots. Colour coding indicates whether attention increased (warm colours) or decreased (cold colours) the GC influence for any given direction (and contact pairing). Only modulation indices which were significantly different to zero are shown in these plots (Wilcoxon signed rank test, $p<0.05$ FDR corrected).

5.5 Summary

This chapter has described how activity in V1 and V4 interacted during the attention task. The analysis mention included noise correlations, field coherence and Granger causality.

The attentional modulation of noise correlations between V1 and V4 matched the decreases which were observed within each area.

In one monkey, clear attentional modulation of field coherence between V1 and V4 was found. In the gamma frequency range coherence was increased by attention, but in the low frequency range there was a mix of increases and decreases. In both frequency ranges the peak frequency was increased by attention into the RF of the recorded cells.

Granger causality showed that gamma activity was feedforward from V1 to V4, whereas low frequency oscillations were feedback, from V4 to V1. Attention modulated Granger causality between the areas, increasing it in the gamma frequency range and decreasing it in the theta/alpha frequency range.

Chapter 6: Discussion

We set out to investigate how attention affects activity in the different layers of V1 and V4 at the levels of spiking activity and local field potentials (see Study Aims, Section 1.4). Overall we found a fairly consistent pattern between monkeys when analysing the spiking activity, but a rather inconsistent pattern between monkeys when analysing the LFP activity.

Figure 6-1 shows the summary of attention effects within V1 and V4 for each of the analyses in our study. The effects of attention on interactions between V1 and V4 are summarised in Figure 6-2. These effects will be discussed further in the subsequent sections of this chapter.

	Monkey 1		Monkey 2 (right)		Monkey 2 (left)	
	V1	V4	V1	V4	V1	V4
MUAE	↑	↑	↑	↑	↑	↑
Firing rate	↑	↑	↑	↑	↑	↑
Fano factor	↓	-	↓	-	↓	-
Gain variance	↓	↓	↓	↓	↓	↓
Noise correlations	↓	↓	-	-	↓	↓
LFP power (theta/alpha)	↓	↓	-	-	↓	↓
LFP power (beta)	↑	↑	↑	-	↑	↑
LFP power (low gamma)	↑	↑	↓	-	↓	↑
LFP power (high gamma)	↑	↑	↑	-	↑	↑
Field coherence (theta/alpha)	↓	↓	-	-	-	-
Field coherence (beta)	mix	mix	-	-	↑	-
Field coherence (low gamma)	mix	↑	↓	-	↓	↑
Field coherence (high gamma)	↑	↑	-	-	-	↑
Granger causality (theta/alpha)	↓	-	↑	-	-	-
Granger causality (beta)	mix	mix	↓	-	-	↓
Granger causality (low gamma)	mix	↑	↓	-	↓	-
Granger causality (high gamma)	-	↑	-	-	-	-

Figure 6-1: Summary of attention effects in V1 and V4. Shown for Monkey 1 and the right and left hemispheres of Monkey 2. Where attention increased a metric, this is indicated by a green arrow and where it decreased a metric this is indicated by a red arrow. If there was a combination of increases and decreases then this is indicated by “mix”.

	Monkey 1	Monkey 2 (right)	Monkey 2 (left)
Noise correlations	↓	-	↓
Field coherence (theta/alpha)	↓	-	mix
Field coherence (beta)	mix	-	mix
Field coherence (low gamma)	↑	-	-
Field coherence (high gamma)	-	-	-
Granger causality (V1-V4, theta/alpha)	↓	-	↓
Granger causality (V1-V4, beta)	↓	-	-
Granger causality (V1-V4, low gamma)	↑	-	↑
Granger causality (V1-V4, high gamma)	-	-	-
Granger causality (V4-V1, theta/alpha)	↓	-	↓
Granger causality (V4-V1, beta)	↑	-	-
Granger causality (V4-V1, low gamma)	-	-	-
Granger causality (V4-V1, high gamma)	-	-	-

Figure 6-2: Summary of attention effects between V1 and V4. Shown for Monkey 1 and the right and left hemispheres of Monkey 2. Where attention increased a metric, this is indicated by a green arrow and where it decreased a metric this is indicated by a red arrow. If there was a combination of increases and decreases then this is indicated by “mix”.

6.1 Spiking activity in the visual cortex

6.1.1 Multiunit responses

As reported in the previous literature (Moran and Desimone, 1985; Motter, 1993; Roelfsema *et al.*, 1998; McAdams and Maunsell, 2000; Roberts *et al.*, 2007), single-cell and multiunit activity in both V1 and V4 was increased with attention into the RFs of the recorded cells in our study. The difference between the attend RF and attend away conditions increased steadily until a dimming occurred, with the strongest modulation occurring immediately prior to the dimming. When the first dimming occurred, we observed a visual response to the dimming when it occurred within the RF of the recorded cells. This was strongest when attention was over the RF. Additionally, when the dimming occurred outside of the RF, the response when attention was also away from the RF was small and when attention was towards the RF the response was inhibitory. Together, these results suggest that attention to the RF acts as a strong (spatial?) filter to eliminate irrelevant responses.

6.1.2 Single cell responses

In the single cell analyses, we observed similar effects in both V1 and V4, so these will be discussed jointly here. Separating cells into narrow spiking and broad spiking cells showed that narrow spiking cells had higher firing rates in our task. This is in line with previous reports from area V4 (Mitchell *et al.*, 2007) and from the FEF (Thiele *et al.*, 2016). Narrow spiking cells in our study had higher variability than broad spiking cells, as measured by both gain variance and Fano factor. The latter finding is not in line with previous results from area V4 (Mitchell *et al.*, 2007) and from area FEF data (Thiele *et al.*, 2016). The rate differences between narrow and broad spiking cells in our V4 population were much smaller than those reported by Mitchell et al. (2007, see their Figure 2). We assume that this could be partly due to sampling procedures. Mitchell *et al.* (2009) recorded from single electrodes, where (at least according to our experience) sampling is biased by activity strength, i.e. highly active cells are more likely to be sampled. The laminar electrodes are unlikely to produce the same bias, as cell quality or response properties cannot be optimized for individual contacts. It might thus be the case that Mitchell *et al.* (2009) sampled preferentially from the most active narrow spiking cells. Our Figure 4-5 shows a rather broad distribution of stimulus induced firing rates in all layers for both cell types.

We observed that Fano factors were lower when aligned to the stimulus or cue onset than when aligned to the first dimming. It has been shown that stimulus onset quenches variability (Churchland *et al.*, 2010; Chang *et al.*, 2012; Purcell *et al.*, 2012; Thiele *et al.*, 2016), which would explain why we see lower Fano factors in these task periods. While this may be one of the contributing factors, aligning to the time of cue onset or to the time first dimming also adds variability of time relative to the stimulus onset. This is because cue onset and first dimming times were variable after stimulus onset. Given that neuronal responses slowly decrease after a response transient, variable amounts of decreases will have occurred when aligned to (variable) cue or first dimming times. This variability would be larger for alignments to the first dimming than to cue onset, and it would inflate the FF. Thus the difference in FF could be due to reduced stimulus onset induced ‘quenching’ of variability, and due to an inflation of FF caused by alignment procedures.

Variability, as measured by both Fano factor and gain variance, was largest in the supragranular layers of V1 and V4, and lowest in infragranular layers. To our

knowledge, no study to date has investigated the layer dependence of rate variability using either measure. Our data show that the (subcortical) output from a processing unit (infragranular layers) exhibits the most reliable code (lowest rate variability), and also has the lowest firing rate.

6.1.3 Attentional modulation of single cell responses

Attention to the RF increased the firing rates of cells compared to when attention was directed away from the RF. Broad and narrow spiking cells did not differ in that respect in either V1 or V4. This was somewhat surprising, as it has been reported that narrow spiking cells in V4 (Mitchell *et al.*, 2009) and in FEF (Thiele *et al.*, 2016) show larger attentional rate modulation than broad spiking cells did. The discrepancy is unlikely due to the task or stimuli used, as the design in this thesis was identical to that used by Thiele *et al.* (2016). Discrepancies could possibly arise from the more opportunistic sampling that is a consequence of laminar electrode recordings, where overall more neurons with lower firing rates were recorded, and these may be the ones with lower attentional rate modulation.

As reported previously (Herrero *et al.*, 2013), we observed that attention significantly reduced the Fano factors of V1 cells in our study. However, this was not found in our V4 cell sample which is unlike previous studies performed in extrastriate cortex (Mitchell *et al.*, 2007; Niebergall *et al.*, 2011). One possibility which could be causing this, is that these previous studies were performed using either static stimuli (Mitchell *et al.*, 2009), or recordings from neurons specialized to analyse moving stimuli (Niebergall *et al.*, 2011), whereas the stimuli in our study were slowly drifting gratings, and cells in V1 and V4 are less specialized for motion analysis. The constant drifting across the receptive fields of neurons could have resulted in an ongoing ‘quenching’ of intrinsic variability in firing rates, similar to a sudden stimulus onset, which may have masked the attentional modulation of FFs. We did however find that attention decreased firing rate variance in both V1 and V4 as measured by gain variance. This effect of attention has also been reported in the FEF (Thiele *et al.*, 2016).

Why would gain variance show a reduction with attention, while FFs did not? Possible reasons have been delineated by Thiele *et al.* (2016), who argued that the expansive nonlinearity that links FFs and firing rates, might cause an increase in FFs with

increased firing rates, that is not overcome by the simultaneous reduction caused by attention. That brings about the question, whether gain variance is equally tied to firing rates, whereby higher rates automatically result in lower gain variance. This problem has been discussed (and addressed) by Thiele *et al.* (2016). Our data add to this, as we find that narrow spiking cells, which have higher firing rates than broad spiking cells, also had higher gain variance. Thus, higher rates are not automatically tied to lower gain variance. The same was found for rate and gain variance layer differences. Firing rates in supragranular layers were higher than in infragranular layers, and gain variance followed that scheme. At the same time, firing rates were higher with attention to the RF whilst gain variance was lower. These results argue against a fixed link between firing rate and gain variance.

There were also several theories of attention which our results could not contribute towards. Within a recording session, each stimuli in our attention task was placed in the same location during each trial and did not vary in size, colour or contrast. This meant that we were unable to treat these as varying factors in our analysis. Therefore our results could not be used to pass comment on the contrast gain, biased competition, feature similarity gain or normalisation models of attention.

6.1.4 Noise correlations of single cells

Noise correlations between neurons within the same layers, between layers within the same area, as well as between areas were relatively small, but on average positive. This is consistent with many other studies (Smith and Kohn, 2008; Cohen and Maunsell, 2009; Mitchell *et al.*, 2009; Herrero *et al.*, 2013; Smith *et al.*, 2013; Ruff and Cohen, 2016). However, it differs from the data reported in a few experimental and theoretical studies, which argue for noise correlations to be on average very close to zero (Ecker *et al.*, 2010; Renart *et al.*, 2010) Positive average noise correlations could arise if cells share common input (Moore *et al.*, 1970; Ruff and Cohen, 2016). Overall, we observed the largest noise correlations within cortical layers. If compared between layers, we found differences between area V1 and V4. Overall noise correlations were larger in V4 than in V1. Moreover, in V1 noise correlations were larger in supragranular layers than in the other layers, while in V4, they were largest in granular layers. However, it has to be noted that the sample size of pairs of neurons from

granular layer in V4 was fairly small, as this layer is comparatively thin. This means that many of the (few) V4 granular pairs may have been recorded from the same electrode. The latter will yield higher noise correlations, when compared to between contact pairs, as spatial proximity is a key factor affecting the size of noise correlations. Future analyses will have to account for this, by e.g. calculating noise correlations for pairs from other layers that were recorded from the same electrode contact.

We found that noise correlations were larger within layers. This was expected, as these neurons are likely to receive more common input, than neurons located in different layers. The fact that neuron pairs located in supragranular layers had on average the largest noise correlations is equally expected, as supragranular layers show a high degree of connectivity (Rockland and Lund, 1983). Moreover, Smith *et al.* (2013) equally found the largest noise correlations in supragranular layers. However, they found the lowest noise correlations in granular layer pairs, while we found the lowest noise correlations in infragranular layer pairs. One difference which might contribute to these differences is the use of awake animals in our study, while Smith *et al.* (2013) recorded from anaesthetized animals.

Our data also showed that attention to the RFs of pairs of neurons reduced noise correlations. This was more profound in area V1 than in area V4. For the analysis of V1 pairs we found the attention induced reduction for pairs residing in the same layers, and between layers. For layer dependent analysis in area V4, mean noise correlations were always lower for attend RF conditions, than attend away conditions, but none of the analyses survived FDR correction. Previous studies have reported a reduction of noise correlation with attention for neuron pairs residing in the same area (Cohen and Maunsell, 2009; Mitchell *et al.*, 2009; Herrero *et al.*, 2013). These studies either recorded from pairs of neurons located at a single electrode (Herrero et al. 2013), or from neurons recorded from chronically implanted Utah arrays (Cohen and Maunsell, 2009), where fixed electrode lengths (1mm) most likely resulted in recordings from the same cortical layer (probably lower layer 3, or layer 4), or they recorded from electrodes located at undefined depths (Mitchell *et al.*, 2009). Thus, none of these studies allowed insight into layer differences of changes to noise correlations with attention. In area V1, we found the largest attention induced noise correlation reduction for pairs located with supragranular layers. Moreover, from eye-balling

Figure 3-17, it would seem that noise correlation reductions (for between layer comparisons) are larger if one of the neurons is located in supragranular layer, than if neurons are both located outside of supragranular layers. However, this has currently not been assessed quantitatively, and will require additional scrutiny, before firm conclusions are possible.

Noise correlations between V1 and V4 were smaller than noise correlations within an area (on average no larger than 0.05 for the stimulus aligned period). This reduction for between area comparisons is expected, as the number of direct connections between V1 and V4 is rather small. These noise correlations are therefore likely to arise from more global activity fluctuations that are shared between larger scale networks (Vincent *et al.*, 2007). Importantly, noise correlations between neuron pairs in these areas were also reduced by attention. While the reduction was not significant for all of the possible layer combinations (see Figure 5-3), the pattern was overall very consistent. This is a rather different finding to what has recently been reported for neuron pairs in V1 and MT (Ruff and Cohen, 2016). The authors reported reduced noise correlations with attention, for within area neuronal pairs, but increased noise correlations for between area neuron pairs. They argued that the increased noise correlations for between area pairs is a consequence of increased communication between areas to process behaviourally relevant (attended) stimuli. Where could the differences with our data arise from? Their experimental design differed from ours in at least one important aspect. For the MT neurons in their study, the attend away and attend RF conditions were both with the neuron's receptive field, while for the V1 neurons one was within the RF (attend RF), and the other was outside. This configuration is rather different to ours, where attend away conditions required attention to be outside the neuron's receptive fields for both areas. The same authors have also demonstrated that noise correlations within an area can be increased by attention in this stimulus configuration (Ruff and Cohen, 2014). Therefore it may be the competition of the stimuli which leads to the increase in noise correlations with attention in these studies.

The effect of attention on noise correlations was similar to that which we observed on theta/alpha coherence in both V1 and V4. Both noise correlations and low frequency coherence were reduced by attention into the RF of the recorded cells. We measured noise correlations within a window of 512ms, which translates to a frequency of

~0.5Hz. Since the minimum frequency which we analysed in our coherence analysis was 2Hz and our multitaper analysis gave a spectral smoothing of ~4Hz, there would have been overlap with this frequency. This means that the reduction in noise correlations and low frequency coherence with attention could be related.

6.2 Spectral LFP power in V1

The analysis of spiking (single cell or MUA_E) activity yielded largely consistent results between the two monkeys, even if small differences may have occurred here and there. These may be down to random sampling. A rather different picture emerged when the spectral power of the LFP was analysed. Not so much in terms of stimulus induced information flow within and between areas, but in relation to the attentional modulation of within and between layer and area interactions.

6.2.1 Stimulus induced effects

The stimuli presented in our study evoked changes of the bipolar LFP power spectrum in the alpha, beta and gamma bands in V1 relative to the pre-stimulus period. Specifically, stimulus onset reduced the power in the theta/alpha band frequencies, and caused increases in the beta, low gamma (30-50Hz) and broad band higher frequency gamma (60-100Hz) range. An increase of gamma band activity after stimulus presentation in the RF has been reported in several past studies (Gieselmann and Thiele, 2008; Chalk *et al.*, 2010; Ray and Maunsell, 2010; Jia *et al.*, 2011; Bosman *et al.*, 2012; Herrero *et al.*, 2013; Van Kerkoerle *et al.*, 2014).

A reduction of low frequency power upon stimulus onset has equally been reported by previous publications (Gieselmann and Thiele, 2008; Chalk *et al.*, 2010; Ray and Maunsell, 2010; Bosman *et al.*, 2012; Herrero *et al.*, 2013; Van Kerkoerle *et al.*, 2014). However, increases in alpha band activity have also been reported (Van Kerkoerle *et al.*, 2014). The influence of stimulus presentation on low frequency power in the study from Van Kerkoerle *et al.* (2014) depended on the type of stimulus presented. If a figure (embedded in a structured background) or a target were shown, alpha (low) frequency power was reduced, while it was increased when only a structured background (or a distractor stimulus) was shown. Whether these changes were indeed a function of the stimulus (and not of a cognitive operation) is however unclear, as the

animals were pre-cued/pre-trained to detect and report the figure (or the target) and ignore the background (or distracters). Therefore it is likely that the increase in alpha frequency in these cases is due to a cognitive process (distracter suppression), rather than the low level visual stimulation.

Increased power in the beta band upon stimulus presentation has been reported widely (Gieselmann and Thiele, 2008; Chalk *et al.*, 2010; Ray and Maunsell, 2010). Conversely, Bosman *et al.* (2012) found a reduction in beta band power after stimulus presentation. There are several possible explanations for this discrepancy. In the Bosman *et al.* (2012) study, stimuli were placed in close proximity to each other (i.e. within a single V4 RF, and neighbouring V1 RFs), which could possibly affect competitive interactions (centre-surround effects and normalisation effects). These in turn might affect beta oscillations in a different way to that seen in my study. At the same time, the Bosman *et al.* (2012) study used multitapers with a spectral smoothing of 14Hz, which could have caused a blurring of alpha and beta band power changes. If the stimuli reduced the alpha power more strongly, than it increased the beta band power, it could have resulted in spurious overall beta decreases.

6.2.2 Stimulus induced spectral power changes across different V1 laminae

A study from Maier *et al.* (2011) compared CSD derived LFP signals across the different layers of V1, showing that stimulus evoked oscillations up to 30Hz were strongest in the infragranular layers, with roughly equal power increases in the low gamma range for the infragranular and supragranular layers, and larger increases in the supragranular than infragranular layers for the high gamma band activity. We equally found the largest stimulus induced changes in infragranular layers for beta band activity, while low gamma band (30-50Hz) increases in V1 were overall most pronounced in the supragranular layers. The results from both these studies are rather different from data reported by Xing *et al.* (2012), who found stimulus induced changes of spectral power to be largely confined to a frequency band of ~40Hz, and most pronounced in layer 4B and layer 2, with some small changes also occurring at the border of layers 5 and 6. Van Kerkoerle *et al.* (2014) found that the largest stimulus induced changes in the alpha frequency band occurred in the infragranular layers

(irrespective of whether figure or ground stimuli were presented), while the largest changes (increases) in the gamma frequency band occurred in the supragranular layers (even if their Figure 2G suggests that the largest increases occurred in layer 6, not in supragranular layers). The latter (not explicitly reported result) would fit our result. Namely, we found roughly equally strong changes in supragranular and in infragranular layers in the gamma frequency band.

The stimulus aligned analysis of Granger causal influence showed that low frequency (4-12Hz and 13-25 Hz bands) GC influences were predominantly from infragranular to supragranular (and some extent granular layers) in both monkeys. This finding is roughly consistent with the data reported by Van Kerkoerle *et al.* (2014). GC influences in the gamma frequency range (low and high, even if more pronounced in the low range) were still predominantly upwards directed (i.e. from infragranular layer to upper supragranular layers), but we also found a downwards dominant component from the lower supragranular layers to the infragranular layers. The latter finding (of a dominant upwards component) is contrary to the results reported by Van Kerkoerle *et al.* (2014). The reasons for this discrepancy could originate in the different task designs used. In our study, the stimulus aligned period had no attentional component, as the cue had not yet been presented, while in the Van Kerkoerle *et al.* (2014) study, the animals had been pre-cued as to what to 'look' for, and thus the stimulus induced activity, will also be affected by 'cognitive' driven network interactions.

Given that we find a Granger causal source of gamma oscillations in the infragranular layers, it could be expected that we also should also see the strongest oscillations there. This was not quite the result we found. However, the gamma frequency oscillation could be initiated in the infragranular layers and then propagate to the supragranular layers (Shipp, 2003) where it is amplified by the high degree of horizontal connectivity between similarly tuned microcolumns (Rockland and Lund, 1983). Such a scenario does not require the strongest gamma oscillations to occur in the infragranular layers, even if GC analysis identifies it as a source thereof. The pulvinar also projects to the supragranular layers and it is proposed that it synchronises oscillations (Saalmann *et al.*, 2012), so this could also be enhancing the power of supragranular power in these layers.

The stimulus induced analysis of GC influences in V4 were even more strongly driven by upwards components, than those seen in area V1. In both monkeys, for all analysed frequency bands, the GC influences from lower contacts were stronger than the GC influences from upper contacts, for almost all contacts. Notable exceptions in both monkeys are influences from layers 2/3 contacts to lower layer 6 across all frequencies (present in both monkeys individually). To the best of my knowledge, these effects have not been reported previously for area V4.

Directionality of GC influences between areas differed strongly according to the spectral frequency band analysed. In both monkeys the GC influences from V4 to V1 were dominant in the low frequency band (4-12 Hz), but this was more pronounced in Monkey 1 than in Monkey 2, where V1-V4 interactions also were dominant occasionally (as a reminder, dominant simply means stronger in one direction than the opposite direction). Difference between monkeys were seen for the beta frequency band (13-25Hz). While Monkey 1 had a clear dominance for feedback (V4 to V1 GC directionality), Monkey 2 showed the opposite pattern. Similarities again were found for both gamma frequency bands analysed, whereby the feedforward component (V1 to V4) GC influence dominated.

6.2.3 Attentional modulation of V1 spectral power

The stimulus induced changes in spectral power were by and large consistent between monkeys, and thus similarities could be highlighted. In this differences have to be emphasized, as these were profound, and sometimes disconcerting, as to the role of oscillatory activity in enabling cognitive functions (Fries, 2005).

In the low gamma (30-50Hz) frequency range we observed different attention effects in V1 of the two monkeys. In one monkey we found an increase in LFP power with attention and in the other a decrease. This was surprising since we used identical stimuli for the experiments in both monkeys. A previous study (Chalk *et al.*, 2010) reported a decrease of V1 gamma power with attention to the RF, which agrees with the effects we observed in Monkey 2. Other studies have reported increases with attention (Buffalo *et al.*, 2011; Bosman *et al.*, 2012). However, it should be pointed out that even in the latter two studies results were not consistent between monkeys in terms of LFP power change, with one of the monkeys either showing no significant

change for the V1 data (Buffalo *et al.*, 2011), or even a small reduction (Bosman *et al.*, 2012). Moreover, Buffalo *et al.* (2011) reported that the changes depended on the cortical layers recorded from, whereby attention induced increases in LFP gamma power were restricted to supragranular layers. We cannot confirm the later result in either of our monkeys. In Monkey 1 increases were found across layers, in Monkey 2 decreases were found across layers. This is unlikely to be a result of poor layer definition in our data, as the use of laminar electrodes probably allowed for better precision than the use of single electrodes along with depth measurements (Buffalo *et al.*, 2011).

It is currently unclear where the difference in results between our monkeys arises from. We cannot exclude difference in strategy of the two monkeys, but these would have been subtle. Alternatively it could be due to damage to the cortex in previous studies. In the right hemisphere of Monkey 1 and both hemispheres of Monkey 2 previous recordings were performed in V4 and the FEF. If these recordings caused damage to the FEF, the potential centre for top-down spatial attention (Moore and Fallah, 2004; Gregoriou *et al.*, 2009; Bichot *et al.*, 2015), then this could cause changes in attentional responses in the visual cortex. Since we recorded in the left hemisphere of Monkey 1, it is unlikely that this could have affected these recordings, so if there was any effect due to cortical damage, it would likely have been in Monkey 2. Moreover, it should be pointed out that all our analyses regarding the effects of attention on spiking activity were consistent between animals, and also largely consistent with previous studies. It has been shown that there is coupling of synchronous activity between the FEF and visual cortex during attention (Gregoriou et al., 2009). This could explain why damage to the FEF would cause discrepancies between monkeys in the effects which we see in LFP activity, but not in spiking activity.

In both V1 and V4, attention to the RF increased the peak frequency of gamma oscillations, which is an effect that has been observed previously in V1 (Bosman *et al.*, 2012). This effect is discussed further in Section 6.4.2.

6.3 Spectral LFP power in V4

6.3.1 Stimulus induced changes in LFP spectral power in area V4

The alpha band spectral power in V4 was reduced by stimulus onset in our data, while beta and gamma band spectral power were increased. The increase of beta and gamma spectral power was largely broadband in V4, i.e. it showed no pronounced frequency peak, unlike it did in our V1 data. However, there were small differences in that respect between the two monkeys. Monkey 1 showed some hints of more pronounced power changes in the beta frequency band (~18-20Hz) and also in the gamma frequency band (~35-40Hz). Bosman *et al.* (2012) also showed a decrease in the lower frequency range (<20Hz) relative to prestimulus power in their V4 data, and an increase in gamma band power. Contrary to our V4 data, the increase in gamma band power in the Bosman study was associated with a distinct peak at ~60Hz for at least one of their monkeys (data for the second monkey were not shown). In that second monkey overall effects seemed more variable (as read from their description) so it is unclear whether a distinct peak in their V4 data set is a common feature across individuals or whether inter-individual differences are common.

6.3.2 Attentional modulation of V4 Spectral Power

In V4 we observed a reduction in alpha power with attention and a broadband increase in the gamma band. A previous study using the same task as ours (Gregoriou *et al.*, 2009) has also reported effects of attention in these frequency bands, showing an increase in gamma power with attention and a decrease in low frequency power. The pattern of decreased alpha and increased gamma power with attention in V4 has also been found in other studies (Fries *et al.*, 2001; Buffalo *et al.*, 2011). The Fries *et al.* (2001) study suggests that a reduction in the low frequency synchrony could improve postsynaptic efficacy by avoiding spike frequency adaptation effects.

6.4 Information flow within and between visual cortical areas - Granger causality analysis

The known pattern of feedback projections is that they arise in infragranular layer of higher areas and terminate in layer 1 and layer 5 of lower areas (Rockland and Pandya, 1979). From layer 5 the information is then influencing processing in supragranular layers within a cortical microcolumn (Rockland and Pandya, 1979). In addition the canonical microcolumn concept (Douglas and Martin, 2004) predicts that within an area, the feedforward flow of information would be from granular layer to supragranular layers to infragranular layers, while the within column feedback would be from infragranular to supragranular layers. Given that low frequency LFP components are supposed to identify feedback influences, while gamma frequency components are supposed to identify feedforward influences (Van Kerkoerle *et al.*, 2014; Bastos *et al.*, 2015), the low frequency GC influences should dominate from infragranular to supragranular layers (within a column), while the gamma frequency influences should take the opposite direction.

6.4.1 Low frequency Granger causal influences

We found a discrepancy between monkeys in GC influence directionality of low frequency information flow between V1 and V4. In Monkey 1 the directionality was feedback from V4 to V1, however in Monkey 2 we observed both feedback and feedforward influences, with a bias for feedforward directionality (at least for beta band influences). Previous studies have argued that alpha and beta frequency oscillations are (markers of) a top-down/feedback mechanism (Van Kerkoerle *et al.*, 2014; Bastos *et al.*, 2015), which is in agreement with the results we observed in Monkey 1, but not Monkey 2.

In both V1 and V4, we found that information in the low frequency bands (alpha and beta) travels upwards within cortical microcolumns. This is in line with the argument that they are markers of feedback signalling (Van Kerkoerle *et al.*, 2014; Bastos *et al.*, 2015).

6.4.2 Gamma band Granger causal influences

We found that GC influences in V1 within the gamma frequency range were, unlike expected, dominant in the upwards direction. This is contrary to the aforementioned predictions, when applied to the canonical microcolumn concept.

Since it has been shown than visually evoked gamma oscillations are not present in the LGN (Bastos *et al.*, 2014) and gamma oscillations are feedforward (Van Kerkoerle *et al.*, 2014), either the oscillations must be generated in V1 or be generated in another subcortical region and then passed on to V1.

In V4, the dominant GC influence directionality of gamma oscillations was upwards from the granular and lower supragranular layers to the upper supragranular layers. This is consistent with the canonical microcircuit (Douglas and Martin, 2004), whereby projections from lower areas target the granular layers and from here the main projections are to the supragranular layers. If the canonical microcircuit described the way in which gamma propagated through visual cortex, then this activity should be received from the supragranular layers of V2. Which in turn would have received its input from the supragranular layers of V1 (via V2 layer 4). However, the dominant direction of GC influence in the gamma frequency range when analysing infra and supragranular layers was still upward directed, contrary to predictions based on canonical microcircuits and gamma frequency being a marker of feedforward signalling.

Although we demonstrated that the directionality of GC influences in the gamma frequency range is feedforward from V1 to V4, we did not find any layer specificity across monkeys for this connection. We targeted our recordings into individual cortical microcolumns, within which cells are highly interconnected. This could lead to a high degree of similarity/synchronisation of the oscillations within the cortical microcolumns. Thus it is perhaps unsurprising that all V1 channels could be used to accurately predict the gamma oscillations in V4.

Another possibility is that V1 gamma oscillations do not directly feedforward to V4, but that both areas receive their oscillations from a third source. If V1 received this before V4, this would also lead to a Granger causality bias from V1 to V4 such as we see. One possible source of such a connection is the pulvinar.

Several previous studies have discussed the potential that a pulvinocortical loop may play in attention (Purushothaman *et al.*, 2012; Saalmann *et al.*, 2012; Zhou *et al.*, 2016). In our study, attentional modulation of gamma oscillations in V4 was most strongly driven by the supragranular layers. This is consistent with the input of the pulvinar into the supragranular layers (Purushothaman *et al.*, 2012). The pulvinar has been suggested to act by synchronising activity between areas in the alpha frequency range and in the gamma frequency range through cross frequency coupling (Saalmann *et al.*, 2012). Given that a common effect which we observed throughout our study was an increase of the peak frequency of gamma oscillations with attention (even if the amplitude was reduced in one monkey), one possibility is that the frequency of gamma oscillations across the visual cortex are being normalised to a common frequency by the pulvinar. This in turn could allow for more efficient information transfer through the cortex when attention is utilised. However, that would predict that coherence between areas is increased by attention in that frequency band, which is not what we found Monkey 2, even if we did find it in Monkey 1.

6.5 Communication through coherence?

The idea behind communication through coherence (Fries, 2005) is that coherent activity between neurons allows for more efficient communication between them. The results of our study cannot fully support this idea. In one of the monkeys, the results are consistent with the idea, whereby coherence and GC influences within and between areas were increased with attention in the gamma frequency band. In the beta frequency band, GC influences were increased for the feedback from area V4 to V1, while they were reduced for the opposite direction. In the other monkey we observed reduced coherence within area V1, but still found some signs of increased coherence between area V1 and V4 in the gamma frequency band with attention. In line with this the GC influence in the gamma frequency range in the feedforward direction was also increased. We observed this increase in coherence/information flow despite coherence within V1 of Monkey 2 being reduced by attention. Given that visually evoked gamma oscillations have been proposed to be generated in V1 (Bastos *et al.*, 2014; Van Kerkoerle *et al.*, 2014), this reduction in coherence may

reflect a conflict between the frequency of the internally generated V1 oscillation and the frequency to which oscillations are shifted to with attention.

There were differences in the patterns of coherence between monkeys in the alpha and beta bands. Although Monkey 1 showed a clear increase with attention in the peak frequency of V1-V4 coherence (in the beta range), we saw no such effect in Monkey 2. Given that we did not observe the suggested top-down flow of information from V4 to V1 (Bosman *et al.*, 2012) in Monkey 2, this may explain why we did not then see attentional modulation in this frequency range.

6.6 Final Remarks

This thesis has described the behaviour of V1 and V4 activity during performance of a covert visuospatial attention task.

We have demonstrated that attention increases firing rates in both V1 and V4, for the supragranular, granular and infragranular layers and both broad and narrow spiking cells. Attention also decreases the variability of cells, which we showed through use of the Fano factor, gain variance and noise correlations. Although the effect of attention on LFP power and coherence differed between subjects, there was a consistent increase in Granger causality with attention in both monkeys.

Within cortical microcolumns of each area, activity was shown to propagate upwards, from the deeper layers to more superficial layers. In line with previous research, the flow of activity between V1 and V4 was shown to be feedforwards in the gamma frequency range and feedback in the alpha and beta frequency ranges.

Using laminar probes inserted in parallel with cortical microcolumns allowed us to determine the layer that was recorded from. This meant that we were able to explore the effects of attention in different cortical layers, where many previous studies were only able to determine the area which was recorded from.

Appendix A. The "Jerky" Stimulus

In recordings performed in the right hemisphere of Monkey 2, the stimuli were rendered such that there was an aliasing artefact in the grating. This meant that as a grating moved through its cycle the bars appeared to increase and decrease in size. The varying size of the grating occurred at a fixed frequency and so manifested as a rhythmic "jerkiness" of the stimulus. We measured the periodicity of this jerky motion using a photodiode placed in front of the monitor, finding it to oscillate at a frequency of around 24Hz (Figure A-1).

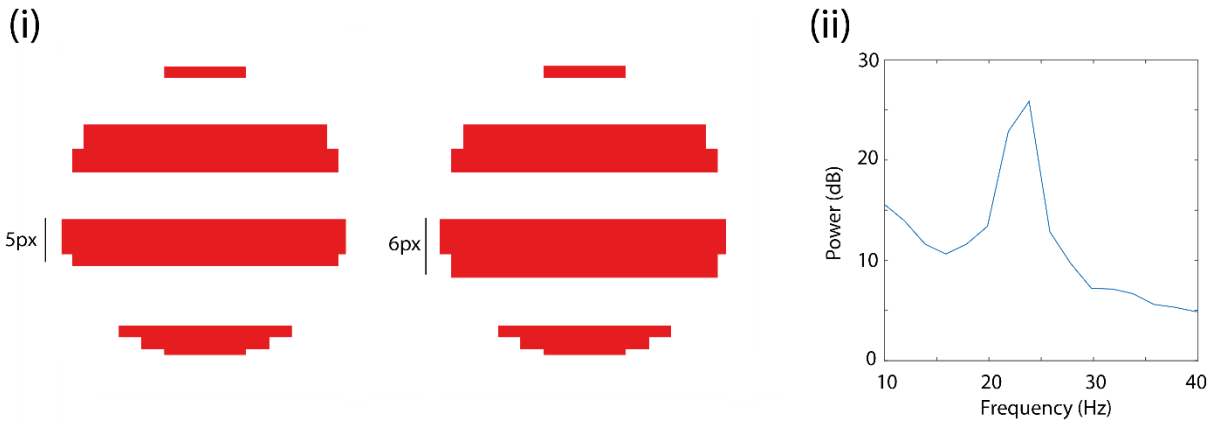

Figure A-1: (i) Two adjacent frames of the jerky stimulus. The third bar in the left stimulus is 5 pixels wide 6 pixels wide in the right stimulus. (ii) Power spectra of the response of a photo diode to the jerky stimulus.

We performed control recordings in the left hemisphere of Monkey 2 where both the normal and jerky stimulus were used in subsequent repetitions of the task during the same recording sessions. By averaging the MUA_E activity for these recordings, the visual response to each of the stimuli can be observed. In V1, the stimulus aligned MUA_E (Figure A-2) showed an oscillation at half the frequency of the jerky stimulus in all layers, but this was not present when using the correctly rendered stimulus. The reason that the frequency was half that detected with the photodiode is likely that the photodiode response peaked whenever there was a change in bar width but the V1 response peaked at either the minimum or maximum bar width.

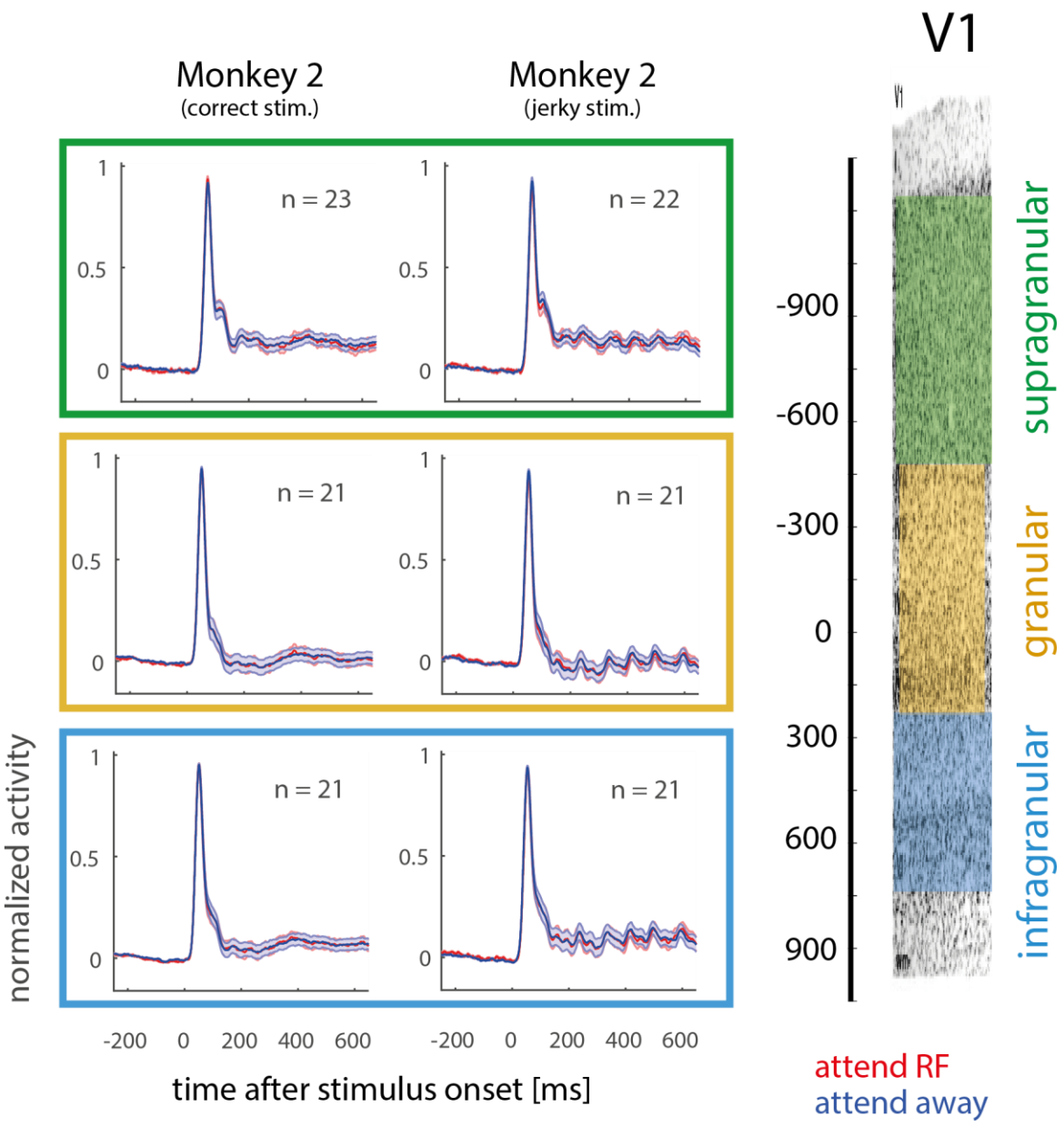

Figure A-2: *Left*: Monkey 2 average envelope multiunit activity (MUA_E) aligned to stimulus onset and calculated separately for the trials with the correctly rendered and jerky stimuli. Grouped into supragranular (top, green), granular (middle, yellow) and infragranular (bottom, blue) layers. Activity is shown separately for trials where the monkey attended into the receptive field (RF, red) and away from it (blue), even though the attention cue had not been presented yet. *Right*: Illustration of V1 architecture, split into supragranular, granular and infragranular cortical layers based on distance (µm) from layer 4cα (Adapted from (Stepanyants et al. (2002))).

Although the stimulus aligned V1 activity was affected by the stimulus, the attentional modulation of V1 MUA_E aligned to the first dimming was present under both stimulus conditions. Additionally there was no rhythmic component to the MUA_E in this time period. This was because the dimming occurred randomly and was not time-locked to the stimulus onset, so once the trials were averaged the stimulus artefact was also averaged out.

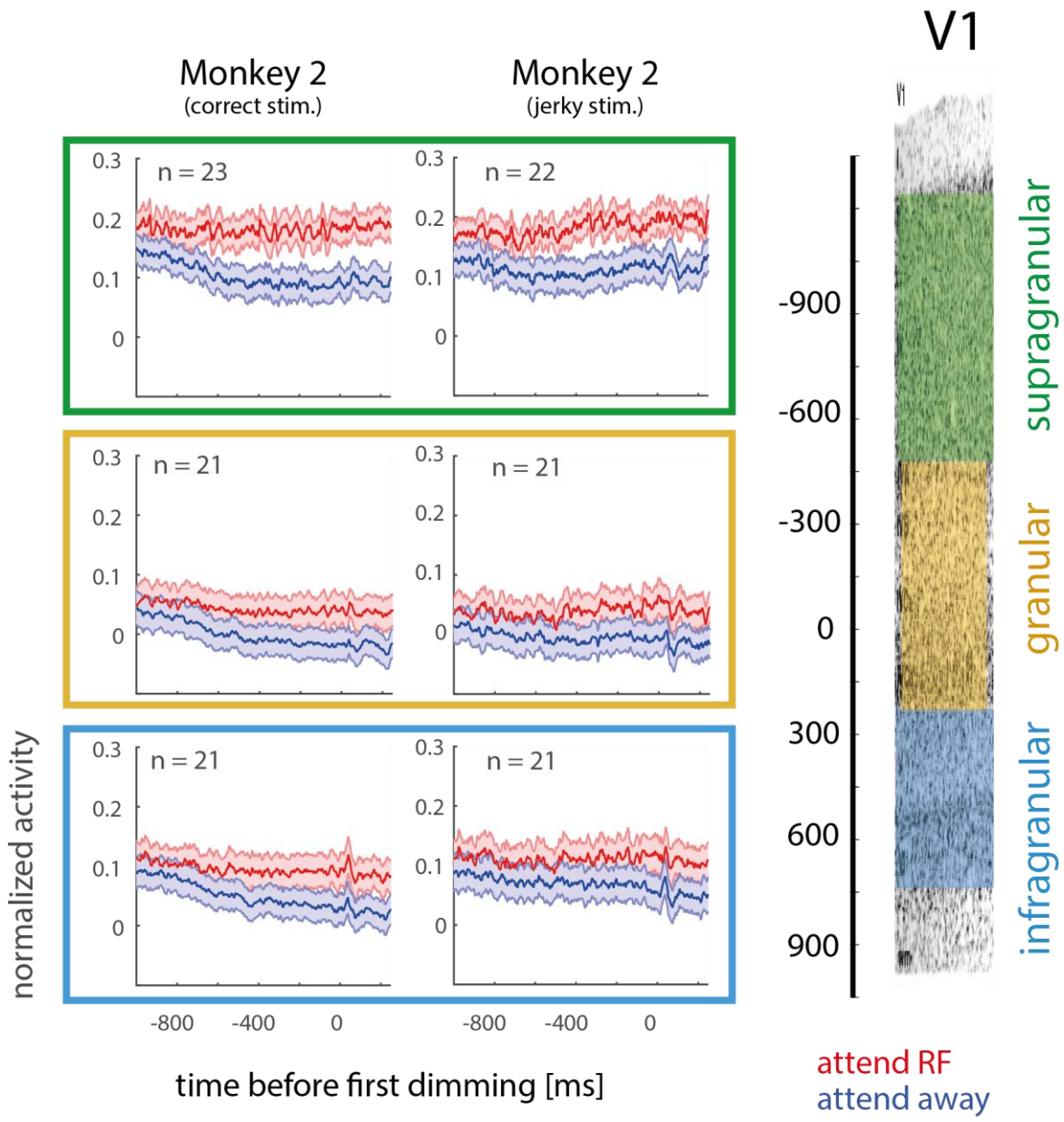

Figure A-3: Monkey 2 average V1 envelope multiunit activity (MUA_E) aligned to the first dimming and calculated separately for the trials with the correctly rendered and jerky stimuli. Attention conditions, depth colours and V1 structure are as defined in Figure A-2.

In V4, there was no effect of the stimulus type observed in either the stimulus aligned (Figure A-4) or the dimming aligned MUA_E response (Figure A-5).

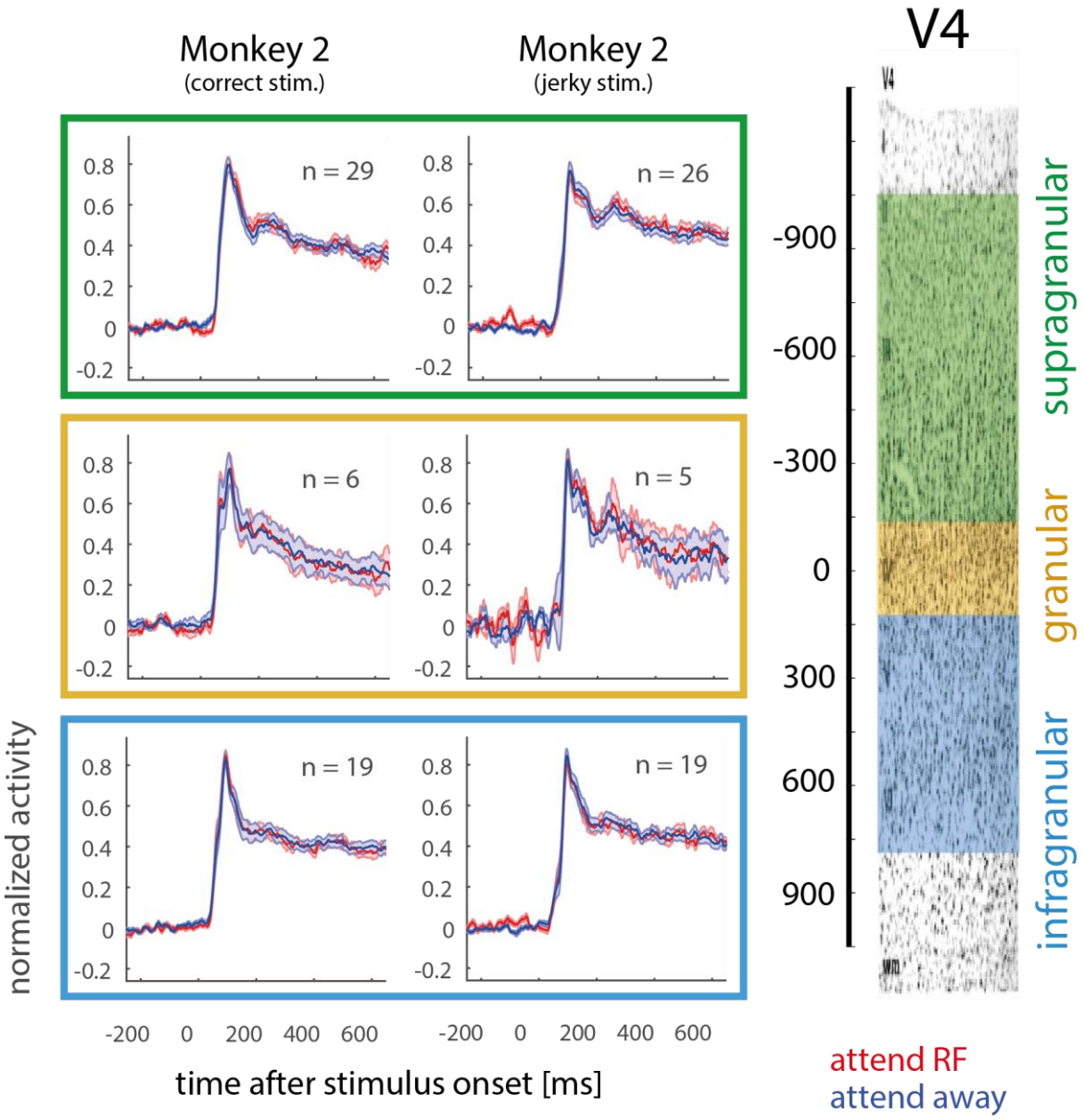

Figure A-4 : Monkey 2 average V4 envelope multiunit activity (MUA_E) aligned to stimulus onset and calculated separately for the trials with the correctly rendered and jerky stimuli. Attention conditions, depth colours and V4 structure are as defined in Figure A-2.

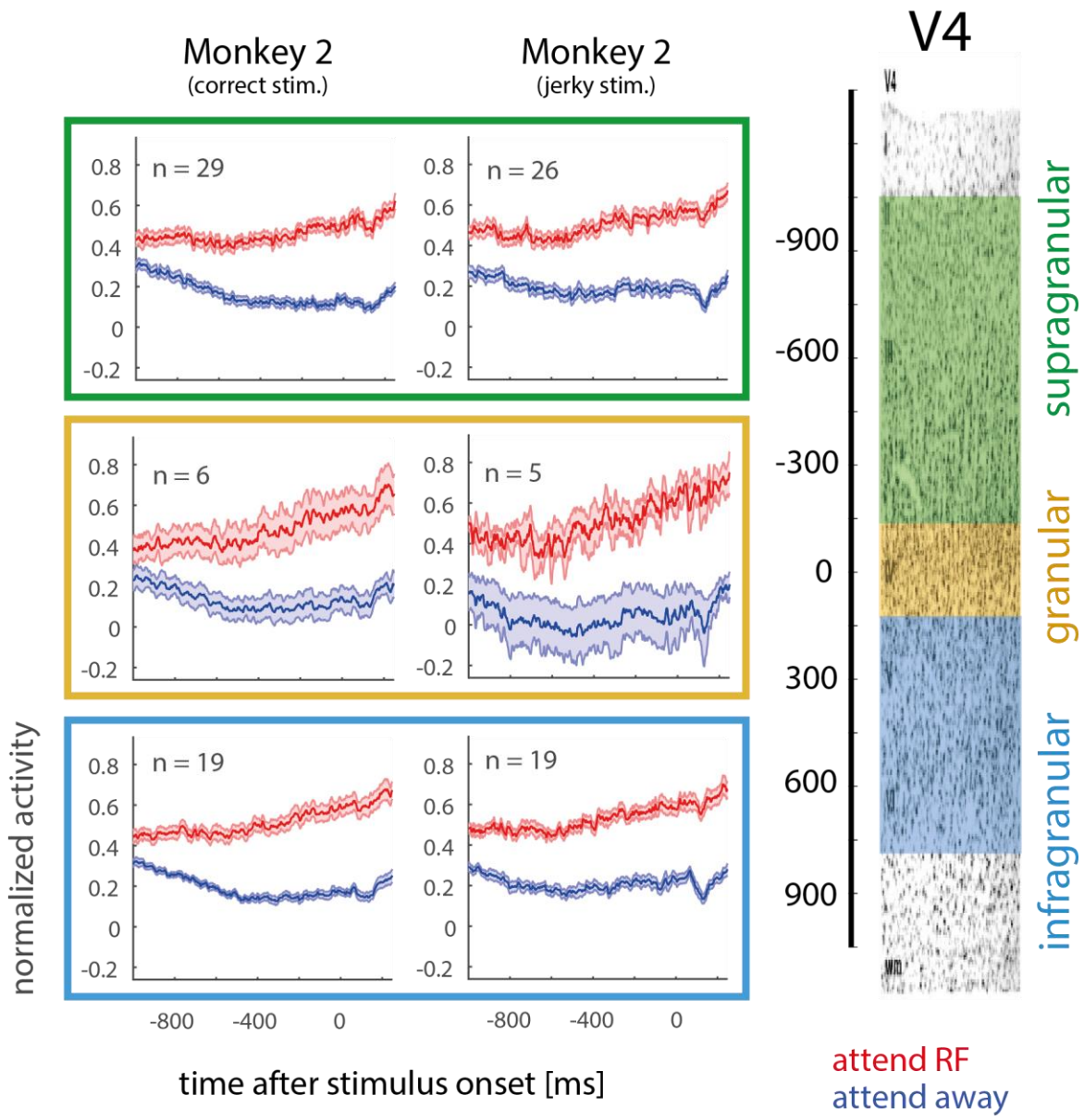

Figure A-5 : Monkey 2 average V4 envelope multiunit activity (MUA_E) aligned to the first dimming and calculated separately for the trials with the correctly rendered and jerky stimuli. Attention conditions, depth colours and V4 structure are as defined in Figure A-2.

We also calculated the LFP spectral power for the two different stimulus types. When the V1 spectral power aligned to the stimulus onset was calculated (Figure A-6), there was a stronger low gamma (30-50Hz) peak when the jerky stimulus was used than when the correctly rendered one was used, particularly in the supragranular layers.

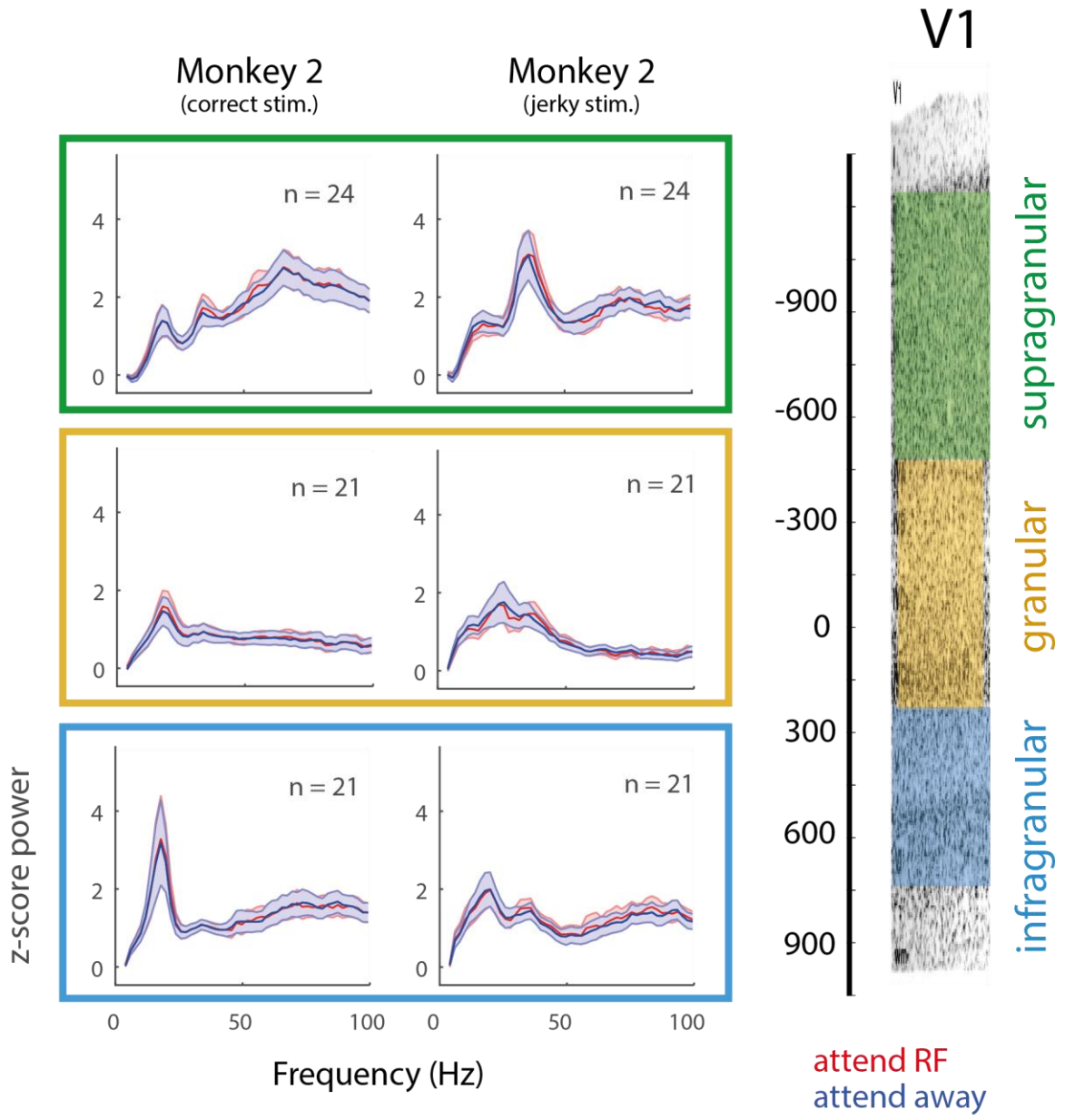

Figure A-6 : Monkey 2 average V1 LFP spectral power aligned to stimulus onset and calculated separately for the trials with the correctly rendered and jerky stimuli. Spectral power calculated using the bipolar derivation of the local field potential, 3 tapers of 4Hz half-bandwidth and expressed as a z-score relative to pre-stimulus power. Attention conditions, depth colours and V1 structure are as defined in Figure A-2.

When using the correctly rendered stimulus and aligning to the first dimming of the task there was a clear attentional modulation of the LFP in the low gamma (30-50Hz) frequency range (Figure A-7). This modulation was reduced when the jerky stimulus was used.

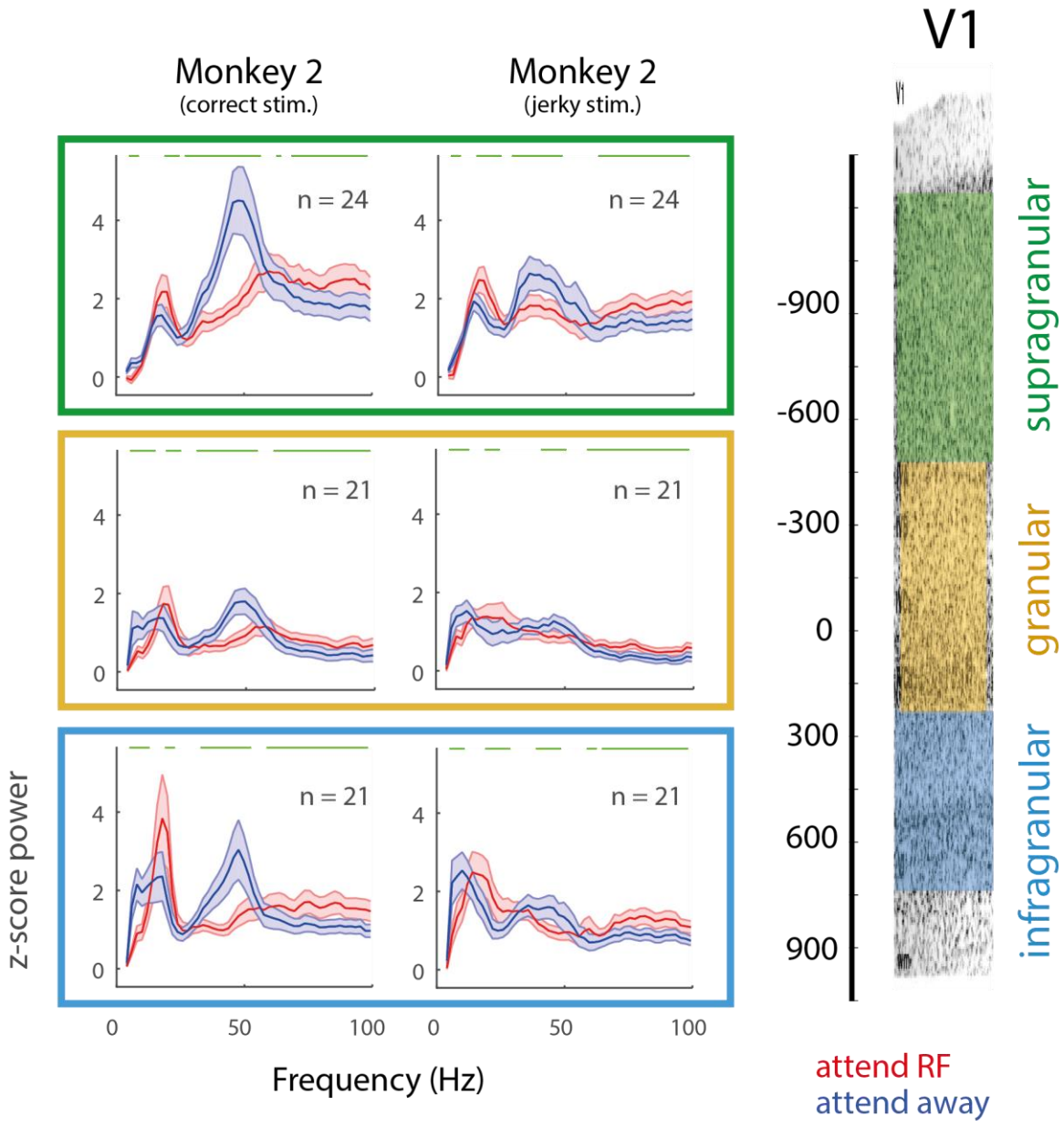

Figure A-7: Monkey 2 average V1 LFP spectral power aligned to the first dimming and calculated separately for the trials with the correctly rendered and jerky stimuli. Power calculation, attention conditions, depth colours and V1 structure are as defined in Figure A-6 .

In V4, there was no effect of the stimulus type observed in either the stimulus aligned (Figure A-8) or the dimming aligned LFP response (Figure A-9).

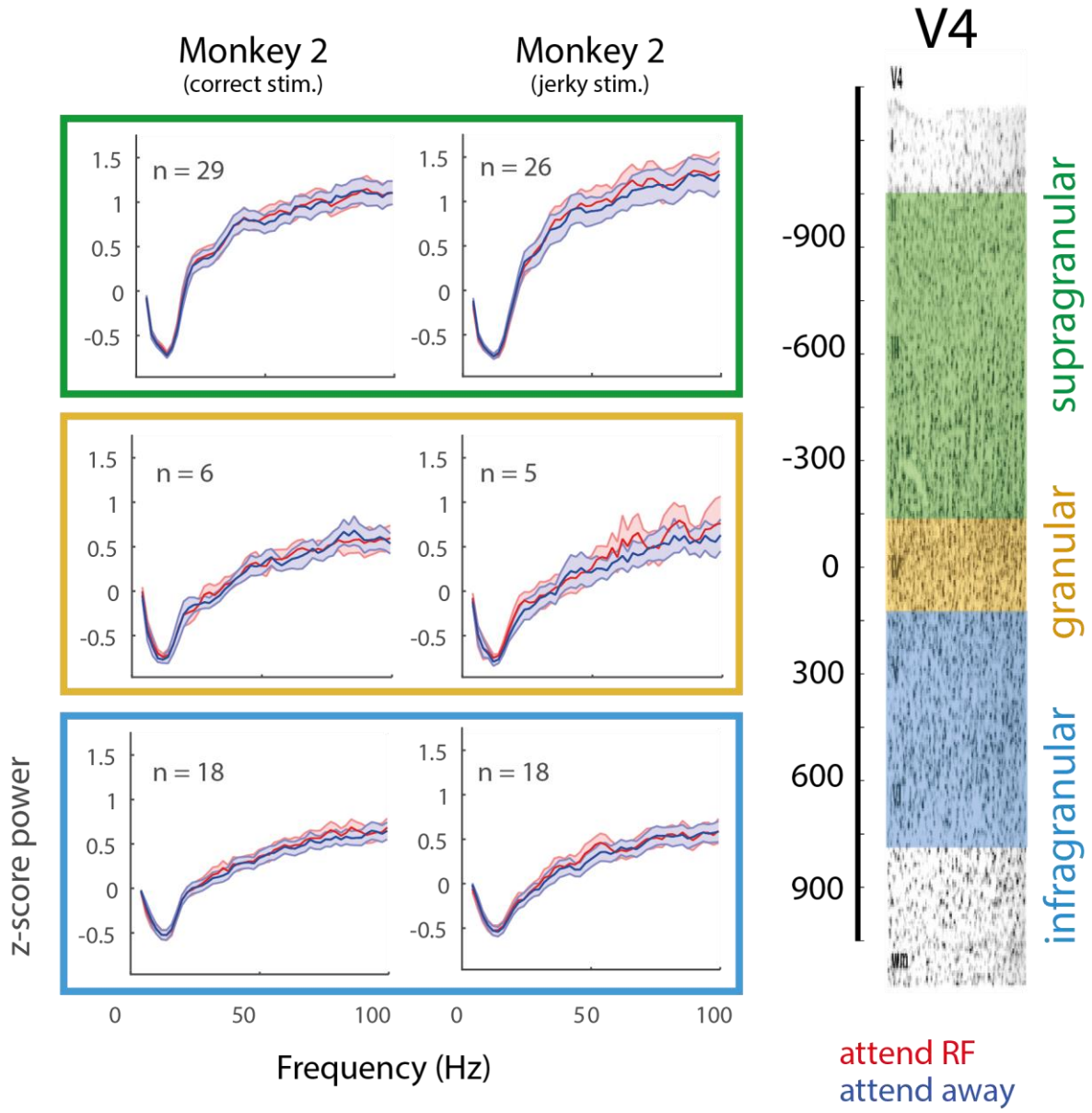

Figure A-8: Monkey 2 average V4 LFP spectral power aligned to stimulus onset and calculated separately for the trials with the correctly rendered and jerky stimuli. Power calculation, attention conditions, depth colours and V4 structure are as defined in Figure A-6 .

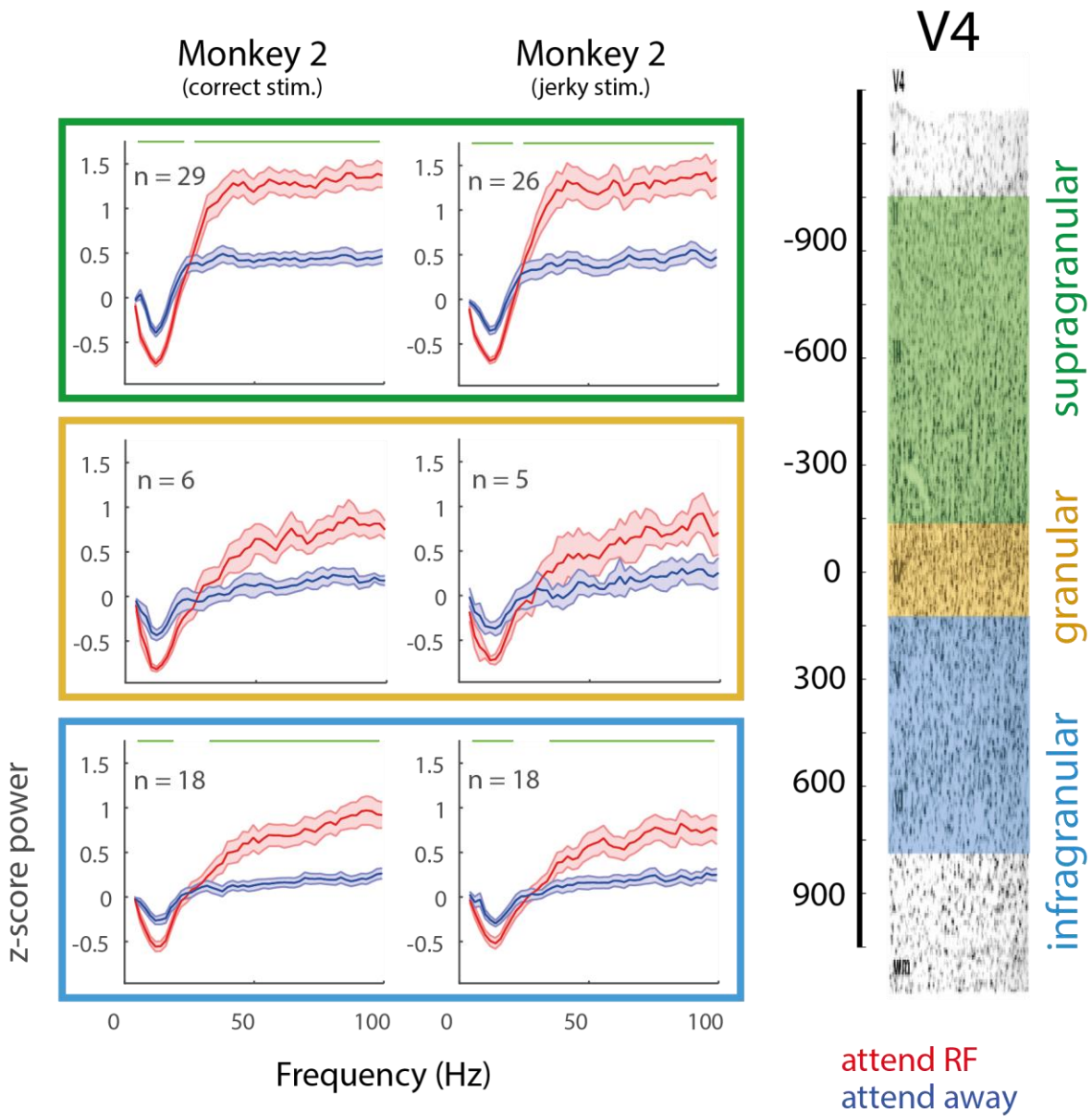

Figure A-9: Monkey 2 average V4 LFP spectral power aligned to the first dimming and calculated separately for the trials with the correctly rendered and jerky stimuli. Power calculation, attention conditions, depth colours and V4 structure are as defined in Figure A-6 .

Together, these results show that a jerky stimulus modulates V1 MUA_E activity. The jerky stimulus thus entrains the cortex on an external oscillation that appear to disrupt the attention effects usually observed in the LFP of V1. This disruption does not appear to propagate further up the visual stream, as visual responses and attentional modulation in V4 were unaffected by the jerky stimulus. This explains why the attentional modulation of low gamma oscillations was weak in the right hemisphere of Monkey 2, however does not explain why strong effects were not observed in V4 in those recordings.

Appendix B. Field Coherence Before the Stimulus Onset

B.1 V1 field coherence before the stimulus onset

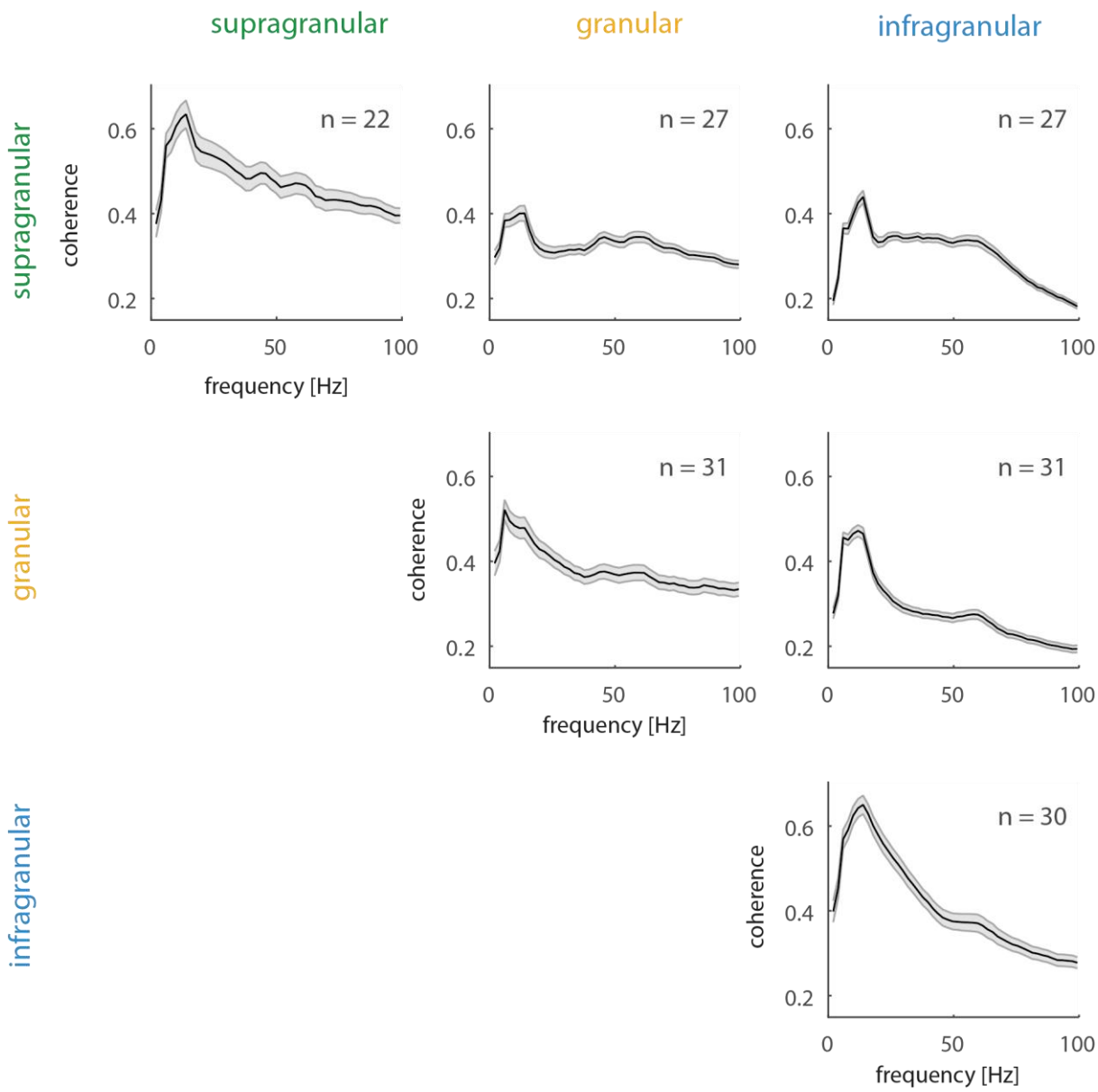

Figure B-1: V1 field-field coherence in Monkey 1 aligned prior to the stimulus onset (-511ms to 0ms) in the attention task. Shown are all possible combinations of supragranular, granular and infragranular layer comparisons, averaged across the channels contributing to the respective sections (n = number of recordings in each plot). Coherence was calculated using the bipolar derivation of the local field potential and 3 tapers of 4Hz half-bandwidth. V1 structure is as defined in Figure 3-1.

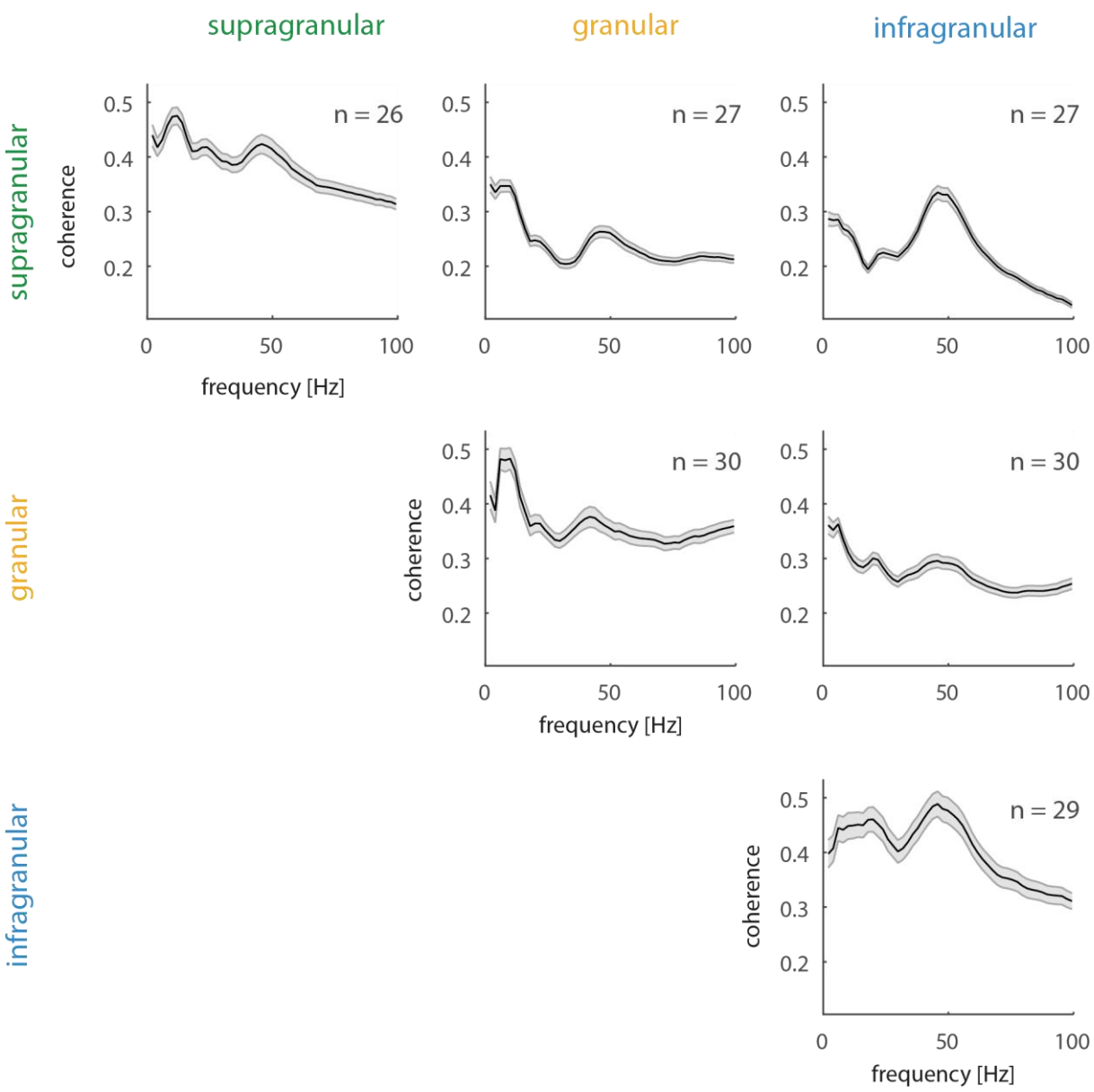

Figure B-2: V1 field-field coherence in Monkey 2 (right hemisphere) aligned prior to the stimulus onset (-511ms to 0ms) in the attention task. Shown are all possible combinations of supragranular, granular and infragranular layer comparisons, averaged across the channels contributing to the respective sections (n = number of recordings in each plot). Coherence was calculated using the bipolar derivation of the local field potential and 3 tapers of 4Hz half-bandwidth. V1 structure is as defined in Figure 3-1.

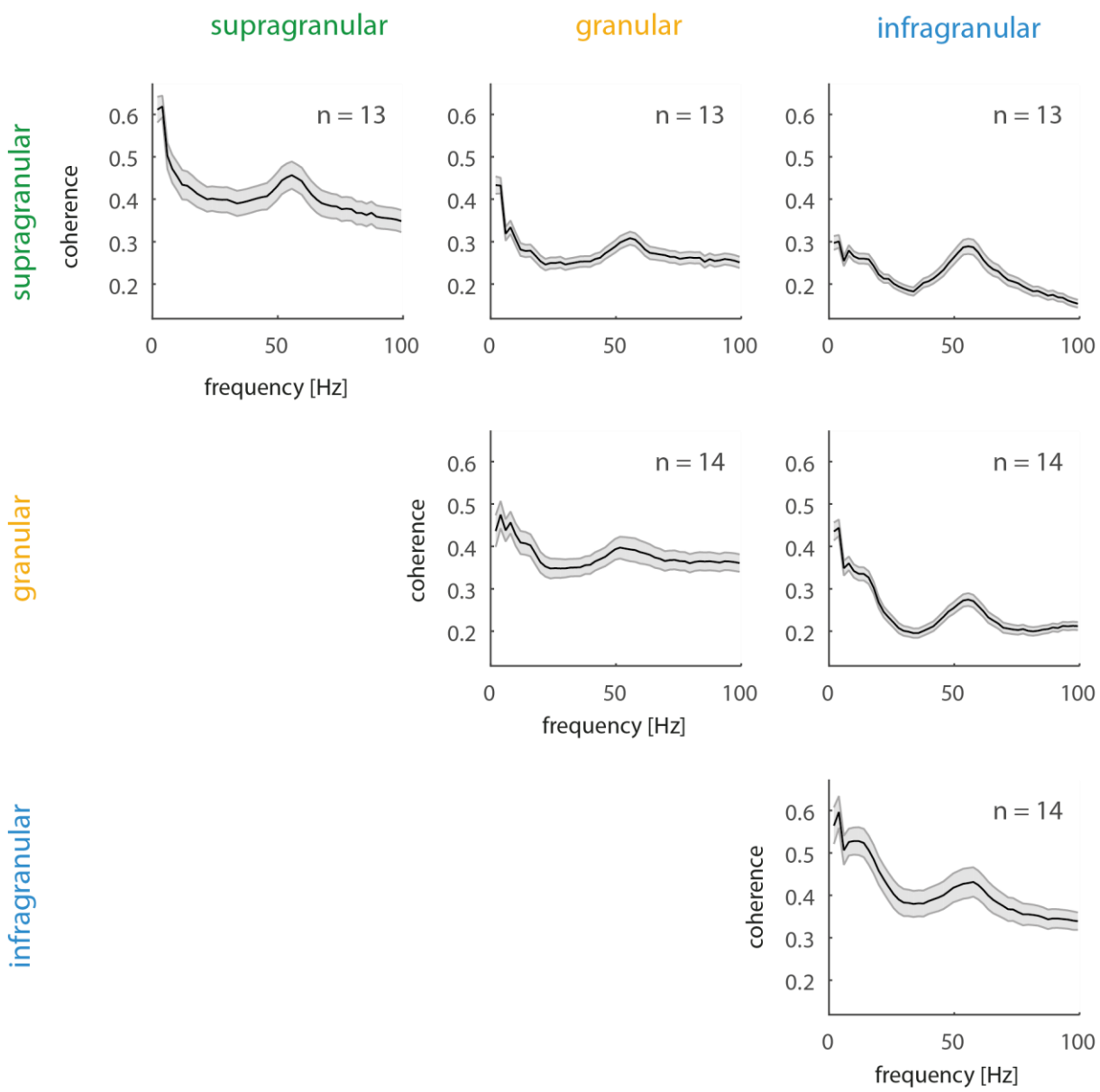

Figure B-3: V1 field-field coherence in Monkey 2 (left hemisphere) aligned prior to the stimulus onset (-511ms to 0ms) in the attention task. Shown are all possible combinations of supragranular, granular and infragranular layer comparisons, averaged across the channels contributing to the respective sections (n = number of recordings in each plot). Coherence was calculated using the bipolar derivation of the local field potential and 3 tapers of 4Hz half-bandwidth. V1 structure is as defined in Figure 3-1.

B.2 V4 field coherence before the stimulus onset

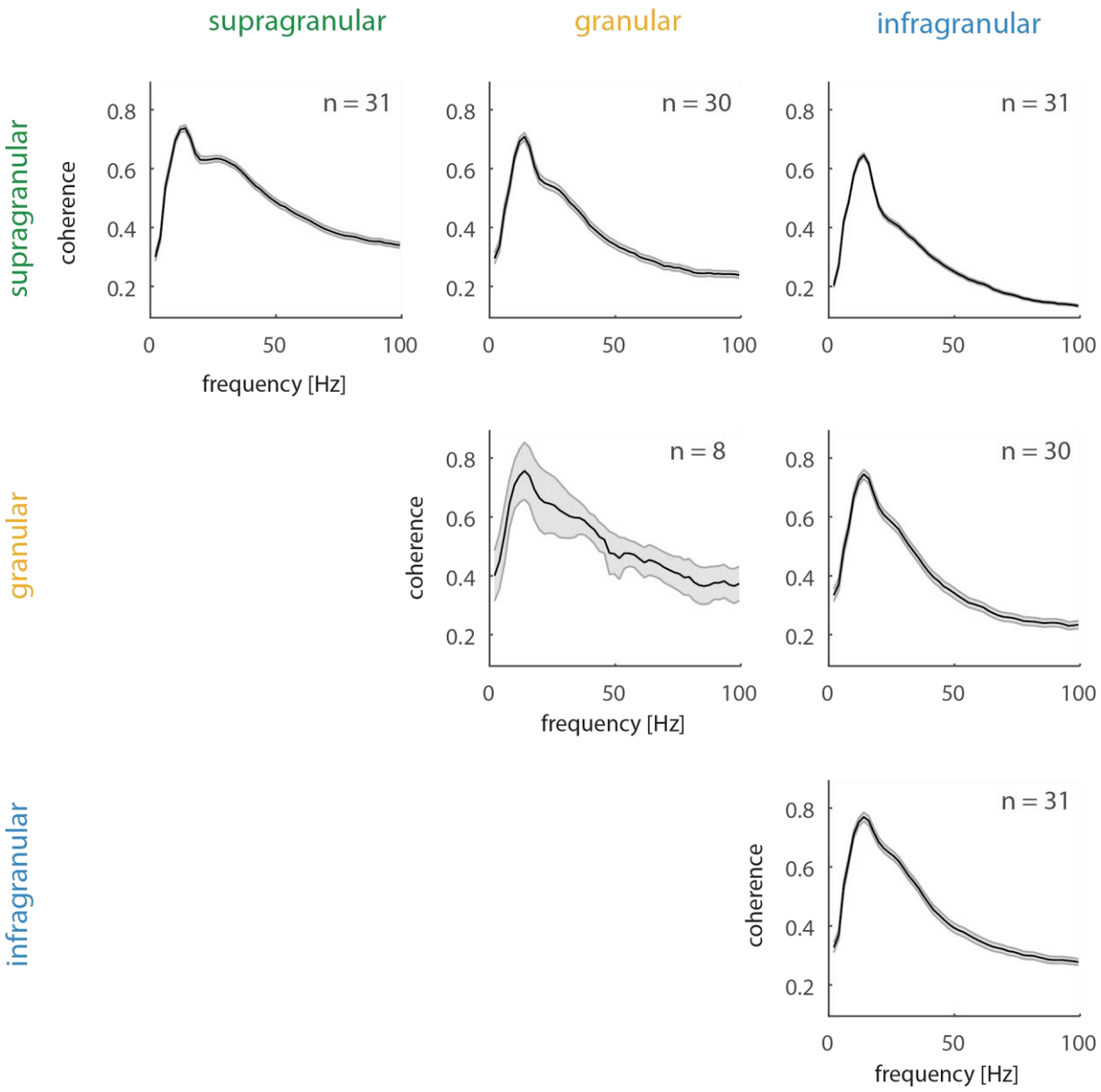

Figure B-4: V4 field-field coherence in Monkey 1 aligned prior to the stimulus onset (-511ms to 0ms) in the attention task. Shown are all possible combinations of supragranular, granular and infragranular layer comparisons, averaged across the channels contributing to the respective sections (n = number of recordings in each plot). Coherence was calculated using the bipolar derivation of the local field potential and 3 tapers of 4Hz half-bandwidth. V4 structure is as defined in Figure 4-1.

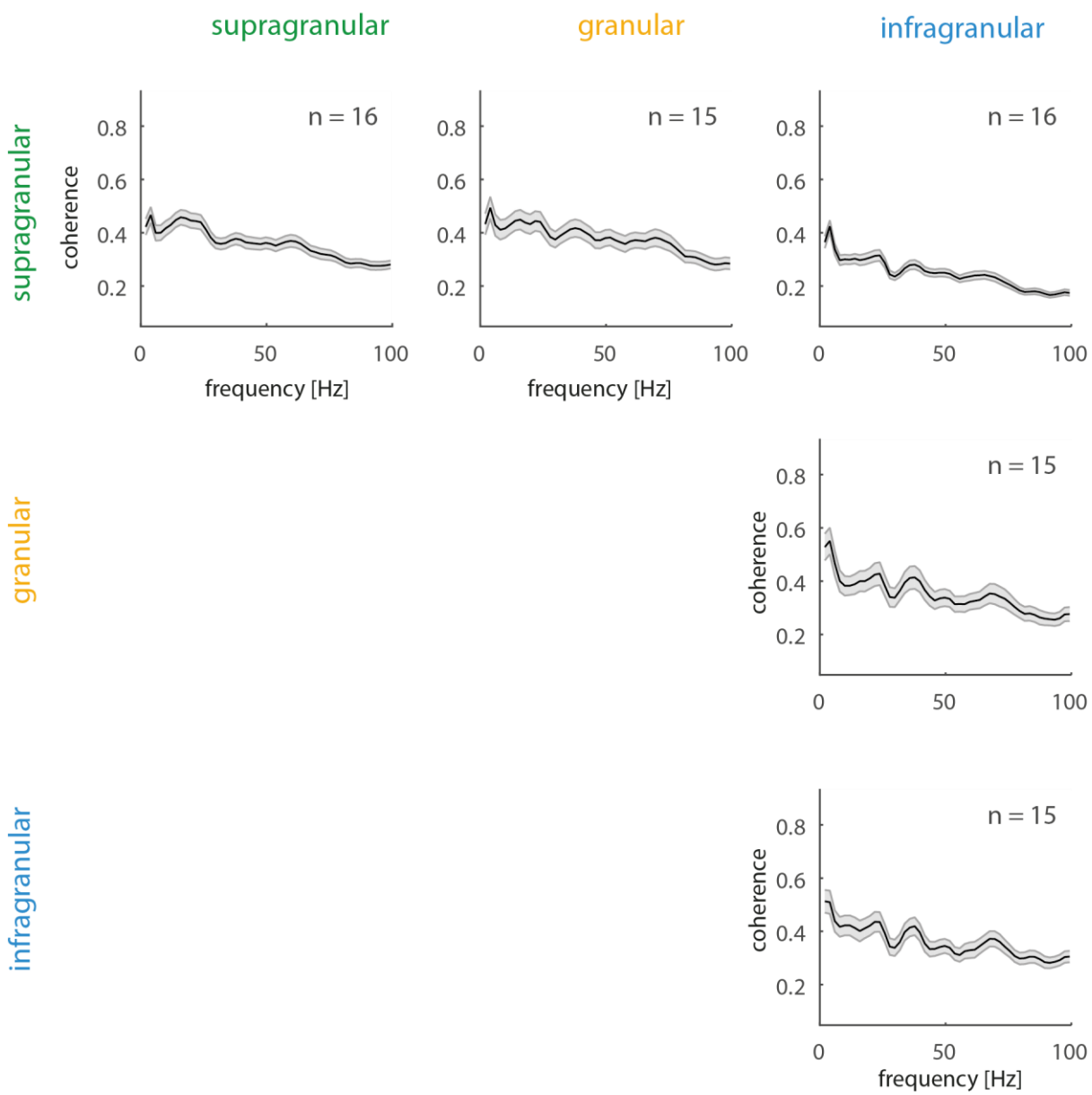

Figure B-5: V4 field-field coherence in Monkey 2 (right hemisphere) aligned prior to the stimulus onset (-511ms to 0ms) in the attention task. Shown are all possible combinations of supragranular, granular and infragranular layer comparisons, averaged across the channels contributing to the respective sections (n = number of recordings in each plot). Coherence was calculated using the bipolar derivation of the local field potential and 3 tapers of 4Hz half-bandwidth. V4 structure is as defined in Figure 4-1.

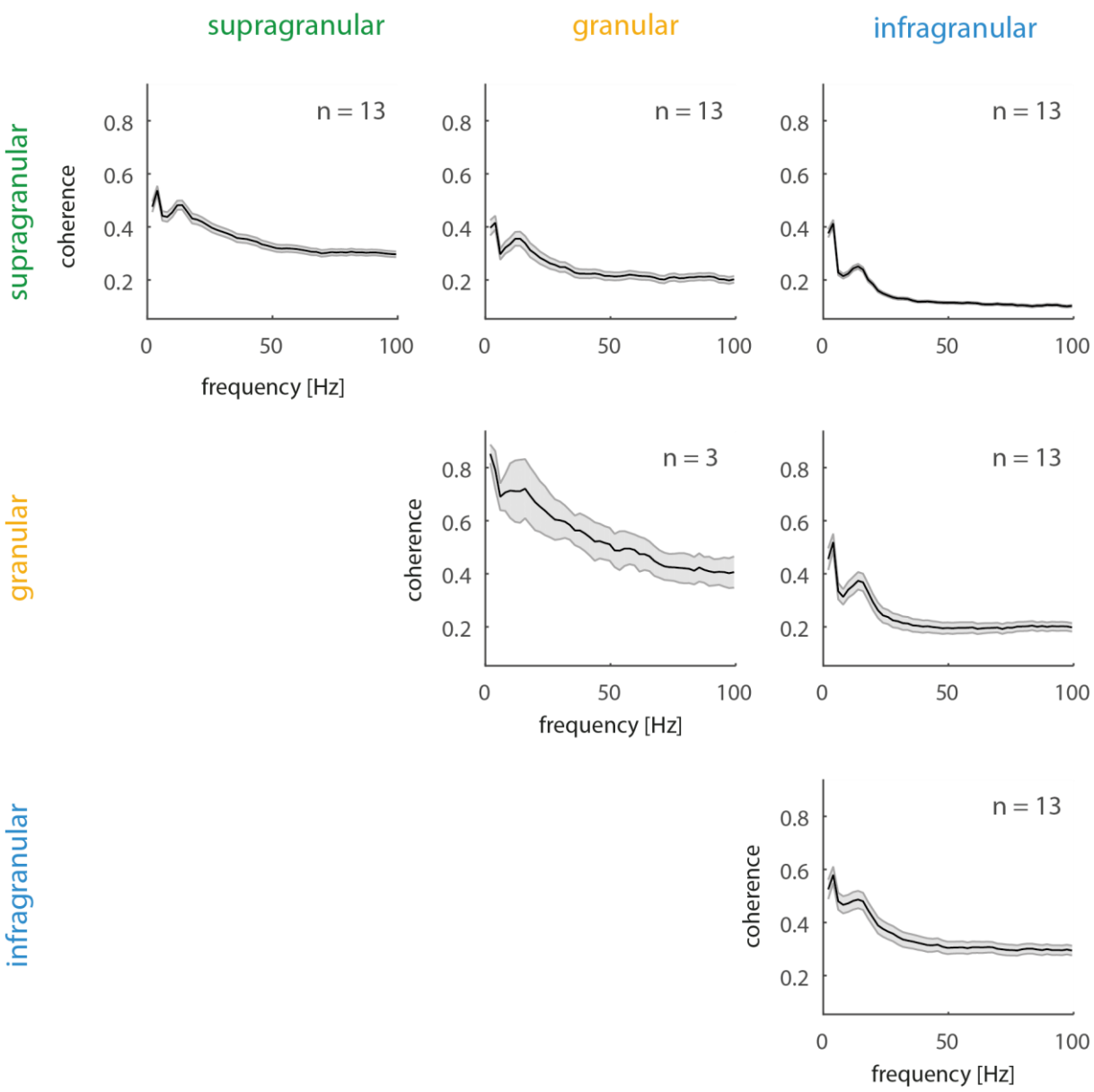

Figure B-6: V4 field-field coherence in Monkey 2 (left hemisphere) aligned prior to the stimulus onset (-511ms to 0ms) in the attention task. Shown are all possible combinations of supragranular, granular and infragranular layer comparisons, averaged across the channels contributing to the respective sections (n = number of recordings in each plot). Coherence was calculated using the bipolar derivation of the local field potential and 3 tapers of 4Hz half-bandwidth. V4 structure is as defined in Figure 4-1.

B.3 V1-V4 field coherence before the stimulus onset

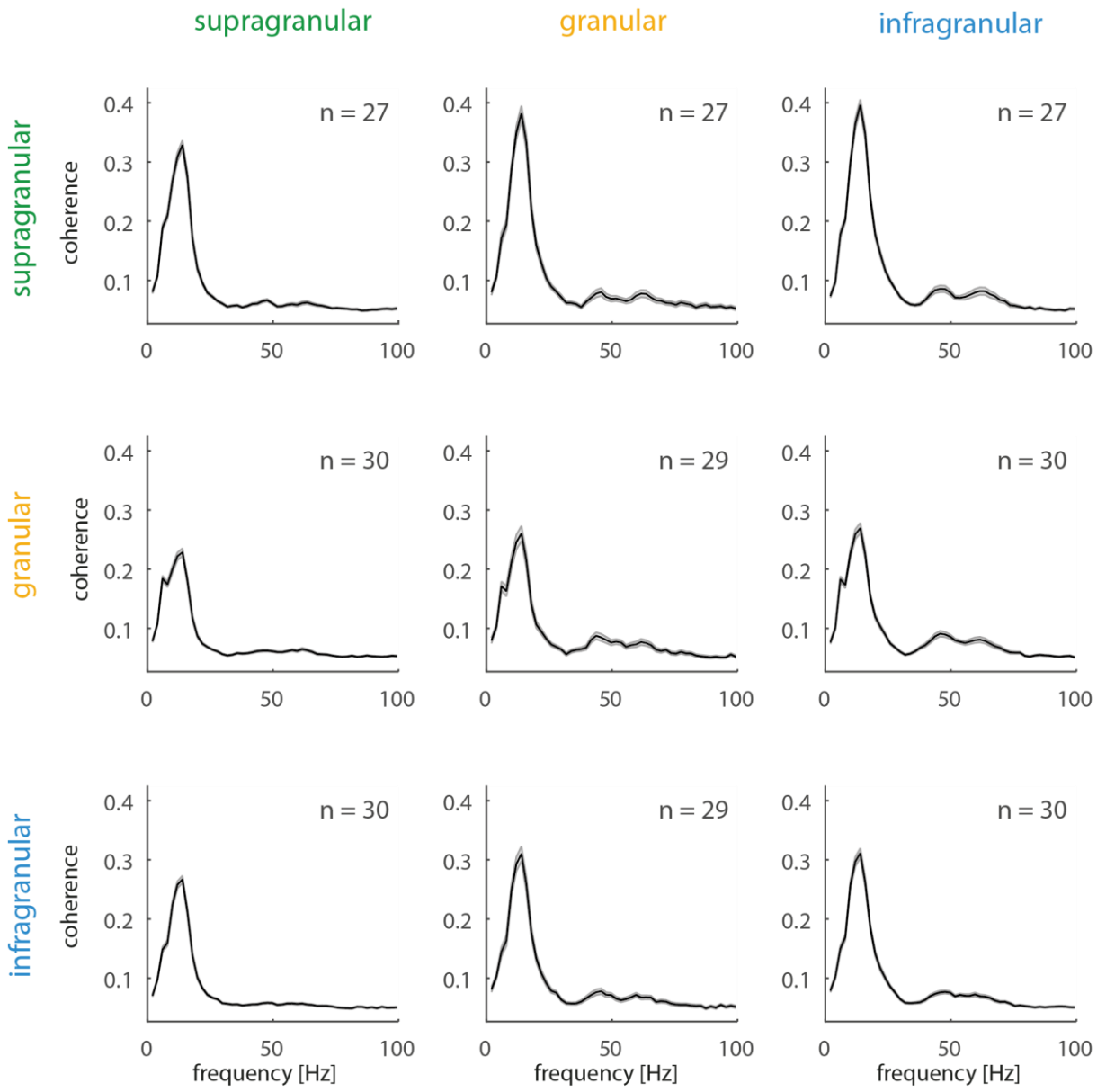

Figure B-7: V1-V4 field-field coherence in Monkey 1 aligned prior to the stimulus onset (-511ms to 0ms) in the attention task. Shown are all possible combinations of supragranular, granular and infragranular layer comparisons, averaged across the channels contributing to the respective sections (n = number of recordings in each plot). Coherence was calculated using the bipolar derivation of the local field potential and 3 tapers of 4Hz half-bandwidth. V1 and V4 structure are as defined in Figure 3-1 and Figure 4-1.

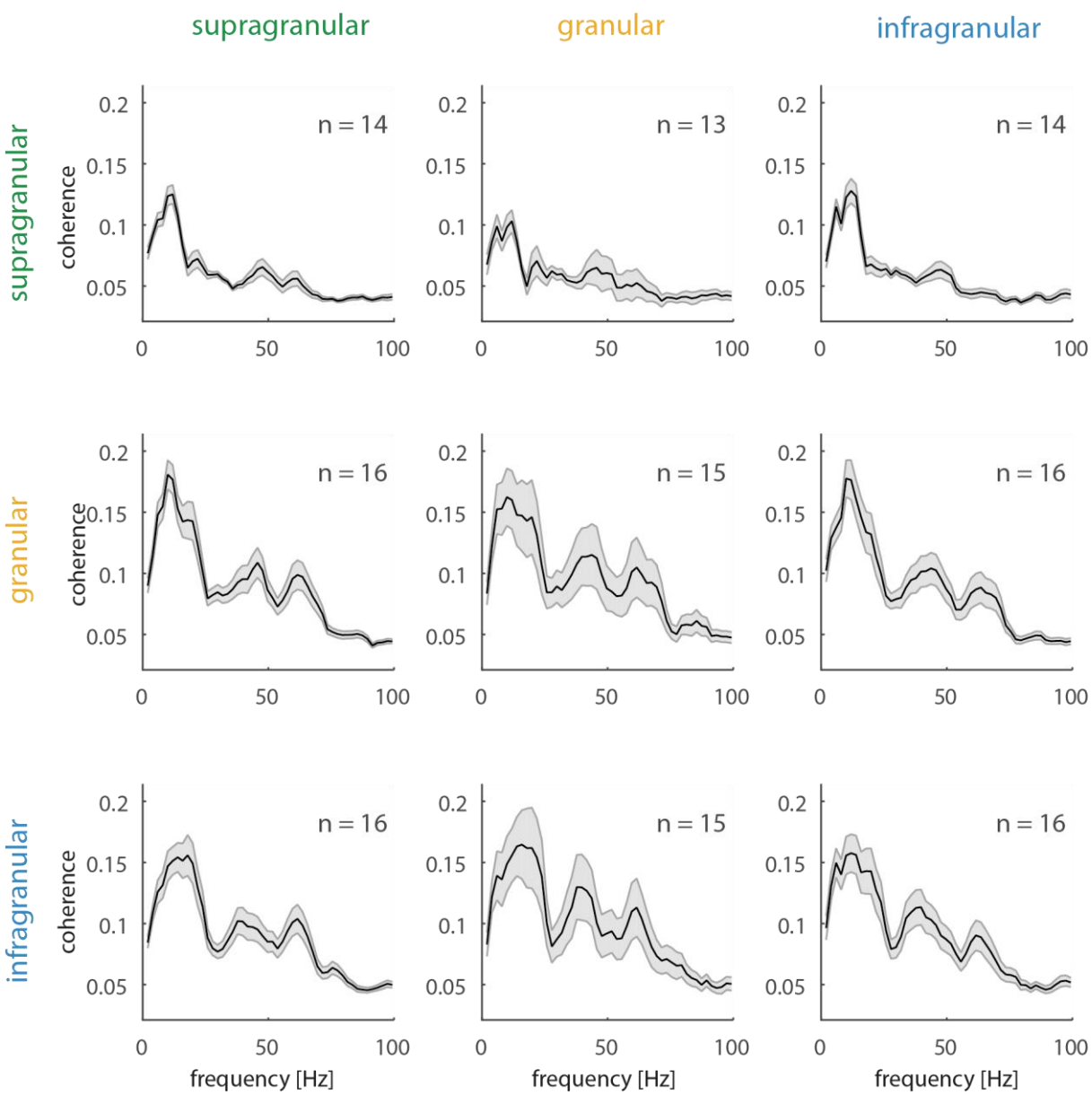

Figure B-8: V1-V4 field-field coherence in Monkey 2 (right hemisphere) aligned prior to the stimulus onset (-511ms to 0ms) in the attention task. Shown are all possible combinations of supragranular, granular and infragranular layer comparisons, averaged across the channels contributing to the respective sections (n = number of recordings in each plot). Coherence was calculated using the bipolar derivation of the local field potential and 3 tapers of 4Hz half-bandwidth. V1 and V4 structure are as defined in Figure 3-1 and Figure 4-1.

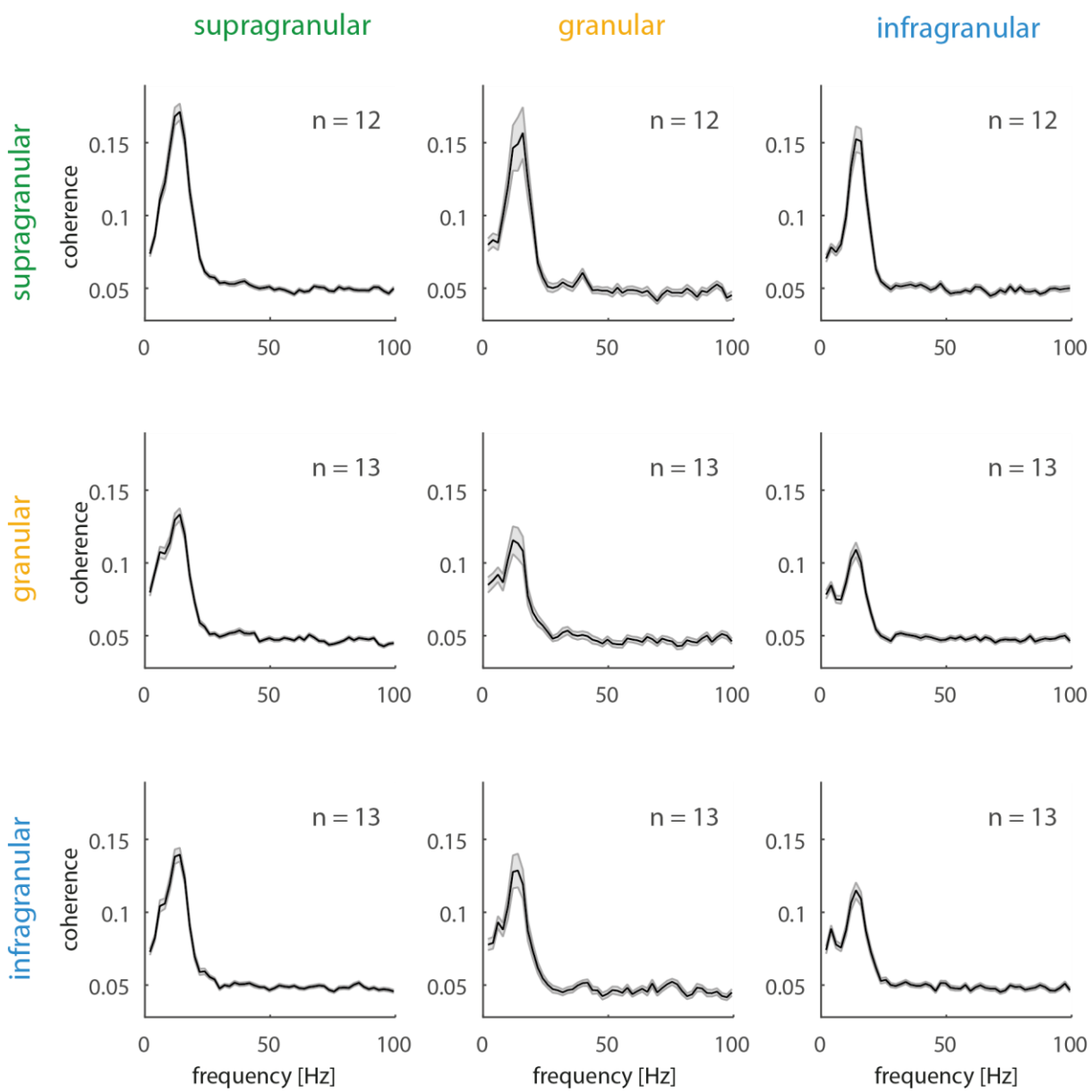

Figure B-9: V1-V4 field-field coherence in Monkey 2 (left hemisphere) aligned prior to the stimulus onset (-511ms to 0ms) in the attention task. Shown are all possible combinations of supragranular, granular and infragranular layer comparisons, averaged across the channels contributing to the respective sections (n = number of recordings in each plot). Coherence was calculated using the bipolar derivation of the local field potential and 3 tapers of 4Hz half-bandwidth. V1 and V4 structure are as defined in Figure 3-1 and Figure 4-1.

Appendix C. Phase Differences

C.1 Phase differences in V1

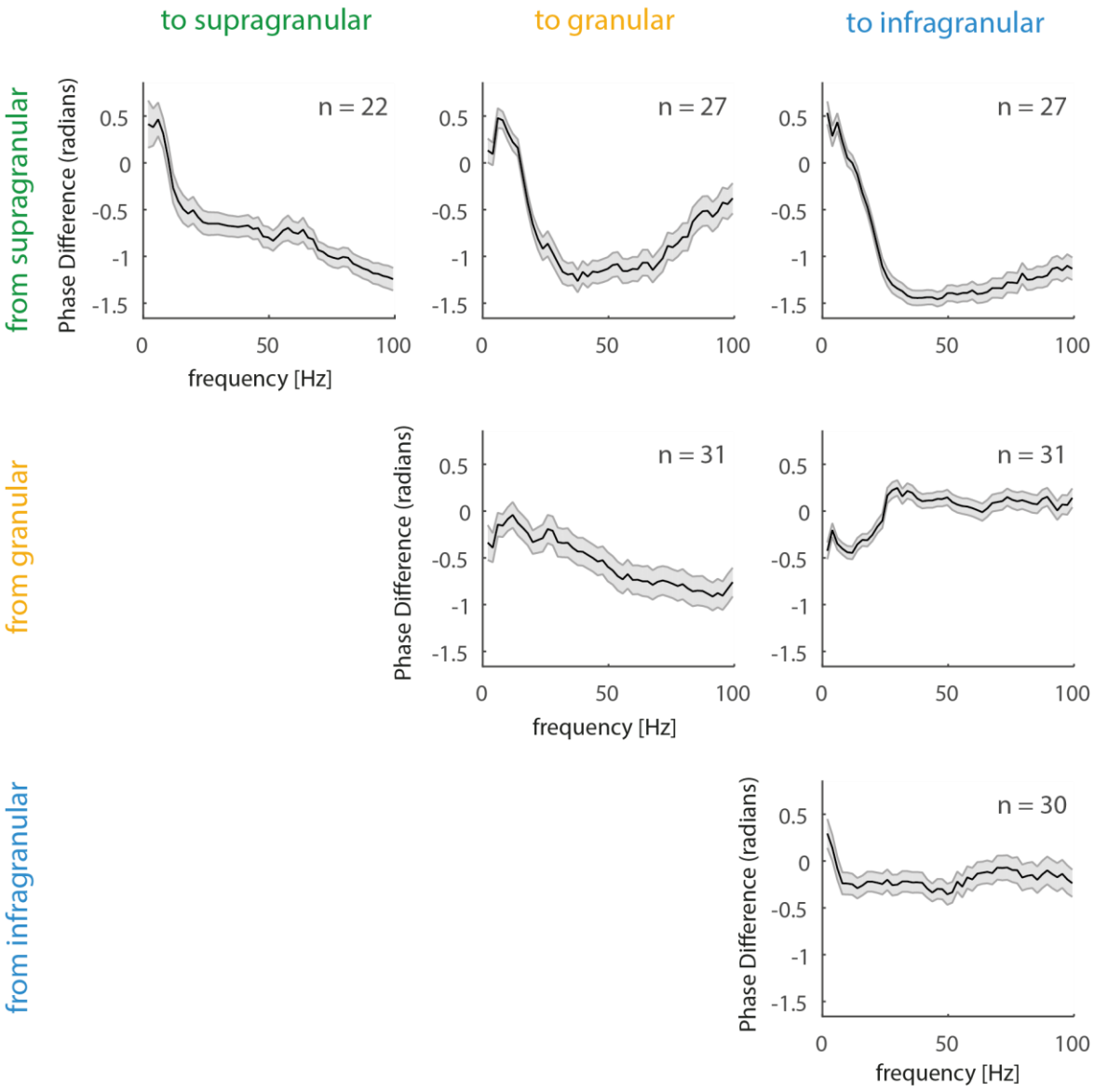

Figure C-6-2: V1 field-field coherence phase differences in Monkey 1 aligned to the stimulus onset (250ms to 761ms) in the attention task. Shown are all possible combinations of supragranular, granular and infragranular layer comparisons, averaged across the channels contributing to the respective sections (n = number of recordings in each plot). The phase differences shown here are from V1 to V4. Phase in the opposite direction (V4 to V1) has the same magnitude and opposite sign. Coherence was calculated using the bipolar derivation of the local field potential and 3 tapers of 4Hz half-bandwidth. V1 structure is as defined in Figure 3-19.

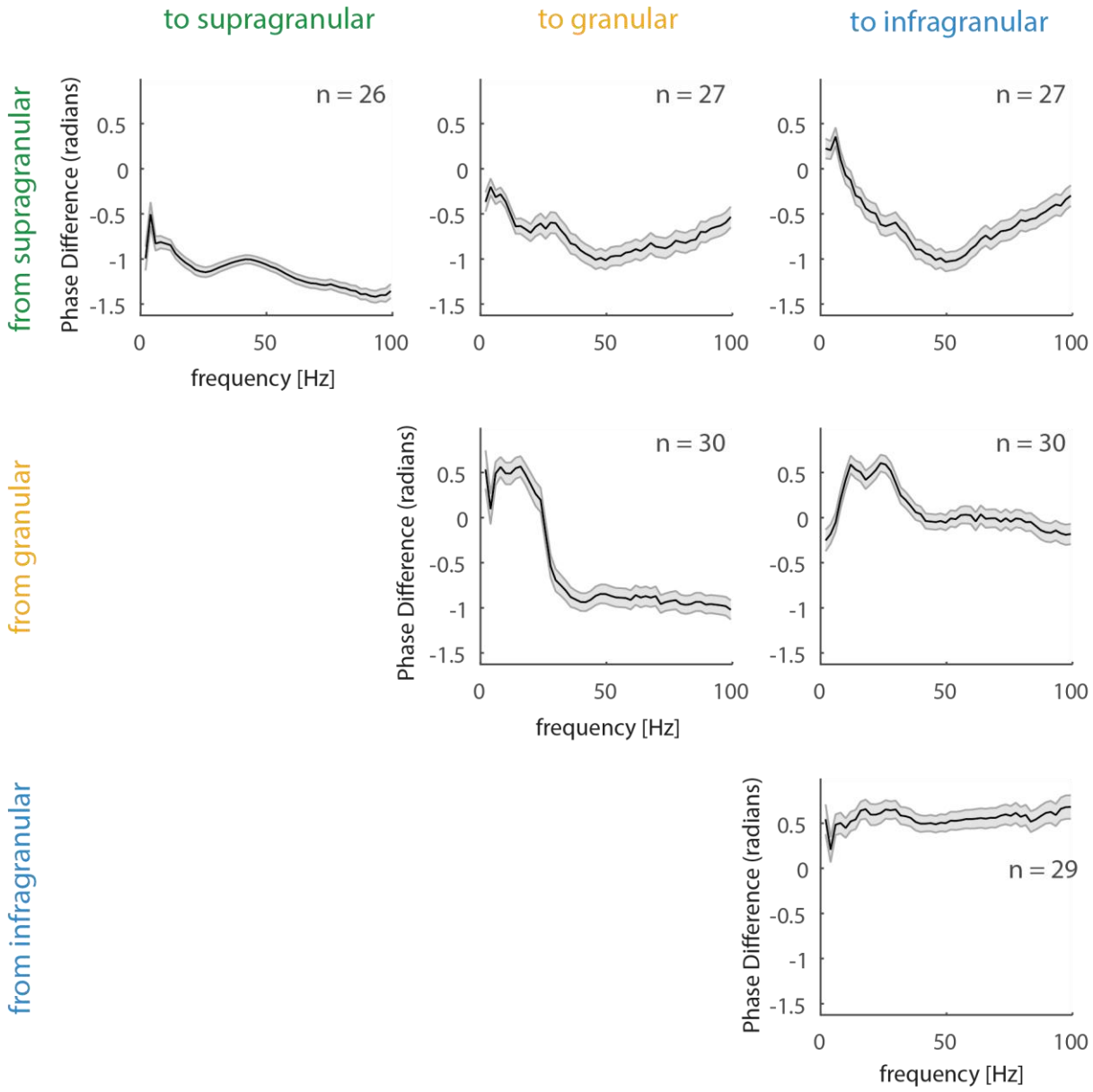

Figure C-2: V1 field-field coherence phase differences in Monkey 2 (right hemisphere) aligned to the stimulus onset (250ms to 761ms) in the attention task. Shown are all possible combinations of supragranular, granular and infragranular layer comparisons, averaged across the channels contributing to the respective sections (n = number of recordings in each plot). The phase differences shown here are from V1 to V4. Phase in the opposite direction (V4 to V1) has the same magnitude and opposite sign. Coherence was calculated using the bipolar derivation of the local field potential and 3 tapers of 4Hz half-bandwidth. V1 structure is as defined in Figure 3-19.

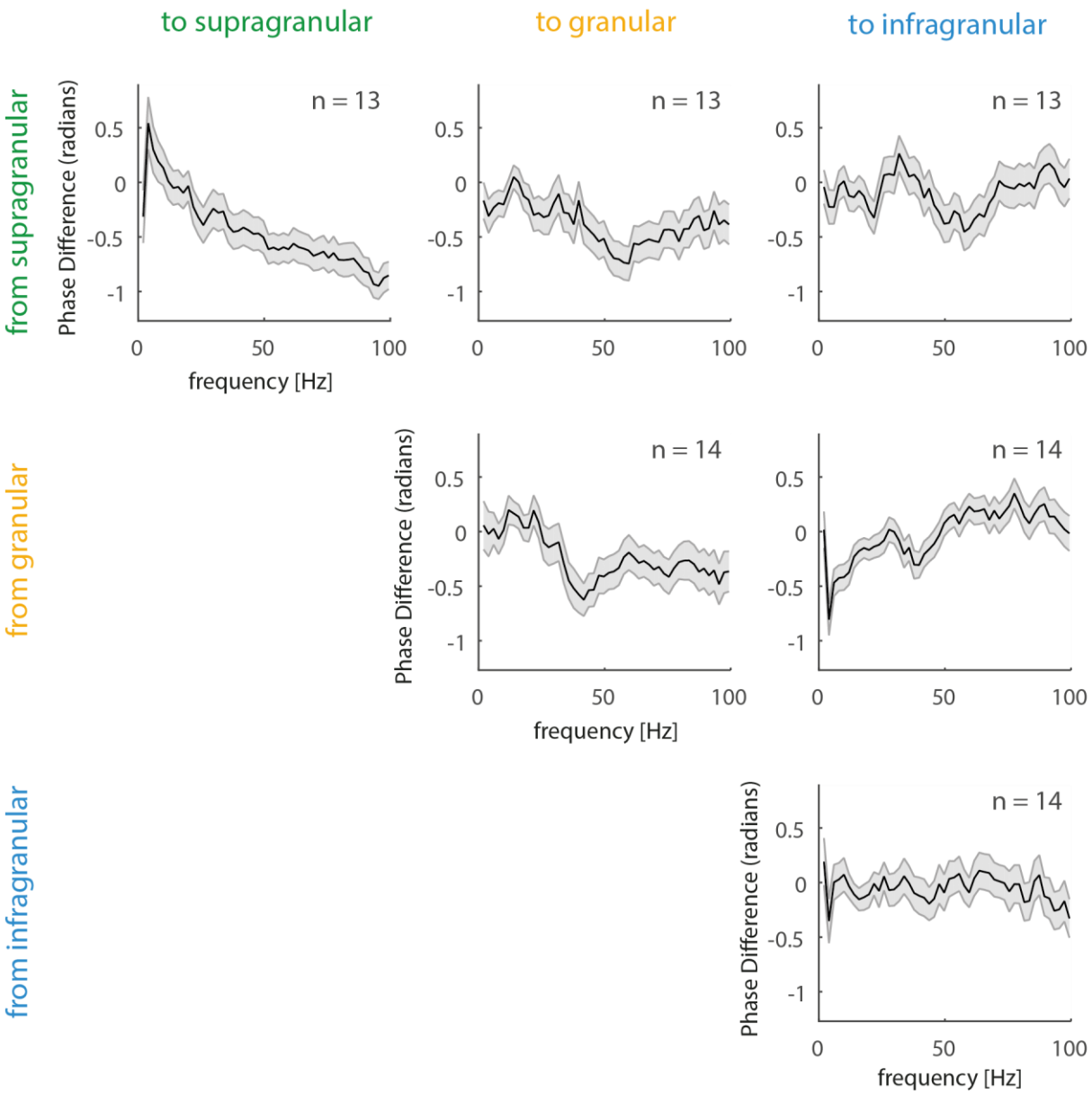

Figure C-3: V1 field-field coherence phase differences in Monkey 2 (left hemisphere) aligned to the stimulus onset (250ms to 761ms) in the attention task. Shown are all possible combinations of supragranular, granular and infragranular layer comparisons, averaged across the channels contributing to the respective sections (n = number of recordings in each plot). The phase differences shown here are from V1 to V4. Phase in the opposite direction (V4 to V1) has the same magnitude and opposite sign. Coherence was calculated using the bipolar derivation of the local field potential and 3 tapers of 4Hz half-bandwidth. V1 structure is as defined in Figure 3-19.

C.2 Phase differences in V4

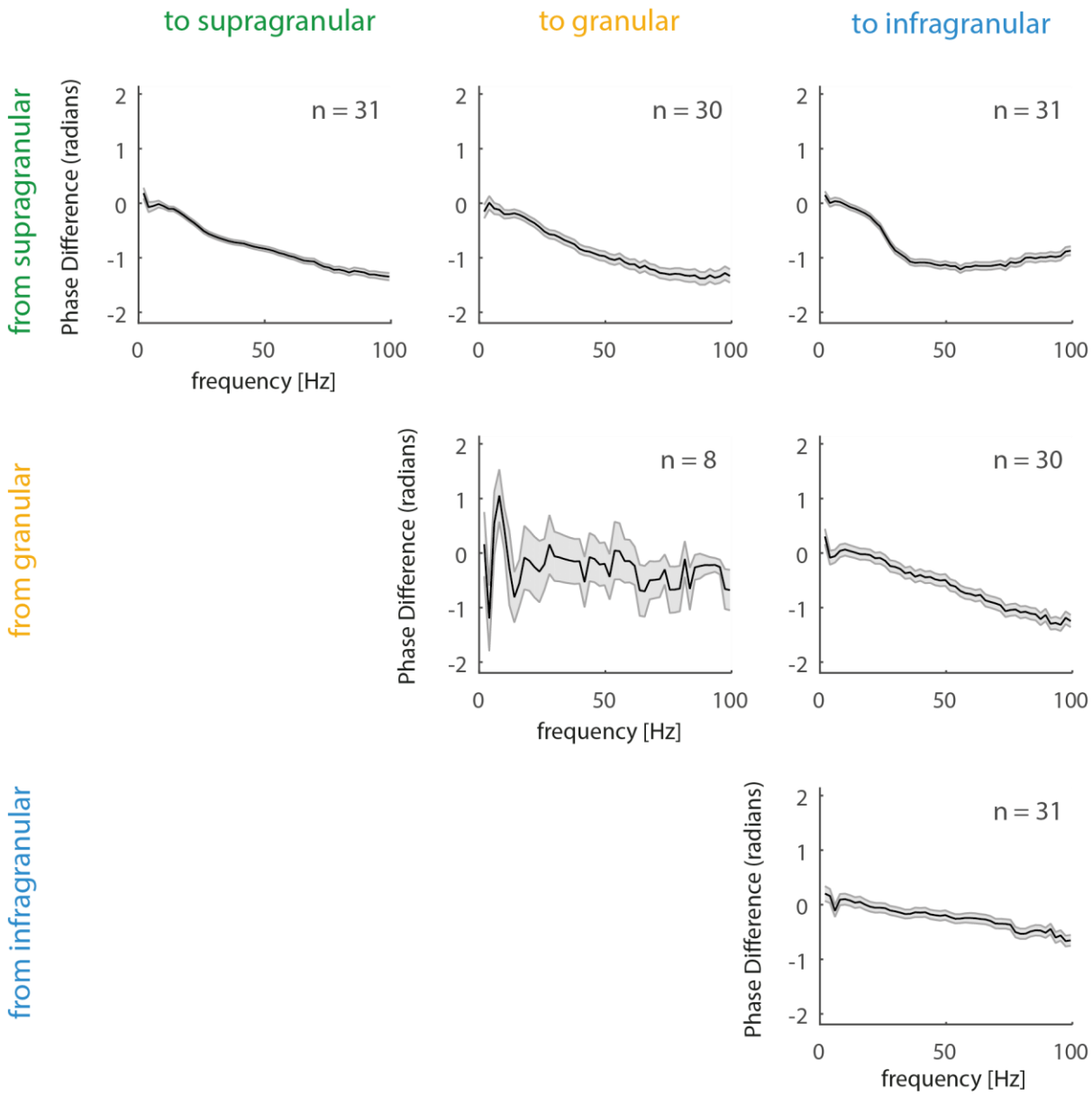

Figure C-4: V4 field-field coherence phase differences in Monkey 1 aligned to the stimulus onset (250ms to 761ms) in the attention task. Shown are all possible combinations of supragranular, granular and infragranular layer comparisons, averaged across the channels contributing to the respective sections (n = number of recordings in each plot). The phase differences shown here are for shallow to deep layers. Phase in the opposite direction (deep to shallow) has the same magnitude and opposite sign. Coherence was calculated using the bipolar derivation of the local field potential and 3 tapers of 4Hz half-bandwidth. V4 structure is as defined in Figure 4-1.

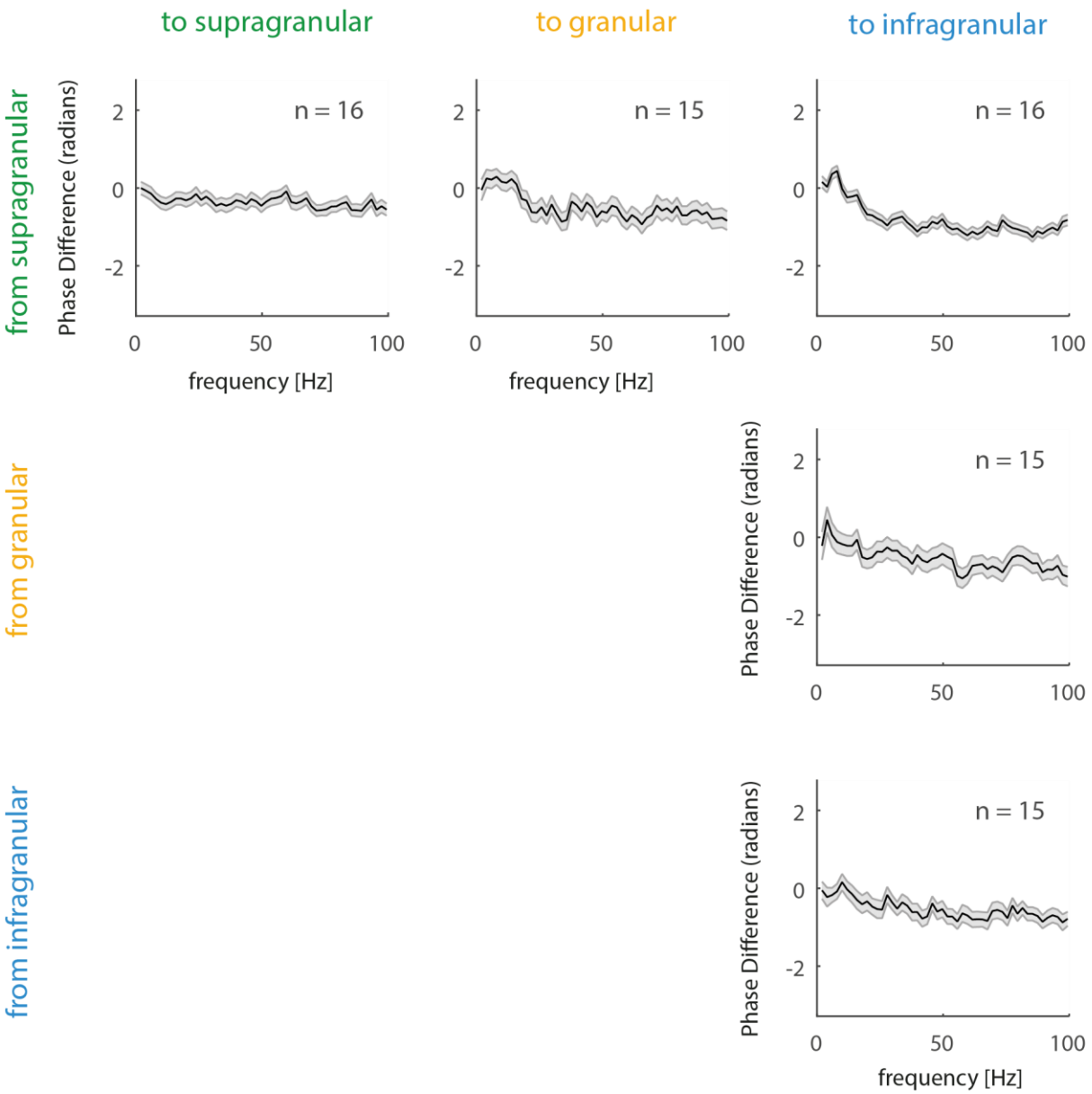

Figure C-5: V4 field-field coherence phase differences in Monkey 2 (right hemisphere) aligned to the stimulus onset (250ms to 761ms) in the attention task. Shown are all possible combinations of supragranular, granular and infragranular layer comparisons, averaged across the channels contributing to the respective sections (n = number of recordings in each plot). The phase differences shown here are for shallow to deep layers. Phase in the opposite direction (deep to shallow) has the same magnitude and opposite sign. Coherence was calculated using the bipolar derivation of the local field potential and 3 tapers of 4Hz half-bandwidth. V4 structure is as defined in Figure 4-1.

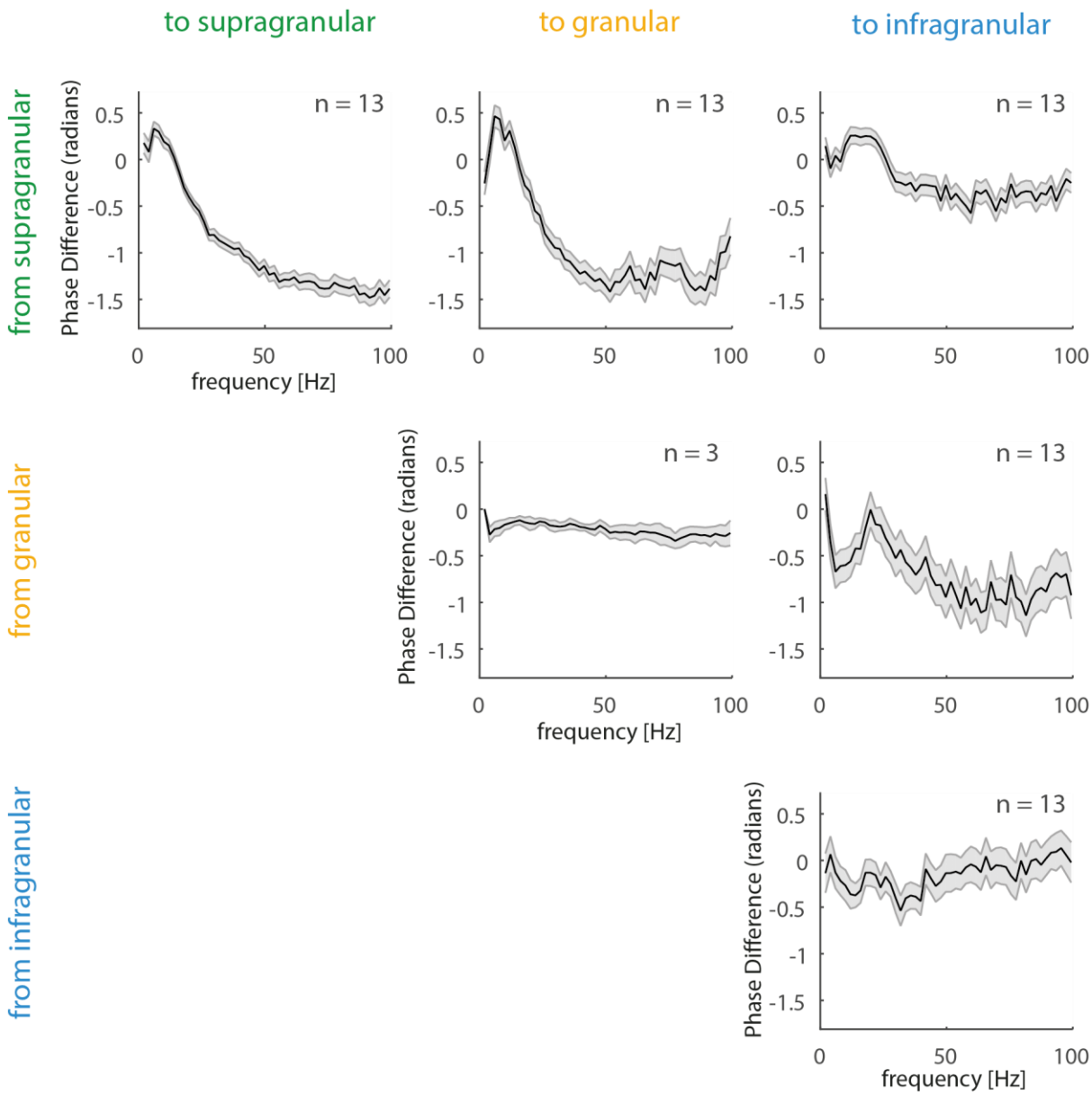

Figure C-6: V4 field-field coherence phase differences in Monkey 2 (left hemisphere) aligned to the stimulus onset (250ms to 761ms) in the attention task. Shown are all possible combinations of supragranular, granular and infragranular layer comparisons, averaged across the channels contributing to the respective sections (n = number of recordings in each plot). The phase differences shown here are for shallow to deep layers. Phase in the opposite direction (deep to shallow) has the same magnitude and opposite sign. Coherence was calculated using the bipolar derivation of the local field potential and 3 tapers of 4Hz half-bandwidth. V4 structure is as defined in Figure 4-1.

C.3 Phase differences between V1 and V4

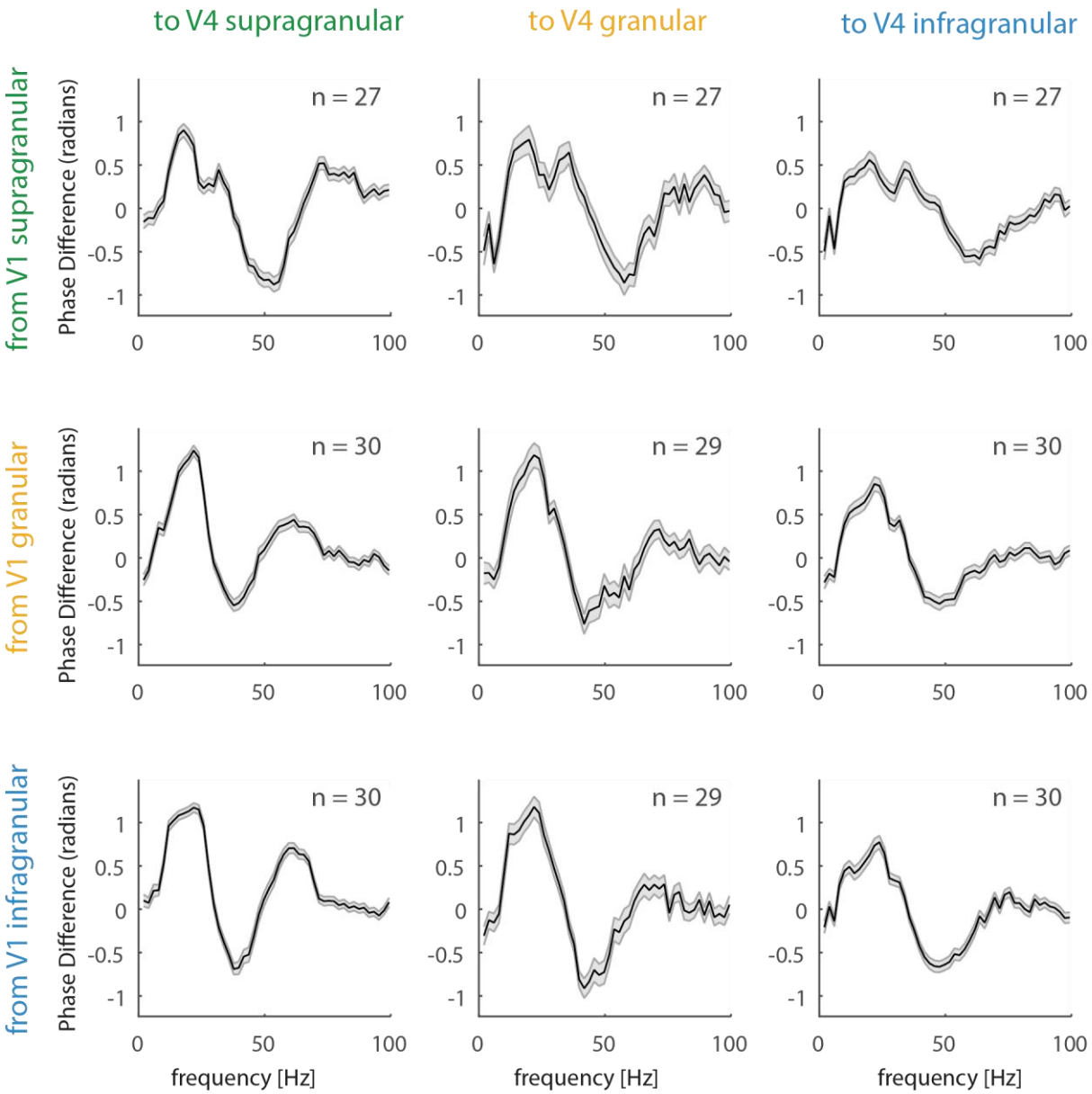

Figure C-7: V4 field-field coherence phase differences in Monkey 1 aligned to the stimulus onset (250ms to 761ms) in the attention task. Shown are all possible combinations of supragranular, granular and infragranular layer comparisons, averaged across the channels contributing to the respective sections (n = number of recordings in each plot). The phase differences shown here are for shallow to deep layers. Phase in the opposite direction (deep to shallow) has the same magnitude and opposite sign. Coherence was calculated using the bipolar derivation of the local field potential and 3 tapers of 4Hz half-bandwidth. V1 and V4 structure is as defined in Figure 3-1 and Figure 4-1.

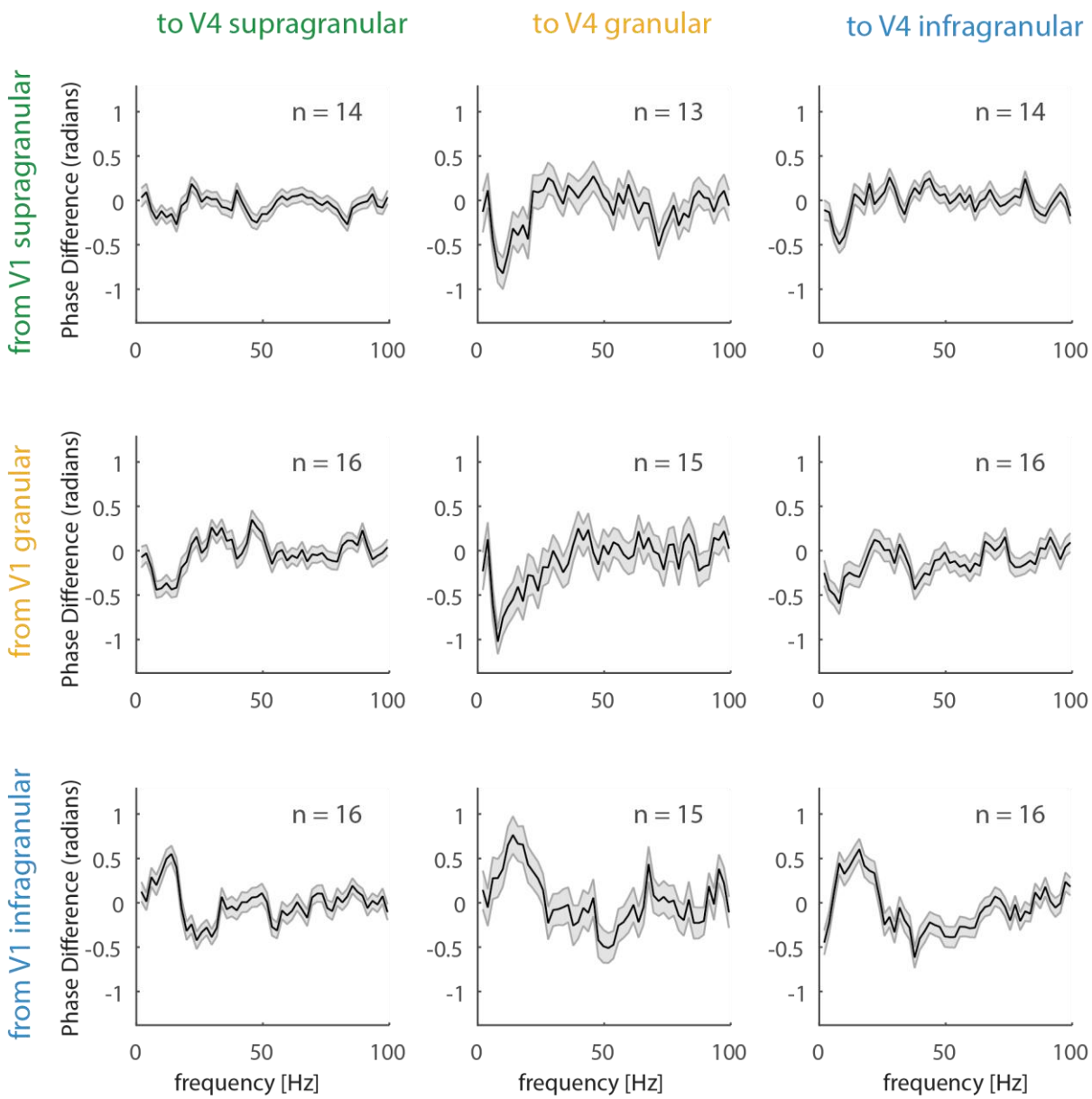

Figure C-8: V4 field-field coherence phase differences in Monkey 2 (right hemisphere) aligned to the stimulus onset (250ms to 761ms) in the attention task. Shown are all possible combinations of supragranular, granular and infragranular layer comparisons, averaged across the channels contributing to the respective sections (n = number of recordings in each plot). The phase differences shown here are for shallow to deep layers. Phase in the opposite direction (deep to shallow) has the same magnitude and opposite sign. Coherence was calculated using the bipolar derivation of the local field potential and 3 tapers of 4Hz half-bandwidth. V1 and V4 structure is as defined in Figure 3-1 and Figure 4-1.

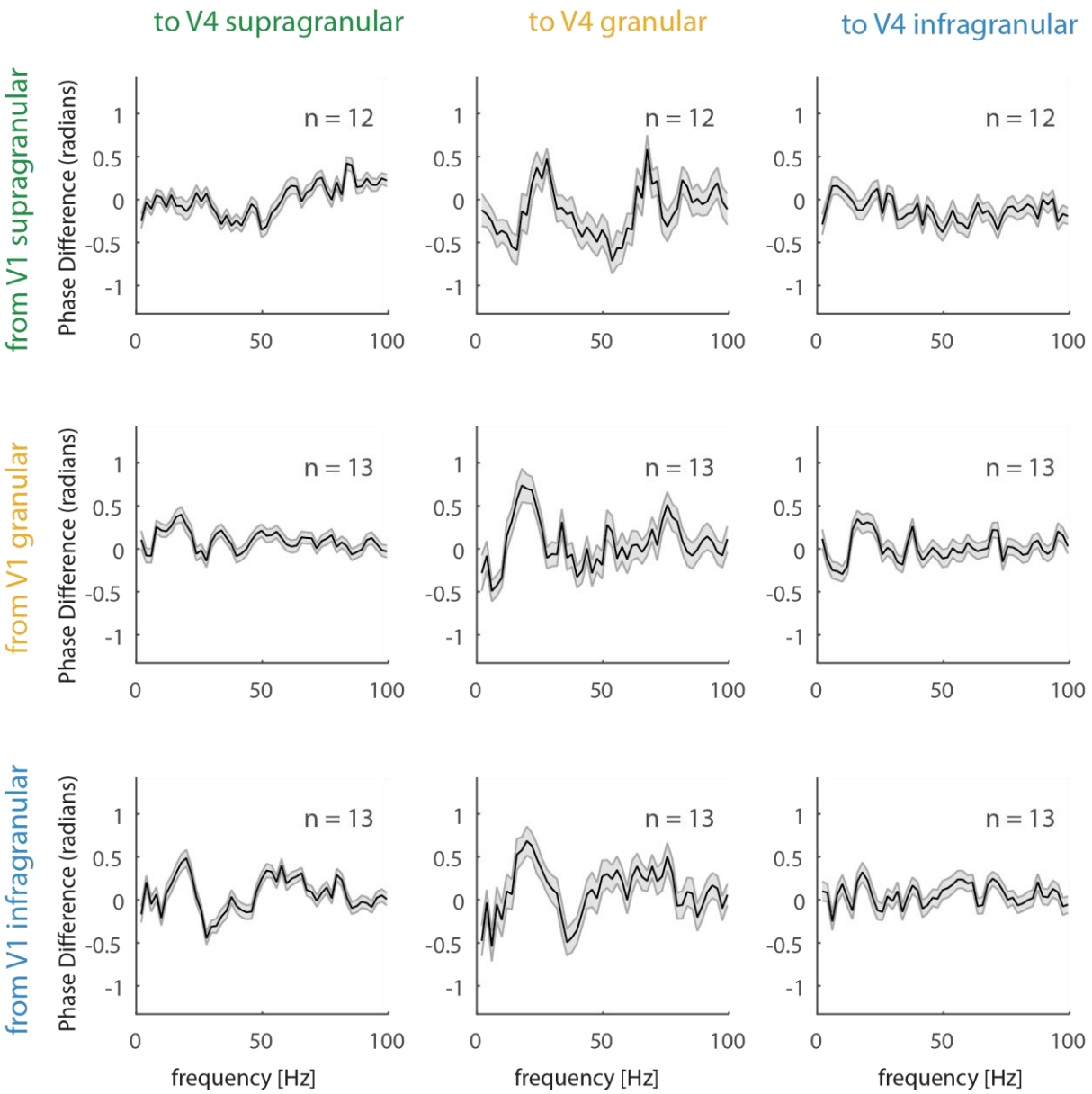

Figure C-9: V4 field-field coherence phase differences in Monkey 2 (left hemisphere) aligned to the stimulus onset (250ms to 761ms) in the attention task. Shown are all possible combinations of supragranular, granular and infragranular layer comparisons, averaged across the channels contributing to the respective sections (n = number of recordings in each plot). The phase differences shown here are for shallow to deep layers. Phase in the opposite direction (deep to shallow) has the same magnitude and opposite sign. Coherence was calculated using the bipolar derivation of the local field potential and 3 tapers of 4Hz half-bandwidth. V1 and V4 structure is as defined in Figure 3-1 and Figure 4-1.

Appendix D. LFP Cross Correlations

D.1 Cross correlations in V1

In order to confirm that the direction of information flow which the Granger causality analyses suggested was not spurious, we performed a separate cross correlation analysis between the different layers of V1. When reading the following figures, it is useful to note that a negative lag from deep to superficial layers indicates that activity in the deep layers leads that in the superficial layers (i.e. upwards directionality), whereas a positive lag indicates downwards directionality. The pattern is then reversed for cross correlations from superficial to deep layers.

In the Granger causality analysis, the main feature which was observed in the low frequency range was that Granger causality in the upwards direction (deep to superficial layers) was stronger than that in the downwards direction (superficial to deep layers). This directionality was also present between the granular and supragranular layers in the cross correlation analysis and between the infragranular layers and granular layers for Monkey 1 and the left hemisphere of Monkey 2 (Figure D-1). Since these layer combinations matched those in which the effect was observed in the Granger causality analysis, this gives confidence in these results.

The cross correlations in the low gamma frequency range (Figure D-2) for Monkey 1 were only significantly different to zero between the infragranular and granular layers, where there was an upwards directionality. In the Granger causality analysis, the opposite directionality was found. In recordings in the right hemisphere of Monkey 2, Granger causality suggested an upwards directionality between infragranular and granular layers and a downwards directionality between supragranular and granular layers. These effects were also present in the cross correlation analysis. Although there were significantly non-zero median lags in the low gamma range for the left hemisphere of Monkey 2, there were no clear effects uncovered in the Granger causality analysis which these could be compared with.

In the high gamma frequency range (50-100Hz), the cross correlation analysis (Figure D-3) showed predominantly an upwards directionality for both monkeys. This matches what was observed in the Granger causality analysis, with the exception of the causality between the granular and infragranular layers of Monkey 1, which showed a

downwards directionality. The cross correlation distribution for this layer pair was not significantly different to zero, so this exception cannot be confirmed or disproven.

Overall the results obtained through cross correlation and Granger causality analysis were mostly in agreement over the direction of information flow in V1.

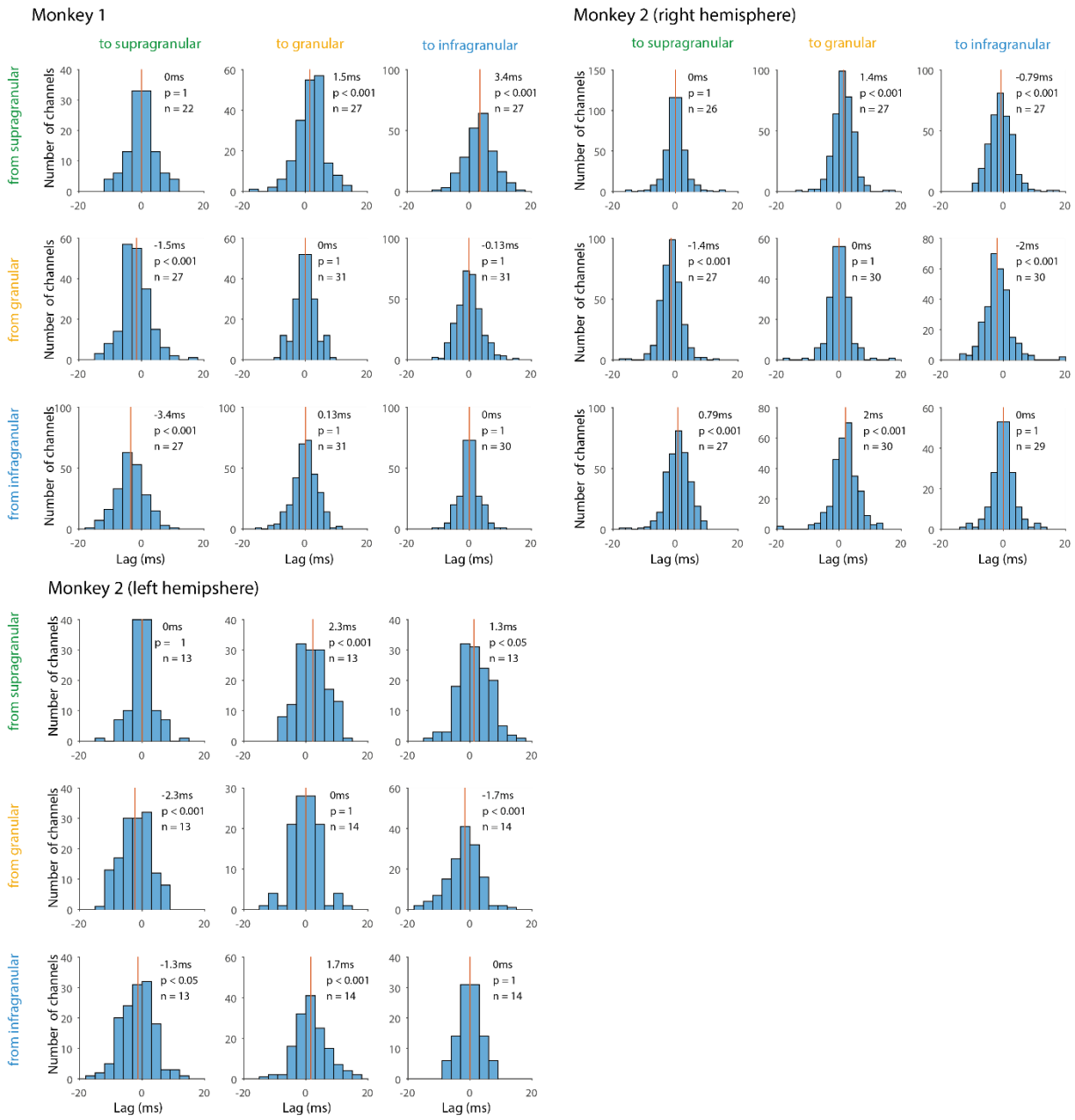

Figure D-1: LFP cross correlation histograms for V1 in the 12-25Hz frequency range. Plotted for Monkey 1 (top left plots) and the right and left hemispheres of Monkey 2 (top right and bottom right respectively plots). Shown for all possible combinations of cortical layers. Red lines indicates the median value of each distribution. The text on the plots quantifies the median value, p value (Wilcoxon signed rank test) and number of recordings (n).

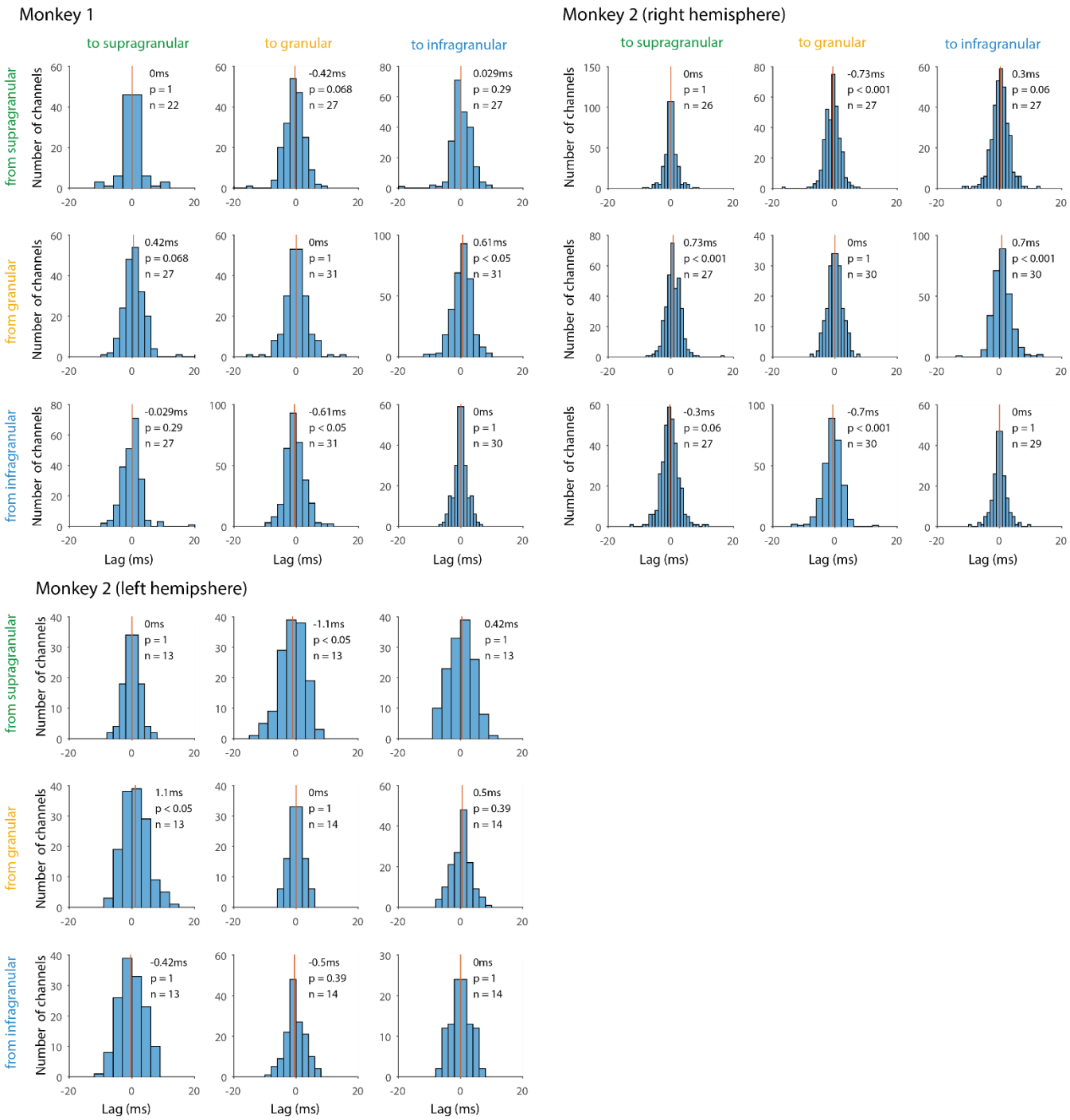

Figure D-2: LFP cross correlation histograms for V1 in the 30-50Hz frequency range. Plotted for Monkey 1 (top left plots) and the right and left hemispheres of Monkey 2 (top right and bottom right respectively plots). Shown for all possible combinations of cortical layers. Red lines indicates the median value of each distribution. The text on the plots quantifies the median value, p value (Wilcoxon signed rank test) and number of recordings (n).

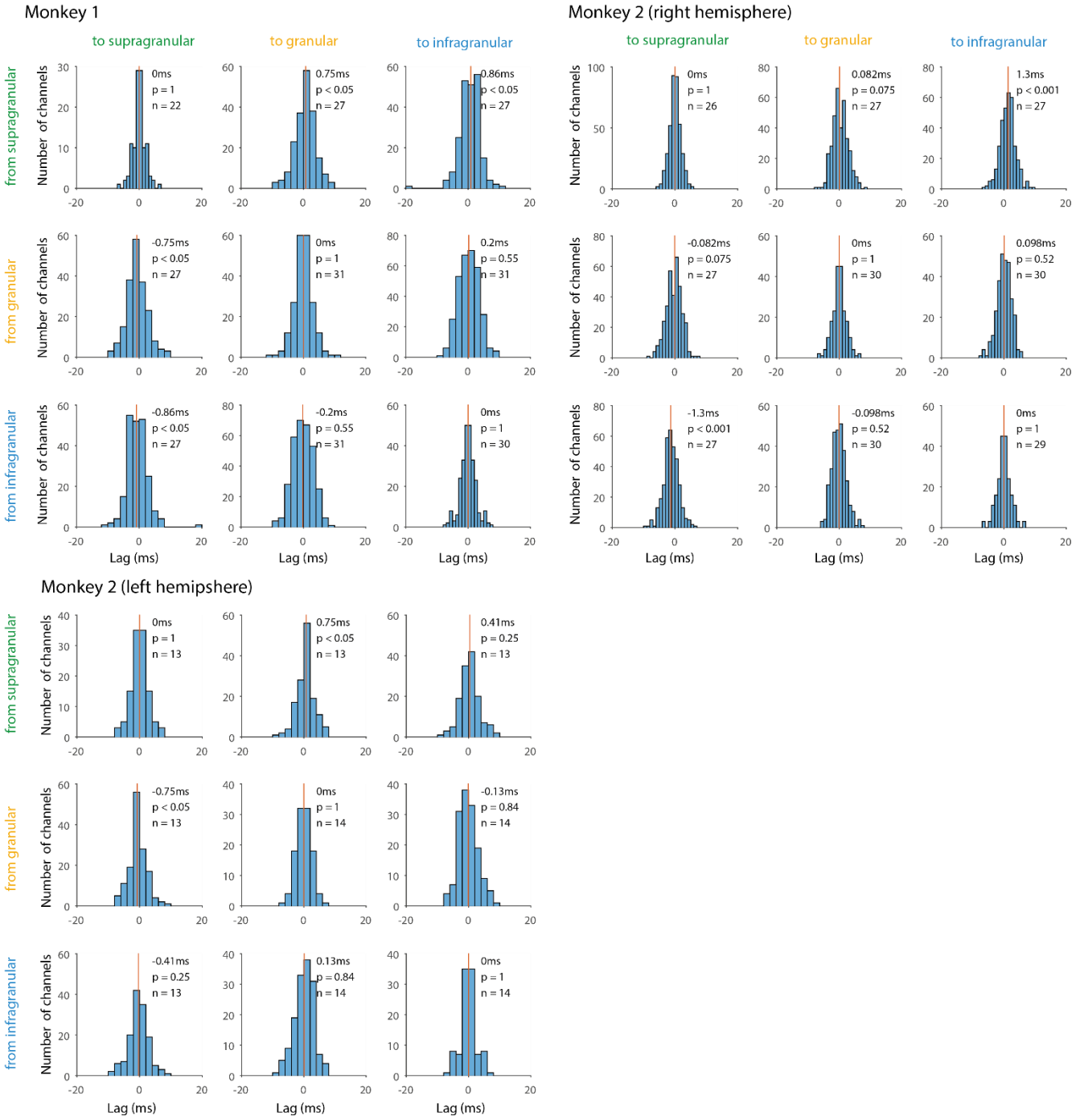

Figure D-3: LFP cross correlation histograms for V1 in the 55-100Hz frequency range. Plotted for Monkey 1 (top left plots) and the right and left hemispheres of Monkey 2 (top right and bottom right respectively plots). Shown for all possible combinations of cortical layers. Red lines indicates the median value of each distribution. The text on the plots quantifies the median value, p value (Wilcoxon signed rank test) and number of recordings (n).

D.2 Cross correlations in V4

We next performed a cross correlation analysis on V4 LFP signals to assess the reliability of directionality which was suggested by our Granger causality analysis (Section 4.6.1).

In Monkey 1, the cross correlation analysis in the low frequency range (12-25Hz, Figure D-4) showed an upwards directionality between the supragranular and granular/infragranular layers, which matched what was shown with Granger causality. The Granger causality in the left hemisphere of Monkey 2 suggested upwards directionality between the supragranular and granular layers, however there was only a trend for this effect in the cross correlation results. As in the Granger causality analysis of recordings in the right hemisphere of Monkey 2, we did not find a clear directionality for the low frequency band.

In both the low gamma frequency range (Figure D-5) and the high gamma frequency range (Figure D-6), the layer combinations which had median lags that were significantly different to zero showed upwards directionality. This matches the directionality which was suggested across monkeys by the Granger causality analysis.

Overall, the directionality of information flow in V4 was found to be upwards by both the cross correlation and Granger causality analysis.

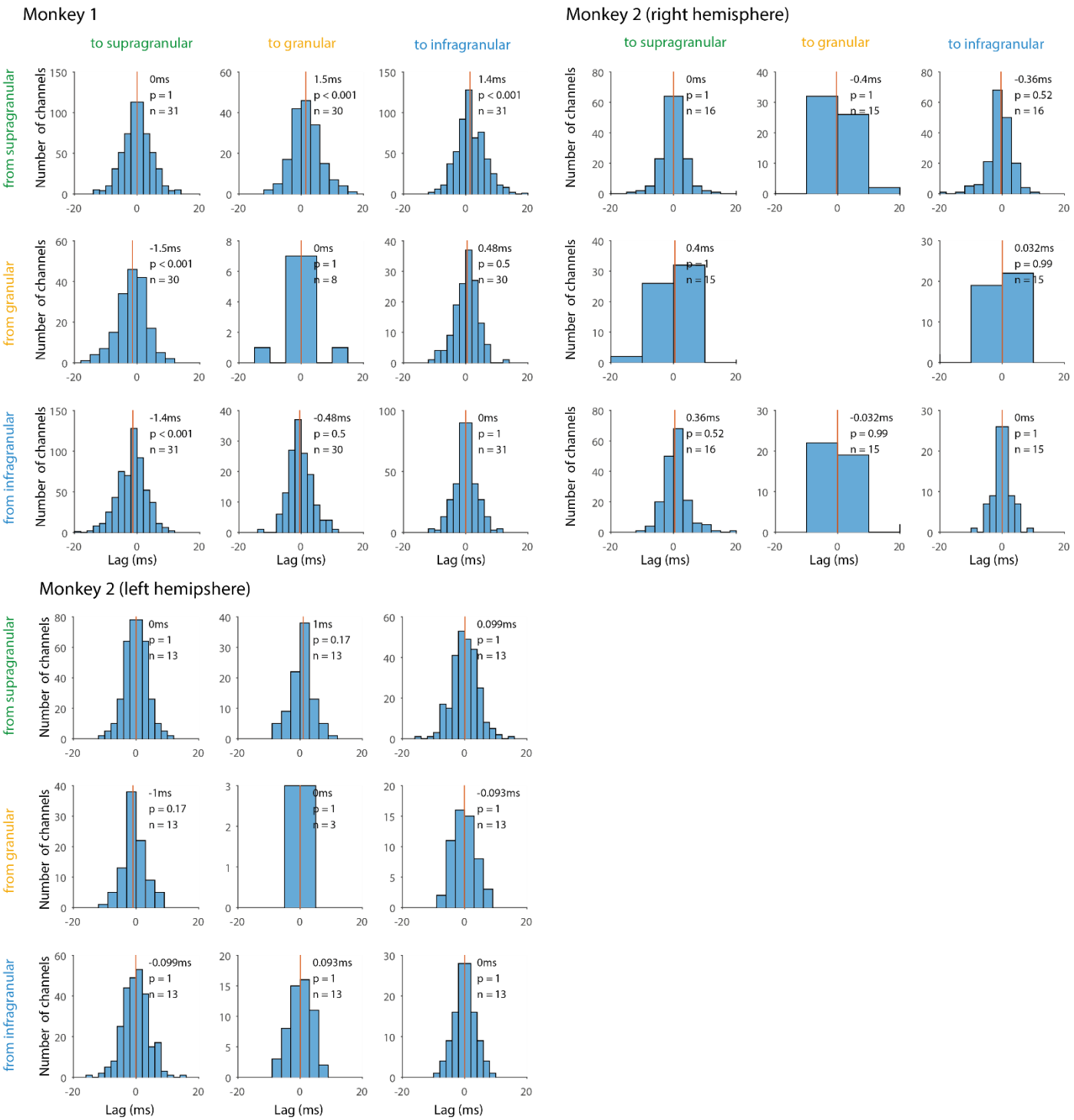

Figure D-4: LFP cross correlation histograms for V4 in the 12-25Hz frequency range. Plotted for Monkey 1 (top left plots) and the right and left hemispheres of Monkey 2 (top right and bottom right respectively plots). Shown for all possible combinations of cortical layers. Red lines indicates the median value of each distribution. The text on the plots quantifies the median value, p value (Wilcoxon signed rank test) and number of recordings (n).

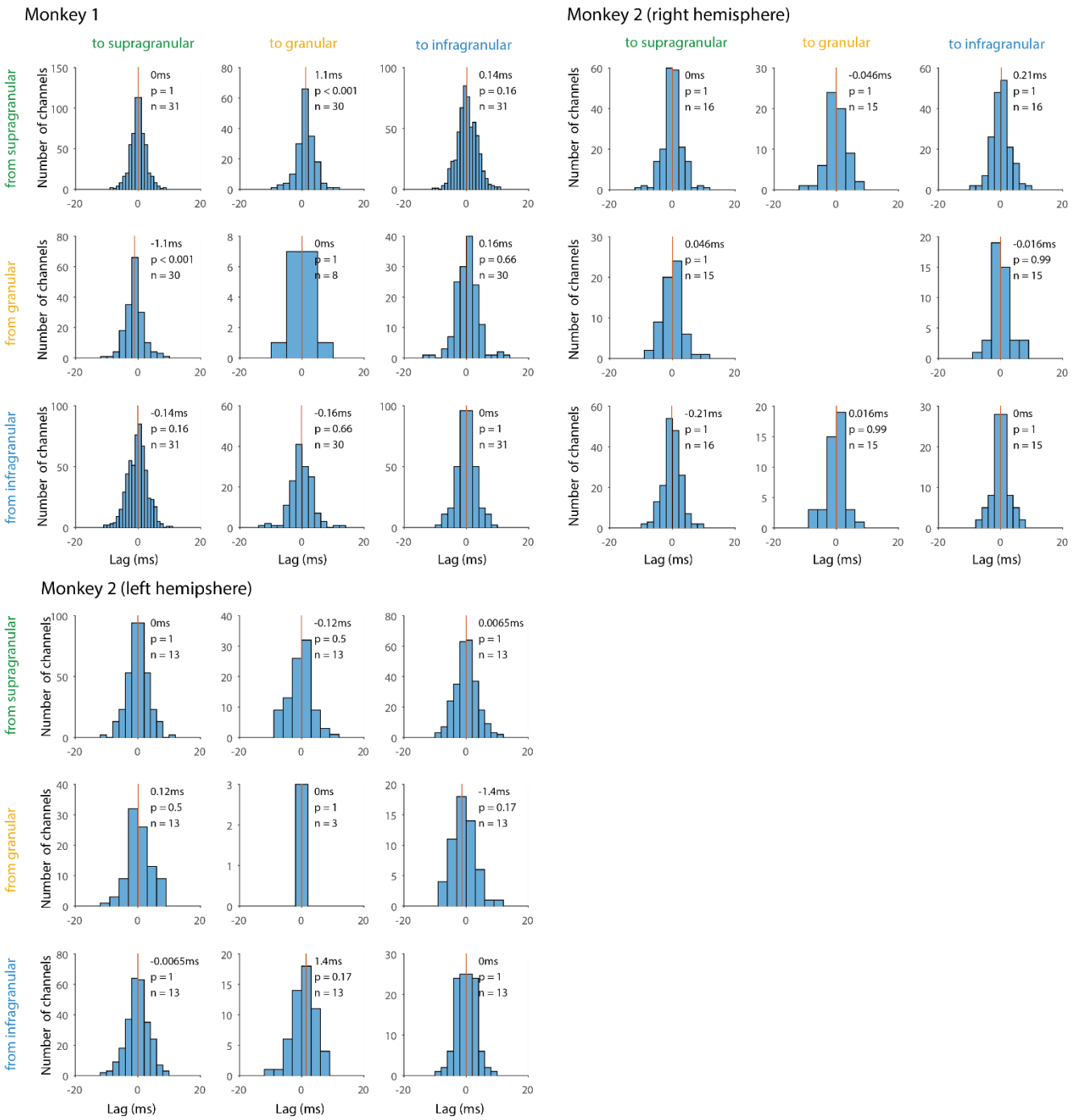

Figure D-5: LFP cross correlation histograms for V4 in the 30-50Hz frequency range. Plotted for Monkey 1 (top left plots) and the right and left hemispheres of Monkey 2 (top right and bottom right respectively plots). Shown for all possible combinations of cortical layers. Red lines indicates the median value of each distribution. The text on the plots quantifies the median value, p value (Wilcoxon signed rank test) and number of recordings (n).

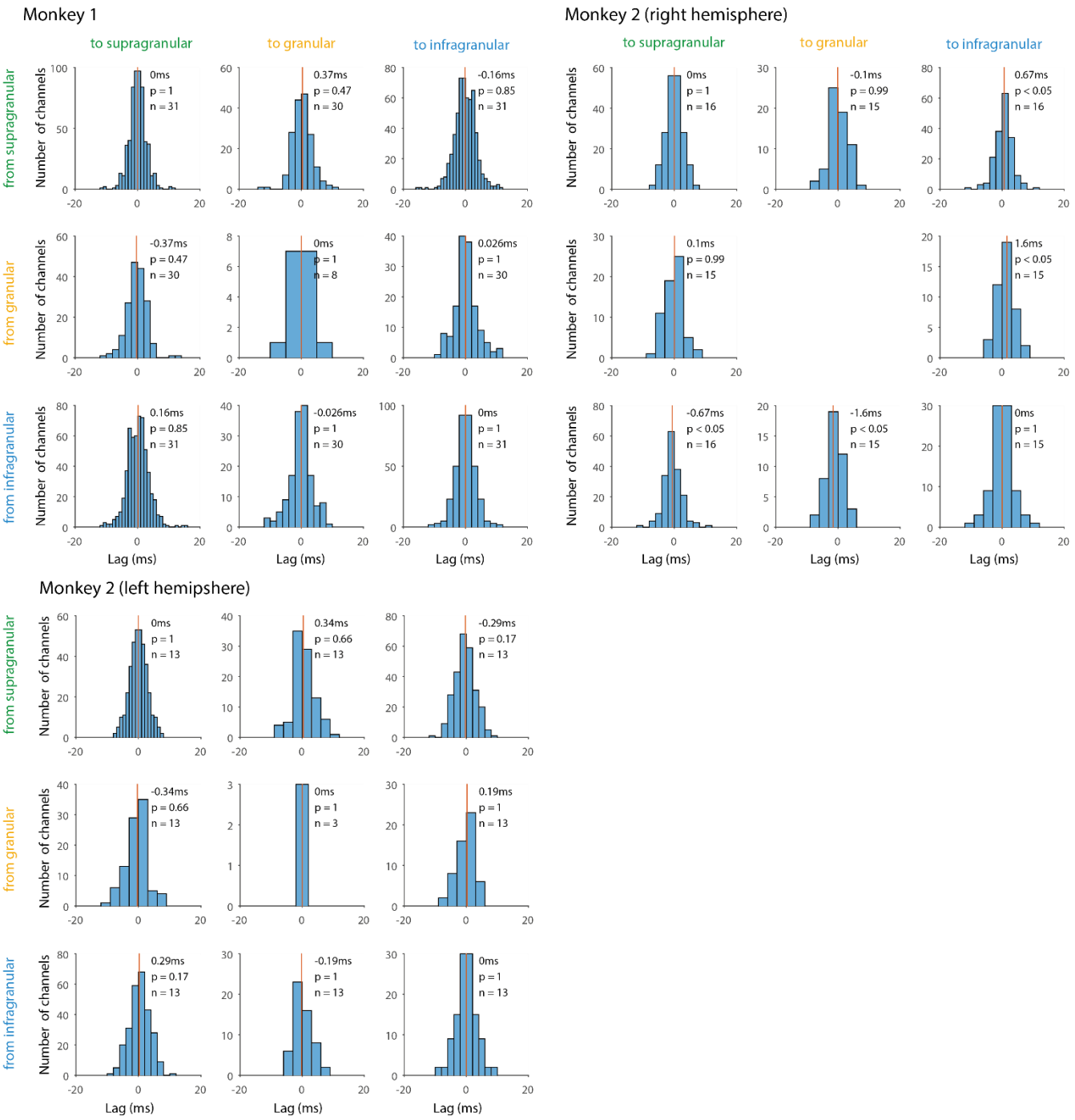

Figure D-6: LFP cross correlation histograms for V1 in the 55-100Hz frequency range. Plotted for Monkey 1 (top left plots) and the right and left hemispheres of Monkey 2 (top right and bottom right respectively plots). Shown for all possible combinations of cortical layers. Red lines indicates the median value of each distribution. The text on the plots quantifies the median value, p value (Wilcoxon signed rank test) and number of recordings (n).

D.3 Cross correlations between V1 and V4

Finally we calculated cross correlations between V1 and V4. It's worth noting that a negative cross correlation from V1 to V4 indicates a feedforward information flow and a positive cross correlation indicates a feedback flow. Cross correlations from V4 to V1 are not shown, but had the same magnitude and opposite sign as those from V1 to V4, so were not needed to draw conclusions from.

In Monkey 1, low frequency cross correlations (Figure D-7) from the V1 supragranular and infragranular layers to all V4 layers had a significantly positive median, suggesting feedback information flow, matching what we observed in the Granger causality analysis (Section 5.4.1). Granger causality from V1 granular layers to V4 showed feedback information flow, however the cross correlation analysis showed feedforward information flow from the V1 granular to V4 supragranular layers. There were no low frequency cross correlation distributions that were significantly different to zero in either hemisphere of Monkey 2.

In both gamma frequency ranges (Figure D-8 and Figure D-9), the median lag was not significantly different to zero for any layer combination in either monkey. Therefore we cannot make any comparisons with the results of the Granger causality analysis.

Since there were few significant results in the V1-V4 cross correlation analysis, it was difficult to back up the conclusions made in the Granger causality analysis. Given that there was a much lower magnitude of coherence between areas compared to within them, it may be that we did not have enough recordings in our study to uncover the subtle underlying effects in our cross correlation analysis.

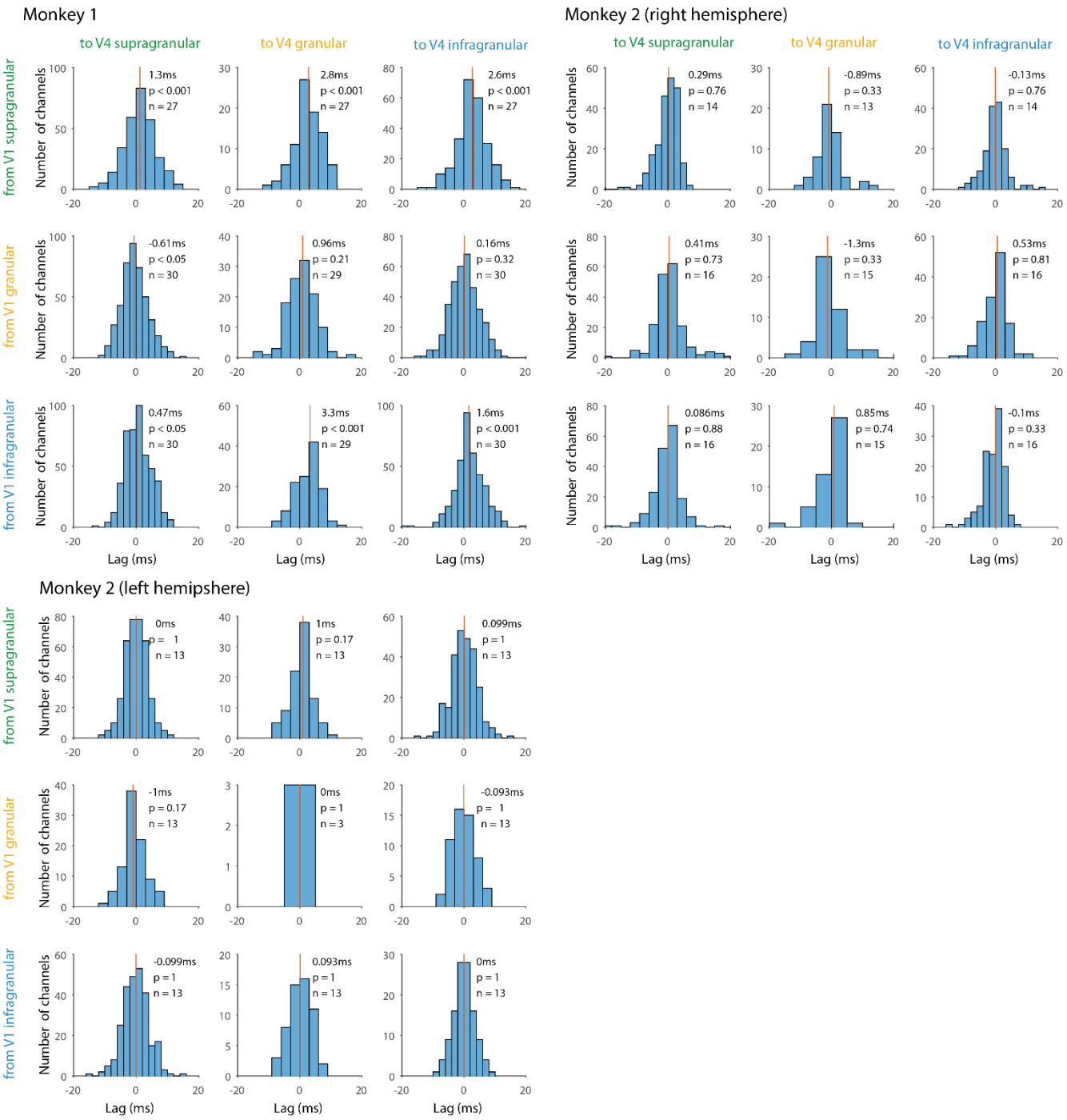

Figure D-7: LFP cross correlation histograms between V1 and V4 in the 12-25Hz frequency range. Plotted for Monkey 1 (top left plots) and the right and left hemispheres of Monkey 2 (top right and bottom right respectively plots). Shown for all combinations of V1 layers to V4 layers, correlations in the opposite direction have the same magnitude and opposite sign. Red lines indicates the median value of each distribution. The text on the plots quantifies the median value, p value (Wilcoxon signed rank test) and number of recordings (n).

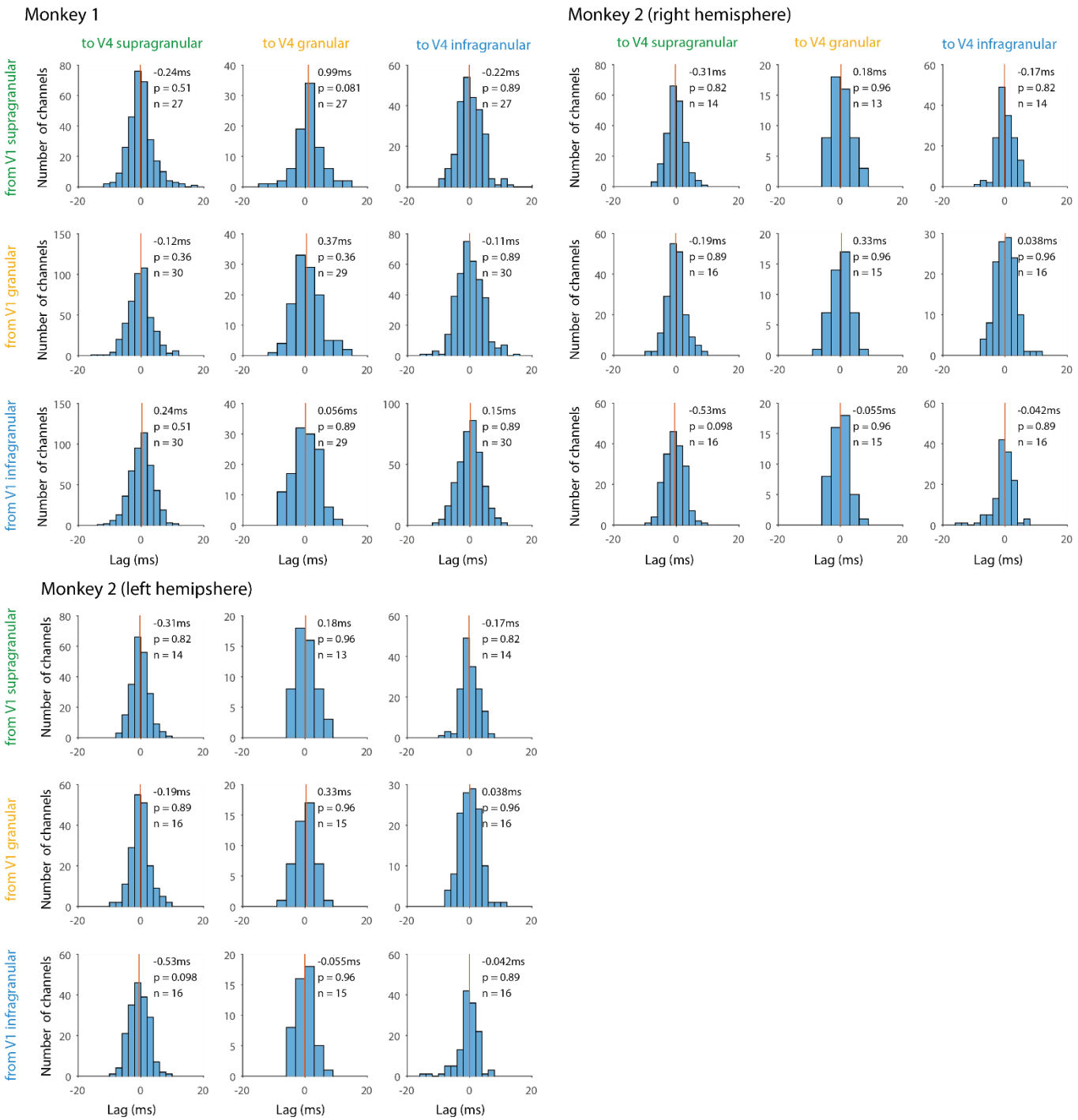

Figure D-8: LFP cross correlation histograms between V1 and V4 in the 30-50Hz frequency range. Plotted for Monkey 1 (top left plots) and the right and left hemispheres of Monkey 2 (top right and bottom right respectively plots). Shown for all combinations of V1 layers to V4 layers, correlations in the opposite direction have the same magnitude and opposite sign. Red lines indicates the median value of each distribution. The text on the plots quantifies the median value, p value (Wilcoxon signed rank test) and number of recordings (n).

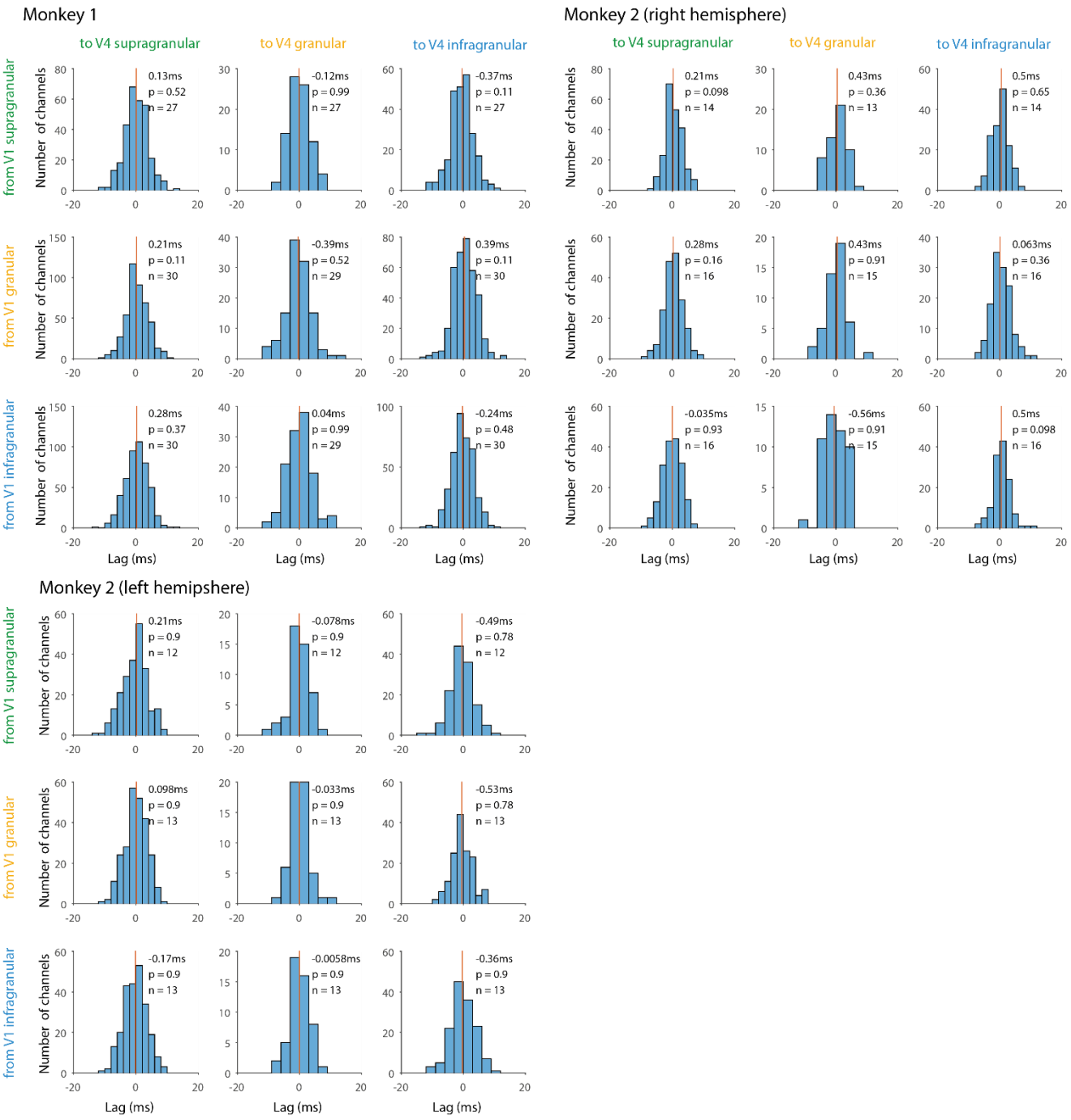

Figure D-9: LFP cross correlation histograms between V1 and V4 in the 55-100Hz frequency range. Plotted for Monkey 1 (top left plots) and the right and left hemispheres of Monkey 2 (top right and bottom right respectively plots). Shown for all combinations of V1 layers to V4 layers, correlations in the opposite direction have the same magnitude and opposite sign. Red lines indicates the median value of each distribution. The text on the plots quantifies the median value, p value (Wilcoxon signed rank test) and number of recordings (n).

Acknowledgements

The initial behavioural training of Monkeys 1 and 2 was performed prior to my starting on the project. Monkey 1 was trained by Miguel Dasilva and Monkey 2 was trained by Christian Brandt. Recordings in Monkey 1 and in the left hemisphere of Monkey 2 were acquired with the assistance of Jochem van Kempen. Animal care and husbandry was handled by the Comparative Biology Centre (CBC) at Newcastle University. Funding for the project was from the Wellcome Trust.

The project was supervised by Alexander Thiele and I would like to personally thank him for his guidance throughout pretty much every stage of my PhD. I almost certainly would have gotten lost down some tangent or other without him steering me through it.

Yet again I must thank my friends and family for supporting me during what you're no doubt hoping is the last stage of my university education (I think I said the same thing last time though…). The biggest thanks go as usual to my wife Ashley. Mostly for putting up with me prior to deadlines, but also for brightening my mood when my motivation was at its lowest.

And thanks to anyone who reads my thesis!

References

Abbott, L.F. and Dayan, P. (1999) 'The effect of correlated variability on the accuracy of a population code', *Neural computation*, 11(1), pp. 91-101.

Adhikari, A., Sigurdsson, T., Topiwala, M. A., Gordon, J. A. (2010) 'Cross-correlation of instantaneous amplitudes of field potential oscillations: A straightforward method to estimate the directionality and lag between brain areas', *J Neurosci Methods*, 191(2), pp. 191

Anderson, J.C., Kennedy, H. and Martin, K.A. (2011) 'Pathways of attention: synaptic relationships of frontal eye field to V4, lateral intraparietal cortex, and area 46 in macaque monkey', *J Neurosci*, 31(30), pp. 10872-81.

Ardid, S., Vinck, M., Kaping, D., Marquez, S., Everling, S. and Womelsdorf, T. (2015) 'Mapping of functionally characterized cell classes onto canonical circuit operations in primate prefrontal cortex', *J Neurosci*, 35(7), pp. 2975-91.

Armstrong, K.M. and Moore, T. (2007) 'Rapid enhancement of visual cortical response discriminability by microstimulation of the frontal eye field', *Proceedings of the National Academy of Sciences of the United States of America*, 104(22), pp. 9499-9504.

Baizer, J.S., Ungerleider, L.G. and Desimone, R. (1991) 'Organization of visual inputs to the inferior temporal and posterior parietal cortex in macaques', *J Neurosci*, 11(1), pp. 168-90.

Barnett, L. and Seth, A.K. (2014) 'The MVGC multivariate Granger causality toolbox: a new approach to Granger-causal inference', *Journal of neuroscience methods*, 223, pp. 50-68.

Bastos, A.M., Briggs, F., Alitto, H.J., Mangun, G.R. and Usrey, W.M. (2014) 'Simultaneous recordings from the primary visual cortex and lateral geniculate nucleus reveal rhythmic interactions and a cortical source for gamma-band oscillations', *J Neurosci*, 34(22), pp. 7639-44.

Bastos, A.M., Vezoli, J., Bosman, C.A., Schoffelen, J.-M., Oostenveld, R., Dowdall, J.R., De Weerd, P., Kennedy, H. and Fries, P. (2015) 'Visual areas exert feedforward and feedback influences through distinct frequency channels', *Neuron*, 85(2), pp. 390-401.

Bedard, C., Kroeger, H. and Destexhe, A. (2006) 'Does the 1/f frequency scaling of brain signals reflect self-organized critical states?', *Physical review letters*, 97(11), p. 118102.

Benevento, L.A. and Yoshida, K. (1981) 'The afferent and efferent organization of the lateral geniculo-prestriate pathways in the macaque monkey', *J Comp Neurol*, 203(3), pp. 455-74.

Benjamini, Y. and Yekutieli, D. (2001) 'The control of the false discovery rate in multiple testing under dependency', *Annals of Statistics*, 29(4), pp. 1165-1188.

Bichot, N.P., Heard, M.T., DeGennaro, E.M. and Desimone, R. (2015) 'A source for feature-based attention in the prefrontal cortex', *Neuron*, 88(4), pp. 832-844.

Blasdel, G.G. and Lund, J.S. (1983) 'Termination of afferent axons in macaque striate cortex', *The Journal of Neuroscience*, 3(7), pp. 1389-1413.

Blasdel, G.G., Lund, J.S. and Fitzpatrick, D. (1985) 'Intrinsic connections of macaque striate cortex: axonal projections of cells outside lamina 4C', *The Journal of neuroscience*, 5(12), pp. 3350-3369.

Borra, E. and Rockland, K.S. (2011) 'Projections to Early Visual Areas V1 and V2 in the Calcarine Fissure from Parietal Association Areas in the Macaque', *Frontiers in Neuroanatomy*, 5, p. 35.

Bosman, C.A., Schoffelen, J.-M., Brunet, N., Oostenveld, R., Bastos, A.M., Womelsdorf, T., Rubehn, B., Stieglitz, T., De Weerd, P. and Fries, P. (2012) 'Attentional stimulus selection through selective synchronization between monkey visual areas', *Neuron*, 75(5), pp. 875-888.

Boussaoud, D., Ungerleider, L.G. and Desimone, R. (1990) 'Pathways for motion analysis: cortical connections of the medial superior temporal and fundus of the superior temporal visual areas in the macaque', *J Comp Neurol*, 296(3), pp. 462-95.

Boyd, J.D., Mavity-Hudson, J.A. and Casagrande, V.A. (2000) 'The connections of layer 4 subdivisions in the primary visual cortex (V1) of the owl monkey', *Cerebral Cortex*, 10(7), pp. 644-662.

Briggs, F., Mangun, G.R. and Usrey, W.M. (2013) 'Attention enhances synaptic efficacy and the signal-to-noise ratio in neural circuits', *Nature*, 499(7459), pp. 476-480.

Buffalo, E.A., Fries, P., Landman, R., Buschman, T.J. and Desimone, R. (2011) 'Laminar differences in gamma and alpha coherence in the ventral stream', *Proceedings of the National Academy of Sciences*, 108(27), pp. 11262-11267.
Buffalo, E.A., Fries, P., Landman, R., Liang, H. and Desimone, R. (2010) 'A backward progression of attentional effects in the ventral stream', *Proceedings of the National Academy of Sciences*, 107(1), pp. 361-365.
Bullier, J. and Kennedy, H. (1983) 'Projection of the lateral geniculate nucleus onto cortical area V2 in the macaque monkey', *Experimental Brain Research*, 53(1), pp. 168-172.
Buschman, T.J. and Miller, E.K. (2007) 'Top-Down Versus Bottom-Up Control of Attention in the Prefrontal and Posterior Parietal Cortices', *Science*, 315(5820), pp. 1860-1862.
Bushnell, M.C., Goldberg, M.E. and Robinson, D.L. (1981) 'Behavioral enhancement of visual responses in monkey cerebral cortex. I. Modulation in posterior parietal cortex related to selective visual attention', *Journal of Neurophysiology*, 46(4), pp. 755-772.
Callaway, E.M. (1998) 'Local circuits in primary visual cortex of the macaque monkey', *Annual review of neuroscience*, 21(1), pp. 47-74.
Callaway, E.M. and Wiser, A.K. (1996) 'Contributions of individual layer 2–5 spiny neurons to local circuits in macaque primary visual cortex', *Visual neuroscience*, 13(05), pp. 907-922.
Casagrande, V.A. and Xu, X. (2004) '31 Parallel Visual Pathways: A Comparative Perspective'.
Chalk, M., Herrero, J.L., Gieselmann, M.A., Delicato, L.S., Gotthardt, S. and Thiele, A. (2010) 'Attention reduces stimulus-driven gamma frequency oscillations and spike field coherence in V1', *Neuron*, 66(1), pp. 114-25.
Chang, M.H., Armstrong, K.M. and Moore, T. (2012) 'Dissociation of response variability from firing rate effects in frontal eye field neurons during visual stimulation, working memory, and attention', *J Neurosci*, 32(6), pp. 2204-16.
Chen, W., Zhu, X.-H., Thulborn, K.R. and Ugurbil, K. (1999) 'Retinotopic mapping of lateral geniculate nucleus in humans using functional magnetic resonance imaging', *Proceedings of the National Academy of Sciences*, 96(5), pp. 2430-2434.
Churchland, M.M., Byron, M.Y., Cunningham, J.P., Sugrue, L.P., Cohen, M.R., Corrado, G.S., Newsome, W.T., Clark, A.M., Hosseini, P. and Scott, B.B. (2010) 'Stimulus onset quenches neural variability: a widespread cortical phenomenon', *Nature neuroscience*, 13(3), pp. 369-378.
Cohen, M.R. and Maunsell, J.H.R. (2009) 'Attention improves performance primarily by reducing interneuronal correlations', *Nature neuroscience*, 12(12), pp. 1594-1600.
Connor, C.E., Gallant, J.L., Preddie, D.C. and Van Essen, D.C. (1996) 'Responses in area V4 depend on the spatial relationship between stimulus and attention', *Journal of Neurophysiology*, 75(3), pp. 1306-1308.
Constantinople, C.M. and Bruno, R.M. (2013) 'Deep cortical layers are activated directly by thalamus', *Science*, 340(6140), pp. 1591-4.
Curcio, C.A., Sloan, K.R., Kalina, R.E. and Hendrickson, A.E. (1990) 'Human photoreceptor topography', *Journal of Comparative Neurology*, 292(4), pp. 497-523.
Dagnino, B., Gariel-Mathis, M.A. and Roelfsema, P.R. (2015) 'Microstimulation of area V4 has little effect on spatial attention and on perception of phosphenes evoked in area V1', *J Neurophysiol*, 113(3), pp. 730-9.
Desimone, R. and Duncan, J. (1995) 'Neural mechanisms of selective visual attention', *Annual review of neuroscience*, 18(1), pp. 193-222.
Douglas, R.J. and Martin, K.A.C. (2004) 'Neuronal circuits of the neocortex', *Annu. Rev. Neurosci.*, 27, pp. 419-451.
Duncan, J. (1984) 'Selective attention and the organization of visual information', *Journal of Experimental Psychology: General*, 113(4), p. 501.
Ecker, A.S., Berens, P., Keliris, G.A., Bethge, M., Logothetis, N.K. and Tolias, A.S. (2010) 'Decorrelated neuronal firing in cortical microcircuits', *science*, 327(5965), pp. 584-587.

Ecker, A.S., Berens, P., Tolias, A.S. and Bethge, M. (2011) 'The effect of noise correlations in populations of diversely tuned neurons', *The Journal of neuroscience : the official journal of the Society for Neuroscience*, 31(40), pp. 14272-14283.
El-Shamayleh, Y., Kumbhani, R.D., Dhruv, N.T. and Movshon, J.A. (2013) 'Visual response properties of V1 neurons projecting to V2 in macaque', *The Journal of Neuroscience*, 33(42), pp. 16594-16605.
Felleman, D.J., Burkhalter, A. and Van Essen, D.C. (1997) 'Cortical connections of areas V3 and VP of macaque monkey extrastriate visual cortex', *The Journal of comparative neurology*, 379(1), pp. 21-47.
Felleman, D.J. and Van Essen, D.C. (1991) 'Distributed hierarchical processing in the primate cerebral cortex', *Cereb Cortex*, 1(1), pp. 1-47.
Ferster, D. and Levy, S. (1978) 'The axonal arborizations of lateral geniculate neurons in the striate cortex of the cat', *Journal of Comparative Neurology*, 182(5), pp. 923-944.
Fries, P. (2005) 'A mechanism for cognitive dynamics: neuronal communication through neuronal coherence', *Trends in cognitive sciences*, 9(10), pp. 474-480.
Fries, P., Reynolds, J.H., Rorie, A.E. and Desimone, R. (2001) 'Modulation of oscillatory neuronal synchronization by selective visual attention', *Science*, 291(5508), pp. 1560-1563.
Fries, W. (1984) 'Cortical projections to the superior colliculus in the macaque monkey: A retrograde study using horseradish peroxidase', *The Journal of Comparative Neurology*, 230(1), pp. 55-76.
Gattas, R., Sousa, A.P., Mishkin, M. and Ungerleider, L.G. (1997) 'Cortical projections of area V2 in the macaque', *Cerebral Cortex*, 7(2), pp. 110-129.
Gattass, R., Galkin, T.W., Desimone, R. and Ungerleider, L.G. (2014) 'Subcortical connections of area V4 in the macaque', *Journal of Comparative Neurology*, 522(8), pp. 1941-1965.
Gieselmann, M.A. and Thiele, A. (2008) 'Comparison of spatial integration and surround suppression characteristics in spiking activity and the local field potential in macaque V1', *Eur J Neurosci*, 28(3), pp. 447-59.
Givre, S.J., Schroeder, C.E. and Arezzo, J.C. (1994) 'Contribution of extrastriate area V4 to the surface-recorded flash VEP in the awake macaque', *Vision research*, 34(4), pp. 415-428.
Goffart, L., Hafed, Z.M. and Krauzlis, R.J. (2012) 'Visual fixation as equilibrium: evidence from superior colliculus inactivation', *The Journal of Neuroscience*, 32(31), pp. 10627-10636.
Gregoriou, G.G., Gotts, S.J. and Desimone, R. (2012) 'Cell-type-specific synchronization of neural activity in FEF with V4 during attention', *Neuron*, 73(3), pp. 581-594.
Gregoriou, G.G., Gotts, S.J., Zhou, H. and Desimone, R. (2009) 'High-frequency, long-range coupling between prefrontal and visual cortex during attention', *Science*, 324(5931), pp. 1207-10.
Gross, C.G., Bender, D.B. and Rocha-Miranda, C.E. (1969) 'Visual receptive fields of neurons in inferotemporal cortex of the monkey', *Science*, 166(3910), pp. 1303-6.
Harris, K.D. and Thiele, A. (2011) 'Cortical state and attention', *Nat Rev Neurosci*, 12(9), pp. 509-23.
Hendry, S.H., Fuchs, J., deBlas, A.L. and Jones, E.G. (1990) 'Distribution and plasticity of immunocytochemically localized GABAA receptors in adult monkey visual cortex', *J Neurosci*, 10(7), pp. 2438-50.
Hendry, S.H.C. and Clay Reid, R. 23 (2000) 'The koniocellular pathway in primate vision' *Annual Review of Neuroscience* [Review]. pp. 127-153.
Herrero, J.L., Gieselmann, M.A., Sanayei, M. and Thiele, A. (2013) 'Attention-induced variance and noise correlation reduction in macaque V1 is mediated by NMDA receptors', *Neuron*, 78(4), pp. 729-39.
Herrero, J.L., Roberts, M.J., Delicato, L.S., Gieselmann, M.A., Dayan, P. and Thiele, A. (2008) 'Acetylcholine contributes through muscarinic receptors to attentional modulation in V1', *Nature*, 454(7208), pp. 1110-4.
Herrington, T.M. and Assad, J.A. (2009) 'Neural activity in the middle temporal area and lateral intraparietal area during endogenously cued shifts of attention', *J Neurosci*, 29(45), pp. 14160-76.
Heywood, C.A., Gadotti, A. and Cowey, A. (1992) 'Cortical area V4 and its role in the perception of color', *The Journal of neuroscience*, 12(10), pp. 4056-4065.

Hof, P.R. and Morrison, J.H. (1995) 'Neurofilament protein defines regional patterns of cortical organization in the macaque monkey visual system: A quantitative immunohistochemical analysis', *Journal of Comparative Neurology*, 352(2), pp. 161-186.
Ito, M. and Gilbert, C.D. (1999) 'Attention modulates contextual influences in the primary visual cortex of alert monkeys', *Neuron*, 22(3), pp. 593-604.
Jia, X., Smith, M.A. and Kohn, A. (2011) 'Stimulus selectivity and spatial coherence of gamma components of the local field potential', *J Neurosci*, 31(25), pp. 9390-403.
Johnson, K.G. and Harris, W.A. (2000) 'Connecting the eye with the brain: the formation of the retinotectal pathway', *Results and problems in cell differentiation*, 31, pp. 157-177.
Kandel, E.R., Schwartz, J.H., Jessell, T.M., Siegelbaum, S.A. and Hudspeth, A.J. (2000) *Principles of neural science*. McGraw-hill New York.
Kaneko, A. (1970) 'Physiological and morphological identification of horizontal, bipolar and amacrine cells in goldfish retina', *The Journal of physiology*, 207(3), p. 623.
Kapadia, M.K., Ito, M., Gilbert, C.D. and Westheimer, G. (1995) 'Improvement in visual sensitivity by changes in local context: parallel studies in human observers and in V1 of alert monkeys', *Neuron*, 15(4), pp. 843-56.
Kaplan, E. and Shapley, R.M. (1982) 'X and Y cells in the lateral geniculate nucleus of macaque monkeys', *Journal of Physiology*, Vol. 330, pp. 125-143.
Kaplan, E. and Shapley, R.M. (1986) 'The primate retina contains two types of ganglion cells, with high and low contrast sensitivity', *Proceedings of the National Academy of Sciences of the United States of America*, 83(8), pp. 2755-2757.
Kennedy, H. and Bullier, J. (1985) 'A double-labeling investigation of the afferent connectivity to cortical areas V1 and V2 of the macaque monkey', *J Neurosci*, 5(10), pp. 2815-30.
Krauzlis, R.J. (2003) 'Neuronal activity in the rostral superior colliculus related to the initiation of pursuit and saccadic eye movements', *Journal of Neuroscience*, 23(10), pp. 4333-4344.
Lee, B.B., Martin, P.R. and Valberg, A. (1989) 'Nonlinear summation of M-and L-cone inputs to phasic retinal ganglion cells of the macaque', *The Journal of Neuroscience*, 9(4), pp. 1433-1442.
Livingstone, M.S. and Hubel, D.H. (1982) 'Thalamic inputs to cytochrome oxidase-rich regions in monkey visual cortex', *Proceedings of the National Academy of Sciences*, 79(19), pp. 6098-6101.
Luck, S.J., Chelazzi, L., Hillyard, S.A. and Desimone, R. (1997) 'Neural mechanisms of spatial selective attention in areas V1, V2, and V4 of macaque visual cortex', *Journal of neurophysiology*, 77(1), pp. 24-42.
Lueschow, A., Miller, E.K. and Desimone, R. (1994) 'Inferior temporal mechanisms for invariant object recognition', *Cerebral Cortex*, 4(5), pp. 523-531.
Lund, J.S. (1987) 'Local circuit neurons of macaque monkey striate cortex: I. Neurons of laminae 4C and 5A', *Journal of Comparative Neurology*, 257(1), pp. 60-92.
Lund, J.S. (1988) 'Anatomical organization of macaque monkey striate visual cortex', *Annu Rev Neurosci*, 11, pp. 253-88.
Lund, J.S., Hawken, M.J. and Parker, A.J. (1988) 'Local circuit neurons of macaque monkey striate cortex: II. Neurons of the laminae 5B and 6', *Journal of Comparative Neurology*, 276(1), pp. 1-29.
Lund, J.S., Lund, R.D., Hendrickson, A.E., Bunt, A.H. and Fuchs, A.F. (1975) 'The origin of efferent pathways from the primary visual cortex, area 17, of the macaque monkey as shown by retrograde transport of horseradish peroxidase', *J Comp Neurol*, 164(3), pp. 287-303.
Lund, J.S. and Wu, C.Q. (1997) 'Local circuit neurons of macaque monkey striate cortex: IV. Neurons of laminae 1-3a', *Journal of Comparative Neurology*, 384(1), pp. 109-126.
Lund, J.S. and Yoshioka, T. (1991) 'Local circuit neurons of macaque monkey striate cortex: III. Neurons of laminae 4B, 4A, and 3B', *Journal of Comparative Neurology*, 311(2), pp. 234-258.
Lund, J.S., Yoshioka, T. and Levitt, J.B. (1993) 'Comparison of intrinsic connectivity in different areas of macaque monkey cerebral cortex', *Cereb Cortex*, 3(2), pp. 148-62.
Maier, A., Aura, C.J. and Leopold, D.A. (2011) 'Infragranular sources of sustained local field potential responses in macaque primary visual cortex', *J Neurosci*, 31(6), pp. 1971-80.

Markov, N.T., Vezoli, J., Chameau, P., Falchier, A., Quilodran, R., Huissoud, C., Lamy, C., Misery, P., Giroud, P., Ullman, S., Barone, P., Dehay, C., Knoblauch, K. and Kennedy, H. (2014) 'Anatomy of hierarchy: Feedforward and feedback pathways in macaque visual cortex', *Journal of Comparative Neurology*, 522(1), pp. 225-259.
Martinez-Trujillo, J.C. and Treue, S. (2004) 'Feature-based attention increases the selectivity of population responses in primate visual cortex', *Curr Biol*, 14(9), pp. 744-51.
Masland, R.H. (2001) 'The fundamental plan of the retina', *Nature Neuroscience*, 4(9), pp. 877-886.
McAdams, C.J. and Maunsell, J.H.R. (1999) 'Effects of attention on orientation-tuning functions of single neurons in macaque cortical area V4', *Journal of Neuroscience*, 19(1), pp. 431-441.
McAdams, C.J. and Maunsell, J.H.R. (2000) 'Attention to both space and feature modulates neuronal responses in macaque area V4', *Journal of Neurophysiology*, 83(3), pp. 1751-1755.
McAdams, C.J. and Reid, R.C. (2005) 'Attention modulates the responses of simple cells in monkey primary visual cortex', *J Neurosci*, 25(47), pp. 11023-33.
McAlonan, K., Cavanaugh, J. and Wurtz, R.H. (2006) 'Attentional Modulation of Thalamic Reticular Neurons', *The Journal of Neuroscience*, 26(16), pp. 4444-4450.
McAlonan, K., Cavanaugh, J. and Wurtz, R.H. (2008) 'Guarding the gateway to cortex with attention in visual thalamus', *Nature*, 456(7220), pp. 391-394.
McGuire, B.A., Gilbert, C.D., Rivlin, P.K. and Wiesel, T.N. (1991) 'Targets of horizontal connections in macaque primary visual cortex', *Journal of Comparative Neurology*, 305(3), pp. 370-392.
Merbs, S.L. and Nathans, J. (1992) 'Absorption spectra of human cone pigments', *Nature*, 356(6368), pp. 433-435.
Merigan, W.H. and Maunsell, J.H.R. (1993) 'How parallel are the primate visual pathways?', *Annual review of neuroscience*, 16(1), pp. 369-402.
Mishkin, M., Ungerleider, L.G. and Macko, K.A. (1983) 'Object vision and spatial vision: two cortical pathways', *Trends in neurosciences*, 6, pp. 414-417.
Mitchell, J.F., Sundberg, K.A. and Reynolds, J.H. (2007) 'Differential attention-dependent response modulation across cell classes in macaque visual area V4', *Neuron*, 55(1), pp. 131-41.
Mitchell, J.F., Sundberg, K.A. and Reynolds, J.H. (2009) 'Spatial attention decorrelates intrinsic activity fluctuations in macaque area V4', *Neuron*, 63(6), pp. 879-88.
Mitra, P. and Bokil, H. (2007) *Observed brain dynamics*. Oxford University Press.
Mitra, P.P. and Pesaran, B. (1999) 'Analysis of Dynamic Brain Imaging Data', *Biophysical Journal*, 76(2), pp. 691-708.
Moore, G.P., Segundo, J.P., Perkel, D.H. and Levitan, H. (1970) 'Statistical Signs of Synaptic Interaction in Neurons', *Biophysical Journal*, 10(9), pp. 876-900.
Moore, T. and Fallah, M. (2001) 'Control of eye movements and spatial attention', *Proceedings of the National Academy of Sciences*, 98(3), pp. 1273-1276.
Moore, T. and Fallah, M. (2004) 'Microstimulation of the Frontal Eye Field and Its Effects on Covert Spatial Attention', *Journal of Neurophysiology*, 91(1), pp. 152-162.
Moran, J. and Desimone, R. (1985) 'Selective attention gates visual processing in the extrastriate cortex', *Frontiers in cognitive neuroscience*, 229, pp. 342-345.
Motter, B.C. (1993) 'Focal attention produces spatially selective processing in visual cortical areas V1, V2, and V4 in the presence of competing stimuli', *Journal of neurophysiology*, 70(3), pp. 909-919.
Mountcastle, V.B. (1957) 'Modality and topographic properties of single neurons of cat's somatic sensory cortex', *Journal of neurophysiology*, 20(4), pp. 408-434.
Nakamura, H., Gattass, R., Desimone, R. and Ungerleider, L.G. (1993) 'The modular organization of projections from areas V1 and V2 to areas V4 and TEO in macaques', *J Neurosci*, 13(9), pp. 3681-91.
Ni, Amy M., Ray, S. and Maunsell, John H.R. (2012) 'Tuned Normalization Explains the Size of Attention Modulations', *Neuron*, 73(4), pp. 803-813.
Niebergall, R., Khayat, P.S., Treue, S. and Martinez-Trujillo, J.C. (2011) 'Multifocal attention filters targets from distracters within and beyond primate MT neurons' receptive field boundaries', *Neuron*, 72(6), pp. 1067-1079.

Ninomiya, T., Sawamura, H., Inoue, K.-i. and Takada, M. (2011) 'Differential architecture of multisynaptic geniculo-cortical pathways to V4 and MT', *Cerebral Cortex*, p. bhr078.
O'Connor, D.H., Fukui, M.M., Pinsk, M.A. and Kastner, S. (2002) 'Attention modulates responses in the human lateral geniculate nucleus', *Nature neuroscience*, 5(11), pp. 1203-1209.
Ogren, M. and Hendrickson, A. (1976) 'Pathways between striate cortex and subcortical regions in Macaca mulatta and Saimiri sciureus: evidence for a reciprocal pulvinar connection', *Experimental neurology*, 53(3), pp. 780-800.
Pesaran, B., Pezaris, J.S., Sahani, M., Mitra, P.P. and Andersen, R.A. (2002) 'Temporal structure in neuronal activity during working memory in macaque parietal cortex', *Nature neuroscience*, 5(8), pp. 805-811.
Pettersen, K.H., Devor, A., Ulbert, I., Dale, A.M. and Einevoll, G.T. (2006) 'Current-source density estimation based on inversion of electrostatic forward solution: Effects of finite extent of neuronal activity and conductivity discontinuities', *Journal of Neuroscience Methods*, 154(1–2), pp. 116-133.
Pooresmaeili, A., Poort, J. and Roelfsema, P.R. (2014) 'Simultaneous selection by object-based attention in visual and frontal cortex', *Proceedings of the National Academy of Sciences*, 111(17), pp. 6467-6472.
Posner, M.I. (1980) 'Orienting of attention', *Quarterly journal of experimental psychology*, 32(1), pp. 3-25.
Posner, M.I., Cohen, Y. and Rafal, R.D. (1982) 'Neural systems control of spatial orienting', *Philosophical Transactions of the Royal Society B: Biological Sciences*, 298(1089), pp. 187-198.
Purcell, B.A., Heitz, R.P., Cohen, J.Y. and Schall, J.D. (2012) 'Response variability of frontal eye field neurons modulates with sensory input and saccade preparation but not visual search salience', *Journal of neurophysiology*, 108(10), pp. 2737-2750.
Purushothaman, G., Marion, R., Li, K. and Casagrande, V.A. (2012) 'Gating and control of primary visual cortex by pulvinar', *Nat Neurosci*, 15(6), pp. 905-12.
Ray, S. and Maunsell, J.H. (2010) 'Differences in gamma frequencies across visual cortex restrict their possible use in computation', *Neuron*, 67(5), pp. 885-96.
Renart, A., de la Rocha, J., Bartho, P., Hollender, L., Parga, N., Reyes, A. and Harris, K.D. (2010) 'The Asynchronous State in Cortical Circuits', *Science (New York, N.Y.)*, 327(5965), pp. 587-590.
Reynolds, J.H., Chelazzi, L. and Desimone, R. (1999) 'Competitive mechanisms subserve attention in macaque areas V2 and V4', *J Neurosci*, 19(5), pp. 1736-53.
Reynolds, J.H. and Desimone, R. (2003) 'Interacting roles of attention and visual salience in V4', *Neuron*, 37(5), pp. 853-63.
Reynolds, J.H. and Heeger, D.J. (2009) 'The normalization model of attention', *Neuron*, 61(2), pp. 168-85.
Reynolds, J.H., Pasternak, T. and Desimone, R. (2000) 'Attention increases sensitivity of V4 neurons', *Neuron*, 26(3), pp. 703-714.
Roberts, M., Delicato, L.S., Herrero, J., Gieselmann, M.A. and Thiele, A. (2007) 'Attention alters spatial integration in macaque V1 in an eccentricity-dependent manner', *Nat Neurosci*, 10(11), pp. 1483-91.
Robinson, D.A. (1972) 'Eye movements evoked by collicular stimulation in the alert monkey', *Vision Research*, 12(11), pp. 1795-1808.
Rockland, K.S. (1992) 'Laminar distribution of neurons projecting from area V1 to V2 in macaque and squirrel monkeys', *Cerebral Cortex*, 2(1), pp. 38-47.
Rockland, K.S. and Lund, J.S. (1983) 'Intrinsic laminar lattice connections in primate visual cortex', *Journal of Comparative Neurology*, 216(3), pp. 303-318.
Rockland, K.S. and Pandya, D.N. (1979) 'Laminar origins and terminations of cortical connections of the occipital lobe in the rhesus monkey', *Brain Res*, 179(1), pp. 3-20.
Roelfsema, P.R., Lamme, V.A.F. and Spekreijse, H. (1998) 'Object-based attention in the primary visual cortex of the macaque monkey', *Nature*, 395(6700), pp. 376-381.
Roelfsema, P.R., Lamme, V.A.F. and Spekreijse, H. (2004) 'Synchrony and covariation of firing rates in the primary visual cortex during contour grouping', *Nature Neuroscience*, 7(9), pp. 982-991.

Roorda, A. and Williams, D.R. (1999) 'The arrangement of the three cone classes in the living human eye', *Nature*, 397(6719), pp. 520-522.
Rossi, A.F. and Paradiso, M.A. (1995) 'Feature-specific effects of selective visual attention', *Vision research*, 35(5), pp. 621-634.
Ruff, D.A. and Cohen, M.R. (2014) 'Attention can either increase or decrease spike count correlations in visual cortex', *Nat Neurosci*, 17(11), pp. 1591-1597.
Ruff, D.A. and Cohen, M.R. (2016) 'Attention Increases Spike Count Correlations between Visual Cortical Areas', *The Journal of Neuroscience*, 36(28), pp. 7523-7534.
Saalmann, Y.B., Pinsk, M.A., Wang, L., Li, X. and Kastner, S. (2012) 'The pulvinar regulates information transmission between cortical areas based on attention demands', *Science*, 337(6095), pp. 753-756.
Sanayei, M., Herrero, J.L., Distler, C. and Thiele, A. (2015) 'Attention and normalization circuits in macaque V1', *European Journal of Neuroscience*, 41(7), pp. 949-964.
Schiller, P.H. and Malpeli, J.G. (1977) 'Properties and tectal projections of monkey retinal ganglion cells', *Journal of Neurophysiology*, 40(2), pp. 428-445.
Schroeder, C.E., Tenke, C.E., Givre, S.J., Arezzo, J.C. and Vaughan, H.G., Jr. (1991) 'Striate cortical contribution to the surface-recorded pattern-reversal VEP in the alert monkey', *Vision Res*, 31(7-8), pp. 1143-57.
Shadlen, M.N., Britten, K.H., Newsome, W.T. and Movshon, J.A. (1996) 'A computational analysis of the relationship between neuronal and behavioral responses to visual motion', *The Journal of neuroscience*, 16(4), pp. 1486-1510.
Shipp, S. (2003) 'The functional logic of cortico–pulvinar connections', *Philosophical Transactions of the Royal Society B: Biological Sciences*, 358(1438), pp. 1605-1624.
Sincich, L.C., Park, K.F., Wohlgemuth, M.J. and Horton, J.C. (2004) 'Bypassing V1: a direct geniculate input to area MT', *Nature neuroscience*, 7(10), pp. 1123-1128.
Singer, W. (1999) 'Neuronal synchrony: a versatile code for the definition of relations?', *Neuron*, 24(1), pp. 49-65, 111-25.
Smith, M.A., Jia, X., Zandvakili, A. and Kohn, A. (2013) 'Laminar dependence of neuronal correlations in visual cortex', *Journal of neurophysiology*, 109(4), pp. 940-947.
Smith, M.A. and Kohn, A. (2008) 'Spatial and temporal scales of neuronal correlation in primary visual cortex', *J Neurosci*, 28(48), pp. 12591-603.
Spearman, C. (1904) 'The proof and measurement of association between two things', *The American journal of psychology*, 15(1), pp. 72-101.
Spitzer, H., Desimone, R. and Moran, J. (1988) 'Increased attention enhances both behavioral and neuronal performance', *Science*, 240(4850), pp. 338-340.
Stepanyants, A., Hof, P.R. and Chklovskii, D.B. (2002) 'Geometry and structural plasticity of synaptic connectivity', *Neuron*, 34(2), pp. 275-288.
Stewart, H.C.H. and Reid, R.C. (2000) 'The Koniocellular Pathway in Primate Vision', *Annual Review of Neuroscience*, 23(1), pp. 127-153.
Supèr, H. and Roelfsema, P.R. 147 (2004) 'Chronic multiunit recordings in behaving animals: Advantages and limitations' *Progress in Brain Research* [Article]. pp. 263-282.
Tassinari, G., Bentivoglio, M., Chen, S. and Campara, D. (1997) 'Overlapping ipsilateral and contralateral retinal projections to the lateral geniculate nucleus and superior colliculus in the cat: a retrograde triple labelling study', *Brain Res Bull*, 43(2), pp. 127-39.
Theeuwes, J. (1991) 'Exogenous and endogenous control of attention: The effect of visual onsets and offsets', *Perception & Psychophysics*, 49(1), pp. 83-90.
Thiele, A., Brandt, C., Dasilva, M., Gotthardt, S., Chicharro, D., Panzeri, S. and Distler, C. (2016) 'Attention Induced Gain Stabilization in Broad and Narrow-Spiking Cells in the Frontal Eye-Field of Macaque Monkeys', *The Journal of Neuroscience*, 36(29), pp. 7601-7612.
Thiele, A., Delicato, L.S., Roberts, M.J. and Gieselmann, M.A. (2006) 'A novel electrode-pipette design for simultaneous recording of extracellular spikes and iontophoretic drug application in awake behaving monkeys', *Journal of Neuroscience Methods*, 158(2), pp. 207-211.

Thiele, A., Pooresmaeili, A., Delicato, L.S., Herrero, J.L. and Roelfsema, P.R. (2009) 'Additive effects of attention and stimulus contrast in primary visual cortex', *Cereb Cortex*, 19(12), pp. 2970-81.
Thiele, A. and Stoner, G. (2003) 'Neuronal synchrony does not correlate with motion coherence in cortical area MT', *Nature*, 421(6921), pp. 366-370.
Tolias, A.S., Moore, T., Smirnakis, S.M., Tehovnik, E.J., Siapas, A.G. and Schiller, P.H. (2001) 'Eye movements modulate visual receptive fields of V4 neurons', *Neuron*, 29(3), pp. 757-767.
Tootell, R.B., Silverman, M.S., Switkes, E. and De Valois, R.L. (1982) 'Deoxyglucose analysis of retinotopic organization in primate striate cortex', *Science (New York, NY)*, 218(4575), pp. 902-904.
Treue, S. and Maunsell, J.H.R. (1999) 'Effects of attention on the processing of motion in macaque middle temporal and medial superior temporal visual cortical areas', *The Journal of Neuroscience*, 19(17), pp. 7591-7602.
Trongnetrpunya, A., Nandi, B., Kang, D., Kocsis, B., Schroeder, C.E. and Ding, M. (2015) 'Assessing Granger Causality in Electrophysiological Data: Removing the Adverse Effects of Common Signals via Bipolar Derivations', *Frontiers in Systems Neuroscience*, 9, p. 189.
Ungerleider, L.G., Galkin, T.W., Desimone, R. and Gattass, R. (2008) 'Cortical connections of area V4 in the macaque', *Cerebral Cortex*, 18(3), pp. 477-499.
Van Kerkoerle, T., Self, M.W., Dagnino, B., Gariel-Mathis, M.-A., Poort, J., Van Der Togt, C. and Roelfsema, P.R. (2014) 'Alpha and gamma oscillations characterize feedback and feedforward processing in monkey visual cortex', *Proceedings of the National Academy of Sciences*, 111(40), pp. 14332-14341.
Vincent, J.L., Patel, G.H., Fox, M.D., Snyder, A.Z., Baker, J.T., Van Essen, D.C., Zempel, J.M., Snyder, L.H., Corbetta, M. and Raichle, M.E. (2007) 'Intrinsic functional architecture in the anaesthetized monkey brain', *Nature*, 447(7140), pp. 83-86.
Williford, T. and Maunsell, J.H.R. (2006) 'Effects of spatial attention on contrast response functions in macaque area V4', *Journal of neurophysiology*, 96(1), pp. 40-54.
Wiser, A.K. and Callaway, E.M. (1996) 'Contributions of individual layer 6 pyramidal neurons to local circuitry in macaque primary visual cortex', *J Neurosci*, 16(8), pp. 2724-39.
Womelsdorf, T., Anton-Erxleben, K., Pieper, F. and Treue, S. (2006) 'Dynamic shifts of visual receptive fields in cortical area MT by spatial attention', *Nature neuroscience*, 9(9), pp. 1156-1160.
Woollard, H.H. (1927) *Proceedings of the Zoological Society of London*. Wiley Online Library.
Xing, D., Shen, Y., Burns, S., Yeh, C.I., Shapley, R. and Li, W. (2012) 'Stochastic generation of gamma-band activity in primary visual cortex of awake and anesthetized monkeys', *J Neurosci*, 32(40), pp. 13873-80a.
Yoshioka, T., Levitt, J.B. and Lund, J.S. (1992) 'Intrinsic lattice connections of macaque monkey visual cortical area V4', *J Neurosci*, 12(7), pp. 2785-802.
Zeki, S.M. (1971) 'Cortical projections from two prestriate areas in the monkey', *Brain Res*, 34(1), pp. 19-35.
Zénon, A. and Krauzlis, R. (2014) 'Superior colliculus as a subcortical center for visual selection', *Medecine/Sciences*, 30(6-7), pp. 637-643.
Zénon, A. and Krauzlis, R.J. (2012) 'Attention deficits without cortical neuronal deficits', *Nature*, 489(7416), pp. 434-437.
Zhou, H., Schafer, R.J. and Desimone, R. (2016) 'Pulvinar-Cortex Interactions in Vision and Attention', *Neuron*, 89(1), pp. 209-220.